

2017

Pathways of NHEJ at Dysfunctional Telomeres and Their Resolution

Roos Anna Karssemeijer

Follow this and additional works at: http://digitalcommons.rockefeller.edu/student_theses_and_dissertations



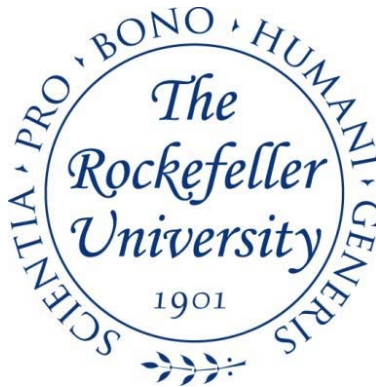
Part of the [Life Sciences Commons](#)

Recommended Citation

Karssemeijer, Roos Anna, "Pathways of NHEJ at Dysfunctional Telomeres and Their Resolution" (2017). *Student Theses and Dissertations*. 396.

http://digitalcommons.rockefeller.edu/student_theses_and_dissertations/396

This Thesis is brought to you for free and open access by Digital Commons @ RU. It has been accepted for inclusion in Student Theses and Dissertations by an authorized administrator of Digital Commons @ RU. For more information, please contact mcsweej@mail.rockefeller.edu.



PATHWAYS OF NHEJ AT DYSFUNCTIONAL TELOMERES AND THEIR RESOLUTION

A Thesis Presented to the Faculty of
The Rockefeller University
in Partial Fulfillment of the Requirements for
the degree of Doctor of Philosophy

by

Roos Anna Karssemeijer

June 2017

PATHWAYS OF NHEJ AT DYSFUNCTIONAL TELOMERES AND THEIR RESOLUTION

Roos Anna Karssemeijer, Ph.D.

The Rockefeller University 2017

Shelterin is a multiprotein complex that prevents DNA damage signaling at chromosome ends. In its absence, DNA repair pathways are activated that can promote the fusion of dysfunctional telomeres resulting in chromosomal instability. The work presented here aims to understand how telomeres are protected from these pathogenic repair pathways.

The first part of this thesis is focused on the DNA damage response factor 53BP1, a key regulator in double strand break (DSB) repair pathways in mammalian cells. By influencing key regulatory events at and near DNA ends, 53BP1 plays an important role in the decision between non-homologous end-joining (NHEJ) and homologous recombination (HR). Telomeres lacking the shelterin protein TRF2 have proven a versatile system for studying 53BP1 in DSB repair since 53BP1 protects dysfunctional telomeres from resection and promotes their mobility. Analysis of separation of function mutants of 53BP1 has identified the domain that is responsible for promoting the mobility of DSBs. Cells expressing 53BP1^{ΔMOB} showed reduced levels of NHEJ at dysfunctional telomeres and damage foci roamed a smaller part of the nucleus. But which

53BP1 interacting factors are responsible for mediating the increased mobility remains unclear.

The second part of this thesis aims to elucidate the DNA repair pathways that are activated when the shelterin component TRF1 is absent. The results provide tantalizing evidence that sister telomeres can fuse via the alternative-NHEJ (a-NHEJ) pathway when replication forks reach the end of the chromosome in cells that are deficient in TRF1. To prevent chromosome instability, mammalian cells appear to employ the Holliday Junction resolvase Gen1, which is capable of cleaving cruciform DNA structures that can be formed when telomeres fuse. The deletion of Gen1 from TRF1 null cells resulted in the accumulation of chromatin bridges and isochromosomes, indicative of genomic instability. The results presented here are of relevance to studies of human cancer cells since the presence of critically short telomeres induces sister telomere fusions via a-NHEJ. It is possible that replication stress underlies these fusion events and that Gen1 has evolved as a mechanism to counteract the consequences of chromosomal fusion events at telomeres.

Acknowledgements

I would first of all like to express my gratitude to my advisor, Titia de Lange. I joined your lab late into the program and I am very grateful for your guidance and support. I am impressed with your dedication to science and have learned a lot during the past three and a half years from your rigorous, distinctive and inspirational approach to solving scientific problems, which will be helpful in any future career. I would also like to thank Tarun Kapoor, Robert Roeder, and John Petrini for serving on my thesis committee. I also thank the Deans office for their continuous support and help over the years. Finally, I would like to thank Daniel Mucida and Sasha Tarakhovsky for being great mentors during my first years in the program.

My experience in the de Lange lab would not have been the same without Francisca, who is an amazing teacher, mentor and friend. I am grateful for all your help and advise and I am so excited that there will soon be a Lottersberger lab! Hiro, thank you for being my bay mate and for sharing your vast knowledge about the lab with me. And I will certainly miss chatting with you about running and climbing mountains! John, I would also like to thank you for our scientific discussions, but even more for all the fun afternoon runs and crazy bike rides that we did (I'll always be terrified of dogs!). I furthermore thank all other members of the de Lange lab for scientific support. I particular Adriana, Stew and Rosie, who do an amazing job making the lab run efficiently.

I have been supported by a fellowship from the Boehringer Ingelheim foundation, which not only provided financial assistance but also scientific support in the form of symposia and workshops. I was also the recipient of a fellowship from the Women & Science initiative at the Rockefeller University.

I also want to thank all the friends that have been there for me over the years, both in New York and back at home. Lianne, Lieke, Lidwien, Sara, Michiel, Evelien, Boaz's, Carlien – your support has meant a lot to me. Special thanks go to my running friends, who kept me sane over the years with our weekly runs, dinners, brunches, crazy races and vacations. Kristina, Lauren, Deirde, Kat, Shin, Dara, Burke, Pete, Will, Kate, Mike, Dima, Andel, Chacko, Laura, Rachel, Nick, Jimmy, I would not have made it to this particular finish line without you.

Importantly, I would like to thank my family, Nico, Ina, Leendertjan and Peter. You have supported me unconditionally over the years for which I am very grateful. I am not the first in our family with a PhD and probably not the last; this would not be possible without your enthusiasm, support and trust in us. Finally, I want to thank Johannes. We met during my first weeks in New York and I have benefited immensely from your love, encouragement, scientific curiosity and patience. Thank you for believing in me no matter what. I am looking forward to spending the next chapter of our lives together.

Table of Contents

Acknowledgements	iii
Table of Contents	v
List of Figures.....	ix
List of Abbreviations	xi
 Chapter 1: Introduction.....	 1
1.1 Mammalian DNA damage response pathways	2
1.1.1 DNA damage	2
1.1.2 ATM kinase and DSB repair	5
1.1.3 Classical and Alternative NHEJ	7
1.1.4 Homologous Recombination	10
1.1.5 ATR kinase activation and replication stress	13
1.1.6 ATR regulates origin firing	14
1.1.7 Fork stabilization by ATR	15
1.1.8 Crosstalk between the ATM and ATR pathway	15
1.2 The role of 53BP1 in the DNA damage response pathway.....	17
1.2.1 53BP1 is a key regulator in the DNA damage response pathway	17
1.2.2 Structure of 53BP1	19
1.2.3 Recruitment of 53BP1	21
1.2.4 Regulation of end-resection in mammalian cells	24
1.2.5 53BP1 mediated chromatin mobility	27
1.3 The structure and function of telomeres	29
1.3.1 Telomeres protect the end of linear chromosomes.....	29
1.3.2 Telomerase counteracts the end-replication problem.....	31
1.3.3 Shelterin protects against the end-protection problem	32
1.3.4 TRF2 prevents ATM activation and NHEJ	35
1.3.5 TRF1 is required for telomere replication.....	37

1.3.6 Fragile sites.....	38
1.3.7 Fragile site cleavage prevents anaphase bridges.....	39
1.3.8 TRF1 recruits BLM to prevent fragile telomeres	40
1.3.9 TRF1 prevents the formation of sister associations.....	41
1.3.10 Dysfunctional telomeres as a model for DNA damage response pathways	42
 Chapter 2: 53BP1 dissociation of function mutants	44
2.1 Introduction	45
2.2 Results	46
2.2.1 Generation of 53BP1 mutants.....	46
2.2.2 Rif1 is the only factor downstream of 53BP1 controlling resection	52
2.2.3 53BP1 mutant alleles promote varying levels of telomere fusions.....	56
2.2.4 Identification of the 53BP1 mobility domain	60
2.2.5 No interaction detected between Sun1 and 53BP1	64
2.2.6 Exploring a role for known 53BP1 interacting partners in chromatin mobility	70
2.2.7 Oligomerization domain of 53BP1	73
2.3 Summary of findings	81
 Chapter 3: The nature of telomere sister associations formed upon loss of	
TRF1	84
3.1 Introduction	85
3.2 Results	92
3.2.1 PARP1 is required for Sister Associations.....	92
3.2.2. Ligase 3 is involved in the formation of Sister Associations	95
3.2.3 Ku does not affect Sister Associations.....	99
3.2.4 Anaphase bridges are seen upon deletion of TRF1	101
3.2.5 PICH localizes to DNA bridges upon deletion of TRF1.....	104
3.2.6 The role of 53BP1 at sites of replication stress.....	111
3.2.7 Rif1 acts downstream of 53BP1 to promote Sister Associations	120
3.2.8 A enigmatic role for Exo1 in the formation of Sister Associations.....	125
3.3 Summary of findings	128

Chapter 4: Gen1 cleaves fused sister telomeres.....	131
4.1 Introduction	132
4.2 Results	136
4.2.1 Gen1 loss induces chromatin bridges after TRF1 loss.....	136
4.2.2 Aphidicolin does not induce chromatin bridges.....	143
4.2.3 Gen1 loss does not affect the frequency of SAs or telomere fragility.....	145
4.2.4 Gen1 loss increases the frequency of isochromosomes.....	147
4.2.5 TRF1 ^{F/F} Gen1 ^{-/-} cells display increased mitotic failure	154
4.2.6 Overexpression of mutant Gen1 alleles in TRF1 ^{F/F} Gen1 ^{-/-} MEFs	156
4.2.7 Chromatin bridges are not an SV40 artifact.....	160
4.2.8 PARP1 deletion rescues chromatin bridge formation	164
4.2.9 Mus81 depletion aggravates the Gen1 ^{-/-} effect	167
4.3 Summary of findings	176
 Chapter 5: Discussion	 179
5.1 Dissociation of function mutants of 53BP1	180
5.1.1 Rif1 is the only factor downstream of 53BP1 inhibiting resection	180
5.1.2 The connection between 53BP1 and the LINC complex	182
5.1.3 The function of chromatin mobility in response to damage.....	186
5.2 The fusion of sister telomeres by a-NHEJ and cleavage by Gen1	188
5.2.1 Telomeres are prone to a-NHEJ in absence of TRF1.....	188
5.2.4 Telomere entanglements in yeast.....	194
5.2.6 The role of Ku in preventing a-NHEJ at telomeres	202
5.2.7 Gen1 cleaves SAs	204
5.2.8 Critically short telomeres in human cells fuse via a-NHEJ.....	207
 Chapter 6: Materials and Methods.....	 210
6.1 Cell culture techniques	211
6.1.1 Mammalian cell culture	211

6.1.2 Calcium phosphate precipitation transfection of 293T and Phoenix cells	212
6.1.3 Retroviral gene delivery	212
6.1.4 Lentiviral gene delivery of shRNAs	213
6.1.5 Cre mediated gene deletion	214
6.1.6 Generation of CRISPR/Cas9 knockout cell lines	214
6.1.7 PARPi treatment of cells	216
6.2 Molecular techniques	216
6.2.1 Cloning techniques	216
6.2.2 Co-immunoprecipitation in 293T cells	219
6.2.3 Co-immunoprecipitation of endogenous Sun1 from MEFs	221
6.2.4 Western blotting	222
6.2.6 Chromatin immunoprecipitation (ChIP)	223
6.2.7 Telomere overhang analysis	224
6.2.8 Quantitative PCR analysis	226
6.3 Imaging techniques	227
6.3.1 IF and IF-FISH	227
6.3.2 Chromatin bridge analysis	228
6.3.3 Metaphase telomeric FISH	229
6.3.4 Isochromosome analysis	230
6.3.5 Live-cell imaging for chromatin mobility analysis	230
6.3.6 Live-cell imaging for mitotic abnormalities	231
6.4 Lists of cell lines used	232
6.5 List of shRNA used	233
References	235

List of Figures

Figure 1.1 ATM and ATR activation	4
Figure 1.2 Pathways for c-NHEJ and a-NHEJ.....	9
Figure 1.3 Homologous recombination.....	12
Figure 1.4 Functions of 53BP1	20
Figure 1.5 Structure of 53BP1	20
Figure 1.6 Recruitment of 53BP1 to DSBs	23
Figure 1.7 Shelterin protects chromosome ends	30
Figure 2.1 Gibson cloning of 53BP1 mutant alleles.....	47
Figure 2.2 53BP1 mutant alleles	48
Figure 2.3 Rif1 recruitment to 53BP1	50
Figure 2.4 53BP1 mutant alleles localize to telomeres.....	51
Figure 2.5 Schematic of telomere overhang assay	54
Figure 2.6 53BP1 ^{ΔRif1} cannot protect telomeres from end resection.....	55
Figure 2.7 Analysis of telomere fusions in cells expressing mutant 53BP1 alleles.....	57
Figure 2.8 Analysis of telomere fusions in cells deficient for the LINC complex.....	58
Figure 2.9 53BP1 ^{ΔMOB} is deficient in stimulating chromatin mobility	62
Figure 2.10 Interaction between 53BP1 and Sun1 is not consistently detected.....	65
Figure 2.12 Telomere fusions upon depletion of potential 53BP1 and Sun1 interaction partners.....	71
Figure 2.13 Telomere CHIP.....	72
Figure 2.14 53BP1 oligo mutants	75
Figure 2.15 Telomere fusions in MEFs expressing oligo mutants.....	77
Figure 2.16 Localization of 53BP1 oligo mutants to telomeres is affected	79
Figure 3.1 TRF1 deletion phenotype	87
Figure 3.3 PARP1 is required for the formation of SAs	93
Figure 3.4 Depletion of Lig3 reduces SAs	96
Figure 3.5 Lig1 and Lig4 do not affect the frequency of SAs.....	97
Figure 3.6 Ku does not affect SAs	100
Figure 3.7 Mitotic abnormalities after TRF1 loss	103
Figure 3.8 PICH localizes to anaphase bridges	106
Figure 3.9 PICH localizes to bridges after deletion of TRF2.....	109

Figure 3.10 Phosphorylation of 53BP1 upon TRF1 or TRF2 deletion	112
Figure 3.12 Telomere overhang gel in TRF1 ^{F/F} 53BP1 ^{-/-} cells	115
Figure 3.13 53BP1 S/TQ sites affect the frequency of SAs	117
Figure 3.14 53BP1 S/TQ sites affect SAs in two additional cell lines	118
Figure 3.15 CRISPR/Cas9 editing of 53BP1 in TRF1 ^{F/F} Rif1 ^{F/F} MEFs	121
Figure 3.16 Analysis of SAs and fragility in TRF1 ^{F/F} Rif1 ^{F/F} 53BP1 ^{-/-} MEFs	122
Figure 3.17 Analysis of SAs and fragility upon deletion of Exo1 or BLM	126
Figure 4.1 A cruciform DNA structure from a telomere fusion and pathways of Holliday Junction resolvases in mammalian cells	133
Figure 4.2 CRISPR/Cas9 editing of Gen1 in TRF1 ^{F/F} MEFs	137
Figure 4.3 Growth curve	138
Figure 4.4 Gen1 null cells display increased chromatin bridges after deletion of TRF1	139
Figure 4.5 CRISPR/Cas9 editing of Gen1 in TRF1 ^{F/F} cell line 9.3	141
Figure 4.6 Aphidicolin treatment does not induce chromatin bridges in TRF1 ^{F/F} Gen1 ^{-/-} MEFs ...	144
Figure 4.7 SAs and telomere fragility in TRF1 ^{F/F} 20.6Gen1 ^{-/-} clones	146
Figure 4.8 Faith of a sister fusion in absence of Gen1	148
Figure 4.9 Verification of isochromosome analysis	149
Figure 4.10 Isochromosomes are increased in Gen1 null cells	153
Figure 4.11 Anaphase bridges in TRF1 ^{F/F} Gen1 ^{-/-} cells persist longer	155
Figure 4.12 TRF1 ^{F/F} Gen1 ^{-/-} cells with overexpressed Gen1	158
Figure 4.13 CRISPR/Cas9 editing of Gen1 in TRF1 ^{F/F} p53 ^{-/-} MEFs	162
Figure 4.14 Knockdown of PARP1 reduces chromatin bridge formation in TRF1 ^{F/F} Gen1 ^{-/-} cells	165
Figure 4.15 Quantification of Mus81 knockdown by qPCR	169
Figure 4.16 Growth curve of Gen1 clones after depletion of Mus81	170
Figure 4.17 Chromatin bridges are increased after depletion of Mus81	171
Figure 4.18 Telomere SAs, fragility and isochromosomes after Mus81 depletion	174
Figure 5.1 Models for the interaction between 53BP1 and Sun1	184
Figure 5.2 Proposed function of 53BP1-dependent mobility of DSBs	187
Figure 5.3 Model for the fork stabilization in absence of TRF1	198
Figure 5.4 Model for the formation of sister telomere fusions upon TRF1 loss	201
Figure 5.5 Model for the role of Gen1 at telomeres fused by a-NHEJ	205

List of Abbreviations

53BP1	p53 binding protein 1	Lig(x)	Ligase (1,3 or 4)
ATM	Ataxia telangiectasia mutated	MDC1	Mediator of DNA damage checkpoint 1
ATR	ATM- and Rad3- related		
BLM	Bloom's syndrome helicase	MEF	Mouse embryonic fibroblast
BRCA1	Breast cancer (early onset) 1		
BRCT	BRCA1 C-terminal	MRN	Mre11-Rad50-Nbs1
CDK	Cyclin-dependent kinase	NCO	Non crossover
CFS	Common fragile site	NHEJ	Non-homologous end joining
ChIP	Chromatin immunoprecipitation	c-NHEJ	Classical NHEJ
co-IP	Co-immunoprecipitation	a-NHEJ	Alternative NHEJ
CO	Crossover	ONM	Outer nuclear membrane
CSR	Class switch recombination	PARP1	Poly [ADP-ribose] polymerase 1
DDR	DNA damage response		
dHJ	Double Holliday Junction	PARPi	PARP inhibitor
DSB	Double strand break	Rif1	Rap1 interacting factor 1
Exo1	Exonuclease 1	RPA	Replication protein A
FISH	Fluorescence in situ hybridization	SA	Sister Association
G4	G-quadruplexes	S/TQ	Serine or Threonine and Glutamine
HR	Homologous recombination	SSB	single stranded break
IF	Immunofluorescence	UDR	Ubiquitin dependent recruitment
INM	Inner nuclear membrane		
IP	Immunoprecipitation	UFB	Ultrafine Bridge
IR	Ionizing radiation	WRN	Werner syndrome helicase
Ku	Ku70/80		
LINC	Linker of Nucleoskeleton and Cytoskeleton		

Chapter 1: Introduction

1.1 Mammalian DNA damage response pathways

1.1.1 DNA damage

The integrity of the DNA in each cell in the human body is under constant attack from thousands of DNA insults every day (Hoeijmakers, 2009). These lesions can block transcription and replication and can lead to mutations and large chromosomal aberrations if not accurately repaired (Jackson and Bartek, 2009). To counteract the consequences of DNA damage, cells have developed complex repair mechanisms to safeguard the integrity of the genome. Defects in these pathways leave cells highly sensitive to DNA damaging agents and are linked to different types of human disease. Furthermore, genome instability resulting from defective DNA repair pathways forms the basis for nearly all types of cancer. A good understanding of the different DNA damage response pathways and their interplay is therefore essential.

Cells are subject to different types of DNA damage including nicks, gaps, single stranded breaks (SSBs), double-stranded breaks (DSBs) and base modifications. Distinct DNA repair mechanisms have evolved to sense and repair each of these lesions. Small base modifications such as deamination or depurination can be repaired through mismatch repair (MMR) or base excision repair (BER). More bulky DNA adducts are repaired via nucleotide-excision repair (NER) whereas SSBs can be repaired via distinct single-strand break repair pathways (SSBR). Ionizing radiation (IR), replication fork collapse or reactive oxygen species (ROS) can form DNA DSBs which can be repaired via

nonhomologous end-joining (NHEJ) or homologous recombination (HR) depending on the stage of the cell cycle.

Key to orchestrating these different DNA repair pathways are members of the phosphatidylinositol 3-kinase-like family of protein kinase (PIKKs) family (ATM kinase, ATR kinase and to a lesser extent DNA-PK), which coordinate rapid and potent signal transduction pathways to initiate repair (Harper and Elledge, 2007). ATM, ATR and DNA-PK are threonine/serine kinases that recognize a common motif, which is their target threonine or serine followed by a glutamine residue (S/TQ site). While this consensus target motif might indicate redundancy, each kinase has a specific function and a different but overlapping set of substrates (Matsuoka et al., 2007). Moreover, ATM and DNA-PK respond to DSBs whereas ATR kinase is activated upon single-stranded DNA formed during replication stress and upon resection of DSBs (Fig. 1.1). Phosphorylation of S/TQ sites in specific target proteins results in the recruitment of a variety of effector proteins that together orchestrate repair of the DNA lesion or activate apoptotic and senescent pathways if the damage is too severe. Activation of ATM and ATR also triggers cell-cycle checkpoints through activation of Chk1 and Chk2 (Sanchez et al., 1997; Matsuoka et al., 1998; Chaturvedi et al., 1999; Liu et al., 2000; Matsuoka et al., 2000). These kinases phosphorylate the Cdc25 family of phosphatases thereby preventing their activity. This leads to cell-cycle arrest in G1 or G2/M as Cdc25 proteins are responsible for activation of cyclin-dependent kinases (CDKs) which control cell cycle progression

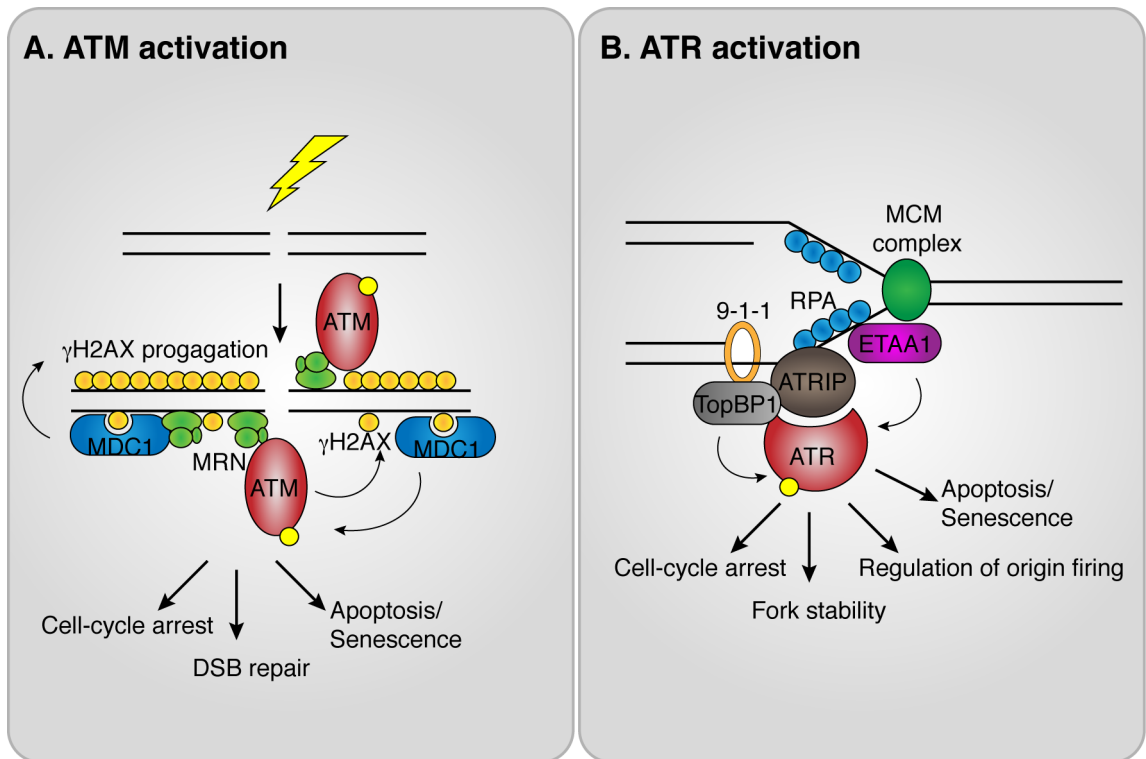


Figure 1.1 ATM and ATR activation

(A) ATM is activated by the MRN complex, which rapidly binds to DSBs. Upon activation, ATM phosphorylates histone H2AX recruiting MDC1 which propagates the γ H2AX signal. MDC1 itself further stimulates ATM activation, resulting in signal amplification. (B) A crucial step for ATR activation is RPA binding to ssDNA resulting in the recruitment of ATR via its binding partner ATRIP. An additional step is needed to activate ATR. The most studied factor is TopBP1, which is recruited to the ssDNA/dsDNA junction via the 9-1-1 complex. A second pathway occurs via ETAA1, which directly binds RPA away from the ssDNA/dsDNA junction and has a similar ATR activating domain as TopBP1.

(Sanchez et al., 1997; Costanzo et al., 2000; Mailand et al., 2000). The delay in cell cycle progression ensures damaged DNA is not transmitted to daughter cells by allowing time for accurate repair. ATM and ATR also activate the p53 tumor suppressor gene to further halt cell-cycle progression and activate proapoptotic or senescence pathways when the DNA damage is extensive (Tibbetts et al., 1999; Shieh et al., 2000).

1.1.2 ATM kinase and DSB repair

DSBs are generated when both strands of the double helix are broken in close proximity. DSBs can arise inadvertently when replication forks collapse or by DNA damage inducing agents such as ionizing radiation or radiomimetic drugs (Jackson and Bartek, 2009). But DSBs are also formed during normal physiological processes such as programmed immune receptor rearrangements in lymphocytes during V(D)J recombination and class switch recombination (CSR) events (Dudley et al., 2005).

An initiating step for DSB repair is sensing of the lesion by the Mre11-Rad50-Nbs1 (MRN) complex. MRN is a multifaceted complex that is required for several DNA repair pathways and its widespread functions are not yet fully understood on a molecular level (Stracker and Petrini, 2011). Among its many functions, MRN can act as DSB sensor, tether broken ends together and provide nucleolytic processing of the DNA ends (Lee et al., 1998; Nelms et al., 1998; de Jager et al., 2001; Mirzoeva and Petrini, 2001; Hopfner et al., 2002; Mimitou and

Symington, 2008; Zhu et al., 2008). Importantly, MRN is essential for the recruitment and activation of ATM at DSBs by promoting monomerization and by acting as cofactor for the catalytic activity of ATM (Carney et al., 1998; Stewart et al., 1999; Lim et al., 2000; Uziel et al., 2003; Lee and Paull, 2004; Lee and Paull, 2005; Paull, 2015).

The Mre11 nuclease forms the core of the MRN complex and harbors both exonuclease and endonuclease activity to initiate resection, the latter of which is stimulated by interaction with CtIP (Sartori et al., 2007; Mimitou and Symington, 2008; Zhu et al., 2008; Wang et al., 2013). The directionality of the exonuclease activity however is towards the break in the 3'-5' direction, opposite of polarity required for resection. The MRN complex therefore only performs the resection initiation step but its activity is thought to be important for the clearance of adducts and blockages from DNA ends, such as topoisomerases or Ku (Mimitou and Symington, 2008; Zhu et al., 2008; Hartsuiker et al., 2009; Garcia et al., 2011; Stracker and Petrini, 2011; Deshpande et al., 2016).

Once MRN has activated ATM kinase, the DNA damage response pathway is activated at DSBs (Fig. 1.1). A key initial function of ATM is phosphorylation of histone variant H2AX on serine 139, which rapidly spreads over a large chromatin domain surrounding the DSB site (Rogakou et al., 1998; Burma et al., 2001). Key to propagating the γ H2AX signal is Mediator of DNA damage Checkpoint 1 (MDC1), which directly binds γ H2AX as well as ATM and the MRN complex thereby further stimulating their activation (Stewart et al., 2003;

Lee et al., 2005; Lou et al., 2006; Chapman and Jackson, 2008). Besides propagating the γ H2AX signal, MDC1 recruits the E3 ubiquitin ligase RING finger 8 (RNF8) and other proteins that eventually result in the recruitment of 53BP1 and other DNA repair proteins, which will be discussed in more detail in Chapter 1.2.

1.1.3 Classical and Alternative NHEJ

Repair of DSBs occurs mainly via two repair pathways in eukaryotic cells: classical NHEJ (c-NHEJ) and HR (Fig. 1.2 and 1.3). The prevailing model in mammalian cells is that most clean, blunt breaks are rapidly repaired by NHEJ in all stages of the cell cycle, in a process that depends on binding of DNA ends by Ku70/80 (Ku) and ligation by DNA ligase VI (Lig4). In S/G2, repair switches to HR, which uses the newly replicated sister chromatid as template for accurate repair. The decisive factor between these two pathways is resection of the 5' ends since HR requires annealing to a homologous template strand.

C-NHEJ is a rapid, reliable, error-free repair mechanism when executed properly and is initiated by loading of Ku onto broken ends (Fig. 1.2)(Lieber, 2010). Ku is a highly abundant ring-shaped heterodimer (Ku70 and Ku80) with high affinity for duplex DNA and the complex rapidly slides onto both ends of the break. There, it serves as docking site for core repair factors such as DNA-PKcs, XRCC4, DNA Lig4, Artemis, XRCC4-like factor (XLF) and PAXX, which help stabilize the repair complex and ligate the broken ends together (Lieber, 2010;

Waters et al., 2014; Ochi et al., 2015; Xing et al., 2015). Not all DNA ends are directly compatible for end-joining by c-NHEJ due to chemical modifications at the break site originating from the source of damage. Therefore several accessory proteins, such as the Artemis nuclease, are recruited to remove damaged bases, hairpins or other obstructions. This allows c-NHEJ to function on a wide range of DNA end substrates (Chang et al., 2016).

C-NHEJ has long been considered an error-prone repair pathway because it does not rely on a homologous sister template to repair the lesion and small deletions at the junction can occur. However, more recently a different mammalian NHEJ pathway has been attributed to mutagenic repair that does not rely on Ku or Lig4. This pathway employs Poly[ADP-ribose] polymerase 1 (PARP1) and DNA Ligase III (Lig3), relies on extensive microhomology at the break site and is known as alternative NHEJ (a-NHEJ) (Fig. 1.3)(Boboila et al., 2010; Simsek et al., 2011; Frit et al., 2014; Pannunzio et al., 2014). This pathway operates when core components of the c-NHEJ machinery are missing, such as Ku or Lig4 (Kabotyanski et al., 1998; Verkaik et al., 2002; Wang et al., 2003; Weinstock et al., 2007). Mechanistically, a DSB is recognized by PARP1 in the a-NHEJ pathway, a step normally inhibited by Ku (Wang et al., 2006). End-resection by MRN, CtIP and Exonuclease1 (Exo1), DNA2 and Bloom's syndrome helicase (BLM) are then thought to expose sufficient microhomology to allow a-NHEJ to take place, although the precise mechanism remains unclear. The Werner syndrome protein (WRN) has also been implicated in resection together

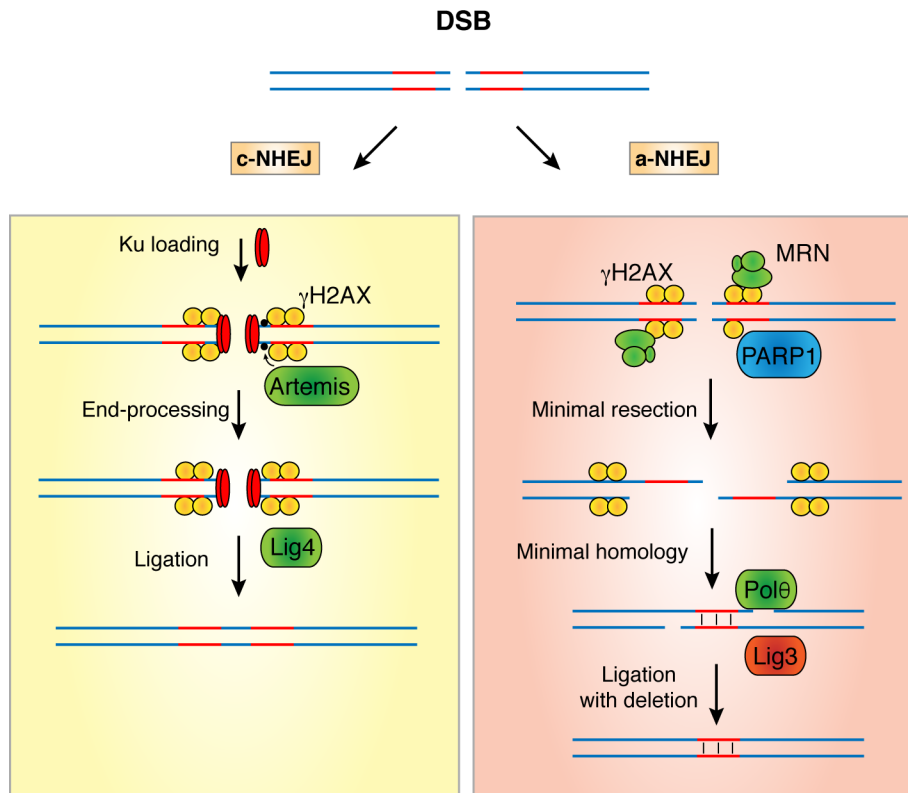


Figure 1.2 Pathways for c-NHEJ and a-NHEJ

c-NHEJ is initiated by Ku loading onto the DNA ends, where it serves as docking sites for additional proteins such as DNK-PKcs, XRCC4 and Artemis that help with end-processing steps if required. The final ligation step is done by DNA ligase 4.

a-NHEJ occurs in absence of cNHEJ components and requires microhomology surrounding the DSB (in red). The break is recognized by PARP1, followed by limited end-resection by the MRN complex and CtIP. Upon annealing of the exposed microhomology domains, Polθ fills in any gaps while Lig3 performs the final ligation step.

with DNA2 (Sturzenegger et al., 2014). However, it is thought that WRN limits the a-NHEJ pathway by suppressing MRN and CtIP although the precise mechanisms are not well understood (Shamanna et al., 2016). Importantly, a-NHEJ has been linked to pathological repair of DSBs resulting in large deletions, insertions and whole chromosomal translocations (Yan et al., 2007; Simsek and Jasin, 2010; Simsek et al., 2011).

There is significant controversy whether a-NHEJ represents a distinct back-up repair pathway or merely pathological processing that occurs when c-NHEJ fails (Deriano and Roth, 2013; Frit et al., 2014; Pannunzio et al., 2014). The reason behind this controversy is that a-NHEJ is highly versatile regarding the proteins involved in the process. For example, DNA ligase 1 (Lig1) can replace Lig3 when the latter is absent (Paul et al., 2013). Furthermore, no physiological relevant function has been uncovered for a-NHEJ, except as backup where others fail. However, given the importance of a-NHEJ in pathological situations, a better understanding of both NHEJ pathways remains important, whether a-NHEJ represents a physiological pathway or not.

1.1.4 Homologous Recombination

Errors during DNA replication give rise to DSBs in S/G2 of the cell cycle that are preferentially repaired using the homologous template to ensure accurate repair without loss of genetic information (Fig. 1.3). Central to HR is end-resection, which is initiated by the MRN complex together with CtIP followed by more

extensive resection by Exo1, and DNA2 together with BLM and WRN (Sartori et al., 2007; Mimitou and Symington, 2008; Nimonkar et al., 2008; Zhu et al., 2008; Sturzenegger et al., 2014). Replication Protein A (RPA) rapidly binds the resulting long 3' single-stranded overhang and has a stabilizing and protective function. For HR to proceed, RPA has to be displaced by Rad51 in a process stimulated by BRCA2 (Baumann et al., 1996; Wong et al., 1997; Davies et al., 2001; Jensen et al., 2010). The Rad51 coated filament catalyzes homology search and strand invasion into a homologous region forming a D-loop, where it forms a primer for new DNA synthesis from using the homologous template to initiate repair.

Completion of HR can proceed via two pathways ending in crossover (CO) or non-crossover (NCO). First, synthesis dependent-strand annealing (SSDA) allows the extended ssDNA to dissociate from the D-loop and anneal back to the other ssDNA end resulting in NCO (Nassif et al., 1994). In a separate pathway called double-strand break repair (DSBR), the other end of the DSB end is captured in the D-loop forming an intermediate structure with a double Holliday junction (dHJ) (Szostak et al., 1983). Processing of this dHJ can involve dissolution by the BLM helicase resulting in harmless NCO. However, the dHJ can also be cleaved by resolvases such as SLX1/SLX4 and Mus81 or Gen1 resulting in NCO or CO. This potential for CO events is toxic for cells as it can lead to loss of heterozygosity (Moynahan and Jasin, 2010). Presumably,

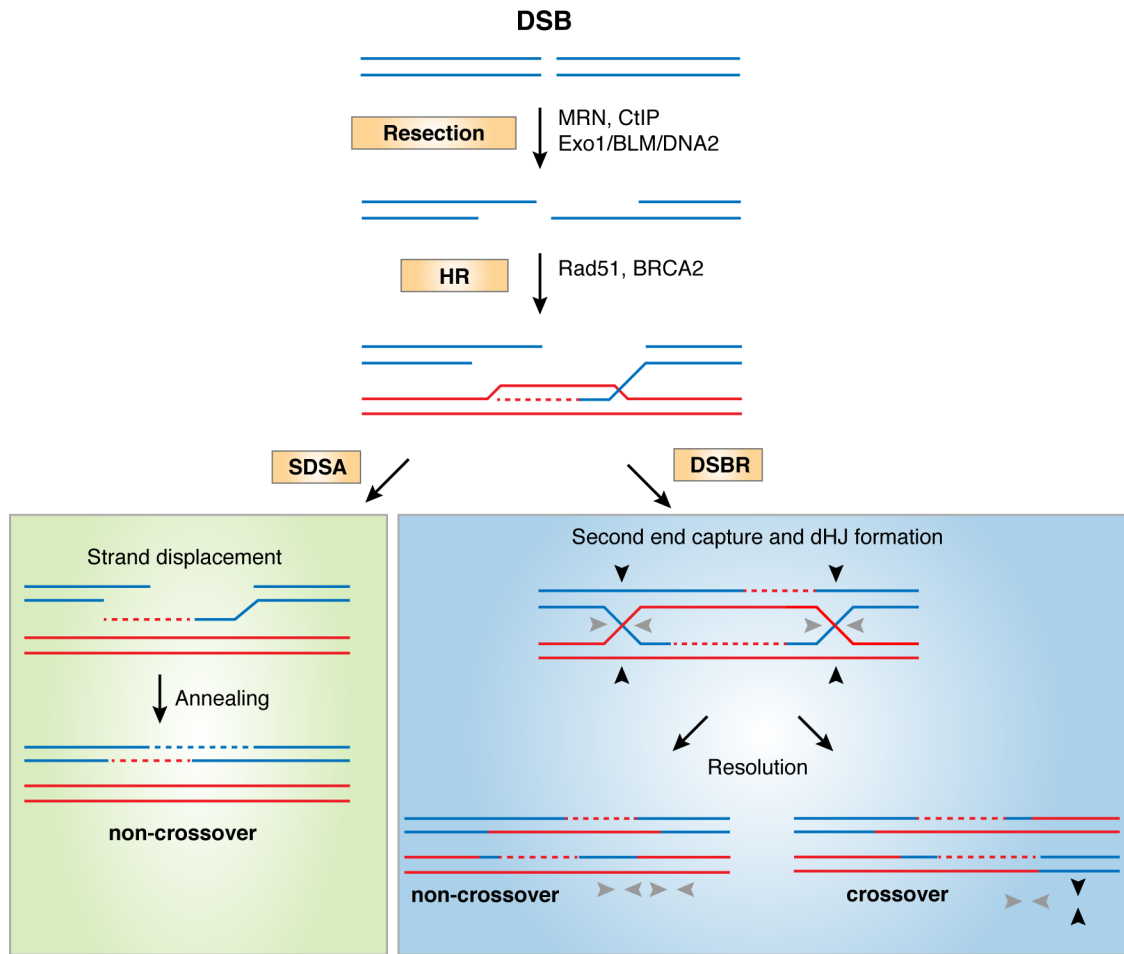


Figure 1.3 Homologous recombination

In S/G₂, DSB are preferentially repaired via HR since a homologous template is available. Central to HR is extensive resection by the MRN complex together with CtIP, Exo1, BLM and DNA2. The ssDNA is coated by RPA, which is replaced by Rad51 in a process dependent on BRCA2. Rad51 catalyzes strand invasion into the homologous template forming a D-loop structure, and DNA synthesis from the homologous template occurs. From here, two separate pathways can occur. In SDSA, the newly synthesized strand dissociates from the D-loop and anneals back to the other ssDNA yielding a NCO. In DSBR, the second end of the DSB is captured in the D-loop creating an intermediate structure with a dHJ. Dissolution can take place by the BLM helicase (not shown). Alternatively, resolution can occur if resolvases cleave the dHJ resulting in either NCO or CO depending on orientation of the cleavage.

SSDA or dissolution by BLM is more prevalent as CO events are suppressed in mitotic cells (Stark and Jasin, 2003).

1.1.5 ATR kinase activation and replication stress

Whereas ATM is dispensable for cell viability, deletion of ATR kinase is lethal, signifying its broad contribution to the DNA damage response (Brown and Baltimore, 2000; Cortez et al., 2001; Brown and Baltimore, 2003). ATR is activated in every S-phase to respond to stalled and collapsed replication forks and regulates origin firing as well as checkpoint activation to prevent premature mitosis in presence of damage (Costanzo et al., 2003; Pichierri and Rosselli, 2004; Woodward et al., 2006). The binding of RPA to ssDNA is a crucial step in the activation process of ATR (Fig. 1.1). RPA is a highly conserved heterotrimeric complex consisting of 70, 32 and 14 kDa subunits that bind ssDNA with high affinity using four OB (oligonucleotide/oligosaccharide binding) folds. The role of RPA is to stabilize the unwound ssDNA, prevent and remove secondary structures and interact with DNA processing proteins to form an appropriate response to ssDNA (Wold and Kelly, 1988; Wold, 1997; Chen et al., 2013). ATR recognizes ssDNA bound RPA together with its interaction partner ATR-interacting protein (ATRIP) (Cortez et al., 2001; Zou and Elledge, 2003). But this interaction alone is not sufficient to activate ATR, as it requires an ATR-activating domain (AAD) containing protein to accomplish this (MacDougall et al., 2007). The most studied ATR activating protein is TopBP1, which is recruited to the

junction of ssDNA and dsDNA via the Rad9-Rad1-Hus1 (9-1-1) complex and RHINO (Bermudez et al., 2003; Kumagai et al., 2006; Delacroix et al., 2007; Cotta-Ramusino et al., 2011). Recently, a second pathway for ATR activation was described in mammalian cells with the discovery of a second AAD-containing protein ETAA1 (Bass et al., 2016; Haahr et al., 2016). In contrast to TopBP1, ETAA1 binds RPA directly and activates ATR in response to replicative stress but not in response to DSB-inducing agents. Furthermore, activation of ATR by ETAA1 causes phosphorylation of distinct ATR substrates as in response to TopBP1, indicative of parallel pathways. The ability of ETAA1 to activate ATR away from the ssDNA/dsDNA junction might signify an ability to propagate the activation of ATR over long stretches of ssDNA although concrete evidence for this idea is lacking.

1.1.6 ATR regulates origin firing

Once activated at a DNA lesion or a stalled replication fork, ATR phosphorylates a multitude of substrates (Matsuoka et al., 2007). Most notably, ATR activates Chk1 via phosphorylation of Ser317 and Ser345, often used as a marker of ATR activation (Walworth and Bernards, 1996; Liu et al., 2000). Chk1 phosphorylates CDC25 to prevent entry into mitosis. Chk1 activation also slows replication by limiting global dormant origin firing (Tercero and Diffley, 2001). However, near the stalled fork the ATR pathway has an opposite effect and promotes dormant

origin firing via activation of PLK1 and CDC45 (Woodward et al., 2006; Ge et al., 2007; Ibarra et al., 2008).

1.1.7 Fork stabilization by ATR

An important function of ATR lies in its ability to stabilize the replication fork, preventing its collapse and the formation of a DSB (Lopes et al., 2001; Tercero and Diffley, 2001). The precise mechanism through which ATR stabilizes the replication fork is still poorly understood. It may involve retaining components of the replisome at the replication fork since DNA polymerases alpha (Pol α) and epsilon (Pol ϵ) are lost in absence of ATR signaling (Cobb et al., 2003; Lucca et al., 2004).

After stabilizing the fork, DNA repair and restart of the replication fork takes place. Depending on the type of damage, ATR phosphorylates and recruits different DNA repair enzymes that regulate phosphorylation of H2AX and recruitment 53BP1, the RecQ helicases BLM and WRN, BRCA1 and many others. Together these enzymes repair the DNA lesion and reinitiate DNA replication at the fork.

1.1.8 Crosstalk between the ATM and ATR pathway

Although ATM and ATR respond to different DNA structures and have many distinct substrates, there is some redundancy between the pathways such as checkpoint activation and H2AX phosphorylation (Ward and Chen, 2001;

Matsuoka et al., 2007). Furthermore, there is significant crosstalk between the pathways as ATM can be activated at DSBs generated at collapsed replication forks and ATR is activated by ssDNA after end-resection at DSBs. What appears to be a defining factor in the cellular response to damage is the kinetics of activation of either pathway.

ATM is rapidly activated at DSBs but resection in S/G2 causes a switch from ATM to ATR activation as a result of ssDNA formation. Interestingly, several studies showed that ATR activation in response to IR induced DSBs requires ATM and the MRN complex (Cuadrado et al., 2006; Jazayeri et al., 2006; Myers and Cortez, 2006). Absence of either ATM or MRN reduces the levels of RPA foci formation indicative of limited end-resection. A key step by which ATM activates ATR is by stimulating initial CtIP dependent resection to form ssDNA. Additionally, ATM recruits and phosphorylates TopBP1, the ATR activating protein (Yoo et al., 2007). Once activated, ATR phosphorylates CtIP at T818, a modification that stabilizes chromatin bound CtIP and promotes robust resection (Peterson et al., 2013). Secondly, ATR mediated activation of Chk1 is essential to activate the G2/M checkpoint and prevents cells from entering mitosis with damaged DNA (Brown and Baltimore, 2003). Chk2 also enforces the G2/M checkpoint, but regulates a more immediate effect whereas long-term arrest is maintained more by Chk1 (Brown and Baltimore, 2003; Rainey et al., 2008).

Conversely, the role of the ATM kinase at stalled replication forks is less understood. Mostly, ATM is activated when ATR signaling is compromised and

replication forks collapse to form DSBs (Chanoux et al., 2009). The role of ATM might be similar to its general DSB repair functions to promote repair of the collapsed replication fork (Cimprich and Cortez, 2008). Interestingly, replication stress results in the formation of 53BP1 nuclear bodies in the next G1, in a process that depends on the activation of ATM kinase (Harrigan et al., 2011; Lukas et al., 2011). The function of these structures remains elusive but they are thought to shield broken or unreplicated DNA from the previous S-phase allowing their repair before the next S-phase. They are present at low frequency in unperturbed cells and often form at Common Fragile Sites (CFS), regions of the genome that are difficult to replicate, further indicating that these 53BP1 nuclear bodies are the result of aberrant replication.

1.2 The role of 53BP1 in the DNA damage response pathway

1.2.1 53BP1 is a key regulator in the DNA damage response pathway

53BP1 was initially discovered as a p53 interacting protein required for activation of the tumor suppressor protein (Iwabuchi et al., 1994; Iwabuchi et al., 1998). However, 53BP1 is much better known for its key role in regulating c-NHEJ and HR at DSBs (Panier and Boulton, 2014; Zimmermann and de Lange, 2014). The role of 53BP1 in regulating DSB repair emerged from work on immunoglobulin gene rearrangements, damaged telomeres and DSB repair defects in BRCA1-deficient cells (Ward et al., 2003; Ward et al., 2004; Difilippantonio et al., 2008; Dimitrova et al., 2008; Bunting et al., 2010; Bothmer et al., 2011; Lottersberger et

al., 2013). Collectively, the data revealed 53BP1 as a multifaceted protein that controls the choice between c-NHEJ and HR by influencing key regulatory events at and near DNA ends. In particular, 53BP1 promotes c-NHEJ and contributes to lethal mis-repair of DSBs in BRCA1-deficient cells by inhibiting 5' end resection (Fig. 1.4). The results also suggested that 53BP1 promotes c-NHEJ by increasing the mobility of damaged telomeric chromatin and by mediating synapsis of DNA ends in CSR (Difilippantonio et al., 2008; Dimitrova et al., 2008).

The role of 53BP1 in c-NHEJ is evident in BRCA1-deficient cells. Upon inhibition of PARP1, transient nicks in DNA primarily resulting from base-excision repair (BER) are not repaired resulting in DSBs in S phase. In BRCA1-deficient cells, HR does not repair these breaks because BRCA1 promotes the 5' resection needed for HR. Instead, 53BP1-dependent c-NHEJ leads to aberrant chromosome structures such as radials (Moynahan et al., 1999; Snouwaert et al., 1999; Cao et al., 2009). Evidence from several systems revealed that the mechanism by which 53BP1 acts is through inhibition of DNA resection by CtIP/MRN (Bouwman et al., 2010; Bunting et al., 2010). Absence of 53BP1 can rescue the embryonic lethality of BRCA1-deficiency and represses the formation of radial chromosomes in PARPi-treated cell lacking BRCA1 (Bothmer et al., 2011).

1.2.2 Structure of 53BP1

53BP1 is a large 1972 amino acids protein that has no enzymatic activity of its own. Instead, 53BP1 functions as a scaffold to recruit DNA repair proteins to damaged chromatin. 53BP1 contains several functional domains as shown in Figure 1.5. The C-terminus of 53BP1 contains a Tudor domain and an ubiquitin dependent recruitment (UDR) motif responsible for binding damaged chromatin through interaction with H4K20me2 and H2AK15ub respectively (Huyen et al., 2004; Fradet-Turcotte et al., 2013). The C-terminus also contains tandem BRCT domains that are important for DNA repair in heterochromatin and for the interaction with p53, but not for the promotion of NHEJ (Noon et al., 2010; Bothmer et al., 2011; Lottersberger et al., 2013; Cuella-Martin et al., 2016). The C-terminus of 53BP1 furthermore contains an oligomerization domain that contributes to optimal recruitment of 53BP1 to chromosome internal DSBs but is dispensable for recruitment to telomeres (Bothmer et al., 2011; Lottersberger et al., 2013). Nuclear localization of 53BP1 is promoted by the NLS signal in the center of the protein. 53BP1 also contains a PRMT1-methylated, glycine-arginine rich (GAR) domain and a dynein light chain 8 (LC8) binding motif, but the function of these domains is still unknown (Adams et al., 2005; Lo et al., 2005).

Importantly, the N-terminus of 53BP1 contains 29 S/TQ sites that are phosphorylated by ATM and ATR in a DNA damage responsive fashion. While the S/TQ sites are not needed for 53BP1 recruitment to DSBs, it has been shown that phosphorylation is required for all of its known functions since they

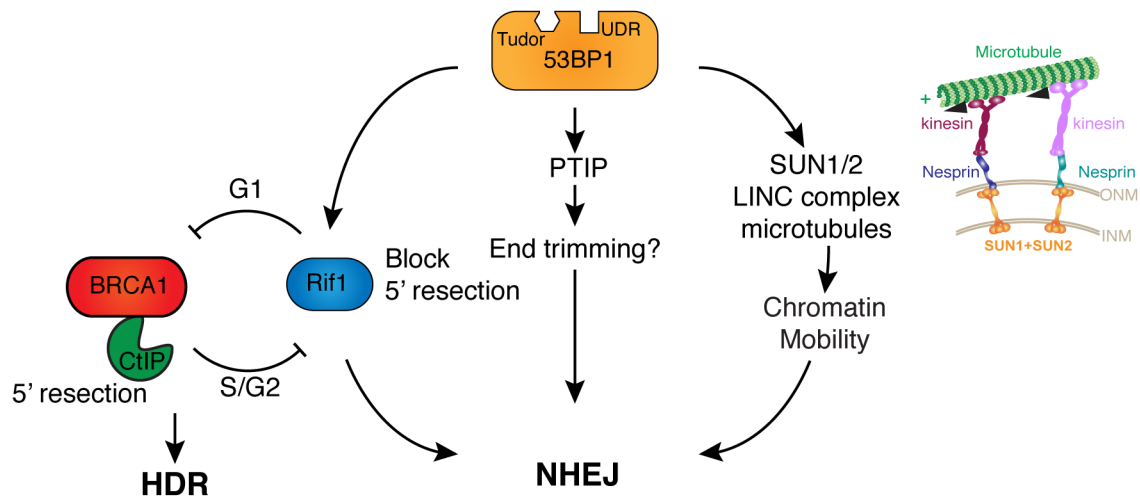


Figure 1.4 Functions of 53BP1

The main role of 53BP1 is to promote NHEJ. It does so via distinct methods. First, 53BP1 recruits Rif1 to block end resection in G1. BRCA1/CtIP counteracts Rif1 in S/G2 to allow for HDR to occur. 53BP1 also promotes NHEJ by stimulating the mobility of damaged chromatin through the LINC complex and cytoplasmic microtubules. Finally, 53BP1 recruits PTIP although the precise function of this interaction is not well understood. Possibly, PTIP is required for end-trimming of incompatible ends for NHEJ.

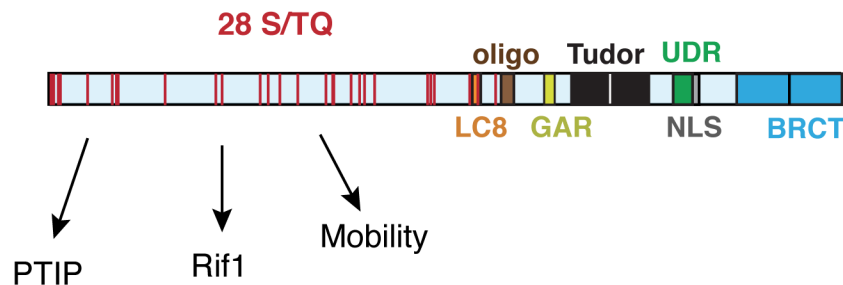


Figure 1.5 Structure of 53BP1

53BP1 binds to chromatin with its Tudor and UDR domain. It contains an NLS signal for nuclear localization and two BRCT domains in the very C-terminus. The LC8 domain binds dynein and the oligo domain is required for oligomerization. The C-terminus furthermore contains a GAR domain with an unknown function. Importantly, the N-terminus contains 28 S/TQ sites (red) that can be phosphorylated by ATM or ATR kinase and recruit proteins such as PTIP and Rif1 to DSBs.

serve as docking sites for interacting proteins such as Rif1 and PTIP (Anderson et al., 2001; Rappold et al., 2001; Bothmer et al., 2011; Lottersberger et al., 2013; Zimmermann et al., 2013). While the function of some interaction partners is known, the role of most binding proteins remains poorly defined.

1.2.3 Recruitment of 53BP1

The precise molecular mechanisms by which 53BP1 accumulates at sites of DNA damage has only recently been defined. It was long known that 53BP1 recognizes H4K20me2 with its tandem Tudor domain (Botuyan et al., 2006). However, this chromatin mark is constitutive and does not distinguish damaged sites from the rest of the genome. How 53BP1 forms foci specifically near DSBs was shown recently by the identification of the UDR motif that binds ubiquitylated H2K15. The signaling cascade that is initiated by ATM mediated phosphorylation of H2AX establishes this mark (Fig. 1.6). MDC1 is recruited to phosphorylated H2AX, which in turn recruits the E3 ubiquitin ligase RNF8/UBC13 complex (Huen et al., 2007; Mailand et al., 2007). The major substrates for RNF8 and UBC13 were long unknown. Recently it was discovered that RNF8 and UBC13 catalyze K63-linked polyubiquitylation of the linker histone H1 at DSB sites (Thorslund et al., 2015). This mark is recognized by yet another E3 ubiquitin ligase, RNF168, which is responsible for the ubiquitylation of H2A at K13/K15, the latter of which is recognized by 53BP1 (Doil et al., 2009; Stewart et al., 2009; Mattioli et al., 2012; Fradet-Turcotte et al., 2013). Thus, 53BP1 functions as a bivalent reader of

histone modifications and is recruited through a multistep signaling cascade that allows for signal amplification or modification when needed.

Another determinant for recruitment of 53BP1 to sites of damage is the oligomerization domain of 53BP1. A 53BP1 mutant lacking this domain is incapable of foci formation at IR induced DSBs and is defective in CSR in lymphocytes (Ward et al., 2006; Zgheib et al., 2009; Bothmer et al., 2011). However, this mutant localizes to dysfunctional telomeres and is capable of partially promoting c-NHEJ at these sites (Lottersberger et al., 2013). Likely, the primary function of the oligomerization domain is to form dimers of 53BP1 as it can be replaced by an ectopic dimerization or tetramerization domain without loss of foci formation (Zgheib et al., 2009; Wilson et al., 2016).

Interestingly, the pathway recruiting 53BP1 is suppressed during mitosis (Giunta et al., 2010; Orthwein et al., 2014). MDC1 is still bound to γ H2AX but RNF8 is no longer recruited due to phosphorylation of RNF8 at Thr198 by CDK1 (Orthwein et al., 2014). In support of this model, a RNF8 T198A mutant is insensitive to CDK1 activity and is able to form foci throughout mitosis whereas the phosphomimetic T198E mutant is incapable of foci formation in interphase cells or mitosis. However, although the T198A mutant restores RNF8 recruitment to DSBs in mitosis, it fails to recruit 53BP1. A second inhibitory pathway acts directly on 53BP1 to suppress its localization to DSBs. Specifically, CDK1 and PLK1 phosphorylate T1609 and S1618 in mitosis, two sites located in the UDR motif of 53BP1 (Orthwein et al., 2014). Thus, 53BP1 focus formation is inhibited

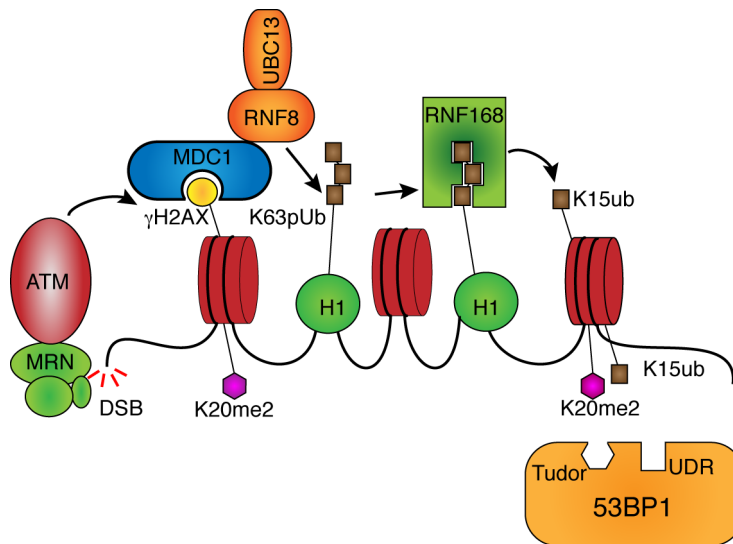


Figure 1.6 Recruitment of 53BP1 to DSBs

53BP1 is recruited in response to a signaling cascade that starts with MRN accumulation at a DSB. MRN activates ATM kinase, which phosphorylates H2AX. This γH2AX forms a docking site for MDC1, which in turn recruits the ubiquitin ligase RNF8 and UBC13. RNF8 catalyzes ubiquitylation of H1 resulting in the recruitment of RNF168. This ubiquitin ligase induces ubiquitylation of lysine15 on H2A, which is recognized by the UDR domain of 53BP1. The Tudor domain of 53BP1 furthermore binds the H4K20me2 group that is constitutively present on H4 independent of DNA damage.

in mitosis by inhibitory phosphorylation of both RNF8 and 53BP1 itself. Why does 53BP1 need to be so strictly suppressed during mitosis? Interestingly, restoring 53BP1 foci formation in mitosis by using phosphomutants resulted in genome instability. These cells were highly sensitive to low dose of IR and showed high rates of micronuclei formation. Furthermore, these cells were prone to sister telomere fusions suggesting spontaneous DSB repair at telomeres. It was speculated that telomeres are transiently uncapped during mitosis thus requiring the inactivation of DSB repair to mitigate this threat to genome integrity (Orthwein et al., 2014).

1.2.4 Regulation of end-resection in mammalian cells

One of the mechanisms by which 53BP1 promotes c-NHEJ is by blocking 5' end resection at broken ends in a cell-cycle dependent manner (Fig. 1.4) (Bothmer et al., 2010; Bunting et al., 2010). Resection is initiated in mammalian cells upon ATM activation by the MRN complex together with the CtIP (Sartori et al., 2007; Buis et al., 2008; Wang et al., 2013). In absence of CtIP, RPA foci do not form after IR and ATR is no longer recruited to DSBs indicating resection is inhibited (Sartori et al., 2007). CtIP is thought to activate the endonuclease activity of MRN to create a nick upstream of the DSB site. The 3'-5' exonuclease activity of MRN towards the DNA end then creates a substrate for more extensive resection by Exo1 or DNA2 with BLM/WRN (Gravel et al., 2008; Nimonkar et al., 2008; Nimonkar et al., 2011; Tomimatsu et al., 2012; Sturzenegger et al., 2014). This initial processing step by MRN and CtIP is especially important with chemically

blocked ends, such as those arising after IR, whereas at clean ends MRN mainly functions to recruit other factors of the resection machinery (Buis et al., 2008; Nimonkar et al., 2011).

The function of 53BP1 to block extensive resection by CtIP and Exo1 was first shown in CSR in lymphocytes (Bunting et al., 2010; Bothmer et al., 2011; Bothmer et al., 2013). Subsequent studies from several groups identified Rif1 as the effector, which is recruited to 53BP1 in an ATM/ATR phosphorylation dependent manner. Rif1 was shown as to be the main factor by which 53BP1 blocks CtIP-initiated resection at DSBs in G1 therefore promoting c-NHEJ while blocking HR (Chapman et al., 2013; Di Virgilio et al., 2013; Escribano-Diaz et al., 2013; Feng et al., 2013; Zimmermann et al., 2013). In S/G2, this inhibition of resection is counteracted by BRCA1, which displaces 53BP1, to allow resection and HR with the sister template to occur. Elegant studies revealed the mechanisms by which this cell cycle depended block to resection is achieved (Escribano-Diaz et al., 2013). In G1, when c-NHEJ is the pathway of choice, 53BP1/Rif1 inhibit binding of BRCA1 at DSBs. Upon entry into S/G2, CDK1 phosphorylates CtIP creating a CtIP/BRCA1 complex that displaces 53BP1/Rif1 from damage foci to allow resection to take place. In absence of BRCA1 or when the interaction between CtIP and BRCA1 is lost, 53BP1/Rif1 form foci in S/G2 and inhibit resection and repair via HR. Conversely, in absence of 53BP1, BRCA1 and CtIP locate to DSBs in G1 thereby promoting resection and inhibiting

c-NHEJ. As such, this regulatory circuit between 53BP1 and BRCA1 controls repair pathway choice.

The importance of pathway choice can easily be seen in BRCA1 deficient cells treated with PARP1 inhibitors (PARPi). Upon treatment, nicks in the DNA are not repaired causing DSBs in S-phase. In BRCA1 deficient cells, these DSBs are repaired by c-NHEJ resulting in aberrant chromosome structures such as radials (Moynahan et al., 1999; Snouwaert et al., 1999; Cao et al., 2009). Deletion of 53BP1 rescues the lethality of PARPi and restores HR, suggesting that the main function of BRCA1 is displacement of 53BP1 in S/G2 (Bunting et al., 2010; Chapman et al., 2013; Di Virgilio et al., 2013; Escibano-Diaz et al., 2013; Feng et al., 2013; Zimmermann et al., 2013).

How Rif1 blocks resection or competes with BRCA1 is still unclear. Genetic screens aimed to find factors that alleviate the synthetic lethality of PARPi and BRCA1 recently discovered MAD2L2 (also called REV7) as a protein that functions downstream of Rif1 to block resection (Boersma et al., 2015; Xu et al., 2015). MAD2L2 is a component of the translesion polymerase Zeta (Pol ζ) but its role in blocking end resection was found to be independent of this function. MAD2L2 localizes to sites of DNA damage in an ATM/53BP1/Rif1-dependent manner but a direct interaction could not be found. The N-terminal HEAT repeats of Rif1 were shown to be required for localization of MAD2L2 to DSBs. This is consistent with the fact that this domain is necessary for the interaction of Rif1

with 53BP1, confirming that MAD2L2 functions downstream of 53BP1/Rif1 (Escribano-Diaz et al., 2013; Boersma et al., 2015).

Another factor implicated downstream of 53BP1 in resection control is PTIP (Fig. 1.6). The N-terminal S25 of 53BP1 is phosphorylated in an ATM dependent manner and required for the interaction with PTIP (Munoz et al., 2007). However, the importance of the interaction with 53BP1 is poorly understood and PTIP does not require 53BP1 to localize to sites of damage (Gong et al., 2009; Wu et al., 2009). Furthermore, PTIP has been suggested to play a role in HR since loss of PTIP results in cell cycle arrest in S-phase due to unrepaired DSBs (Wang et al., 2010). The function of PTIP is even more complex with regards to c-NHEJ. While loss of PTIP had no effect on CSR in B cells, radial formation in PARPi-treated BRCA^{-/-} cells was diminished in absence of PTIP (Callen et al., 2013). Perhaps this phenotype reflects an S-phase specific role for the interaction of PTIP with 53BP1 as PARPi results in nicks during DNA replication whereas CSR occurs in G1.

1.2.5 53BP1 mediated chromatin mobility

Although loss of Rif1 suppresses NHEJ at dysfunctional telomeres and in CSR, the effect is not as severe as loss of 53BP1, indicating that other factors downstream of 53BP1 are required. A second function for 53BP1 in regulating c-NHEJ is promotion of chromatin mobility upon DNA damage (Fig. 1.4) (Dimitrova et al., 2008). Live-cell imaging has shown that telomeres become more mobile

and occupy larger territories when TRF2 is removed, which renders telomeres dysfunctional and activates ATM kinase. This increase in mobility is dependent on the N-terminal S/TQ sites of 53BP1, as a phosphorylation mutant (53BP1^{Δ28}) was unable to promote mobility. However, neither Rif1 nor MAD2L2 is required for this effect (Zimmermann et al., 2013; Boersma et al., 2015). The effect of 53BP1 on mobility is not limited to dysfunctional telomeres as IR-induced DSBs show an ATM dependent increase in mobility in G1 as well (Krawczyk et al., 2012; Neumaier et al., 2012; Becker et al., 2014). However, other studies have shown that I-SceI induced DSBs are immobile unless Ku is removed (Soutoglou et al., 2007).

Preliminary data from the de Lange lab had pointed to the possibility that 53BP1 acts through the LINC (Linker of Nucleoskeleton and Cytoskeleton) complex and uses kinesin-mediated movement on microtubules to increase the mobility of damaged telomeres. The LINC complex is composed of Sun proteins (including Sun1 and Sun2 in mammals) that span the inner nuclear membrane (INM) and associate with KASH (Klarsicht, Anc-1, Syne1 homology) domain containing proteins situated in the outer nuclear membrane (ONM) (Mejat and Misteli, 2010). Mammalian KASH proteins include the nesprins and the KMS proteins, which can link to microtubules with kinesins and dynein. Experiments suggest the involvement of Sun1, Sun2, Nesprin-4, and the kinesin components KIF3A, KIF5B, and Klc1. Using shRNAs against these proteins, telomere fusions are diminished by 30-50%. Importantly, the mobility of damaged chromatin is

diminished in a Sun1/2 deficient background to the same extent as in the absence of 53BP1. How 53BP1 connects to the LINC complex and which S/TQ sites are required remains unknown.

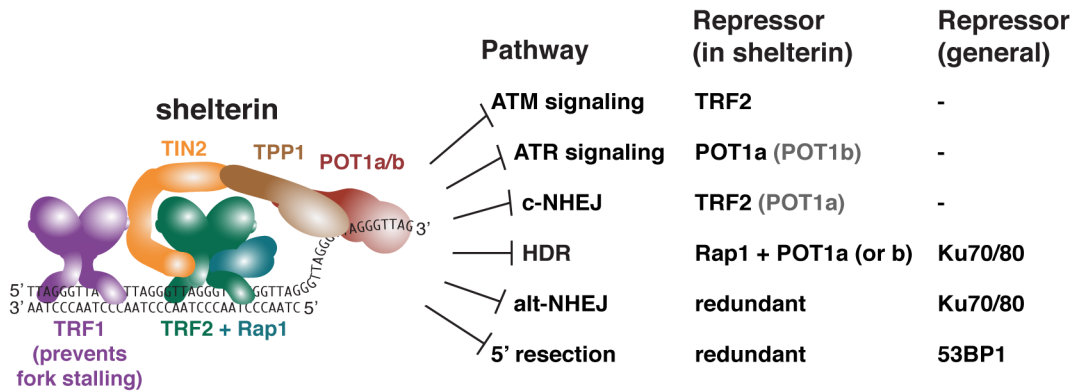
1.3 The structure and function of telomeres

1.3.1 Telomeres protect the end of linear chromosomes

Telomeres are nucleoprotein structures containing of short tandem repetitive sequences that cap the natural ends of linear eukaryotic chromosomes. In mammalian cells, telomeres consist of 5'-TTAGGG-3' repeats that can be 10-15 kb (human) to 20-50 kb (mouse) in length, ending with a 3' overhang (de Lange et al., 1990; Lejnine et al., 1995). Electron microscopy has shown that telomeres are organized in large lariat-like t-loop structures that are formed by strand invasion by the 3' overhang (Griffith et al., 1999; Nikitina and Woodcock, 2004). A telomere specific protein complex, shelterin, together with telomerase protects the telomere from two threats that arise at chromosome ends: the end-replication and end-protection problem (Fig. 1.7).

The end-replication problem arises due to the inability of the DNA replication machinery to fully replicate the 3' ends of linear DNA. Replicative polymerases function in the 5' to 3' direction and require a free 3' hydroxyl group to initiate synthesis of nascent DNA. At the leading-strand the DNA polymerase move in the same direction as the replication fork allowing the replication until the end. At the lagging-strand, the DNA is synthesized in opposite direction of the

A.



B.

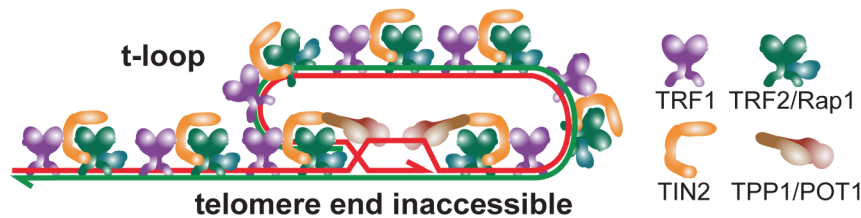


Figure 1.7 Shelterin protects chromosome ends

(A) The six protein shelterin complex binds telomeric DNA via TRF1 and TRF2. The function of each shelterin in blocking DNA damage pathways is shown on the right. (B) Shelterin and particularly TRF2 keep the telomeric DNA in a T-loop configuration. This physically hides the DNA end from recognition by the MRN complex and protects against ATM activation. Loss of TRF2 results in T-loop unwinding and activation of ATM kinase and NHEJ at the chromosome end. Adapted from Doksani and de Lange 2014 (Doksani and de Lange, 2014).

replication fork resulting in short stretches of nascent DNA, Okazaki fragments, which are initiated at RNA primers that provide the free 3' hydroxyl group. The RNA primers are subsequently removed and the Okazaki fragments ligated together. Yet, the removal of the very last RNA primer produces a gap at the end of the lagging strand, incompletely replicating the 3' end. This causes telomeres to gradually shorten during every cell division, eventually resulting in loss of genetic information thus limiting the replicative potential of the cell (Hayflick, 1965; Watson, 1972; Olovnikov, 1973). Additionally, nucleolytic processing of the 3' overhang adds to the end-replication problem. Leading end DNA synthesis results in blunt ends that require processing by Apollo and CST to produce the 3' overhang (Wu et al., 2010; Wu et al., 2012).

The end-protection problem refers to the possibility of the chromosome end to be recognized as a DSB that could initiate apoptosis or inappropriate repair via the DDR pathway.

1.3.2 Telomerase counteracts the end-replication problem

To counteract telomere erosion, most eukaryotic cells possess a specialized enzyme called telomerase. The presence of a specialized enzyme capable of replicating the terminal TTAGGG repeats was first shown and isolated in *Tetrahymena* (Greider and Blackburn, 1985). Subsequent studies revealed telomerase as a ribonucleoprotein that uses a catalytic subunit with reverse transcriptase activity (TERT) to synthesize TTAGGG repeats from an RNA

primer, TERC (Greider and Blackburn, 1987; Greider and Blackburn, 1989; Lingner et al., 1997; Nakamura et al., 1997). Telomerase is highly regulated during development, being active in germline tissue but not somatic cells (Kim et al., 1994). This ensures a limited lifespan of normal somatic cells, with telomeres shortening every cell division. The inactivation of telomerase in somatic cells represents an important tumor suppressor pathway to limit immortalization of cells. Indeed, about 90% of tumor biopsies tested have reactivated telomerase (Kim et al., 1994). The remaining 10% of tumors may either lack telomere maintenance or rely on a recombination based mechanism, Alternative Lengthening of Telomeres (ALT), to prevent loss of telomeric sequences (Bryan et al., 1997; Dunham et al., 2000). The fact that all tumor cells possess some mechanisms to prevent telomere attrition illustrates the importance of telomeres.

1.3.3 Shelterin protects against the end-protection problem

The end-protection problem emerged from landmark studies by Herman Muller and Barbara McClintock in the 1930's and 1940's (Muller, 1938; McClintock, 1941). First, Muller observed that induced chromosomal translocations and rearrangements never occurred at chromosomes ends, which he called telomeres. He concluded that the terminal "gene" must have a protective function by sealing the chromosome end. Barbara McClintock independently found that broken chromosomes are prone to fusions and rearrangement, but that the natural ends of chromosomes are somehow protected from this genetic

instability. We now know that a protective telomere specific protein complex, shelterin, associates with chromosome ends (Palm and de Lange, 2008). Shelterin associates with telomeres through TRF1 and TRF2, which bind specifically to double stranded TTAGGG repeats. POT1 (POT1a and POT1b in mice) binds the single stranded TTAGGG repeats that are present in a 50-400 nt TTAGGG repeat 3' overhang at the telomere terminus. POT1 is connected to TRF1 and TRF2 through two other shelterin components, TIN2 and TPP1. A sixth component, Rap1, binds to TRF2.

Studies using telomeres lacking components of shelterin or the entire complex revealed how shelterin represses different deleterious damage pathways that are activated at unprotected DNA ends (Fig. 1.7a) (Palm and de Lange, 2008; Sfeir and de Lange, 2012; Doksani and de Lange, 2014). TRF2 represses ATM activation and c-NHEJ by sequestering telomeres in a t-loop configuration (van Steensel et al., 1998; Griffith et al., 1999; Karlseder et al., 1999; Celli and de Lange, 2005; Doksani et al., 2013). This conformation is proposed to inhibit loading of Ku70/80 and the MRN complex onto DNA ends, steps that are essential for initiation of c-NHEJ and ATM signaling, respectively (Lieber, 1999; Walker et al., 2001; Lee and Paull, 2004). TRF2 has long been implicated in t-loop formation, but only recent STORM imaging techniques have enabled direct evidence for this in vivo (Doksani et al., 2013). These experiments have shown that TRF2 is the sole shelterin component involved in t-loop formation.

TRF1 has similar domain architecture as TRF2 but its main function lies in promoting telomere replication (Sfeir et al., 2009; Zimmermann et al., 2014). The telomeric TTAGGG sequence poses a problem for the replication machinery, similar to common fragile sites (CFS) elsewhere in the genome. Upon deletion of TRF1, multiple telomeric signals are observed at a single chromatid end, indicative of replication problems and fork stalling in the telomeric DNA can be observed by DNA combing. Furthermore, ATR kinase is activated at telomeres lacking TRF1 in a process that requires progression through S-phase, consistent with a role for TRF1 in replication. The mechanism by which TRF1 supports replication is not completely understood, but involves recruitment of BLM and Rtel1 helicases to unwind G-quadruplexes that are formed by telomeric TTAGGG sequences (Sfeir et al., 2009; Vannier et al., 2012; Zimmermann et al., 2014).

In contrast to TRF1 and TRF2, POT1 binds the single stranded DNA in the telomeric overhang. Interestingly, humans and mice differ with regards to POT1. Where mouse telomeres require two distinct paralogs, POT1a and POT1b, the function of these proteins is carried out by one POT1 protein in human cells (Hockemeyer et al., 2006). POT1 has several functions at telomeres. First of all it shields the single stranded overhang from RPA binding and unwanted ATR activation (Hockemeyer et al., 2005; Hockemeyer et al., 2006; Denchi and de Lange, 2007; Gong and de Lange, 2010). Furthermore, POT1 (POT1b) is required for postreplicative processing of telomeres by blocking excessive resection by the Apollo nuclease (Wu et al., 2012). Leading-strand DNA

synthesis results in blunt ended telomeres that are at risk for ATM activation and NHEJ. TRF2 recruits Apollo to process the leading ends into minimal overhang that enables the t-loop configuration. In absence of POT1b, resection by Apollo and also Exo1 is extreme (Wu et al., 2010). Besides its inhibitory effect on Apollo, POT1 (POT1b) recruits CST to regulate the overhang length at the telomere end. CST-mediated fill-in synthesis corrects the extended overhang created by Exo1 (Wu et al., 2012; Takai et al., 2016). Another role for POT1 lies in telomere length control as POT1 is thought to block access of telomerase to single stranded overhangs (Loayza and de Lange, 2003). POT1 is therefore a negative regulator of telomere length.

Rap1 binds TRF2 but unlike TRF2 it has no role in the repression of ATM or c-NHEJ. However, deletion of Rap1 in a Ku70/80^{-/-} background revealed a role for Rap1 in repressing HR, similarly as seen previously seen for POT1a and POT1b (Palm et al., 2009; Sfeir et al., 2010). Shelterin as well Ku70/80 thus block HR at telomeres, perhaps to ensure greater protection.

1.3.4 TRF2 prevents ATM activation and NHEJ

By sequestering telomeres in the t-loop configurations, TRF2 is thought to inhibit loading of Ku and MRN at the end. Indeed, when TRF2 is deleted from mouse embryonic fibroblasts (MEFs), ATM is rapidly activated as indicated by Chk2 phosphorylation and accumulation of 53BP1, MDC1 and γH2AX in foci that overlap with telomeres called telomere dysfunction induced foci (TIFs) (Karlseder

et al., 1999; Takai et al., 2003; Celli and de Lange, 2005; Dimitrova and de Lange, 2006; Denchi and de Lange, 2007). NHEJ is unleashed when TRF2 is missing causing telomere end-to-end fusions that are visible as chromosome trains on metaphase spreads. These chromosome fusions occur mostly in G1 and are fully dependent on ATM, Lig4 and Ku, supporting their dependency on NHEJ and DNA damage signaling (Smogorzewska et al., 2002; Celli and de Lange, 2005; Celli et al., 2006; Konishi and de Lange, 2008). Furthermore, 53BP1 mediated mobility of chromatin and inhibition of end resection are required for these telomere fusions, which are drastically reduced in absence of 53BP1 (Dimitrova et al., 2008; Lottersberger et al., 2013; Zimmermann et al., 2013). The resection that occurs at telomeres when TRF2 is deleted in absence of 53BP1 is dependent on ATM and CtIP (Lottersberger et al., 2013). Similar to chromosome internal DSBs, 53BP1 recruits Rif1 and MAD2L2 to suppress extensive end-resection (Zimmermann et al., 2013; Boersma et al., 2015).

TRF2 binds specifically to telomeric DNA through a C-terminal SANT/Myb domain and forms homodimers with its N-terminal TRFH domain (Palm and de Lange, 2008). TRF2 furthermore contains a Gly/Arg rich domain Basic domain in its N-terminus that can bind and stabilize dHJs that can be formed at the base of the t-loop by branch-migration (Fouche et al., 2006; Poulet et al., 2009). While the t-loop is required for protection against NHEJ and ATM activation, the dHJs can be cleaved by Holliday junction resolvases resulting in excision of the t-loop and loss of telomeric DNA (Wang et al., 2004). Expression of a TRF2 mutant

lacking the Basic domain results in t-loop excision and telomere shortening, while NHEJ is still suppressed (Wang et al., 2004; Saint-Leger et al., 2014).

1.3.5 TRF1 is required for telomere replication

Studies in yeast and mammals have shown that telomere replication mostly originates from the subtelomeric regions (Makovets et al., 2004; Sfeir et al., 2009). Therefore, leading-strand replication produces the G-rich strand whereas the C-rich strand is made by lagging-strand synthesis. However, the repetitive telomeric sequence poses a problem for the replication machinery as the G-rich DNA can form G-quadruplexes (G4), a secondary structure held together by G-G Hoogsteen base-pairing (Henderson et al., 1987). Fork stalling is frequently observed in telomeric sequences and treatment of cells with G4-stabilizing drugs induces ATR activation and telomeric aberrations (Miller et al., 2006; Salvati et al., 2007; Rizzo et al., 2009; Sfeir et al., 2009). Interestingly, fork stalling also occurs when the telomeric sequence is located internally in chromosomes, further indicating that the DNA sequence itself forms a problem for the replication machinery (Miller et al., 2006; Bosco and de Lange, 2012).

TRF1 is required to aid replication fork progression through telomeric DNA (Martinez et al., 2009; Sfeir et al., 2009). Deletion of TRF1 from MEFs results in frequent fork stalling in telomeric sequences and activation of an ATR signaling cascade, and the appearance of fragile telomeres. The fragile telomeres are

reminiscent of fragile sites that arise at other genomic regions that are challenging to replicate.

1.3.6 Fragile sites

Two different types of fragile sites have been described in human cells. Rare fragile sites are only present in certain individuals that have expansions of genomic repeat regions such as Fragile X syndrome (Kremer et al., 1991). In contrast, all individuals have common fragile sites (CFSs), which represent regions of the genome that are late to replicate or have a low density of replication origins. As a result, CFSs are often incompletely replicated at the onset of mitosis. Fragile sites manifest as breaks and gaps on metaphase chromosomes, especially upon treatment with drugs that affect replication such as aphidicolin, which blocks DNA synthesis by inhibiting polymerase alpha. The inherent genetic instability of CFSs is thought to be a driving force in the onset of cancer because many chromosome translocations and rearrangements in tumors originate from CFSs (Hecht and Glover, 1984; Hellman et al., 2002; Le Tallec et al., 2011; Ozeri-Galai et al., 2012). The mechanisms of genetic instability at CFSs are not very well understood. Secondary structure formation at CFSs could be a causative factor for their instability (Durkin and Glover, 2007). Upon replication stress, single stranded DNA formed ahead of the DNA polymerase upon uncoupling from the replicative helicase could form a secondary structure resulting in fork stalling and breakage. Consistent with this model, loss of

enzymes that remove secondary structures, such as the RecQ helicases BLM and WRN, increases fragile site expression (Pirzio et al., 2008). More recent studies challenged this model and postulated that it is the lack of replication origins that cause CFSs instability (Ozeri-Galai et al., 2011). CFSs are thought to replicate late in S-phase and additional delay upon treatment with aphidicolin results in incomplete replication (Le Beau et al., 1998; Pelliccia et al., 2008). Another contributing factor to CFS expression is thought to be a collision between transcription and replication forks (Helmrich et al., 2011). Likely, all these pathways play a varying role in CFS expression, which could explain why expression levels of CFSs differ between cell types. One unifying factor in CFSs expression is the observation that replication is not finished at these sites, yielding DNA structures with replication intermediates at the onset of mitosis.

1.3.7 Fragile site cleavage prevents anaphase bridges

Cleavage of CFSs was long thought to cause genetic instability, but this view was recently challenged by two studies indicating that cleavage by Mus81-Eme1 is actually protective (Naim et al., 2013; Ying et al., 2013). The structure-specific endonuclease Mus81-Eme1 was shown to localize to CFSs at the onset of mitosis and cleave replication intermediates, triggering the appearance of the characteristic breaks and gaps associated with CFSs. Unexpectedly however, depletion of Mus81-Eme1 caused more severe genetic instability due to accumulation of anaphase bridges and mitotic failure. Thus, cleavage of under-

replicated DNA by Mus81-Eme1 appears to be beneficial to cells as it helps sister chromatid disjunction and prevents the formation of anaphase bridges. The gaps and breaks in DNA caused by Mus81-Eme1 cleavage are protected in 53BP1 nuclear bodies in the next G1 to allow for their repair (Lukas et al., 2011).

The anaphase bridges that appear at CFSs, especially when Mus81 is missing, are not always detectable with conventional DNA dyes. These bridges are called ultrafine bridges (UFBs) and can be visualized by immunofluorescent staining of either BLM or PICH (Chan et al., 2009; Naim and Rosselli, 2009). The presence of BLM on these UFBs is dependent on PICH and provides cells with a final attempt to resolve unrepaired DNA intermediates before anaphase (Chan et al., 2007).

1.3.8 TRF1 recruits BLM to prevent fragile telomeres

It is not completely understood how TRF1 promotes faithful telomere replication. TRF1 lacks enzymatic activity and is assumed to function by recruiting additional proteins to aid fork progression. Two proteins of interest are BLM and RTEL1, since telomere fragility is seen upon shRNA mediated depletion of these proteins (Ding et al., 2004; Lillard-Wetherell et al., 2004; Sfeir et al., 2009). Recent studies have shown that BLM interacts with TRF1 and that this interaction is required to prevent telomere fragility, specifically on the telomere replicated by lagging strand DNA synthesis (Zimmermann et al., 2014). The lagging-strand TTAGGG template is particularly prone to G-quadruplex formation. Since BLM possesses

G-4 unwinding activity, it is likely that TRF1 recruits BLM to unwind Hoogsteen bonding between guanines in the lagging-strand template and thus prevents telomere fragility (Sun et al., 1998; Huber et al., 2002). How TRF1 prevents leading-strand telomere fragility remains unknown but might require RTEL1.

1.3.9 TRF1 prevents the formation of sister associations

A separate phenotype that emerges upon deletion of TRF1 are sister associations (SA), which are visible as fused sister telomeres in metaphase spreads. However, the molecular nature of SA is not yet known. They are not fused by c-NHEJ, as deletion of Lig4 has no effect on their prevalence (Sfeir et al., 2009). SAs are also not dependent on the interaction of TRF1 with BLM and therefore likely form through a mechanism distinct from fragile telomeres (Zimmermann et al., 2014). The only known contributing factor to the formation of SAs is the activation of ATR kinase. When ATR is depleted from TRF1 null cells, the frequency of SAs is significantly reduced (Sfeir et al., 2009). Supporting this model, it was shown that TRF1 uses the interaction with TIN2/TPP1 and POT1 to prevent sister associations (Zimmermann et al., 2014). POT1a is thought to compete with RPA for binding single-stranded TTAGGG repeats and thereby prevent ATR activation. However, activation of ATR alone is not sufficient to form SAs as deletion of TPP1 or POT1 by itself results in only low levels of SAs (Hockemeyer et al., 2006; Kibe et al., 2010). Thus, TRF1 deletion combined with

ATR activation is required for the formation of SAs indicating that it requires an activity that occurs at a stalled replication fork.

1.3.10 Dysfunctional telomeres as a model for DNA damage response pathways

All six shelterin protein repress different components of the DNA damage response, from c-NHEJ and HR to ATM and ATR activation (Sfeir and de Lange, 2012). Conditional deletion of shelterin proteins has therefore emerged as useful model system to study DNA damage response pathways. There are several advantages of using shelterin depletion over traditional drug or irradiation induced DNA damage. First, the defined location of the DNA damage allows for separation of the damaged DNA from the rest of the chromatin. This allows the use of molecular techniques such as telomere overhang assays, ChIP and other physical assays to study the effect of DNA damage. Secondly, the highly specific function of shelterin components allows studying DNA damage pathways separately from one each other, a feat difficult to accomplish with drugs or irradiation which often stimulate a more complex response. However, care should be taken before extrapolating results from telomere specific studies to other sites in the genome without appropriate controls.

For the purpose of this thesis, telomeres lacking TRF2 will be used to study the role of 53BP1 in promoting chromatin mobility. Telomeres devoid of TRF2 were previously successfully used to shown the role of 53BP1 in the c-NHEJ pathway and in blocking extensive end-resection (Dimitrova et al., 2008;

Lottersberger et al., 2013; Zimmermann et al., 2013). Furthermore, deletion of TRF1 will be used to analyze the role of 53BP1 at sites of replication stress and to analyze the molecular activities underlying sister telomere associations.

Chapter 2: 53BP1 dissociation of function mutants

2.1 Introduction

It is known that 53BP1 is a key regulator in the decision between NHEJ and HR at DSBs. However, specifically how 53BP1 promotes NHEJ is not completely understood. One mechanism by which 53BP1 stimulates NHEJ is via inhibition of end-resection using its interaction with Rif1. However, loss of Rif1 does not reduce NHEJ to the same extent as loss of 53BP1 indicating other factors are involved (Zimmermann et al., 2013). We also know that 53BP1 promotes NHEJ by stimulating the mobility of damaged chromatin but the molecular mechanisms are not well understood (Dimitrova et al., 2008). Preliminary data from the de Lange lab has shown that the 53BP1-mediated mobility involves cytoplasmic microtubules since it is diminished upon treatment with nocodazole, which depolymerizes microtubules. Furthermore, treatment of cells with the microtubule-stabilizing drug Taxol also reduced the mobility of dysfunctional telomeres. In addition, it was shown that the effect of 53BP1 on mobility involves the LINC complex (Linker of Nucleoskeleton and Cytoskeleton), which spans the inner and outer nuclear membranes (INM and ONM) (Starr and Fridolfsson, 2010). The LINC complex is composed of Sun proteins (Sun1 and Sun2) in the INM that interact with nesprins spanning the ONM. The nesprins connect to the cytoskeleton, including microtubules, through interactions with kinesins amongst other proteins. How 53BP1 connects to the LINC complex is unknown.

The function of the interaction between PTIP and 53BP1 remains controversial. Loss of PTIP has no effect on CSR in B cells but radial formation in

PARPi-treated BRCA^{-/-} cells is diminished in absence of PTIP. This was attributed to increased resection after loss of PTIP (Callen et al., 2013). At telomeres, fusions were reduced in PTIP^{-/-} MEFs treated with an shRNA against TRF2, which was speculated to be due to the increased resection. However, these experiments were done with a TRF2 shRNA and in PTIP^{-/-} MEFs and it is unclear if these results represent a function of PTIP downstream of 53BP1.

53BP1 uses its N-terminal S/TQ phosphorylation sites to interact with proteins that perform essential functions in DNA repair, such as Rif1 and PTIP. A proteomics screen in B cells identified hundreds of proteins that interact with the S/TQ sites in a damage inducible way, but the relevance of most of these factors remains unknown (Di Virgilio et al., 2013).

The first part of my thesis is focused on understanding the role of phosphorylation dependent interaction partners of 53BP1 in regulating DNA repair. Telomeres depleted of TRF2 are used as a model system since 53BP1 mediated NHEJ results in extensive telomere fusions that are easily visible in metaphase spreads. Furthermore, resection can be analyzed with telomere overhang assays using a telomere specific probe.

2.2 Results

2.2.1 Generation of 53BP1 mutants

To study the role of 53BP1 interaction partners, a panel of mutant 53BP1 alleles was generated in which clusters of the 28 S/TQ sites are mutated to alanine.

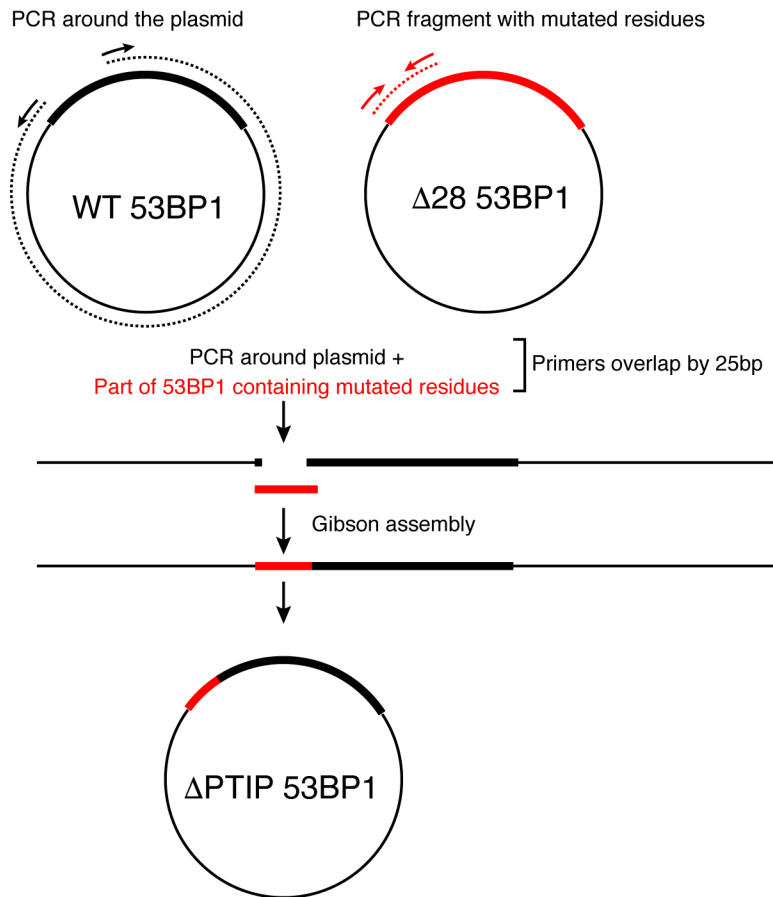


Figure 2.1 Gibson cloning of 53BP1 mutant alleles

Mutant 53BP1 alleles were created from 53BP1^{WT} and 53BP1 ^{$\Delta 28$} via Gibson cloning. Primer pairs were designed containing short overlap with each other. One pair (black) was used to do a PCR around the plasmid copying the backbone and most of the 53BP1^{WT} construct. A second PCR (red) on the 53BP1 ^{$\Delta 28$} vector copies part of the N-terminal region containing mutated S/TQ residues. The two PCR products are isolated and ligated together using Gibson cloning dependent on the overlap between the primer pairs. This strategy allows mixing parts of the 53BP1^{WT} and 53BP1 ^{$\Delta 28$} constructs

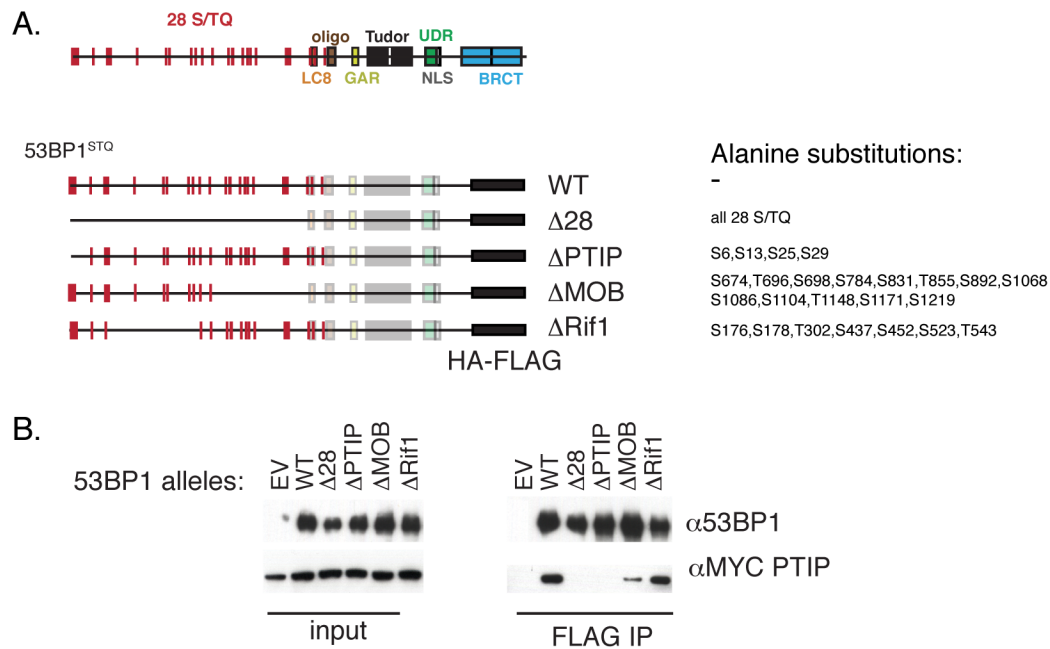


Figure 2.2 53BP1 mutant alleles

(A) Schematic of 53BP1 and the mutant alleles. (B) Co-IP in 293T cells expressing MYC-tagged PTIP and FLAG-tagged 53BP1. Co-IP demonstrates that the interaction between 53BP1 and PTIP is lost with 53BP1^{Δ28} and 53BP1^{ΔPTIP} but not with the other alleles. Left panel shows input DNA and the co-IP using FLAG antibody is shown on the right. Immunoblot was done with antibodies against 53BP1 and MYC.

These mutants were generated via Gibson cloning using WT and 53BP1^{Δ28} as template allowing the exchange of different parts of the plasmids (Fig. 2.1). This approach was taken since 53BP1 is a very large construct that hinders regular cloning protocols. Constructs were sequenced throughout to verify the correct change. All constructs contain a C-terminal FLAG-tag for IP and western blotting and lack the C-terminal BRCT domains, which were previously shown to be dispensable for NHEJ at telomeres (Lottersberger et al., 2013). These constructs will collectively be called S/TQ mutants or specifically named for their mutant domain. The different mutants are shown in Fig. 2.2a.

For 53BP1^{ΔPTIP}, the first 4 S/TQ sites were mutated to alanine based on previous studies that showed these to be required for the interaction with PTIP (Munoz et al., 2007; Callen et al., 2013). Co-IP experiments with FLAG tagged 53BP1 and myc-tagged PTIP showed that the interaction with PTIP was indeed lost in the 53BP1^{ΔPTIP} mutant but not the other alleles (Fig. 2.2c). The interaction between 53BP1 and Rif1 was previously mapped to 7 S/TQ sites in a central domain of 53BP1, in a mutant called 53BP1^{Δ3} (Callen et al., 2013) (Fig. 2.3a). However, this mutant still displayed residual Rif1 binding at telomeres after deletion of TRF2 (Fig 2.3a). Therefore a different subset of mutant 53BP1 alleles was created in which additional domains of S/TQ sites were mutated (Fig. 2.3b). The interaction between 53BP1 and Rif1 was examined by analyzing Rif1 recruitment to 53BP1 by IF-FISH at dysfunctional telomeres in TRF2^{F/F}53BP1^{-/-}

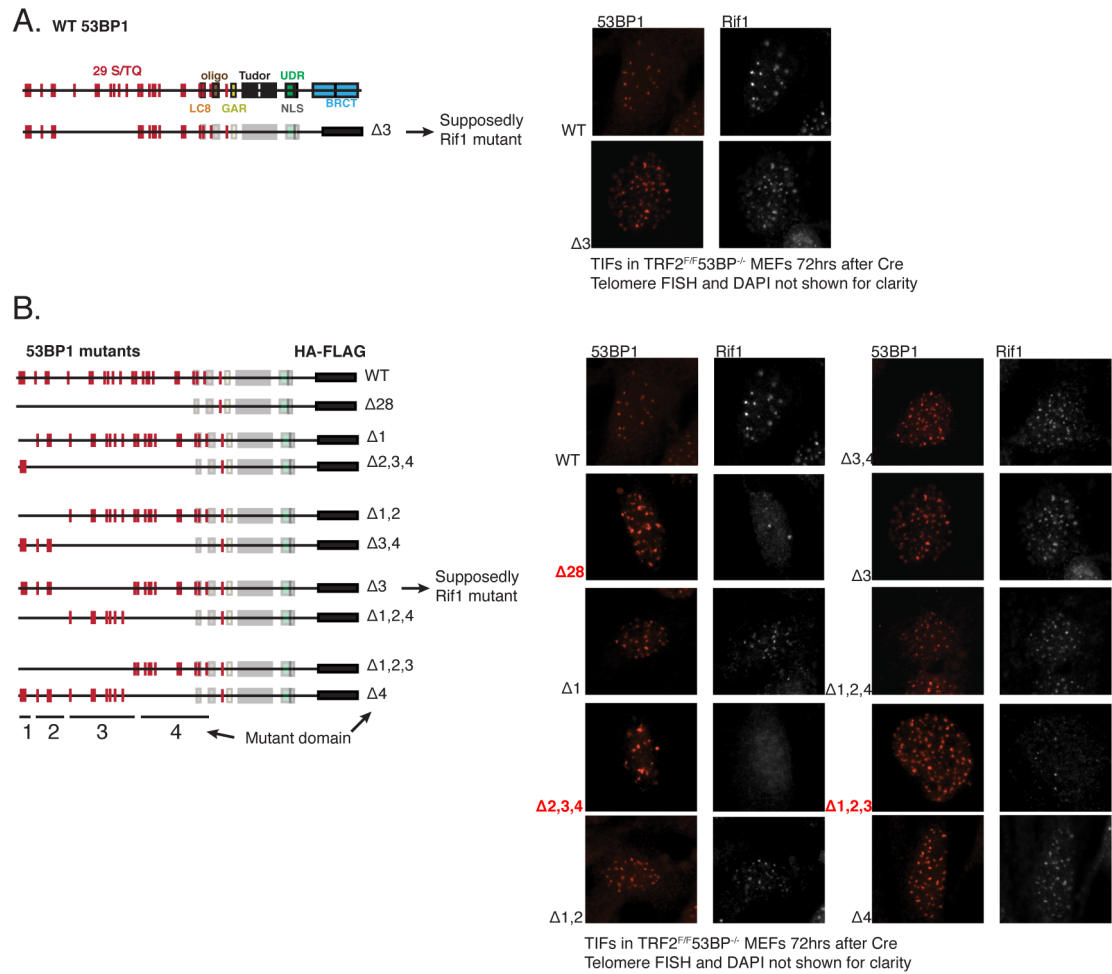


Figure 2.3 Rif1 recruitment to 53BP1

(A) Schematic of 53BP1 WT and 53BP1^{Δ3}, which is supposedly deficient in Rif1 recruitment (Callen et al., 2013). Right panel shows Rif1 (white) recruitment to 53BP1 (red) by IF-FISH upon expression of the constructs in TRF2^{F/F} 53BP1^{-/-} MEFs, 72 h after deletion of TRF2. Rif1 is still recruited to 53BP1^{Δ3}. For clarity, panels with DAPI and telomere FISH signals are not shown in these images, but 53BP1 localizes to telomeres. (B) Generation of additional 53BP1 mutant constructs, shown on left. The domains of mutated S/TQ sites are depicted at the bottom. For example, 53BP1^{Δ1,2} has S/TQ sites in both domain 1 and 2 mutated to alanine. Right panel shows IF-FISH of Rif1 (white) recruitment to 53BP1 (red) upon expression of constructs in TRF2^{F/F} 53BP1^{-/-} MEFs, 72 h after deletion of TRF2. The interaction between 53BP1 and Rif1 is only lost in mutants that have both domain 2 and 3 mutated or in the complete phosphorylation mutant 53BP1^{Δ28} (highlighted in red).

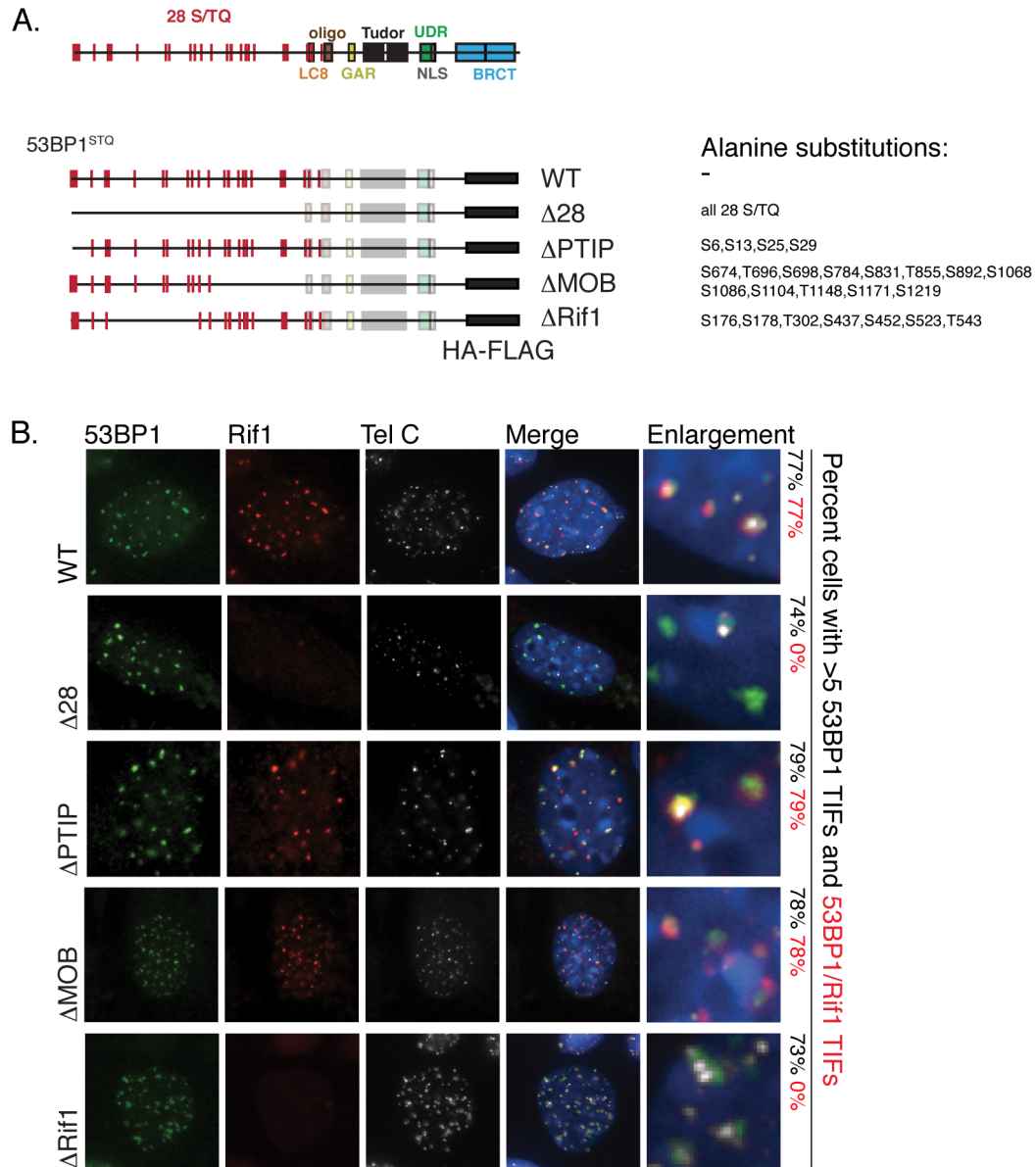


Figure 2.4 53BP1 mutant alleles localize to telomeres

(A) Schematic of 53BP1 and the mutant alleles. (B) 53BP1 constructs were expressed in TRF2^{F/F} 53BP1^{-/-} MEFs and localization analyzed via IF-FISH at 72 h after deletion of TRF2. IF-fish shows 53BP1 (green) recruitment to telomeres (white). Rif1 (red) localizes to 53BP1 foci except in cells expressing the 53BP1^{Δ28} or 53BP1^{ΔRif1} alleles. Numbers on the right represent the quantification of the average percentage of cells with >5 53BP1 or 53BP1/Rif1 foci at telomeres from 3 independent experiments.

cells expressing the mutant 53BP1 alleles. Interestingly, only the 53BP1 alleles that have the S/TQ sites mutated in both domain 2 and 3 showed complete loss of Rif1 recruitment (Fig. 2.3b). The precise interaction between Rif1 and 53BP1 was further mapped by mutating subsets of the S/TQ sites in this region. Especially S176 and S178 appeared to be required for Rif1 foci formation. The resulting 53BP1^{ΔRif1} allele contains 7 mutated S/TQ sites (different from 53BP1^{Δ3}) and has lost all interaction with Rif1 (Fig. 2.4a and 2.4b).

The 53BP1^{ΔMOB} allele was initially generated to examine whether S/TQ sites in this domain influence any of the known functions of 53BP1. As will be described in detail in chapter 2.2.4, this mutant affected the ability of 53BP1 to promote the mobility of dysfunctional telomeres and was thus called 53BP1^{ΔMOB}. Importantly, all S/TQ mutants expressed equally well in TRF2^{F/F} 53BP1^{-/-} MEFs and each localized to sites of damage (Fig. 2.2b and 2.4b).

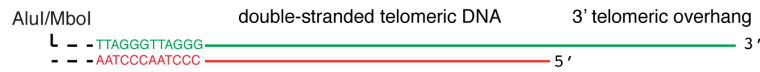
2.2.2 Rif1 is the only factor downstream of 53BP1 controlling resection

53BP1 blocks CtIP-dependent end resection thereby promoting c-NHEJ in G1. At telomeres, 53BP1 also blocks CtIP-independent end-resection by Exo1/BLM in response to ATR activation upon loss of TPP1/POT1a/b (Kibe et al., 2016). In absence of 53BP1, hyper-resection occurs at DSBs and dysfunctional telomeres that inhibit c-NHEJ. The ability of 53BP1 to block resection is dependent on phosphorylation of the S/TQ sites and Rif1 was identified as the main 53BP1 interacting factor responsible for this function (Di Virgilio et al., 2013;

Zimmermann et al., 2013). To analyze if any 53BP1-S/TQ binding factors other than Rif1 are required to block resection, the 53BP1 mutant alleles were expressed in TRF2^{F/F}Lig4^{-/-}53BP1^{-/-} MEFs and resection was analyzed by telomere overhang assays. These experiments are done in a Ligase 4 (Lig4) deficient setting since telomere fusions would mask a defect in protection from hyper-resection.

Telomere overhang assays are native in-gel hybridization assays that enable quantification of the amount of ssDNA at telomeres (Fig. 2.5). Briefly, genomic DNA is isolated and digested with AluI and MboI, which frequently cleave anywhere in the genome except for the telomeric repeats. The generated telomeric fragments are then separated on a gel, which is hybridized with a telomere specific probe ([CCCTAA]₄) under native conditions, resulting in a quantifiable signal for the amount of ssDNA at telomeres. The gel is then denatured and hybridized with the same telomeric probe to control for the total amount of DNA in the lane allowing normalization of the ssDNA signal, as explained in Figure 2.5. The measured ssDNA can be either internal or at the 3' overhang. Treatment of the telomeric DNA with *E. coli* ExoI can distinguish between these two possibilities since ExoI removes 3' overhangs but does not act on internal ssDNA. As it is already known that ssDNA formed after TRF2 deletion is solely at the 3' overhang, ExoI treatment was not included in these experiments (Celli and de Lange, 2005; Lottersberger et al., 2013).

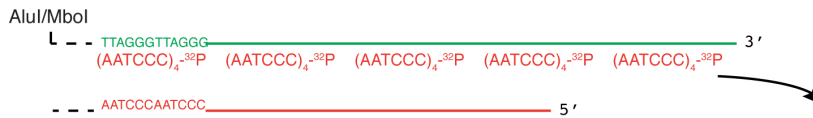
1) Separate Alul/Mbol-digested genomic DNA by PFGE



2) Hybridize with a ^{32}P labeled telomeric probe under native conditions. Quantify ssDNA signal.



3) Denature and hybridize gel with same probe. Quantify total telomeric DNA signal.



4) Normalize ssDNA quantification to total telomeric DNA amount.

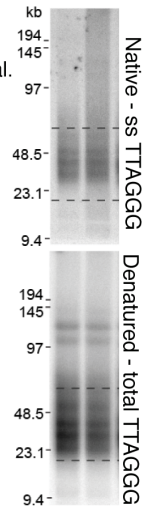


Figure 2.5 Schematic of telomere overhang assay

Genomic DNA is isolated and digested with Alul and Mbol, which cannot cleave the telomeric sequence. Isolated telomeric DNA is separated on by PFGE and hybridized under native conditions with a telomere specific probe that binds to the ssDNA. The gel is then denatured and hybridized with the same probe to quantify the total telomeric DNA present to allow normalization of the amount of telomeric ssDNA to the total amount of telomeric DNA. To compare lanes, the normalized ssDNA signal in a control lane is set to 1.0 and the treated sample is quantified compared to this number. Figure provided by Titia de Lange.

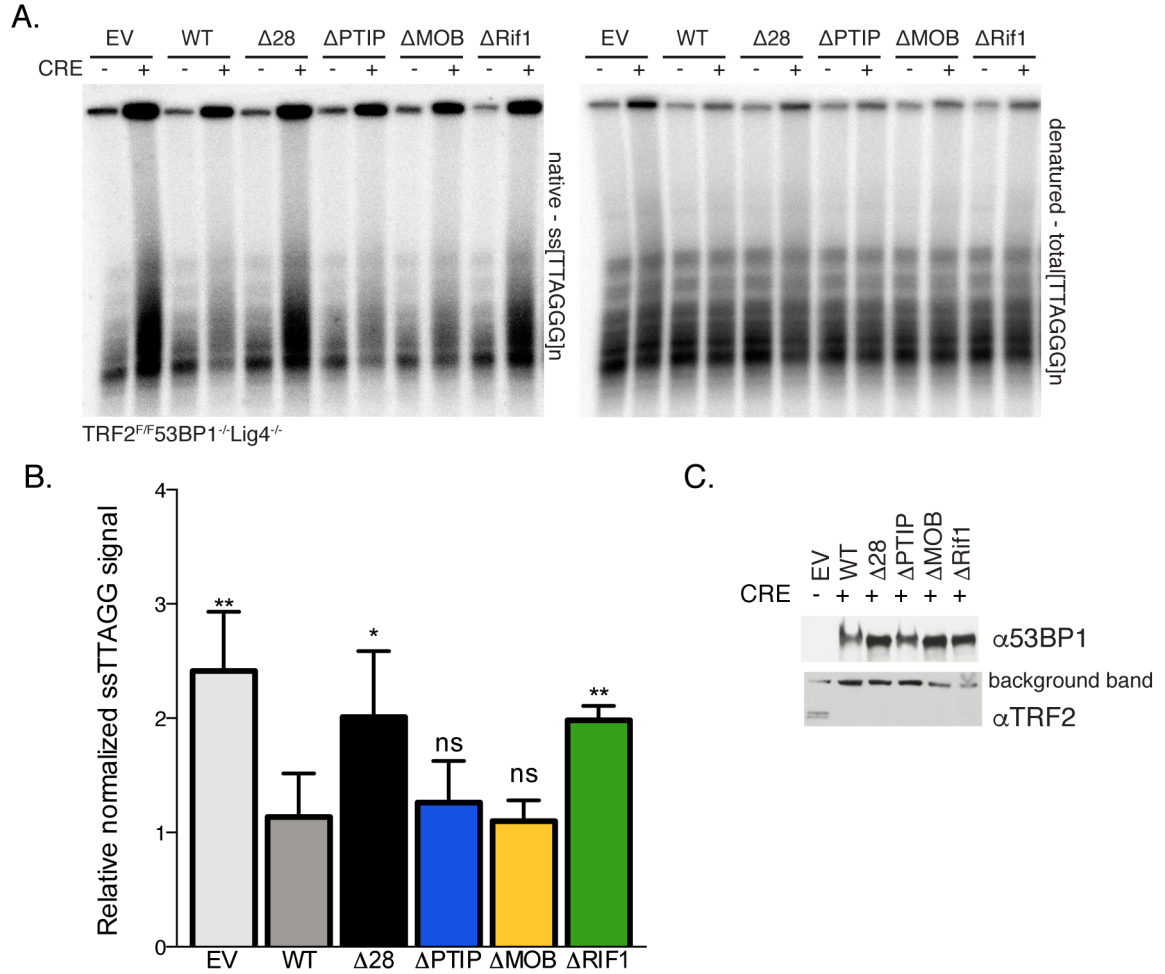


Figure 2.6 53BP1 ^{$\Delta Rif1$} cannot protect telomeres from end resection

(A) Telomere overhang assay of Mbol/Alul digested DNA from TRF2^{F/F}Lig4^{-/-}53BP1^{-/-} MEFs expressing the mutant 53BP1 alleles. Telomeric DNA was analyzed 96 h after Cre-mediated deletion of TRF2 using the in-gel hybridization assay. Left panel shows native telomeric ssDNA signal, right panel displays the denatured total amount of telomeric DNA as explained in Fig. 2.5 (B) Quantification of the overhang signal as in (A) from three independent experiments. Only the values from the Cre-treated samples are shown. Numbers were obtained by normalizing the native ssDNA signal to the total telomeric DNA signal in the denatured gel. The values of the Cre-treated samples were obtained by comparison with the untreated control samples, which were set to 1.0. Means and SDs from three independent experiments are shown. P-values were determined compared to WT by a two-sided Students T-test (* $p < 0.05$, ** $p < 0.01$). (C) Western blot control showing the equal expression level of the 53BP1 alleles and the deletion of TRF2. Cells were harvested 72 h after deletion of TRF2 and antibodies against 53BP1 and TRF2 were used.

As expected, hyper-resection was observed in TRF2^{F/F}Lig4^{-/-}53BP1^{-/-} MEFs upon deletion of TRF2 and expression of empty vector control and in cells expressing 53BP1^{Δ28} (Fig. 2.6a-c). The overhang signal increased 2 to 2.5 fold, similar to previous studies using TRF2^{F/F}Lig4^{-/-}53BP1^{-/-} MEFs (Dimitrova et al., 2008; Lottersberger et al., 2013; Zimmermann et al., 2013). Cells expressing 53BP1^{ΔRif1} showed a similar overhang increase as 53BP1^{Δ28} suggesting that Rif1 is the only factor downstream of 53BP1 required to block end resection. Furthermore, 53BP1^{ΔPTIP} behaved as WT 53BP1 with regards to end resection indicating that PTIP is not involved downstream of 53BP1 contrary to previous reports (Callen et al., 2013). It is possible that PTIP is recruited independent of 53BP1 to inhibit end resection since these experiments were not done in a PTIP deficient setting. However, other experiments from the lab using TRF2^{F/F}Lig4^{-/-}PTIP^{-/-} MEFs indicate that PTIP does not affect resection at telomeres contradicting this explanation (Lottersberger et al., 2015).

2.2.3 53BP1 mutant alleles promote varying levels of telomere fusions

53BP1 promotes c-NHEJ of dysfunctional telomeres via at least two distinct mechanisms: blocking end-resection and stimulating chromatin mobility. To understand which domain of 53BP1 is required to induce chromatin mobility and whether other factors might be involved, the ability of the S/TQ mutants to induce c-NHEJ was analyzed. These experiments were done in TRF2^{F/F}53BP1^{-/-} cells expressing the S/TQ mutants and telomere fusion analyzed in metaphase

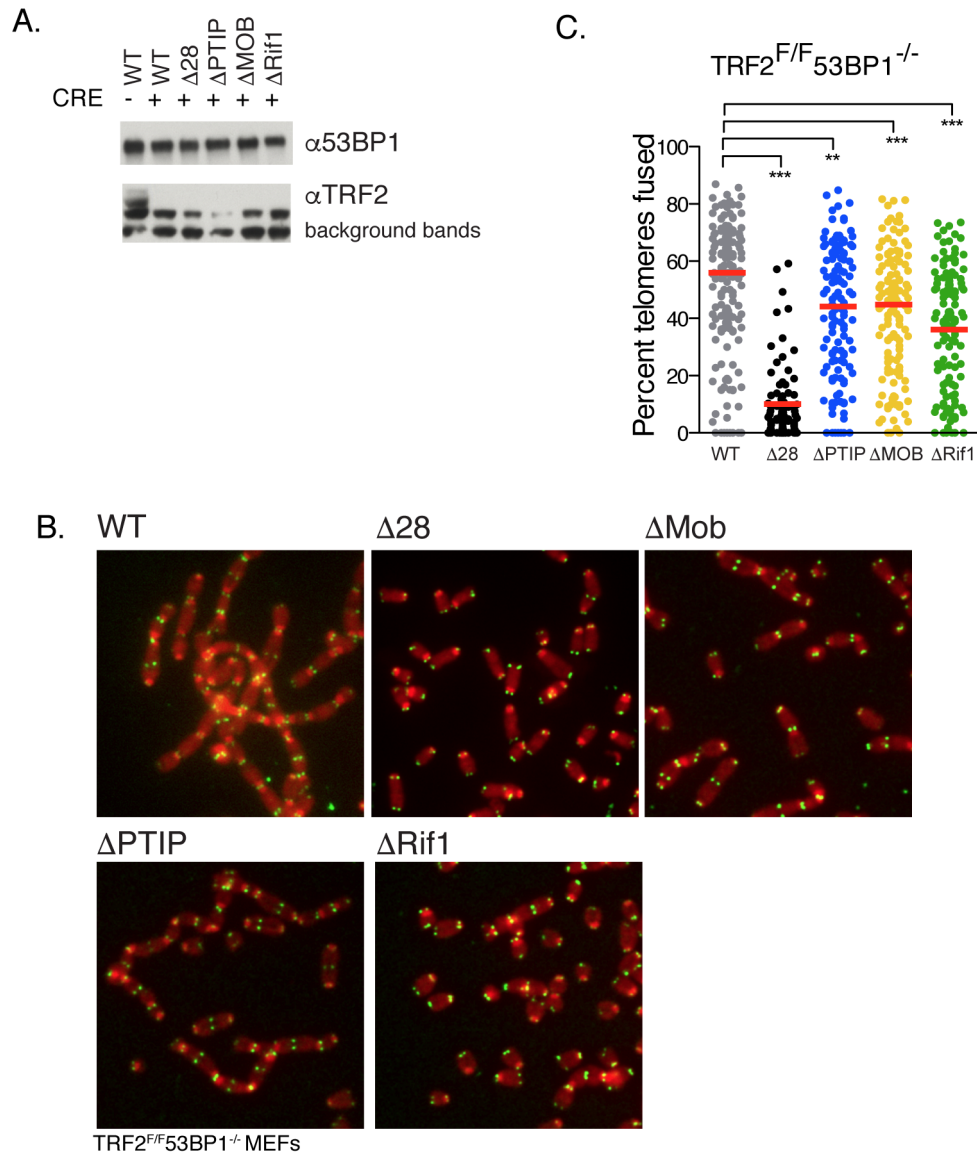
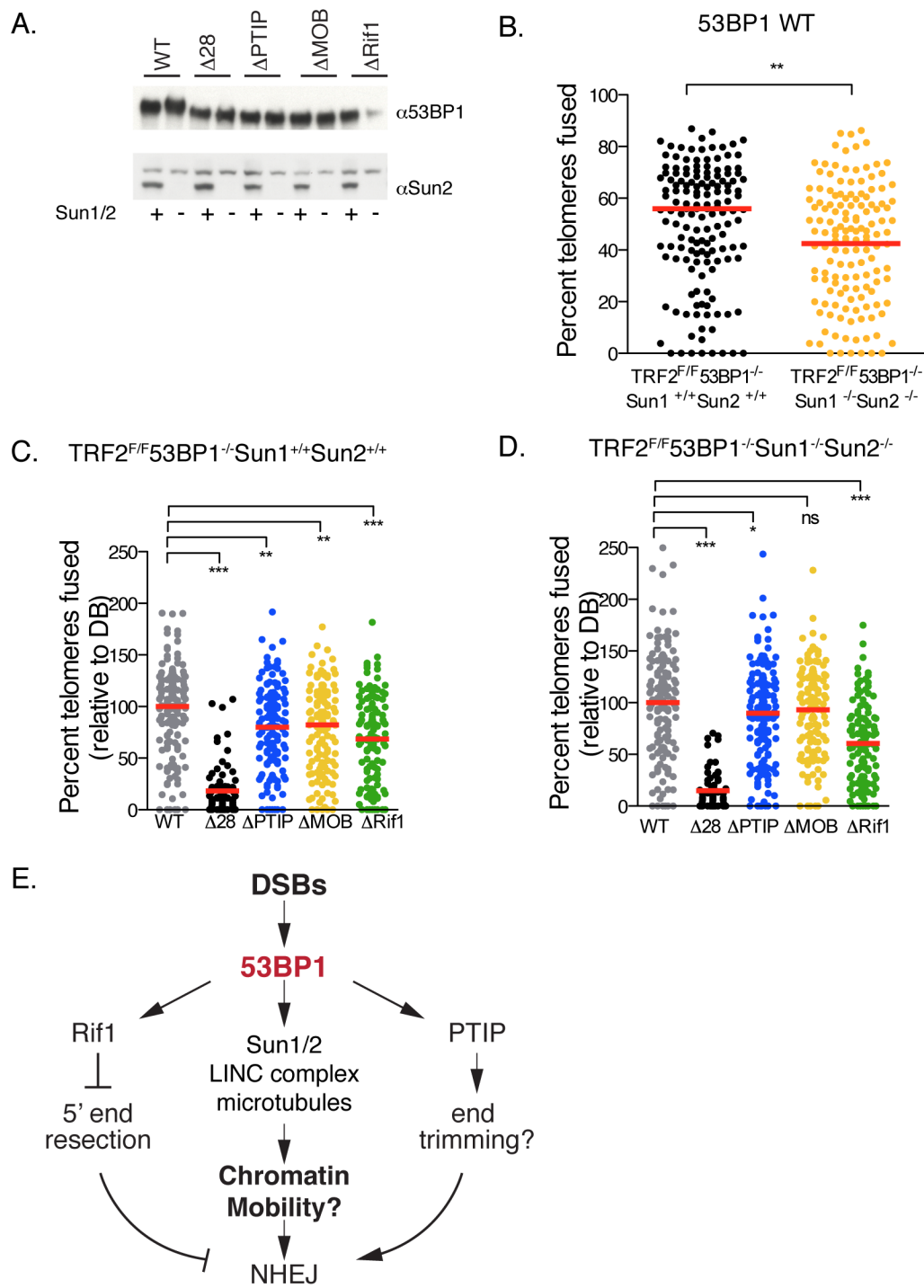


Figure 2.7 Analysis of telomere fusions in cells expressing mutant 53BP1 alleles.

(A) Western blot control for the equal expression level of 53BP1 alleles and deletion of TRF2 from MEFs 72 h after Cre. (B) Metaphase spreads of TRF2^{F/F}53BP1^{-/-} MEFs expressing mutant 53BP1 alleles. Cells were harvested 84 h after Cre-mediated deletion of TRF2. Metaphase spreads were stained with DAPI (red) and a telomeric TelG FISH probe (green). (C) Quantification of the percentage of telomere fusions. Results from 4 independent experiments are shown, each dot represents a metaphase spread. Bars represent the median % of telomere fusions. P-values determined by a two-sided Students T-test (* $p < 0.05$, ** $p < 0.01$, *** $p < 0.001$).

Figure 2.8 Analysis of telomere fusions in cells deficient for the LINC complex

(A) Immunoblot showing expression of 53BP1 alleles and Sun2 in TRF2^{F/F}53BP1^{-/-}Sun1^{-/-}Sun2^{-/-} and TRF2^{F/F}53BP1^{-/-}Sun1^{+/+}Sun2^{+/+} MEFs expressing the indicated mutant alleles of 53BP1. (B) Telomere fusions of MEFs expressing 53BP1^{WT} analyzed 84 h after deletion of TRF2. Bars represent the median % of telomeres fused in 4 independent experiments. (C and D) Telomere fusions of the mutant 53BP1 alleles in TRF2^{F/F}53BP1^{-/-}Sun1^{-/-}Sun2^{-/-} (C) and TRF2^{F/F}53BP1^{-/-}Sun1^{+/+}Sun2^{+/+} (D) MEFs. To allow comparison of telomere fusions in these two separate MEF cell lines, the median fusion frequency in cells expressing WT 53BP was set to 100% (this is the same data as in B). Telomere fusions of the mutant 53BP1 alleles were compared relative to the fusion frequency in the cells expressing WT 53BP1. This allows correction for variability between experiments. The frequency of telomere fusions was scored on metaphases harvested 84 h after TRF2 deletion. Bars represent the median % of telomeres fused in 4 independent experiments; each dot represents a metaphase spread. P-values determined by a two-sided Students T-test (* p<0.05, ** p<0.01, *** p<0.001). (E) Schematic of the mechanisms by which 53BP1 promotes NHEJ



spreads 84 h after deletion of TRF2. As expected, telomeres of cells expressing wild type 53BP1 became extensively fused after deletion of TRF2 whereas expression of 53BP1^{Δ28} did not support c-NHEJ (Fig. 2.7a-c). Furthermore, 53BP1^{ΔRif1} displayed reduced levels of c-NHEJ while 53BP1^{ΔPTIP} showed only a mild fusion defect (Fig. 2.7b). Importantly, 53BP1^{ΔMOB} showed a mild fusion defect as well, even though this mutant is fully capable of blocking end-resection (Figs. 2.7b and 2.6b).

2.2.4 Identification of the 53BP1 mobility domain

The mild fusion defect seen in 53BP1^{ΔMOB} could be due to lack of the chromatin mobility promoted by 53BP1. To test whether this was the case, telomere fusions were analyzed in TRF2^{F/F}53BP1^{-/-}Sun1^{-/-}Sun2^{-/-} cells, which lack the LINC complex and are therefore defective for DNA damaged induced chromatin mobility (Lottersberger et al., 2015). If 53BP1^{ΔMOB} is indeed responsible for inducing chromatin mobility, expression of this mutant should behave as wild type 53BP1 with regards to c-NHEJ in cells lacking the LINC complex (Fig. 2.8e). This experiment was carried out in TRF2^{F/F}53BP1^{-/-}Sun1^{-/-}Sun2^{-/-} and TRF2^{F/F}53BP1^{-/-}Sun1^{+/+}Sun2^{+/+} littermate controls expressing the S/TQ alleles (Fig. 2.8a). As expected, the level of fused telomeres in cells expressing wild type 53BP1 was lower in cells deficient in the LINC complex (Fig. 2.8b). Next, all S/TQ alleles were analyzed in these two cell lines. To correct for variability between experiments, the median level of fusion in cells expressing wild type 53BP1 was

set to 100% in each set of parallel experiments and percent reduction was calculated for the S/TQ mutants tested (Fig. 2.8c and d). This comparison to the levels of fusions observed with wild type 53BP1 served as an internal control for the timing of each experiment. Such a control is needed because in different experiments, the timing of Cre mediated deletion can vary slightly. Since telomere fusions represent a cumulative phenotype that is affected by the duration of the TRF2 deficiency, variations in Cre timing can affect fusion frequencies.

Interestingly, whereas telomere fusions were reduced in $\text{TRF2}^{\text{F/F}}53\text{BP1}^{-/-}$ $\text{Sun1}^{+/+}\text{Sun2}^{+/+}$ cells expressing $53\text{BP1}^{\Delta\text{MOB}}$, this construct behaved similar to wild type 53BP1 in $\text{TRF2}^{\text{F/F}}53\text{BP1}^{-/-}\text{Sun1}^{-/-}\text{Sun2}^{-/-}$ cells (Fig. 2.8c-d). This suggests that $53\text{BP1}^{\Delta\text{MOB}}$ harbors the S/TQ sites needed to induce chromatin mobility.

To test the effect of the $53\text{BP1}^{\Delta\text{MOB}}$ mutations further, the ability of this mutant to induce chromatin mobility was studied via live cell imaging using the same experimental settings as used previously to describe 53BP1 induced chromatin mobility (Fig. 2.9a) (Dimitrova et al., 2008; Lottersberger et al., 2015). Briefly, a stable cell line was created by expressing the Tudor and UDR domains of 53BP1 fused to mCherry (mCherry-BP1-2) in $\text{TRF2}^{\text{F/F}}53\text{BP1}^{-/-}$ cells. This construct localizes to sites of damage but has no effect on DNA damage repair since it lacks all other functional domains of 53BP1 (Dimitrova et al., 2008). Upon deletion of TRF2, mCherry-BP1-2 localizes to telomeres and the dynamic movement of telomeres can be tracked via live cell time-lapse imaging and the

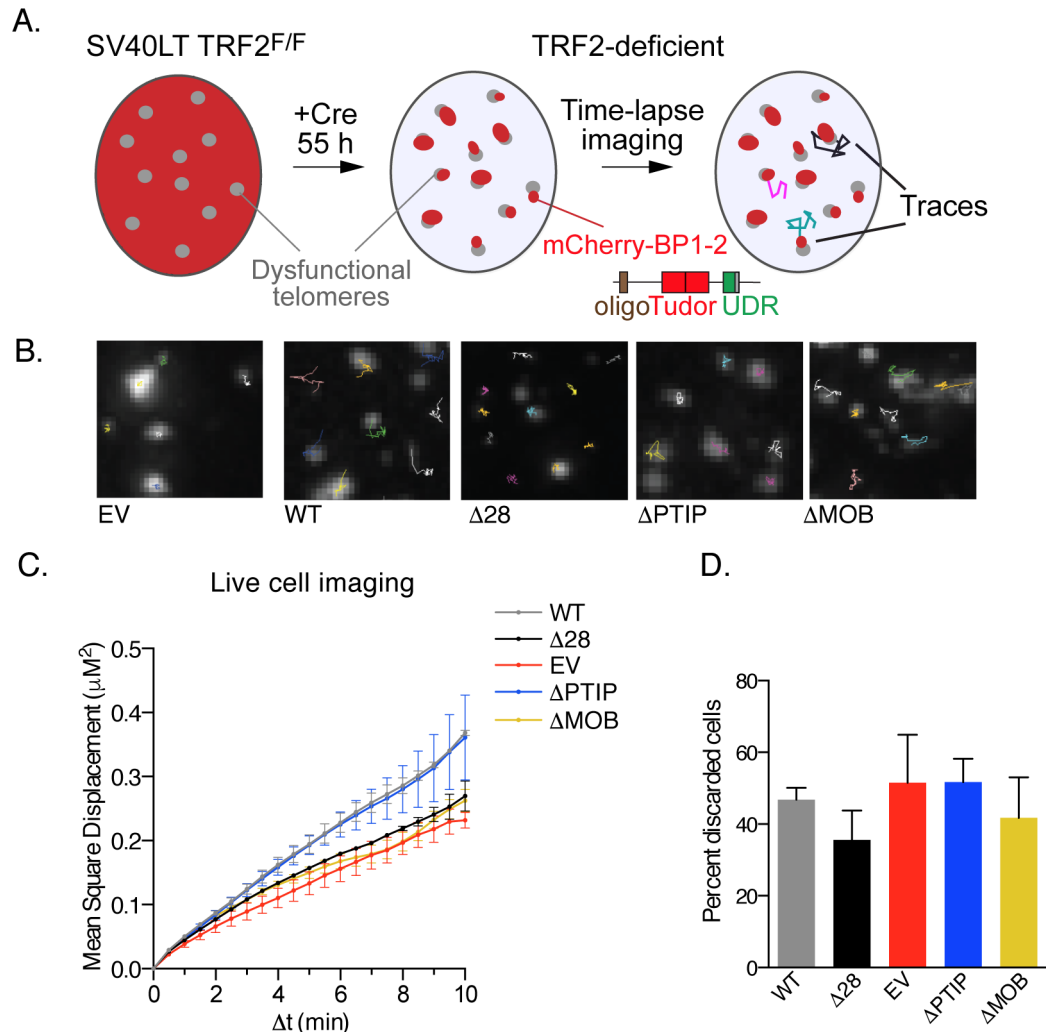


Figure 2.9 53BP1^{ΔMOB} is deficient in stimulating chromatin mobility

(A) Experimental setup for analysis of telomere mobility. TRF2^{F/F} 53BP1^{-/-} MEFs expressing a mCherry-BP1-2 construct are used in time-lapse imaging experiments. This protein localizes to damage sites upon deletion of TRF2. Z-stack images are acquired every 30 seconds during a 10 minute timelapse experiment. Figure adapted from Lotterberger et al. 2015. (B) Examples of mCherry-53BP1 traces in TRF2^{F/F} 53BP1^{-/-} cells expressing the indicated mutant 53BP1 alleles, as described in A. (C) The MSD calculated from the traces of mCherry-BP1-2 foci from 3 independent experiments as described in A. (D) Percent of cells discarded from the analysis by the parameters described in 2.2.4. Values represent mean and SD from the 3 experiments from C and differences are not significant.

Mean Square Displacement (MSD) measured from the track lengths (Fig. 2.9b). Movies were 10 minutes long and the tracks were analyzed from 2D-maximum intensity projected images since MEF nuclei are flat (2-4 μm in z compared to 15-20 μm in x and y). The resulting traces can be corrected for nuclear rotation and movement, but large-scale nuclear deformations, such as expansion, contraction or twisting can confound the results. Therefore, cells showing extensive distortion were discarded from the analysis according to parameters described in Lottersberger et al. 2015 (Lottersberger et al., 2015). Briefly, extensive distortion was measured by a shift in the geometrical center of the nucleus. Expansion and contraction of nucleus was measured by the maximal difference between the average distances of the foci from the geometrical center. For example, in an expanding nucleus all foci would increase their distance from the geometrical center. A folding or twisting nucleus was measured as groups of foci all moving in the same direction. Arbitrary parameters were set for all these conditions and cells were discarded based on whether their parameters were outside the set thresholds. In most experiments, approximately half the nuclei passed the selection criteria and were used for the mobility analysis. DNA damage induction and 53BP1 status did not affect the frequency of discarded cells (Fig. 2.9d).

As expected, cells expressing 53BP1^{WT} displayed the expected DNA damage induced chromatin mobility with an MSD of 0.35 μm^2 that is consistent with previous measurements (Fig. 2.9c). The 53BP1 ^{$\Delta 28$} allele was defective and

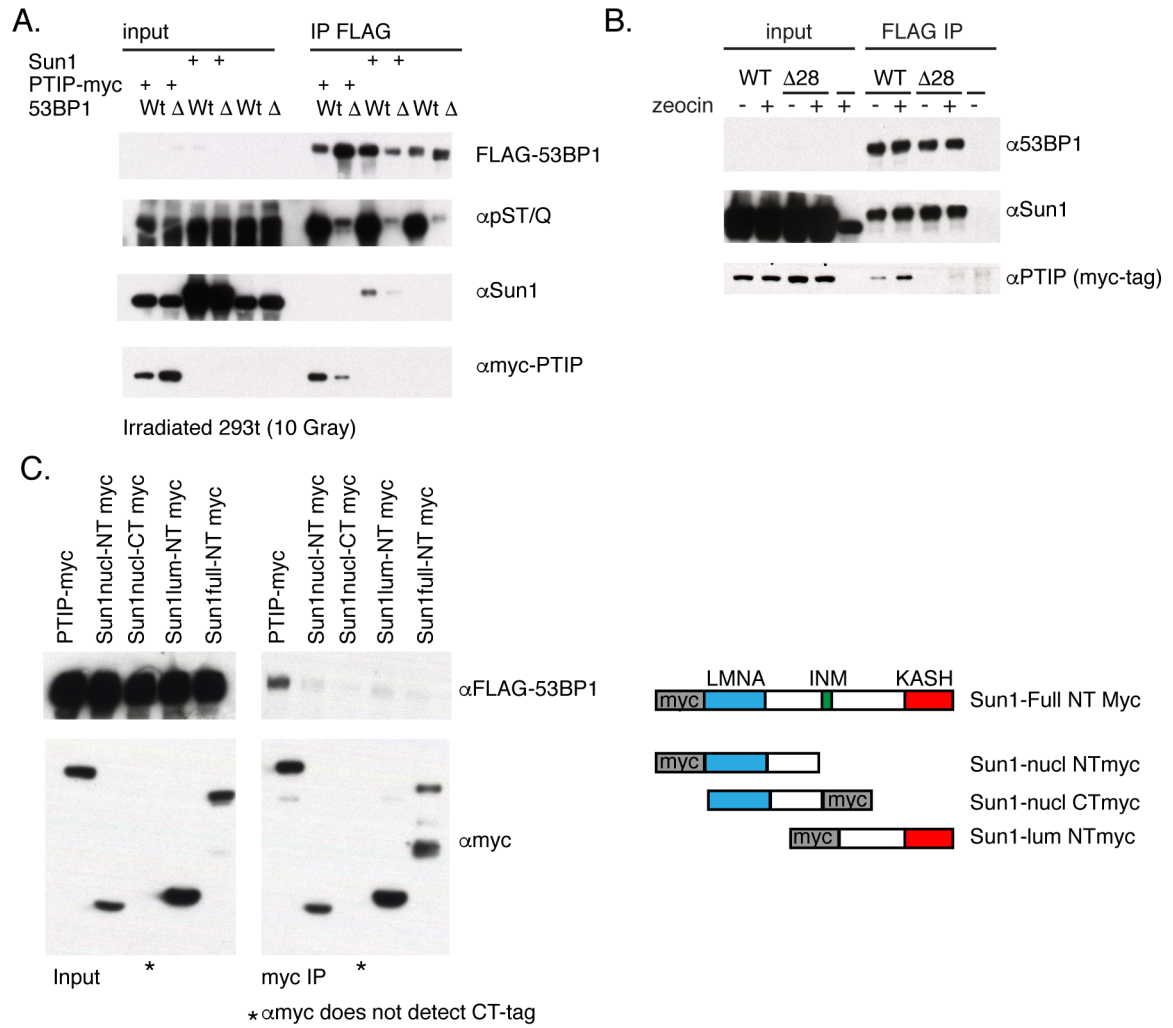
similar to an empty vector control showed an MSD of $0.25 \mu\text{m}^2$. Interestingly, the MSD of $53\text{BP1}^{\Delta\text{MOB}}$ was also $0.25 \mu\text{m}^2$, similar to $53\text{BP1}^{\Delta 28}$ and the empty vector control, indicating that this mutant has a complete defect in inducing chromatin mobility (Fig. 2.9c). Together with the c-NHEJ results from LINC complex deficient cells, the data argue that $53\text{BP1}^{\Delta\text{MOB}}$ indeed contains mutations in the residues needed to promote chromatin mobility. Furthermore, $53\text{BP1}^{\Delta\text{PTIP}}$ had no effect on stimulating chromatin mobility indicating that the mild fusion defect seen with this mutant is due to a different function of 53BP1 (Fig. 2.7c).

2.2.5 No interaction detected between Sun1 and 53BP1

Although the experiments described above argue that $53\text{BP1}^{\Delta\text{MOB}}$ harbors the S/TQ sites needed to promote mobility, it is unknown how 53BP1 connects to the LINC complex on a molecular level. Previous experiments in the lab have shown that Sun1 and Sun2 are redundant and therefore only the interaction with Sun1 was tested. To investigate whether an interaction exists between Sun1 and 53BP1, co-IP experiments were carried out in 293T cells overexpressing Sun1 and FLAG-tagged 53BP1^{WT} or $53\text{BP1}^{\Delta 28}$. Overexpressed myc-PTIP was used as positive control. Cells were irradiated or treated with zeocin to induce DNA damage signaling and phosphorylation of 53BP1. An IP was performed using antibodies against FLAG to pull down 53BP1 together with its interacting factors (Fig. 2.10a and b). The results were inconclusive. An interaction was seen between 53BP1 and Sun1 in some but not all experiments (compare Fig. 2.10a

Figure 2.10 Interaction between 53BP1 and Sun1 is not consistently detected

(A) Co-IP of 53BP1, Sun1 and myc-PTIP in 293T cells using FLAG antibody. FLAG tagged 53BP1, Sun1 and myc-PTIP were transiently expressed in 293t cells. After irradiation with 10Gray, a co-IP was performed using FLAG antibodies and interacting factors visualized by western blot with myc and Sun1 antibodies. An antibody against phosphorylated S/TQ sites was used to demonstrate 53BP1 phosphorylation. (B) Co-IP of 53BP1, Sun1 and myc-PTIP in 293T cells using FLAG antibody. FLAG tagged 53BP1, Sun1 and myc-PTIP were transiently expressed in 293T cells. After treatment with/without zeocin, a co-IP was performed using FLAG beads and interacting factors detected by western blot with myc and Sun1 antibodies. (C) Co-IP of 53BP1, myc-Sun1 and myc-PTIP in 293T cells using myc antibody. FLAG tagged 53BP1, Myc-tagged truncated Sun1 constructs and myc-PTIP were transiently expressed in 293T cells. After IP with myc reactive antibody, interacting factors were visualized by immunoblot with 53BP1 and myc specific antibodies. Schematics of the Sun1 constructs are drawn on the right. The full length Sun1 construct is indicated at the top with LMNA interaction domain (blue), transmembrane domain (green) and KASH domain (red) shown.



and b). There was a correlation between the overexpression levels of Sun1 and the amount recovered in co-IP suggesting that this might be non-specific binding of Sun1 to the beads. The positive control, myc-PTIP, was pulled down specifically by 53BP1^{WT} but not 53BP1^{Δ28} in a zeocin inducible manner indicating that the experimental setup was correct (Fig. 2.10a and b). To try to minimize non-specific binding of Sun1, different wash buffers and magnetic beads were used but the results remained inconclusive (see materials and methods for details).

The reverse IP reaction was also attempted, using antibodies against the myc-tag and western blotting for FLAG-53BP1 (Fig. 2.10c). The positive control, myc-PTIP, was pulled down with 53BP1, but an interaction was not observed with myc-Sun1. In these experiments, truncated versions of Sun1 were used in addition to the full-length protein. Both a nuclear and luminal Sun1 mutant were used, both lacking the transmembrane domain and thus soluble (Fig. 2.10c). Possibly, the soluble nuclear truncation mutant of Sun1 interacts more strongly with 53BP1 due to its localization throughout the nucleus. A luminal version of Sun1 was used as a negative control since the interaction between 53BP1 and Sun1 is not expected in the perinuclear space between INM and ONM. A potential caveat to this experiment is that the nuclear or luminal localization of these constructs was not verified. However, an interaction was not observed between these constructs and 53BP1.

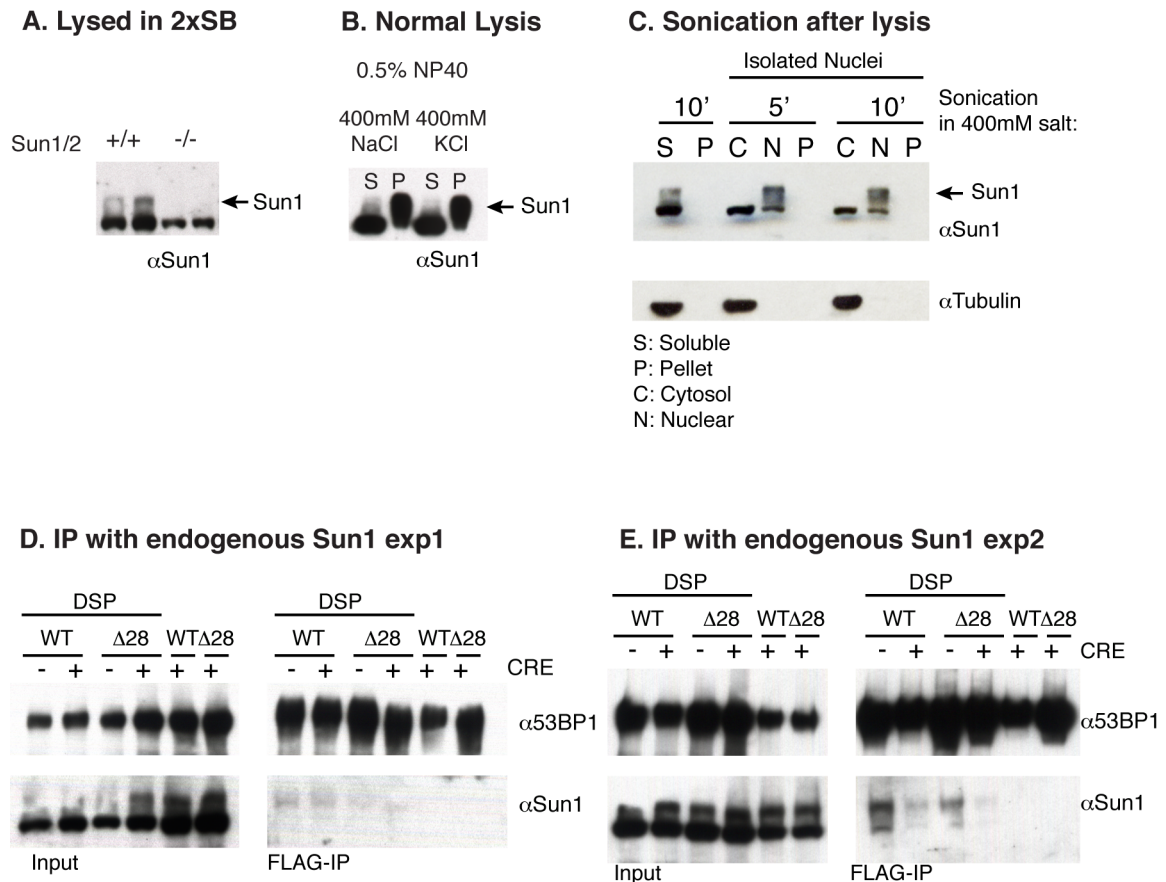


Figure 2.11 Interaction between 53BP1 and endogenous Sun1 in MEFs

(A) Levels of endogenous Sun1 in MEFs lysed in 2x sample buffer. The MEFs are either TRF1^{F/F}53BP1^{-/-}Sun1^{+/+}Sun2^{+/+} or TRF1^{F/F}53BP1^{-/-}Sun1^{+/+}Sun2^{+/+} as indicated. Two samples of each MEF line were analyzed on western blot stained with a Sun1 reactive antibody. (B) Immunoblot of TRF1^{F/F} MEFs lysed in 0.5% NP40 and high salt concentrations (see materials and methods for further details). Sun1 presence in soluble (S) and Pellet (P) fraction was visualized by immunoblot with a Sun1 specific antibody. (C) Immunoblot of TRF1^{F/F} MEFs lysed in high salt lysis buffer with/without prior isolation of nuclei as indicated. Lysate was sonicated for 5 or 10 minutes. Sun1 extraction in the indicated fractions was visualized by western blot with Sun1 specific antibody. Immunoblot for tubulin suggests correct separation of fractions. (D) Co-IP of 53BP1 and Sun1 using FLAG-beads from TRF2^{F/F}53BP1^{-/-} MEFs expressing the indicated 53BP1 allele with a 3xFLAG tag at its C-terminus. Cells were harvested 72 h after Cre mediated deletion of TRF2 or untreated control cells. MEFs were treated with/without DSP crosslinker prior to lysis and sonication for 5 minutes as in C. A co-IP was performed using magnetic FLAG beads and interacting factors detected by western blot with Sun1 and 53BP1 specific antibodies. (E) Same experiment as in D, only now minimal interaction is seen between Sun1 and 53BP1.

Since co-IP experiments with overexpressed Sun1 were unconvincing, the experiments were carried out with endogenous Sun1 in MEFs. The rationale for these experiments was that overexpressed nuclear envelope proteins often accumulate in other cellular compartments where an interaction with 53BP1 might not be found. However, extraction of endogenous Sun1 is difficult since it is not released in most common lysis buffers, unless 2xSample buffer is used (Fig. 2.11a and b). Different approaches were tested and the most consistent release of Sun1 was found when nuclei were isolated and subsequently lysed in a high salt lysis buffer followed by brief sonication (Fig. 2.11c). Cells were briefly treated with dithiobis(succinimidylpropionate) (DSP) prior to IP, a reversible crosslinker that reacts with primary amines in lysine residues to form stable amide bonds (Lomant and Fairbanks, 1976). The DSP crosslinker was used to increase the IP strength in case the interaction is transient. The addition of the reducing agent dithiothreitol (DTT) to the sample buffer prior to western blot removes the crosslinks to allow separation of proteins by SDS page. Furthermore, for these experiments 3xFLAG tagged 53BP1 constructs were used to increase the efficiency of the co-IP. The indicated 53BP1 constructs were overexpressed in TRF2^{F/F}53BP1^{-/-} cells, which were treated with Cre 72 h prior to harvest. To reduce potential background binding due to pelleting of large complexes, magnetic anti-FLAG beads were used. However, an interaction between 53BP1 and Sun1 was still not consistently observed (Fig. 2.11d and e).

2.2.6 Exploring a role for known 53BP1 interacting partners in chromatin mobility

It is possible that the interaction between 53BP1 and the LINC complex is either transient or indirect, explaining why co-IP experiments failed to show an interaction. To test whether known interaction partners of 53BP1 are involved in chromatin mobility, a candidate list of proteins from a proteomics screen in B-cells was examined (Di Virgilio et al., 2013). Several Coiled-Coil Domain-Containing (CCDC) proteins are found on this list, including CCDC124, CCDC9 and CCDC79. This is of interest given that during meiosis, CCDC proteins connect telomeres to Sun1 (Shibuya et al., 2014). To test whether any of these proteins are involved in 53BP1 mediated chromatin mobility, shRNAs were used to knockdown CCDC124, CCDC9 or CCDC79 in TRF2^{F/F} cells and telomere fusions assessed 96 h after deletion of TRF2. Although the level of knockdown was not assessed, none of the shRNA yielded a significant reduction in c-NHEJ upon deletion of TRF2 (Fig. 2.12a and b). For CCDC9, a small reduction was seen but knockdown of this protein significantly affected cell growth. Since telomere fusions are a cumulative phenotype, the reduced cell growth is expected to decrease telomere fusions and the results with the shCCDC9 are therefore inconclusive. The shRNA against CCDC79 was also toxic to cells and resulted in endoreduplication. Telomere fusions were therefore not assessed.

Another protein that surfaced in the proteomics screen for 53BP1 is TopBP1. Despite the potentially confounding roles of TopBP1 in the ATR mediated DNA damage response pathway and DNA replication, the effect of

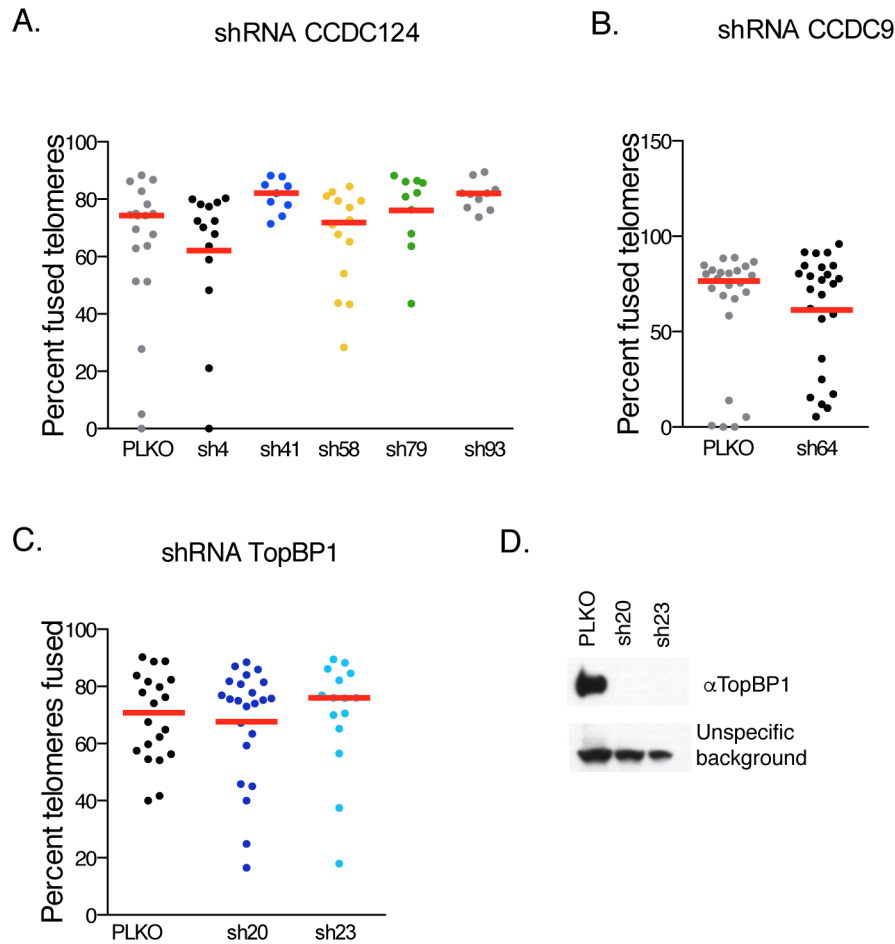


Figure 2.12 Telomere fusions upon depletion of potential 53BP1 and Sun1 interaction partners

(A) Frequency of telomere fusions in TRF2^{F/F} MEFs after shRNA mediated depletion of CCDC124. Five independent shRNAs were used. Metaphase spreads were analyzed 96 h after deletion of TRF2. Each dot represents a metaphase spread and bars represent the median % of telomeres fused in one experiment. (B) Frequency of telomere fusions in TRF2^{F/F} MEFs after shRNA mediated depletion of CCDC9. Metaphase spreads were analyzed 96 h after deletion of TRF2. Bars represent the median % of telomeres fused in one experiment. (C) Frequency of telomere fusions in TRF2^{F/F} MEFs after shRNA mediated depletion of TopBP1. Metaphases were analyzed 96 h after deletion of TRF2. Bars represent the median % of telomeres fused in one experiment. (D) Western blot from TRF2^{F/F} MEFs after depletion of TOPBP1. Cells were harvested 72 h after deletion of TRF2 and shRNA effectiveness analyzed with a TOPBP1 specific antibody.

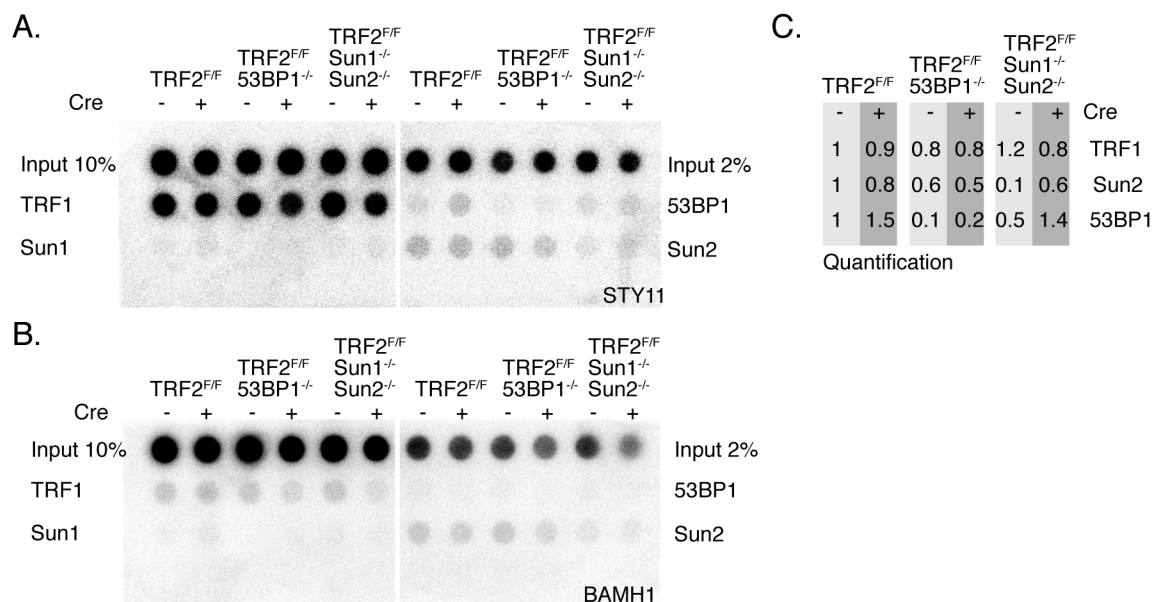


Figure 2.13 Telomere CHIP

(A) Telomere ChIP performed in the indicated MEFs (top) 72 h after deletion of TRF2. ChIP was done with the antibodies indicated on either sides and recovered telomeric DNA visualized by dot-blot using a telomere specific probe (Sty11, TTAGGG). (B) ChIP samples from A were hybridized on dot-blot with a BAMH1 probe to control for unspecific binding. (C) Quantification of the recovered telomeric DNA in ChIP from A. Signals of telomeric DNA recovered with indicated antibodies were normalized to the input and are given relative to the signal in no-Cre TRF2^{F/F} cells. The Sun1 antibodies did not result in a ChIP signal and was therefore not quantified.

shRNA-mediated knockdown of TopBP1 was analyzed (Kumagai et al., 2006)(Delacroix et al., 2007),. Whereas the knockdown of TopBP1 was efficient, no reduction in telomere fusions was observed indicating that TopBP1 is not required for NHEJ of telomeres depleted of TRF2 and thus is unlikely to constitute the link between 53BP1 and the LINC complex (Fig. 2.12c and d).

In a final attempt to show an interaction between 53BP1 and the LINC complex, a telomeric chromatin immunoprecipitation (CHIP) experiment was done using Sun1 or Sun2 specific antibodies. As a positive control, antibodies against TRF1 and 53BP1 were used. Whereas a DNA damage inducible accumulation of 53BP1 was seen at telomeres, there was no increase in telomeric DNA seen with Sun2 specific antibodies (Fig. 2.13a-c) and the Sun1 ChIP failed altogether. It thus remains unclear how 53BP1 connects to the LINC complex.

2.2.7 Oligomerization domain of 53BP1

The C-terminus of 53BP1 contains an oligomerization domain that is required for efficient IR-induced focus formation, although chromatin binding itself is partially retained (Zgheib et al., 2009; Bothmer et al., 2011). The oligomerization domain is also crucial for CSR in B cells but at dysfunctional telomeres, NHEJ is only partially affected when this domain is deleted (Lottersberger et al., 2013). It was previously shown that the oligomerization domain does not affect the ability of

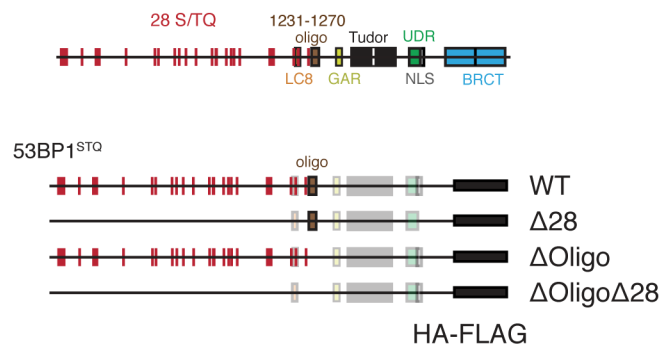
53BP1 to protect against resection and does not affect the mobility of dysfunctional telomeres (Lottersberger et al., 2013).

To further understand the role of the oligomerization domain at dysfunctional telomeres, a mutant 53BP1 allele was made in which the oligomerization domain was deleted and the N-terminal S/TQ sites mutated to alanine (53BP1^{ΔOligoΔ28}) (Fig. 2.14a). This mutant and the control 53BP1 alleles were expressed in TRF2^{F/F}53BP1^{-/-} cells and resection and telomere fusions analyzed after Cre mediated deletion of TRF2 (Fig. 2.14b). As expected, 53BP1^{ΔOligoΔ28} behaved similar to 53BP1^{Δ28} with regards to blocking resection since the interaction with Rif1 is lost in both mutants (Fig. 2.14c and d). The overhang signal increased 2.5 fold upon expression of either 53BP1^{ΔOligoΔ28} or 53BP1^{Δ28} similar to the empty vector control. Next, telomere fusions were analyzed on metaphase spreads. Interestingly, NHEJ was more strongly affected in cells expressing the 53BP1^{ΔOligoΔ28} mutant compared to 53BP1^{ΔOligo} or 53BP1^{Δ28} as telomere fusions in the 53BP1^{ΔOligoΔ28} expressing cells were reduced to levels similar to empty vector control (Fig. 2.15). In contrast, cells expressing the 53BP1^{Δ28} allele show residual telomere fusions with a small percentage of metaphases containing significant telomere fusions (20-60% telomeres fused) even though the median remains below 10% when analyzed 96 h after deletion of TRF2. These cells with higher levels of telomere fusions are never observed in empty vector control cells and are also not observed in cells expressing 53BP1^{ΔOligoΔ28}.

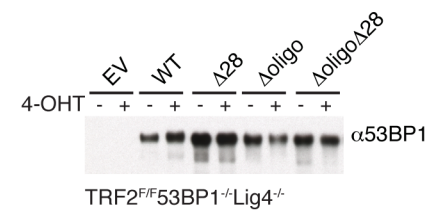
Figure 2.14 53BP1 oligo mutants

(A) Schematic of 53BP1 oligo mutants. (B) Western blot control for the equal expression level of the 53BP1 oligo alleles and the deletion of TRF2. Cells were harvested 72 h after deletion of TRF2 and antibodies against 53BP1 and TRF2 were used. C. Telomere overhang assay of Mbol/Alul digested DNA from TRF2^{F/F}Lig4^{-/-}53BP1^{-/-} MEFs expressing the indicated 53BP1 alleles. Telomeric DNA was analyzed 96 h after Cre-mediated deletion of TRF2 using the in-gel hybridization assay (Fig. 2.5). Left panel shows native telomeric ssDNA signal, right panel displays the denatured total amount of telomeric DNA. (D) Quantification of the overhang signal from three independent experiments. Only the values from the Cre-treated samples are shown. Numbers were obtained by normalizing the native ssDNA signal to the total telomeric DNA signal in the same lane in the denatured gel. The values of the Cre-treated samples were obtained by comparison with the untreated control samples, which were set to 1.0. Means with SD from three independent experiments are shown. P-values were determined compared to WT by a two-sided Student's t-test (* p<0.05, ns = non significant)

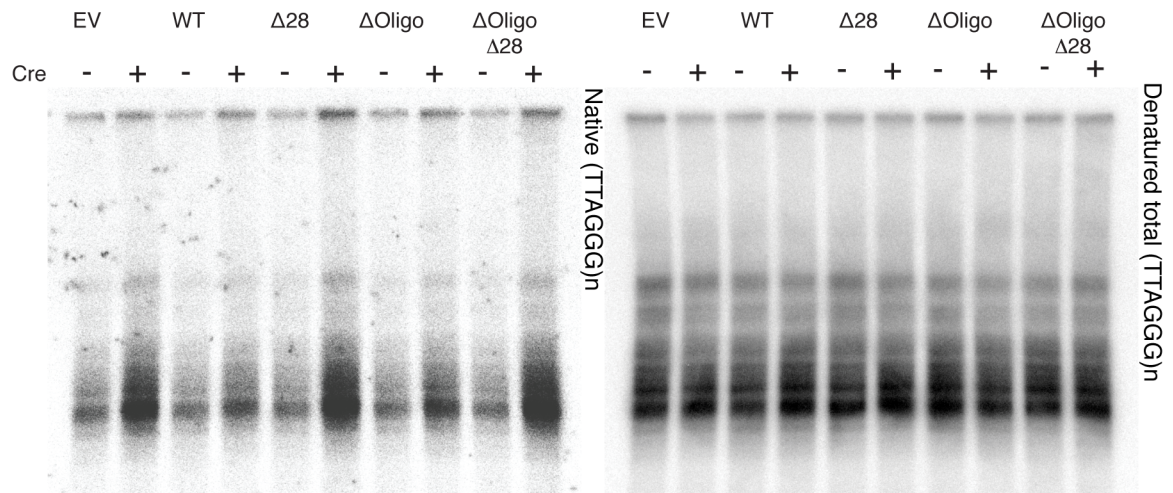
A.



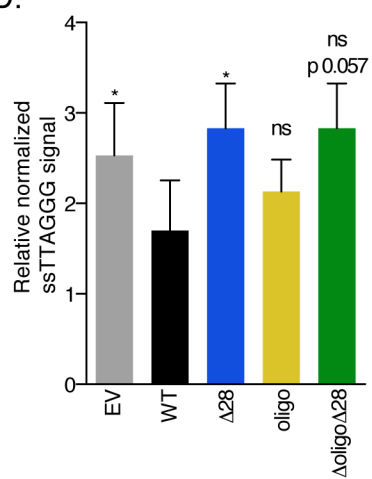
B.



C.



D.



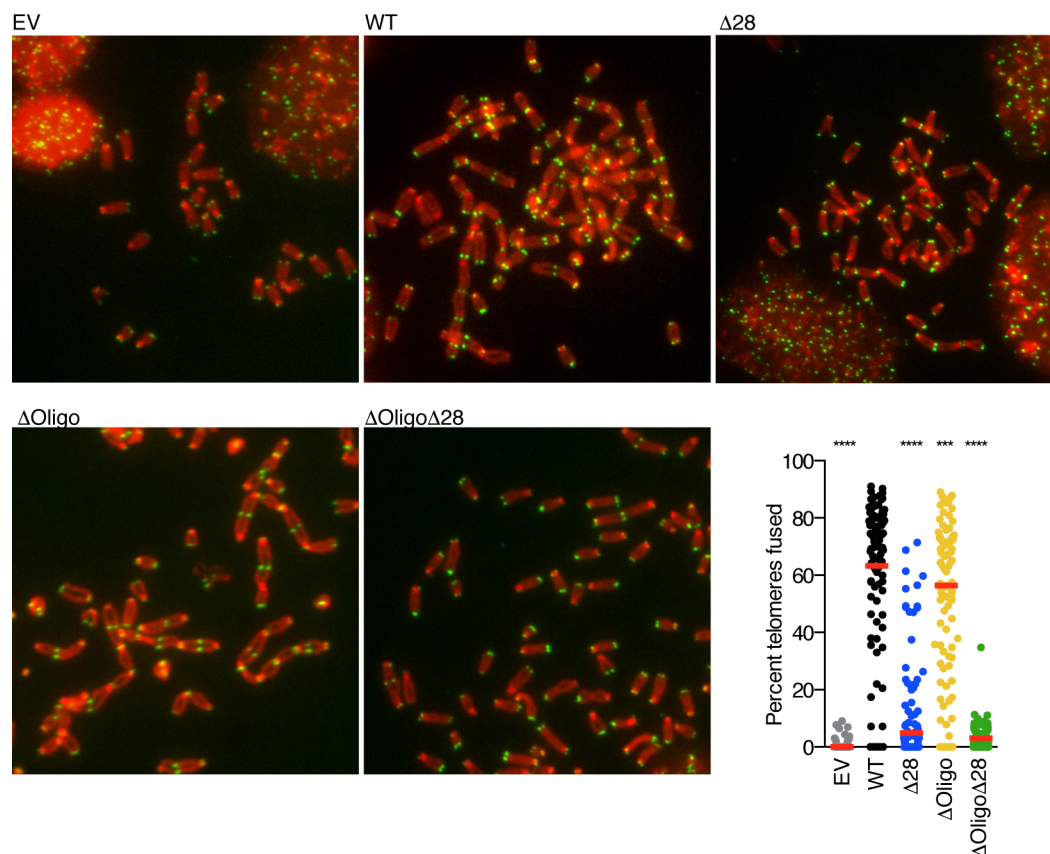


Figure 2.15 Telomere fusions in MEFs expressing oligo mutants

Example of metaphase spreads from TRF2^{F/F}53BP1^{-/-} MEFs, expressing the indicated 53BP1 allele. Cells were harvested 96 h after Cre-mediated deletion of TRF2. Metaphase spreads were stained with DAPI (red) and a telomeric TelG FISH probe (green). Quantification of the level of telomere fusions is shown on the right. Bars represent median % of telomere fusions from 4 independent experiments, each dot represents a metaphase spread. P-values were determined compared to WT with a two-sided Student's t-test (* p<0.05, ** p<0.01, *** p<0.001).

Interestingly, this reduction in NHEJ appeared to be due to an inability of 53BP1^{ΔOligoΔ28} to form foci at telomeres as shown in Fig. 2.16a (left panel). Whereas the localization of 53BP1^{ΔOligo} to telomeres was somewhat reduced compared to wild type 53BP1, the 53BP1^{ΔOligoΔ28} mutant failed to localize effectively explaining the behavior similar to the empty vector control. Of interest, whereas 53BP1^{ΔOligo} recruitment to dysfunctional telomeres was only mildly disrupted, it could not localize to IR induced foci suggesting an alternative mode of localization to telomeres (Zgheib et al., 2009; Lottersberger et al., 2013).

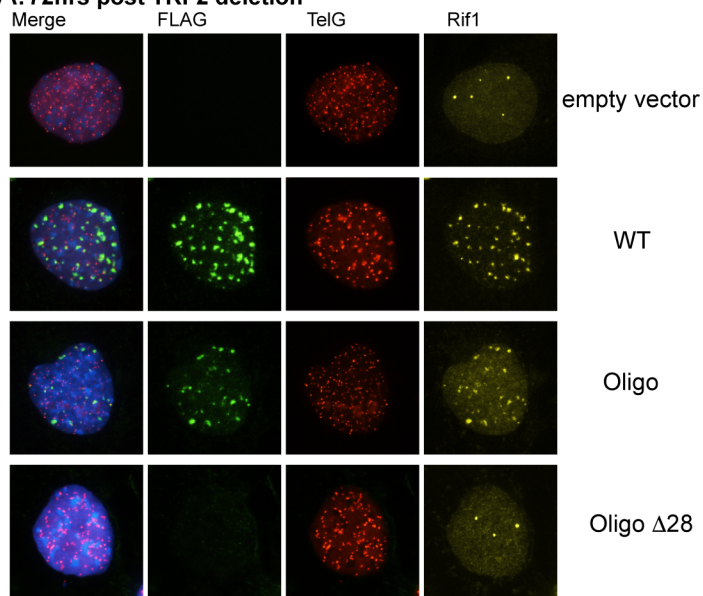
To further validate these results, TRF2^{F/F} 53BP1^{-/-} cells expressing the mutant 53BP1 alleles were irradiated and recruitment to γH2AX-marked sites was analyzed 30 min later by IF (Fig. 2.16a, right panel). Upon irradiation, neither 53BP1^{ΔOligo} nor 53BP1^{ΔOligoΔ28} was efficiently recruited to DSBs in agreement with published experiments (Zgheib et al., 2009). Thus, whereas the oligomerization domain is necessary for foci formation at IR-induced DSBs, 53BP1 can use an alternative method to localize to telomeres in absence of the oligomerization domain, and this recruitment requires a phosphorylation dependent interaction partner of 53BP1.

To analyze which S/TQ sites might be required for localization of 53BP1 to telomeres in absence of the oligomerization domain, a second subset of mutant alleles was made with clusters of the S/TQ sites mutated to alanine (Fig. 2.16b). These mutants were made prior to identification of the proper Rif1 binding site but domain 2 and 3 contain the required sites for Rif1 binding, as explained in

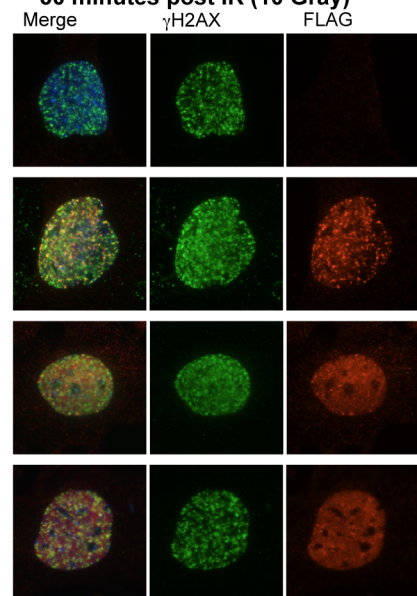
Figure 2.16 Localization of 53BP1 oligo mutants to telomeres is affected

(A) IF-FISH images of TRF2^{F/F}53BP1^{-/-} MEFs expressing the indicated 53BP1 construct. Left panel shows recruitment of 53BP1 (FLAG tag, green) to telomeres (red) 72 h after deletion of TRF2, recruitment of Rif1 is shown in yellow. The right panel shows the foci formation of the 53BP1 alleles (FLAG tag-red) 30 minutes after treatment with IR (10Gray). Staining for γ H2AX (green) indicates IR induced DSB formation. (B) Schematic of additional 53BP1 oligo mutants created with subsets of the S/TQ sites mutated to alanine, similar to Fig. 2.3. (C) IF-FISH images of TRF2^{F/F}53BP1^{-/-} MEFs expressing the additional 53BP1 constructs after deletion of TRF2 (left) or IR (right), with the same experimental conditions as in A. (D) Quantification of 53BP1 recruitment to telomeres 72 h after deletion of TRF2. The percentage of cells with >5 53BP1 foci at telomeres is shown, the values represent the mean and SEM from 2 independent experiments.

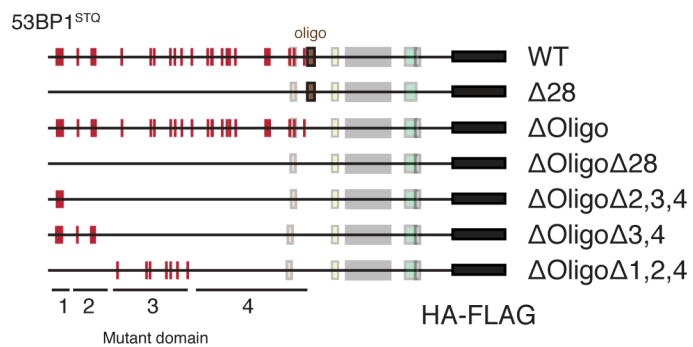
A. 72hrs post TRF2 deletion



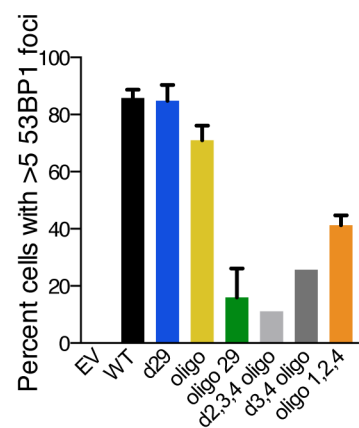
30 minutes post IR (10 Gray)



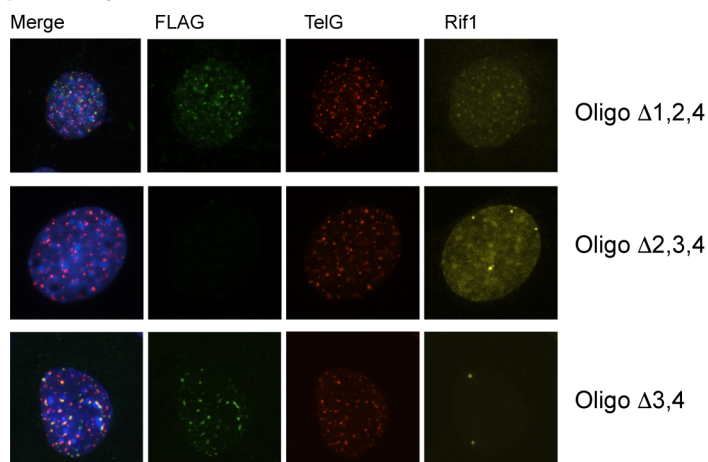
B.



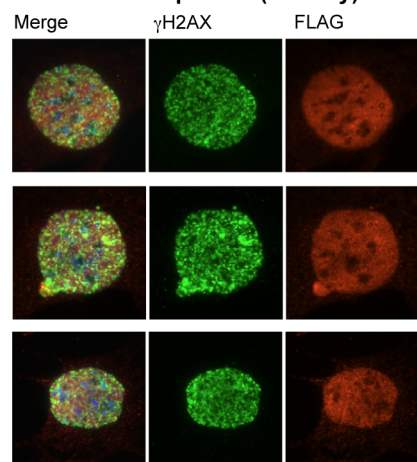
D. 53BP1 recruitment to telomeres



C. 72hrs post TRF2 deletion



30 minutes post IR (10 Gray)



Figures 2.2.1 and 2.3. Localization of these constructs to telomeres after deletion of TRF2 was analyzed via IF-FISH (Fig. 2.16c and d). Preliminary data indicates that the S/TQ sites needed for Rif1 binding are also required for localization of 53BP1 to dysfunctional telomeres in absence of the oligomerization domain since the mutant lacking S/TQ sites in both domain 2 and 3 showed deficient 53BP1 recruitment (Fig. 2.16c and d). However, these are very preliminary results, which need to be repeated before any conclusion can be made. Repeating this experiment in a Rif1 deficient and proficient setting would ascertain that this phenotype is dependent on Rif1 and not another interacting factor of 53BP1.

2.3 Summary of findings

The creation of a panel of mutant 53BP1 alleles enabled analysis of the function of 53BP1 interaction partners in DNA repair at telomeres lacking TRF2. The results indicate that the S/TQ domain needed for the Rif1 interaction is the only domain required for inhibiting end resection downstream of 53BP1 (Fig. 2.6). However, the 53BP1^{ΔRIF1} allele was not tested in TRF2^{F/F}53BP1^{-/-}Rif1^{-/-} cells. Thus even though the results suggest that Rif1 is the only factor downstream of 53BP1 required for blocking end resection, this cannot be fully confirmed based on these experiments. Furthermore, the results suggest that PTIP is not required to control end resection at telomeres since 53BP1^{ΔPTIP} behaved as a wild type allele in telomere overhang assays. Even though PTIP does not have a role in preventing hyper resection, the telomere fusions are slightly delayed in cells

expressing 53BP1^{ΔPTIP} (Fig. 2.7). It is possible that this reduction is due to the role of PTIP in recruiting the Artemis nuclease that is required for end-trimming of obstructed ends (Wang et al., 2014). Possibly, a subset of telomeres requires Artemis mediated processing before NHEJ can occur explaining the lower levels of telomere fusions in absence of PTIP.

The results also describe a separation of function mutant of 53BP1 that is deficient in inducing chromatin mobility. Cells expressing the 53BP1^{ΔMOB} allele failed to induce chromatin mobility in live cell imaging experiments and had lower levels of telomere fusions (Fig. 2.7 and 2.9). Furthermore, the reduction in telomere fusions was absent in cells lacking SUN1/SUN2 indicating that 53BP1^{ΔMOB} lacks activity in the same pathway as the LINC complex, confirming that this domain contains the S/TQ sites that are required for mobility (Fig. 2.8). Importantly, 53BP1^{ΔMOB} had no effect on resection, firmly placing chromatin mobility in a NHEJ-promoting pathway separate from resection (Fig. 2.6).

Unfortunately, attempts to show an interaction between the LINC complex and 53BP1 were unsuccessful. Possibly, the interaction is transient and therefore difficult to detect. Furthermore, antibodies against endogenous LINC complex components are not very effective, hindering co-IP experiments.

Lastly, experiments using the 53BP1^{ΔOligoΔ28} mutant suggest that 53BP1 has a unique mechanism to efficiently accumulate at dysfunctional telomeres. Whereas the oligomerization domain is required for optimal recruitment to IR-induced DSBs, this domain is dispensable at telomeres. However, a mutant

lacking the oligomerization domain in combination with mutated S/TQ sites no longer binds to dysfunctional telomeres (Fig. 2.16). These experiments suggest that a 53BP1 interaction partner can replace the function of the 53BP1 oligomerization domain for accumulation at dysfunctional telomeres but not at other sites of DNA damage. Preliminary data indicate that it might be Rif1 that is required for this function, but further studies are needed to confirm this.

**Chapter 3: The nature of telomere sister associations formed
upon loss of TRF1**

3.1 Introduction

The main role for TRF1 at telomeres is to aid progression of the replication fork. The telomeric TTAGGG repeat sequence represents a problem for the replication machinery since the G-rich strand has the tendency to form G-quadruplexes (G4), a secondary structure held together by Hoogsteen hydrogen bonds (Henderson et al., 1987). In absence of TRF1, replication forks often stall in the telomeric repeat array resulting in activation of the ATR signaling cascade (Martinez et al., 2009; Sfeir et al., 2009). Fork stalling also occurs when the telomeric sequence is located internally in chromosomes, further indicating that the DNA sequence itself forms a problem for the replication machinery (Miller et al., 2006; Bosco and de Lange, 2012). One consequence of TRF1 deletion is the appearance of fragile telomeres, which appear as multiple telomeric signals on chromosome ends in staining on metaphase spreads (Sfeir et al., 2009). Fragile telomeres are thought to be similar to the breaks and gaps seen on metaphase spreads at Common Fragile Sites (CFSs), which are regions of the genome that are difficult to replicate and show 'broken' chromatin in metaphase cells after treatment with aphidicolin (Hecht and Glover, 1984). Low dose aphidicolin treatment induces the appearance of fragile telomeres similar to the expression CFSs. TRF1 was shown to recruit BLM and possibly the RTEL1 helicase to prevent G4-formation and fork stalling and aid the replication machinery (Sfeir et al., 2009). A TRF1 mutant lacking the BLM interaction site displays increased levels of fragile telomeres (Zimmermann et al., 2014). This fragility was observed

primarily on telomeres formed by lagging strand DNA synthesis (lagging end telomeres) indicating that BLM specifically functions to remove secondary structures formed by the TTAGGG repeat array which is the template for lagging strand DNA synthesis. However, loss of TRF1 results in both leading and lagging strand fragility and how leading strand telomere fragility is prevented by TRF1 is still unknown. Possibly, the RTEL1 helicase is involved in preventing telomere fragility in the leading strand since BLM and RTEL1 prevent telomere fragility in an additive manner (Vannier et al., 2012). RTEL1 contains a PCNA interacting domain that is required for its ability to suppress telomere fragility but the molecular details and function of this interaction are not yet understood (Ding et al., 2004; Vannier et al., 2013).

A second phenotype observed after deletion of TRF1 is the formation of telomeric sister associations (SAs) (Martinez et al., 2009; Sfeir et al., 2009). These structures are visible on metaphase spreads as fused sister telomeres but their molecular nature remains unclear (Fig. 3.1). They are not dependent on c-NHEJ since an shRNA against Lig4 has no effect on their prevalence (Sfeir et al., 2009). It is possible that SAs are formed via a-NHEJ, a relatively recently described pathway that operates when core components of the c-NHEJ machinery are missing, such as Ku or Lig4 (Kabotyanski et al., 1998; Verkaik et al., 2002; Wang et al., 2003; Weinstock et al., 2007). In a-NHEJ, a DSB is recognized by PARP1, a step normally inhibited by Ku (Wang et al., 2006). A-NHEJ is furthermore thought to be dependent on microhomology at the junction

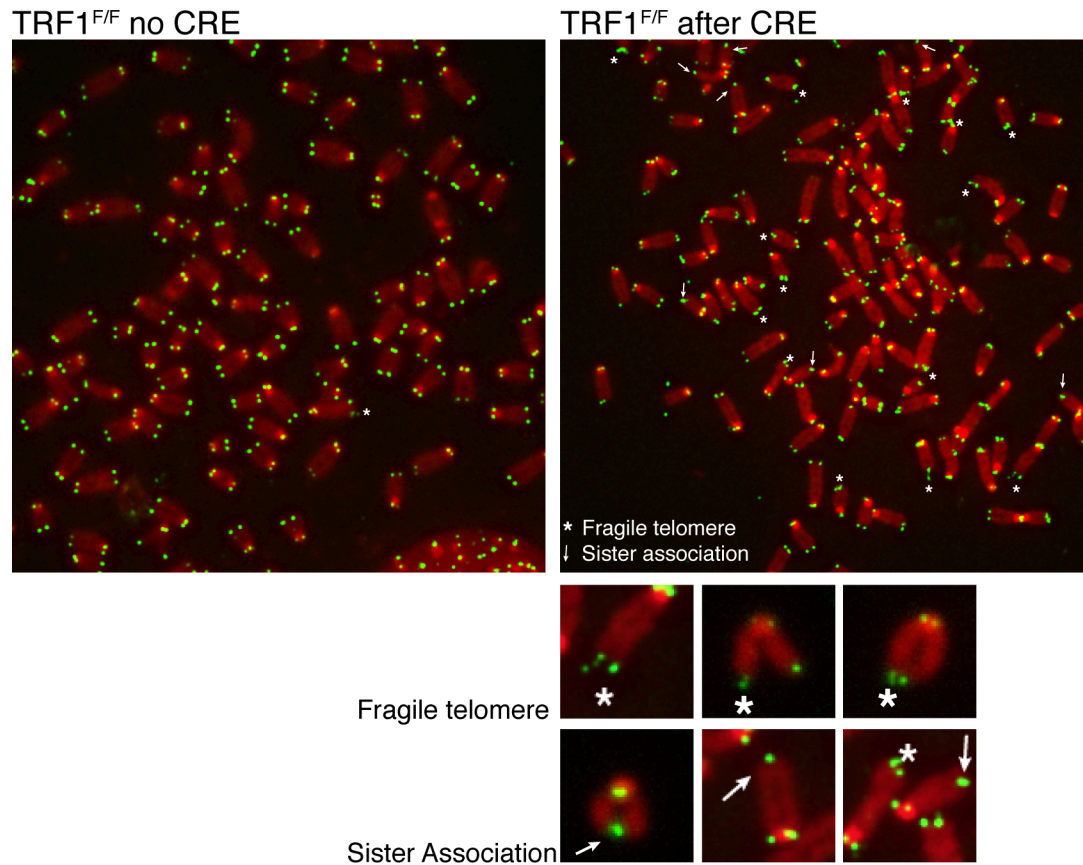


Figure 3.1 TRF1 deletion phenotype

Metaphase spreads of TRF1^{F/F} cells before (left) and 96 h after (right) Cre mediated deletion of TRF1. Telomeres are in green (TelC FISH) and chromosomes in red (DAPI). Fragile telomeres and sister associations are marked with an asterisk and arrow respectively. Enlargements are shown in the bottom right.

that is exposed upon limited resection by the MRN complex and CtIP (Truong et al., 2013). After annealing of the microhomology regions, fill-in synthesis occurs by Pol θ , which lacks proofreading capacity and is therefore prone to produce mutagenic insertions (Mateos-Gomez et al., 2015). Ligation of the DSB is independent of the c-NHEJ Lig4, but requires Lig3 or Lig1 instead (Frit et al., 2014). Deletions are frequently observed in a-NHEJ and the pathway is considered pathogenic and has been linked to chromosomal translocations in cancer cells (Simsek and Jasin, 2010).

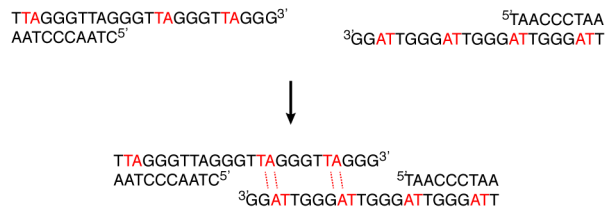
The telomeric 3' overhangs of the TTAGGG repeat strand have microhomology (2 bp/repeat) so that a-NHEJ could take place (Fig. 3.2a). Interestingly, analysis of telomere fusion junctions in human tumors revealed the presence of microhomology and fusions of critically short telomeres are dependent on Lig3 and the a-NHEJ (Letsolo et al., 2010; Lin et al., 2010; Jones et al., 2014). The molecular mechanism underlying these fusions is unknown and why they occur by a-NHEJ instead of c-NHEJ remains unclear. Under normal circumstances, a-NHEJ is strictly suppressed at telomeres by shelterin and Ku. However, in the absence of the entire shelterin complex and Ku, a-NHEJ takes place at telomeres as evidenced by chromosome type fusions dependent on Lig3 and Parp1 (Sfeir and de Lange, 2012; Mateos-Gomez et al., 2015). The a-NHEJ pathway can thus be activated at telomeres that lack shelterin protection.

However, if SAs were telomeres fused via a-NHEJ, a covalent linkage would be formed. Around 15-20% of chromosomes contain SAs after loss of

TRF1 and as a result, isochromosomes should appear in the next metaphase if a chromosome with sister fusions missegregates into one daughter cell and is replicated (Fig. 3.2b). However, isochromosomes are not readily detected upon deletion of TRF1 (Sfeir et al., 2009). It is therefore also possible that SAs represent a different structure. Possibly, they are non-covalent interactions resulting from replication intermediates formed upon fork stalling in the telomeric sequence.

SAs are not simply a consequence of telomere fragility since loss of BLM or expression of a TRF1 mutant lacking the BLM interaction domain does not induce SAs although telomere fragility is observed (Zimmermann et al., 2014). Instead, the prevalence of SAs appears to correlate with the level of ATR activation. TRF1 inhibits ATR activation through its association with TIN2, allowing TPP1/POT1 binding to the ssDNA that can arise at the replication fork (Zimmermann et al., 2014). When TRF1 is removed from telomeres, TIN2 is no longer effectively recruited to telomeres (Frescas and de Lange, 2014). However, some residual TIN2 remains at telomeres through its interaction with TRF2, and the associated TPP1 and POT1 are capable of protecting the 3' overhang since there is no evidence for a POT1 null phenotype when TRF1 is missing. But apparently, the residual TRF2 bound TIN2 is not enough to block replication associated ATR activation in cells lacking TRF1 since replication dependent ATR activation is observed at telomeres (Sfeir et al., 2009). By enforcing the interaction between TRF2 and TIN2, using a TIN2 fusion to the TRF2 binding

A. Microhomology within telomeres



B. Isochromosomes

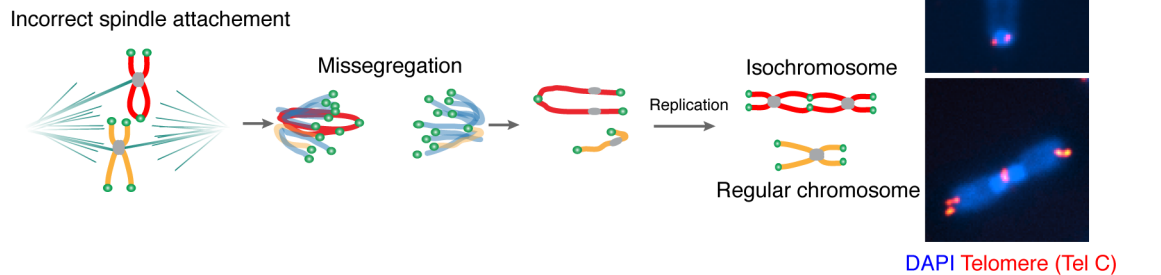


Figure 3.2 Sister telomere fusions

(A) Microhomology within telomeres. Two telomere ends are shown with potential microhomology shown in red. Upon 5' resection of the ends, the TA-AT nucleotides can anneal explaining how telomeres provide a substrate for a-NHEJ. (B) Model for the generation of an isochromosome from a sister telomere fusion. When an entire chromosome with sister fusion (red) is missegregated into one daughter cell, replication through the sister fusion in the next S-phase would result in the formation of an isochromosome. Examples of potential isochromosomes from MEF metaphases are shown on the right (DAPI in blue and telomeres in red (TelG)). Note, mouse chromosomes are acrocentric and the short arm thus appears to be absent.

domain of RAP1, the localization of TIN2 to telomeres after deletion of TRF1 is rescued. Expression of this TIN2 mutant completely represses the ATR activation upon loss of TRF1 indicating that replication associated ATR activation is blocked by TRF1 using TIN2 (and TTP1/POT1) (Zimmermann et al., 2014). Interestingly, expression of this TIN2 mutant in TRF1 null cells does not rescue telomere fragility whereas SAs are repressed (Zimmermann et al., 2014). This strongly suggests that SAs require ATR activation. In agreement with this, shRNA mediated knockdown of ATR represses SAs (Sfeir et al., 2009). However, ATR activation at telomeres by itself is not enough to induce SAs as only low levels of SAs are detected in a POT1 null setting (~3%), where ATR signaling occurs at most telomeres (Hockemeyer et al., 2006; Denchi and de Lange, 2007). Low levels of SAs are also observed after deletion of TPP1 (~3%) or TIN2 (~7%), presumably due to the loss of POT1a/b (Kibe et al., 2010; Takai et al., 2011; Frescas and de Lange, 2014). Thus, SAs require ATR activation but also a replication associated event that is normally repressed by TRF1 since much higher levels are seen after TRF1 loss (15%) compared to TIN2/TPP1/POT1 (3-7%). Possibly, the low levels of SAs observed upon loss of TIN2/TPP1/POT1 are due to residual replication stress at telomeres that occurs even when TRF1 is present.

In this chapter, I use a genetic approach to illuminate the nature of the telomere associations formed upon loss of TRF1.

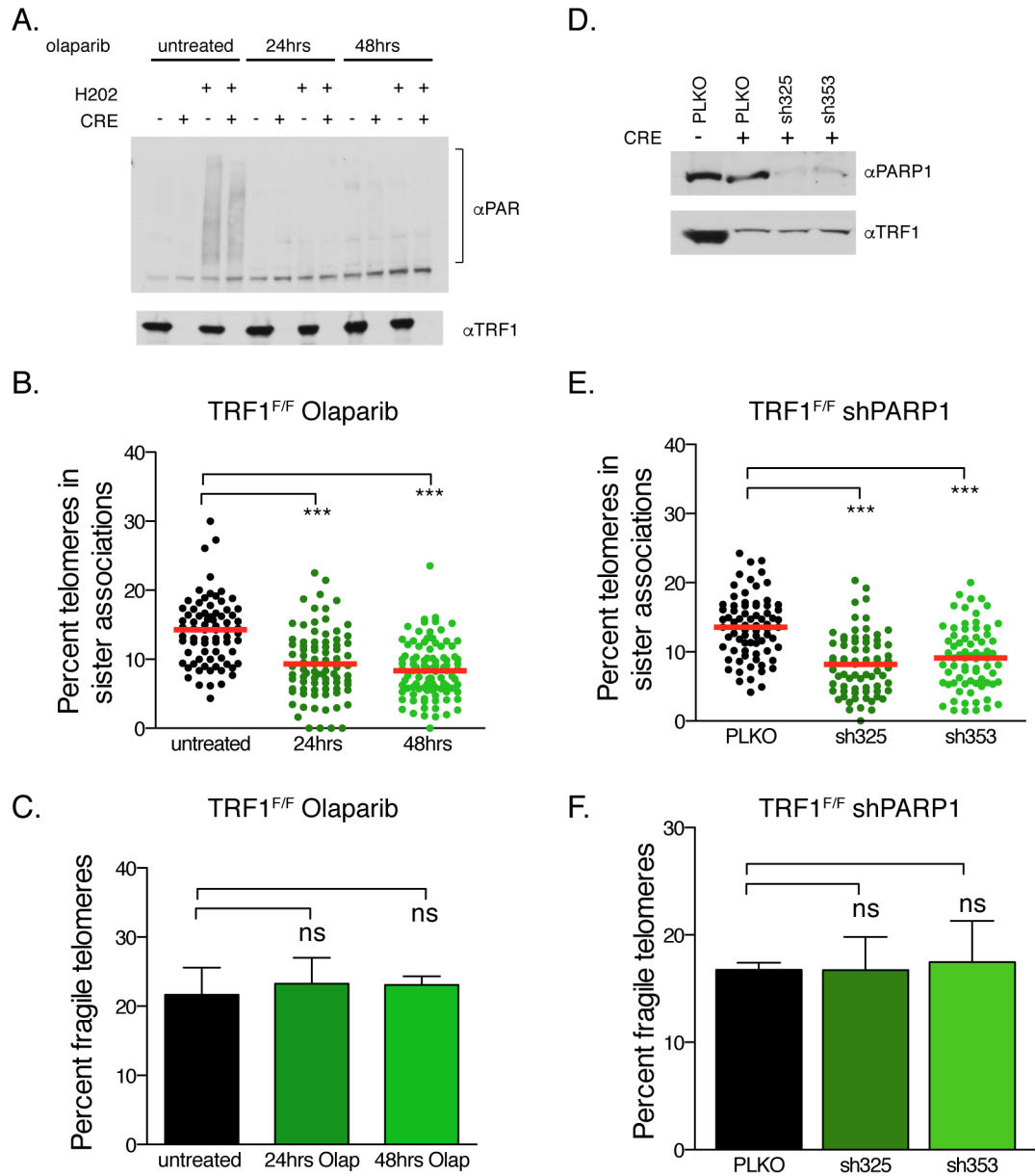
3.2 Results

3.2.1 PARP1 is required for Sister Associations

To examine whether the a-NHEJ pathway might create SAs, the role of PARP1 was tested. First, the PARP1 inhibitor (PARPi) olaparib was used to prevent PARP1 function. For this experiment, TRF1^{F/F} MEFs were first treated with Cre and olaparib was added for the final 24 or 48 h prior to harvest, and 96 h after deletion of TRF1. To test the efficacy of olaparib treatment, cells were briefly treated with H₂O₂, which produces robust PARsylation. Samples were analyzed by western blot and indeed, both 24 and 48 h of olaparib treatment completely abolished the H₂O₂ induced PARsylation indicating that the PARPi treatment worked (Fig. 3.3a). Metaphase spreads of cells treated with PARPi were analyzed and SAs and fragile telomeres scored 96 h after Cre mediated deletion of TRF1. Because the short arm of mouse chromosomes is too short to detect a separation of the arms, both SAs and fragility were scored on long arm chromosomes only for all experiments. Interestingly, PARPi treatment for 24 or 48 h significantly reduced the levels of SAs compared to untreated control cells from around 15% to 8% (Fig. 3.3b). Telomere fragility was not affected by PARPi and remained around 20% (Fig. 3.3c). To confirm that the reduction in SAs was due to PARP inhibition and not a side effect of the olaparib treatment, PARP1 was depleted using shRNA. Two different shRNAs were used and western blot analysis indicated knockdown of PARP1 (Fig. 3.3d). When metaphase spreads were analyzed 96 h after deletion of TRF1, a similar reduction in SAs was

Figure 3.3 PARP1 is required for the formation of SAs

(A) Western blot of TRF1^{F/F} MEFs treated with olaparib. Cells were harvested at 72 h after deletion of TRF1 with the indicated duration of olaparib (2 μ M) treatment. MEFs were treated with H₂O₂ prior to harvest when indicated and parylation and TRF1 deletion visualized on western blot with TRF1 and PAR reactive antibodies. (B) Frequency of SAs on metaphase spreads from olaparib treated TRF1^{F/F} MEFs 96 h after deletion of TRF1. Duration of olaparib treatment (2 μ M) is shown below. Bars represent median % of SAs from 5 independent experiments, each dot represents a metaphase spread. (C) Frequency of telomere fragility on the metaphase spreads from (B). Means and SD from 5 independent experiments is shown. (D) Western blot of shPARP1 treated TRF1^{F/F} MEFs. Cells were harvested 72hrs after deletion of TRF1 and deletion of PARP1 and TRF1 visualized on western blot with indicated antibodies. (E) Frequency of SAs on metaphase spreads from shRNA treated cells, 96 h after Cre. Bars represent the median % of SAs from 3 independent experiments. (F) Frequency of telomere fragility on the metaphase spreads from (E). Means and SD from 3 independent experiments is shown. P-values determined by a two-sided Students T-test (* p<0.05, ** p<0.01, *** p<0.001, ns: not significant).



observed as after the olaparib treatment (Fig. 3.3e and 3.3b). The frequency of SAs was reduced to around 8% with both shRNAs against PARP1. Again, telomere fragility was not affected upon depletion of PARP1 (Fig. 3.3f). The data thus suggest that PARP1 activity is needed for the formation of SAs, implicating the a-NHEJ pathway.

However, the activity of PARP1 in DNA repair is extensive and there are additional explanations why PARP1 could be required for SAs. First of all, PARP1 is known for its role in BER where it detects ssDNA breaks and attracts repair proteins (Dantzer et al., 2000). Furthermore, PARP1 has been implicated in HR mediated restart of replication forks (Bryant et al., 2009). Thus, additional experiments are needed to firmly establish the a-NHEJ pathway in the formation of SAs.

3.2.2. Ligase 3 is involved in the formation of Sister Associations

To further examine whether a-NHEJ is involved in the formation of SAs, Lig3 was deleted using shRNA because this ligase is an important component of the a-NHEJ pathway (Simsek et al., 2011). Unfortunately, whereas the function of Lig3 in the nucleus is not essential, it has a vital role in mitochondria and cells without Lig3 are not viable. Long-term shRNA-mediated depletion of Lig3 is therefore toxic to cells and not achievable. To circumvent this problem, TRF1^{F/F} cells were first treated with Cre immediately followed by lentiviral infection with two different shRNA. This allowed analysis of the effect of Lig3 depletion before cells are too

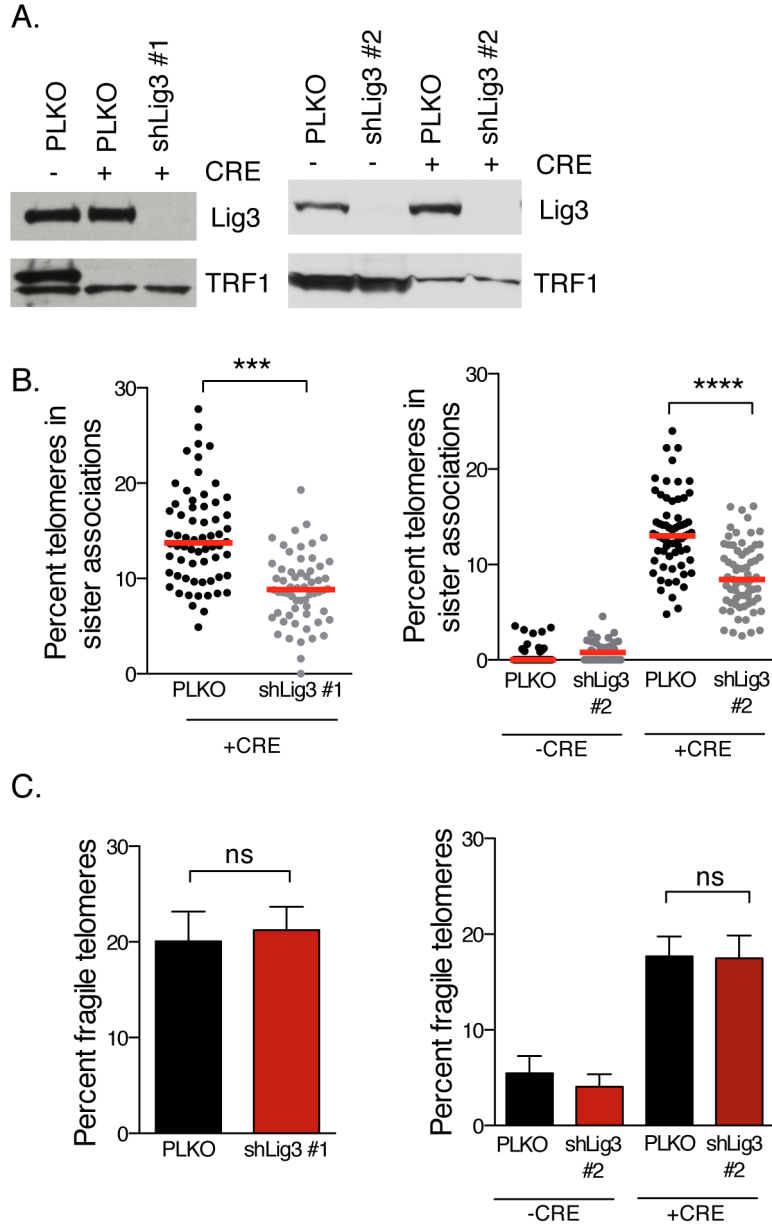


Figure 3.4 Depletion of Lig3 reduces SAs

(A) Western blots of TRF1^{F/F} MEFs treated with two different shRNA against Ligase 3. Cells were harvested 72 h after deletion of TRF1 and analyzed on western blot with Lig3 and TRF1 reactive antibodies. (B) Frequency of SAs on metaphase spreads from shRNA treated TRF1^{F/F} MEFs 96 h after deletion of TRF1. Bars represent median % of SAs from 3 independent experiments, each dot represents a metaphase spread. (C) Analysis of telomere fragility on the metaphase spreads from (B). Means and SD from 3 independent experiments is shown. P-values determined by a two-sided Students T-test (***) $p < 0.001$, **** $p < 0.0001$, ns: not significant).

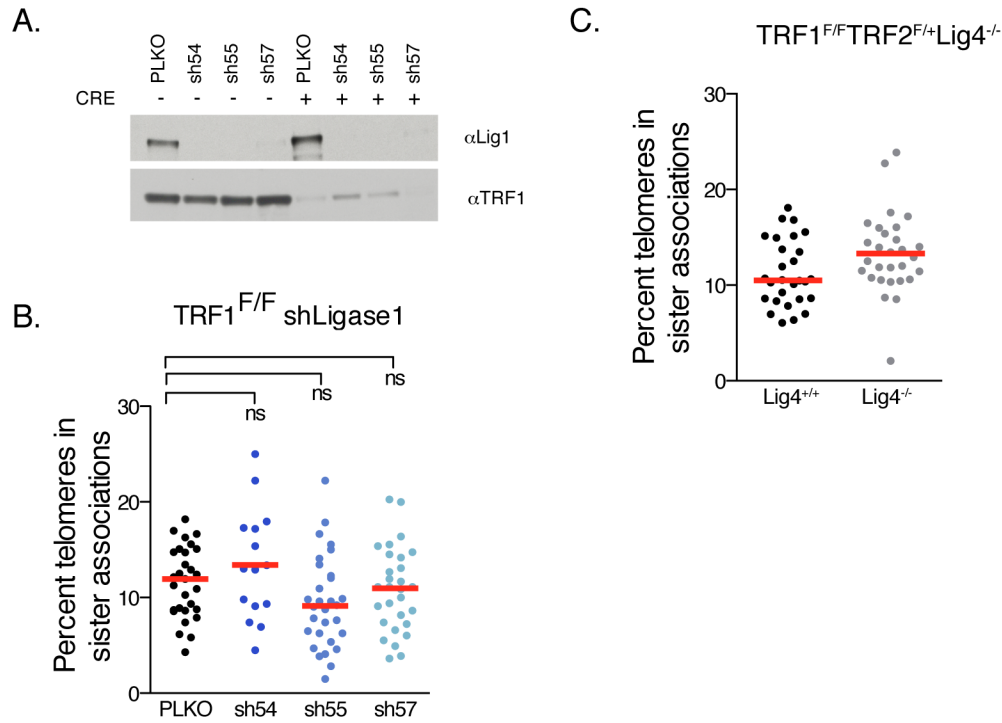


Figure 3.5 Lig1 and Lig4 do not affect the frequency of SAs

(A) Western blots of TRF1^{F/F} MEFs treated with three different shRNA against Ligase 1. Cells were harvested 72 h after deletion of TRF1 and analyzed on western blot with Lig1 and TRF1 reactive antibodies. (B) Frequency of SAs on metaphase spreads from shRNA treated TRF1^{F/F} MEFs 96 h after deletion of TRF1. Bars represent median % of SAs from 3 independent experiments, each dot represents a metaphase spread. (C). Frequency of SAs on metaphase spreads from TRF1^{F/F}Lig4^{+/+} and TRF1^{F/F}Lig4^{-/-} MEFs 96 h after Cre. Bars represent median % of SAs from one experiment. P-values determined by a two-sided Students T-test (ns: not significant).

sick for analysis. The proliferation rate of cells after shRNA against Lig3 is still somewhat lower compared to control cells (~40% or ~20% fewer cells with shRNA1 and 2 respectively, at time of harvest 2 days after plating). However, this is not expected to affect the level of SAs as they are formed in the last S/G2 phase before analysis. SAs therefore do not represent a cumulative phenotype, unlike the chromosome type fusions seen after TRF2 loss. A lower proliferation rate is thus not expected to reduce the prevalence of SAs.

Western blot analysis indicates that both shRNA are effective in knocking down Lig3 expression (Fig. 3.4a). Metaphase spreads were analyzed 96 h after deletion of TRF1 and SAs and fragile telomeres were scored. Interestingly, both shRNA against Lig3 significantly reduced the level of SAs to around 8% (Fig. 3.4b). No effect on the frequency of fragile telomeres was observed after depletion of Lig3 (Fig. 3.4c). The reduction in SAs with the shRNA against Lig3 is similar to the reduction seen with olaparib and the shRNA against PARP1 (Fig. 3.3b,e and Fig 3.4b).

Another ligase implicated in a-NHEJ is Ligase 1 (Lig1). This ligase has been shown to mediate a-NHEJ in absence of Lig3 (and Lig4) and could thus be involved in the formation of SAs (Liddiard et al., 2016; Lu et al., 2016). To examine the role of Lig1, three different shRNA against Lig1 were tested in TRF1^{F/F} MEFs and SAs analyzed 96 h after deletion of TRF1. Western blot analysis indicates good knockdown of Lig1 with all shRNA (Fig. 3.5a). However, the levels of SAs were not affected by the absence of Lig1 (Fig. 3.5b). It is

possible that Lig1 functions as a backup enzyme for Lig3. This was suggested in earlier experiments where an effect for Lig1 in a-NHEJ was only seen in absence of Lig3 (Liddiard et al., 2016). However, given that knockdown of Lig3 is toxic for cells, the combined knockdown of Lig3 and Lig1 was not attempted. Nevertheless, the results clearly establish that Lig1 is not involved in the formation of SAs when Lig3 is present. Furthermore, as previously shown, SAs were still present in TRF1^{F/F}Lig4^{-/-} MEFs establishing that the fusions are not formed via c-NHEJ (Fig. 3.5c) (Sfeir et al., 2009). The combined results of the effect of PARP1 and Lig3 strongly suggest that SAs are formed via a-NHEJ.

3.2.3 Ku does not affect Sister Associations

The fact that telomeric sequences contain microhomology (Fig. 3.2a) and that a-NHEJ can take place under certain circumstances supports the hypothesis that SAs may represent a-NHEJ mediated fused telomeres. It was previously shown that a-NHEJ takes place at telomeres when the entire shelterin complex is missing (Sfeir and de Lange, 2012). However, the pathway was only fully unleashed when Ku was absent. Ku prevents a-NHEJ by at least two mechanisms. It prevents DNA resection and competes with PARP1 for DNA binding thus inhibiting its activation (Wang et al., 2006). To test whether Ku has a similar role in preventing a-NHEJ after TRF1 deletion, SAs were analyzed in TRF1^{F/F}Ku70^{-/-} MEFs. If Ku prevents a-NHEJ, SAs are expected to increase in absence of Ku. Metaphase spreads of TRF1^{F/F}Ku70^{-/-} cells were analyzed

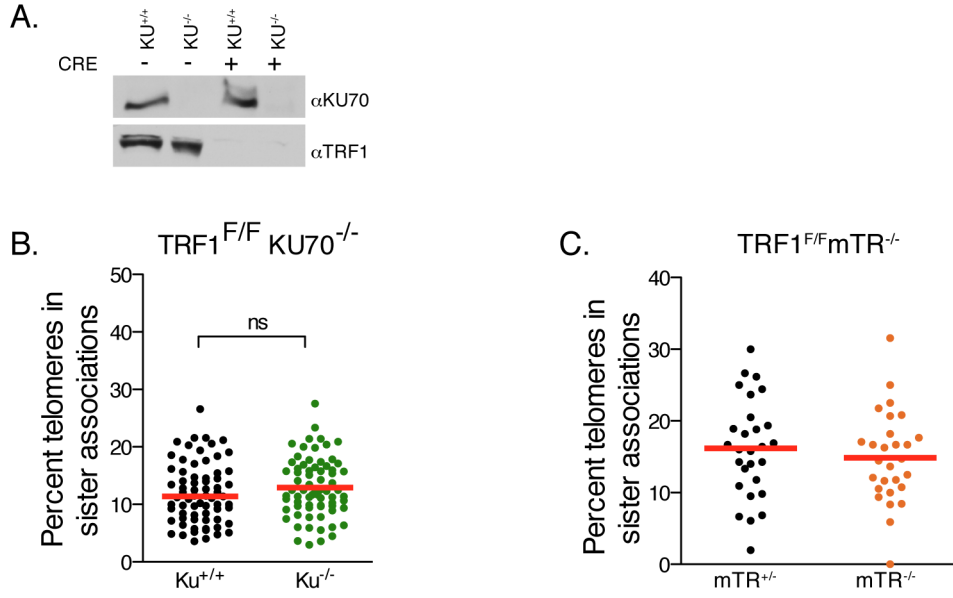


Figure 3.6 Ku does not affect SAs

(A) Western blot of TRF1^{F/F}Tin2^{+/+}Ku70^{+/+} and TRF1^{F/F}Tin2^{+/+}Ku70^{-/-} littermate MEFs. Cells were harvested 72 h after deletion of TRF1 and analyzed with TRF1 and Ku70 reactive antibodies. (B) Frequency of SAs on metaphase spreads from TRF1^{F/F}Tin2^{+/+}Ku70^{+/+} and TRF1^{F/F}Tin2^{+/+}Ku70^{-/-} MEFs 96 h after deletion of TRF1. Bars represent median % of SAs from 3 independent experiments, each dot represents a metaphase spread. (C) Frequency of SAs on metaphase spreads from TRF1^{F/F}mTR^{+/+} and TRF1^{F/F}mTR^{-/-} littermate MEFs 96 h after Cre. Bars represent the median % SAs from one experiment. P-values determined by a two-sided Students T-test (ns: not significant).

together with Ku positive littermate controls (Fig. 3.6a and b). Unexpectedly, lack of Ku did not significantly increase the level of SAs upon deletion of TRF1 indicating that Ku does not prevent a-NHEJ in this setting. Possibly, the presence of TRF2 prevents Ku from acting at telomeres lacking TRF1 (Ribes-Zamora et al., 2013). In vitro experiments suggested that TRF2 directly interacts with Ku to prevent it from stimulating NHEJ. Thus, upon deletion of TRF1, Ku may continue to be inhibited by TRF2 explaining why loss of Ku does not result in higher levels of SAs.

Recently, unpublished experiments from the Boulton lab suggested a role for the telomerase enzyme in the formation of fragile telomeres. In absence of telomerase, the prevalence of telomere fragility upon RTEL1 deletion was drastically reduced. To ascertain that SAs are not affected by telomerase, metaphase spreads from cells deficient for mTR, the RNA component of telomerase complex, were analyzed. Yet, SAs were unchanged in TRF1^{F/F}mTR^{-/-} cells compared to littermate controls, suggesting that telomerase does not affect their formation (Fig. 3.6c).

3.2.4 Anaphase bridges are seen upon deletion of TRF1

If SAs are truly fused telomeres, abnormalities should be visible during mitosis as dicentric chromosomes form anaphase bridges, which can result in Breakage-Fusion-Bridge cycles (BFB) and genome instability (Maciejowski et al., 2015). To analyze whether cells lacking TRF1 display abnormalities, the behavior of

chromosomes in mitosis was examined using spinning-disk confocal imaging. For these experiments, a TRF1^{F/F} cell line was created that stably expresses H2B-venus to allow visualization of chromosome dynamics in live cell imaging experiments. Cells were imaged before and 72 h after deletion of TRF1 using a Yokogawa spinning-disk confocal system and a Z-stack set of images was acquired every 5 minutes. This experimental setup permits imaging adjacent fields that are computationally stitched together to follow the fate of mitotic cells (Stephens et al., 2011). Interestingly, more than 80% of mitotic cells displayed anaphase bridges upon deletion of TRF1 versus only 20% of untreated control cells (Fig. 3.7a and b). The high background of chromatin bridges in the no-Cre control cells might be due to the repression of p53/Rb in these SV-40 immortalized MEFs, since these MEFs bypass cell cycle arrest upon DNA damage.

TRF1 loss has previously been linked to mitotic abnormalities in a mouse model of tissue specific TRF1 deletion (Martinez et al., 2009). When TRF1 was conditionally deleted from epithelial cells, mice deficient for p53^{-/-} spontaneously developed squamous cell carcinomas in the tail and ear skin. These lesions contained many multinucleated giant cells and anaphase bridges consistent with chromosome segregation problems in TRF1 deficient cells. However, the reason for the appearance of these anaphase bridges was not further analyzed.

The presence of anaphase bridges further suggests that SAs are fused telomeres (Fig. 3.7a). However, one caveat of these experiments is that TRF1^{F/F}

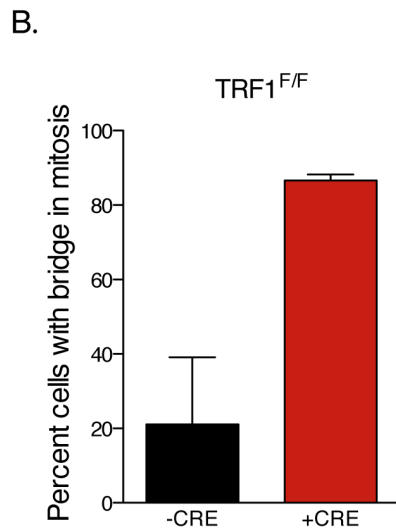
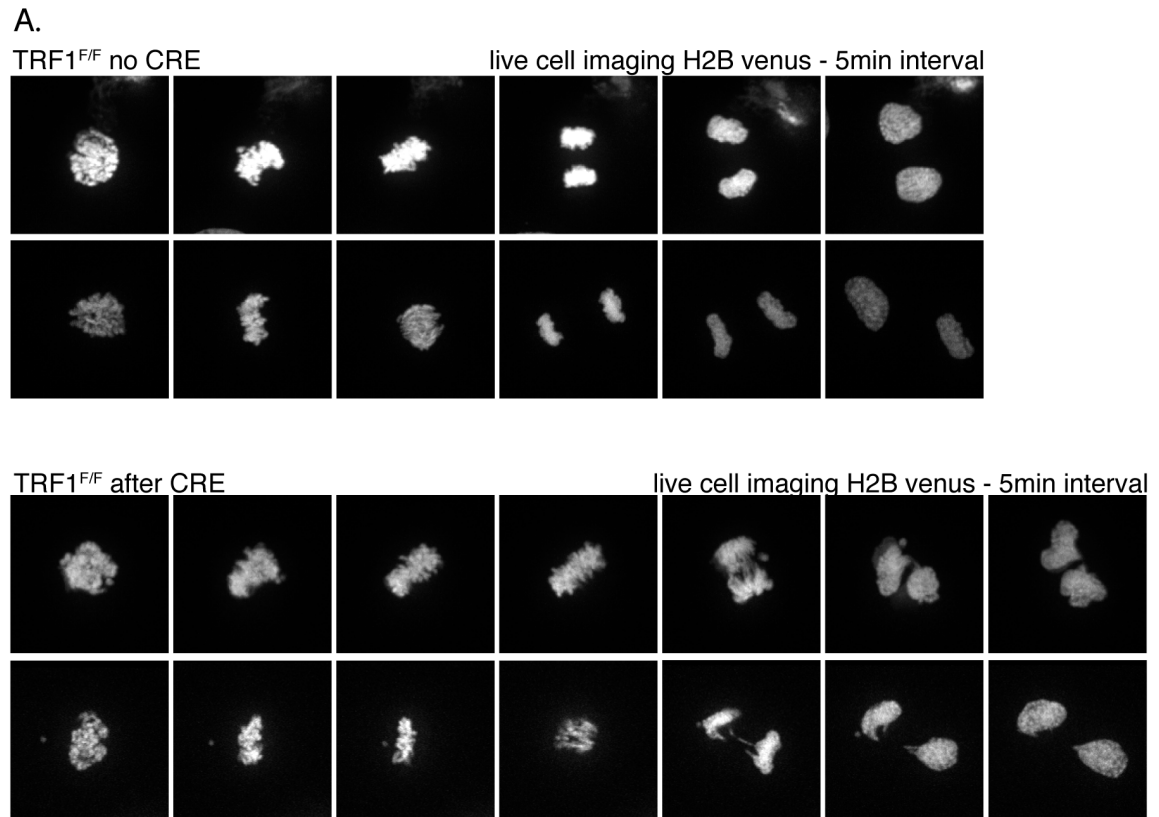


Figure 3.7 Mitotic abnormalities after TRF1 loss

(A) Images of H2B-Venus marked chromatin of a mitotic cell from TRF1^{F/F} MEFs left untreated (top) or 72hrs after Cre. Image stills were taken from movies made on a confocal spinning disk microscope with Z-stacks taken 5 minutes apart. (B) Analysis of the frequency of mitotic bridges in movies from A. At least 60 mitotic cells were analyzed per condition. Numbers represent mean and SDs from 3 movies per condition from 2 independent experiments.

MEFs also display low levels of chromosome type fusions after deletion of TRF1 that could explain the appearance of the mitotic abnormalities. Unfortunately, these chromosome type fusions are still present in TRF1^{F/F}Lig4^{-/-} and in TRF1^{F/F} MEFs depleted of Lig3. Therefore it is not possible to strictly ascertain that the anaphase bridges upon deletion of TRF1 are the result of SAs or due to the low level of chromosome type fusions present in these cells. Most metaphases contain at least one chromosome type fusion 96 h after deletion of TRF1 but the percentage of SAs is much higher (5-10 per metaphase). Analysis of the mitotic cells in the movies of TRF1^{F/F} cells after Cre suggests that multiple anaphase bridges are present, arguing that they represent the SAs. However, it is difficult to quantify the exact numbers with this imaging setup, hindering a direct correlation with the numbers of SAs or chromosome type fusions. Possibly, imaging experiments at very early time points after deletion of TRF1 would offer a solution as chromosome type fusions will not have accumulated to such an extent.

3.2.5 PICH localizes to DNA bridges upon deletion of TRF1

Plk1-interacting checkpoint helicase (PICH) is a DNA translocase that is activated by Plk1 during mitosis and is recruited to a special class of anaphase bridges, ultrafine bridges (UFBs) (Baumann et al., 2007; Chan et al., 2007). These bridges are not detectable with conventional DNA dyes but can be visualized with antibodies to BLM and PICH. UFBs appear in every anaphase between centromeres but are resolved as mitosis proceeds. These centromeric

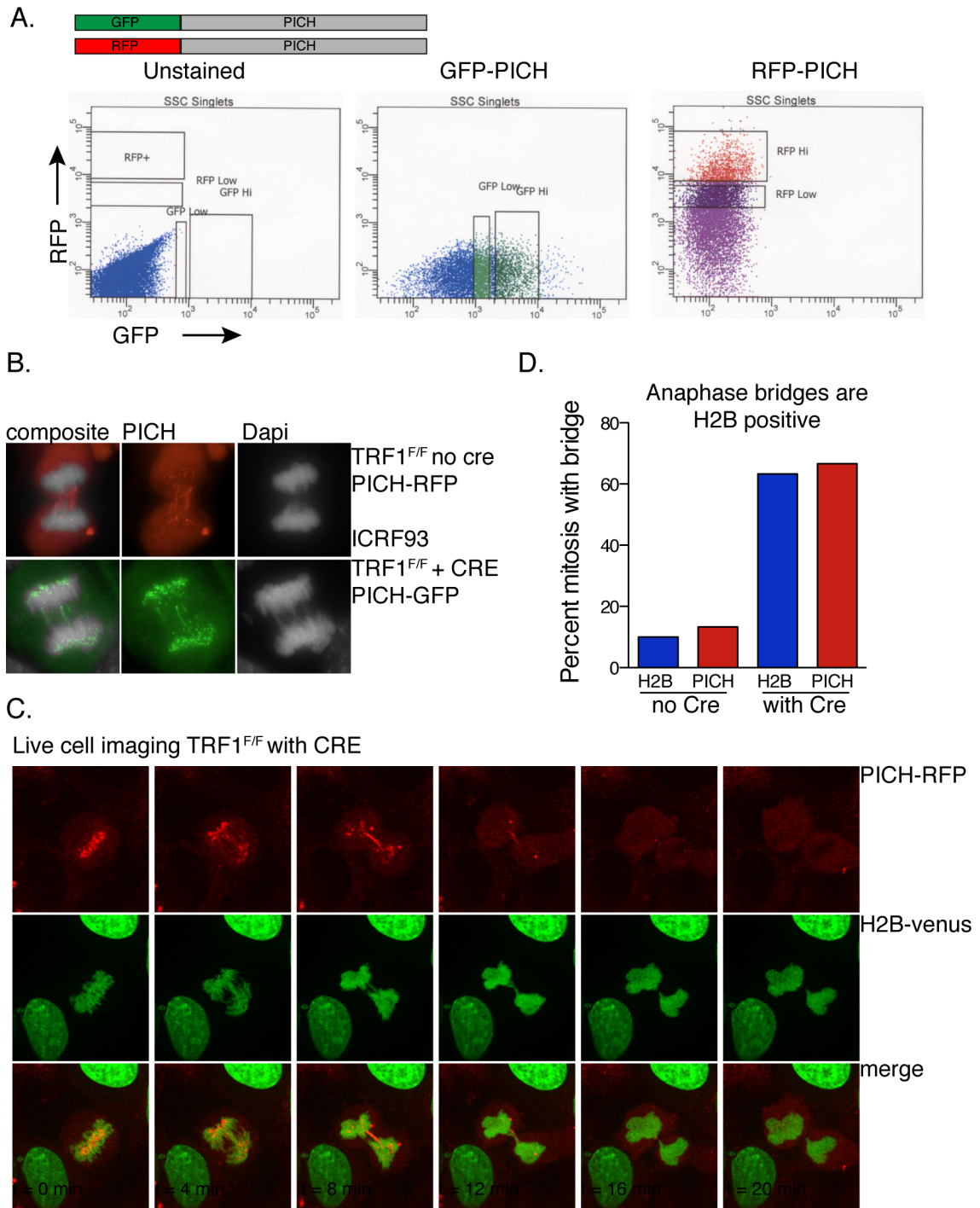
UFBs represent intertwined DNA structures that require decatenation by Topoisomerase IIa (TopoIIa) and BLM, a process stimulated by PICH (Nielsen et al., 2015). UFBs not only originate from centromeres but can also arise at fragile sites and telomeres (Chan et al., 2009; Barefield and Karlseder, 2012). These UFBs are increased in cells lacking BLM and are thought to represent replication intermediates.

Since TRF1 loss induces anaphase bridging and replication stress, it is possible that telomeric UFBs appear as a results of TRF1 deletion. In human cells, a small increase in UFBs was detected when TRF1 was depleted by shRNA from IMR90 cells but these results were difficult to interpret due to concomitant telomere loss hindering the classification of telomeric UFBs versus those at CFSs or centromeres (Barefield and Karlseder, 2012). Since mouse telomeres are much longer than human telomeres, deletion of TRF1 in MEFs might be a better experimental setup to examine the appearance of telomeric UFBs.

Unfortunately, antibodies against mouse BLM or PICH are not available for IF analysis since most of the prior work was done in human cells. To enable visualization of UFBs, a GFP or RFP tagged PICH construct was therefore generated (Fig. 3.8a). These constructs were stably expressed in TRF1^{F/F} cells and high expressing cells were isolated by FACS sorting (Fig. 3.8a). To show that the N-terminal tag had no effect on PICH localization, cells were treated with ICRF-193, a topoisomerase inhibitor that is known to induce centromeric UFBs.

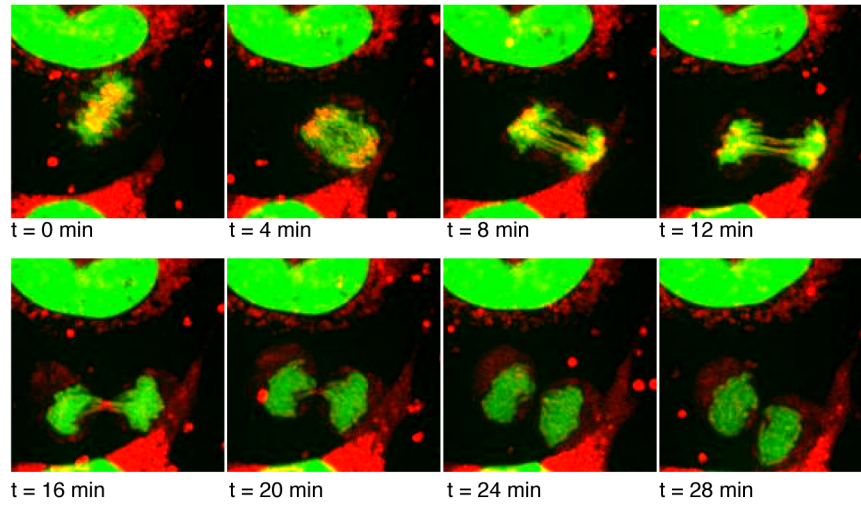
Figure 3.8 PICH localizes to anaphase bridges

(A) Schematic of PICH-RFP and PICH-GFP constructs (top) and FACS plots of the isolation of TRF1^{F/F} MEFs expressing these constructs by FACS sorting (bottom). The fraction of GFP high and RFP high expressing MEFs were sorted. (B) Examples of PICH localization to anaphase bridges in PFA fixed cells. Sorted PICH expressing TRF1^{F/F} MEFs from A were treated with ICRF93 (top) or analyzed 72 h after TRF1 deletion (bottom) by microscopy. DNA is stained with DAPI and PICH is either RFP or GFP positive. (C) Example of a mitotic cell from live cell imaging experiments of TRF1^{F/F} PICH^{RFP} H2B^{venus} MEFs 72 h after deletion of TRF1. Z-stacks were taken 4 minutes apart on a confocal spinning disk microscope. (D) Quantification of the percentage of cells with H2B-venus and PICH positive mitotic bridges before and 72 h after deletion of TRF1. Values represent the mean from one experiment with at least 60 mitotic cells analyzed per condition. All H2B-venus bridges have PICH staining and only few PICH only bridges are seen.



Indeed, PICH positive bridges were readily detected in anaphase cells upon ICRF-193 treatment of TRF1^{F/F} RFP-PICH expressing cells (Fig. 3.8b, top). To examine the effect of TRF1 deletion, TRF1^{F/F} GFP-PICH cells were treated with Cre and mitotic cells analyzed IF 72 h later. Interestingly, PICH positive threads were seen upon TRF1 loss, although their abundance was not as high compared to treatment with ICRF-193 (Fig. 3.8b, bottom). To better understand the dynamics of PICH positive anaphase bridges upon deletion of TRF1, H2B-venus was expressed in TRF1^{F/F} PICH-RFP cells to enable live cell imaging. Cells were imaged 72 h after deletion of TRF1 on the Yokogawa spinning-disk confocal system and images (Z-stack) were acquired every 4 minutes. Again, PICH positive threads were detected in anaphase similar to live cell imaging or fixed samples (Fig. 3.8c). Around 70% of anaphases analyzed displayed PICH localization. However, most PICH positive threads contained histones as indicated by the overlap with H2B-venus (Fig. 3.8d). Therefore, it is unclear whether these bridges represent genuine UFBs or regular anaphase bridges. Possibly, the resolution of the microscope is not sufficient to visualize UFBs using this method. The PICH positive threads seen in fixed cells using regular imaging suggests that more bridges might be present than detected in live cell imaging experiments (compare Fig. 3.8b and 3.8c). The PICH structures seen in live cell imaging show a speckled pattern compared to the full threads seen in fixed cells indicating that microscope resolution might be an issue. However, even in fixed cells, the PICH positive threads appear to overlap with DAPI signals suggesting

A. Live cell imaging TRF2^{F/F} PICH-RFP-H2B-venus with CRE



B. Live cell imaging TRF2^{F/F} PICH-RFP-H2B-venus with CRE

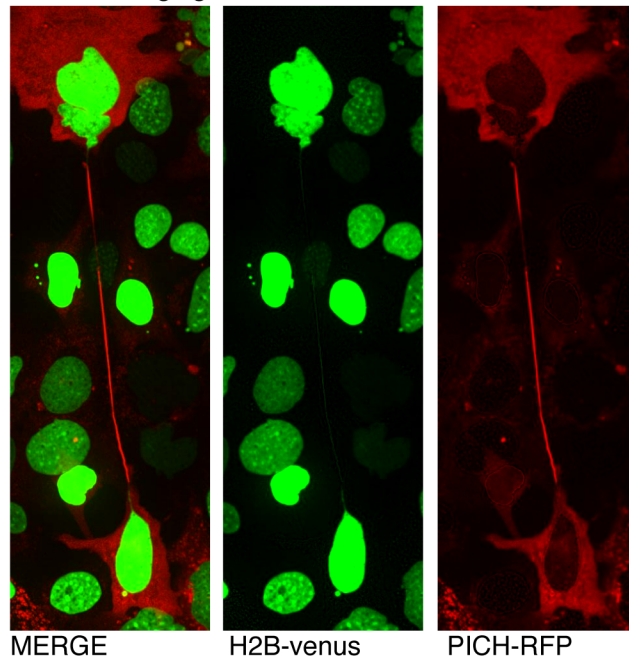


Figure 3.9 PICH localizes to bridges after deletion of TRF2

(A) Example of a mitotic cell from a live cell imaging experiment of TRF2^{F/F}PICH^{GFP}H2B^{venus} expressing MEFs 72 h after deletion of TRF2. Z-stacks were taken 4 minutes apart on a confocal spinning disk microscope. (B) PICH recruitment to a chromatin bridge remaining after mitosis from the same movie as in A.

that they represent regular anaphase bridges instead of genuine UFBs (Fig. 3.8b).

To better understand the distinction between UFBs and regular anaphase bridges, the effect of TRF2 loss was analyzed. Deletion of TRF2 results in massive chromosome type fusion and the appearance of anaphase bridges but there is no replication stress and telomeric UFBs are therefore not expected. A TRF2^{F/F} cell line was created expressing H2B-venus and PICH-RFP and high expressing cells isolated by FACS sorting. Live cell imaging experiments were done using the same conditions as for TRF1^{F/F} cells using the Yokogawa spinning-disk confocal system. Remarkably, deletion of TRF2 resulted in the appearance of PICH positive threads similar to those seen upon TRF1 deletion (Fig. 3.9a). In some cases, a PICH positive thread remained long after cell division (Fig. 3.9b). Thus, it appears as though PICH is not just recruited to UFBs but also to regular DAPI positive chromatin bridges formed upon telomere dysfunction.

Because PICH recruitment was not specific to TRF1 deletion and microscope resolution prohibits definitive analysis of telomeric UFBs by live cell imaging, this line of experimentation was not continued. Therefore, it cannot be concluded whether TRF1 loss leads to the appearance of UFBs at telomeres. It would be interesting to repeat the experiment in fixed cells since the resolution of PICH-GFP imaging appears to be higher.

3.2.6 The role of 53BP1 at sites of replication stress

53BP1 is mostly known for its role in DSB repair. However, 53BP1 is also recruited to sites of replication stress (Jowsey et al., 2007), including replication stress at telomeres (Sfeir et al., 2009). While ATM is the main kinase that acts on 53BP1 in response to DSBs, phosphorylation by ATR occurs in response to UV damage or loss of TRF1. Whether similar or different S/TQ sites are phosphorylated in response to DSBs or replication stress remains unclear. At DSBs, the main role for 53BP1 is to promote NHEJ by blocking extensive end resection. However, stalled replication forks are not repaired by NHEJ and it is therefore unclear what the role (if any) of 53BP1 is at these sites. It is possible that 53BP1 only localizes to collapsed replication forks that have turned into DSBs and have activated ATM kinase. However, 53BP1 is recruited to telomeres in TRF1^{F/F}ATM^{-/-} cells, arguing against this hypothesis (Sfeir et al., 2009). Furthermore, phosphorylation of 53BP1 by ATR occurs independently of ATM (Jowsey et al., 2007). A recent study from this lab provided evidence that 53BP1 is capable of blocking resection at telomeres in an ATR dependent manner (Kibe et al., 2016). This was shown at cells lacking TPP1/POT1a/b, which are incapable of protecting the 3' overhang at telomeres. Deletion of 53BP1 from these cells resulted in a hyper resection phenotype at telomeres. Interestingly, this resection pathway was dependent on BLM and Exo1, instead of the ATM mediated CtIP resection pathway. Furthermore, the results showed that 53BP1 recruits Rif1 to inhibit the ATR mediated resection pathway, similar to the

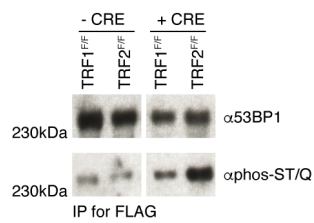


Figure 3.10 Phosphorylation of 53BP1 upon TRF1 or TRF2 deletion

Western blot of 53BP1 isolated from TRF1^{F/F}53BP1^{-/-} and TRF2^{F/F}53BP1^{-/-} MEFs expressing FLAG-53BP1. Cells were harvested 72 h after deletion of either TRF1 or TRF2 and 53BP1 was isolated using FLAG-beads. Isolated 53BP1 was analyzed by western blot for phosphorylation using an antibody specific for phosphorylated S/TQ sites. Total levels of 53BP1 were visualized with a 53BP1 reactive antibody.

situation at DSBs (Kibe et al., 2016). Whether there is a similar role for 53BP1/Rif1 in response to ATR activation at the replication fork remain unknown.

To analyze whether 53BP1 is phosphorylated in a different manner in response to ATR activation versus ATM, a phosphorylation status of 53BP1 was compared after TRF1 and TRF2 deletion. A FLAG-tagged 53BP1 wild type allele was expressed in TRF1^{F/F}53BP1^{-/-} and TRF2^{F/F}53BP1^{-/-} cells. Upon deletion of either TRF1 or TRF2, 53BP1 was isolated using FLAG antibodies to recover 53BP1. An immunoblot against 53BP1 or with an antibody specifically reactive with phosphorylated S/TQ residues revealed the phosphorylation status of 53BP1 (Fig. 3.10). In absence of Cre, some background phosphorylation of 53BP1 is detected in both TRF1^{F/F} and TRF2^{F/F} cells. Interestingly, whereas deletion of TRF2 results in considerable S/TQ phosphorylation of 53BP1, this effect is much less when TRF1 is deleted (Fig. 3.10). This could indicate that fewer sites are phosphorylated in response to ATR activation but it is also possible that a smaller fraction of the 53BP1 pool is affected after TRF1 deletion versus TRF2. This experimental approach does not allow distinction between these two possibilities. However, the results suggest that ATR does not affect 53BP1 phosphorylation as strongly as ATM activation at telomeres.

To evaluate the role of 53BP1 at telomeres upon ATR activation, TRF1^{F/F}53BP1^{-/-} MEFs were examined. The mutant 53BP1 alleles described in Chapter 2 were expressed in these cells to enable analysis of 53BP1 function (Fig. 3.11a). All 53BP1^{S/TQ} alleles expressed equally well as shown by western

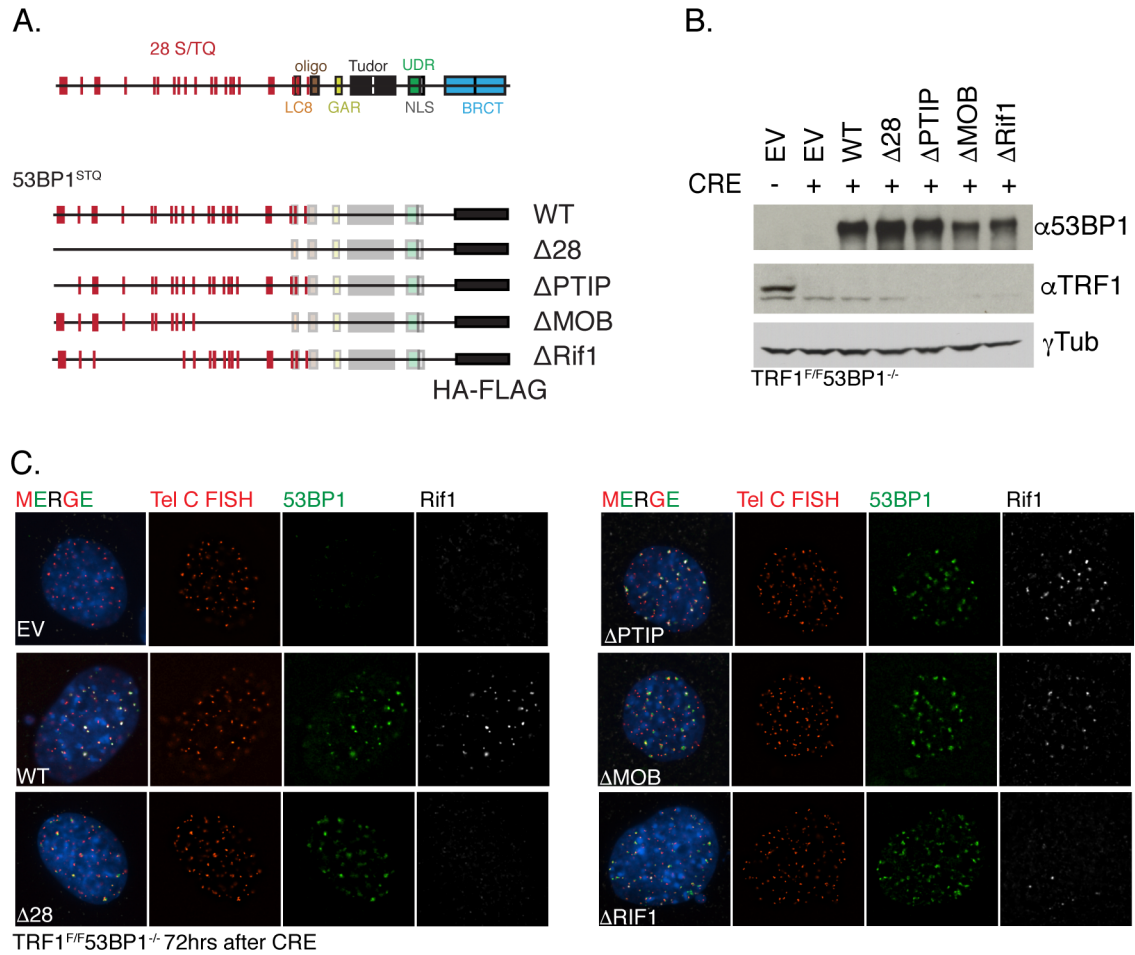


Figure 3.11 53BP1 mutants in TRF1^{F/F}53BP1^{-/-} MEFs

(A) Schematic of the 53BP1 mutant alleles with the S/TQ sites illustrated in red (B) Immunoblot showing the expression level of the 53BP1 mutant alleles in TRF1^{F/F}53BP1^{-/-} MEFs. Cells were harvested 72 h after deletion of TRF1 and visualized on western blot with 53BP1 or TRF1 specific antibodies. (C) Recruitment of 53BP1 and Rif1 to telomeres. Example of IF-FISH images from TRF1^{F/F}53BP1^{-/-} MEFs expressing the indicated mutant 53BP1 allele. Cells were imaged 72 h after deletion of TRF1. Telomeres are shown in red, 53BP1 in green and Rif1 in white.

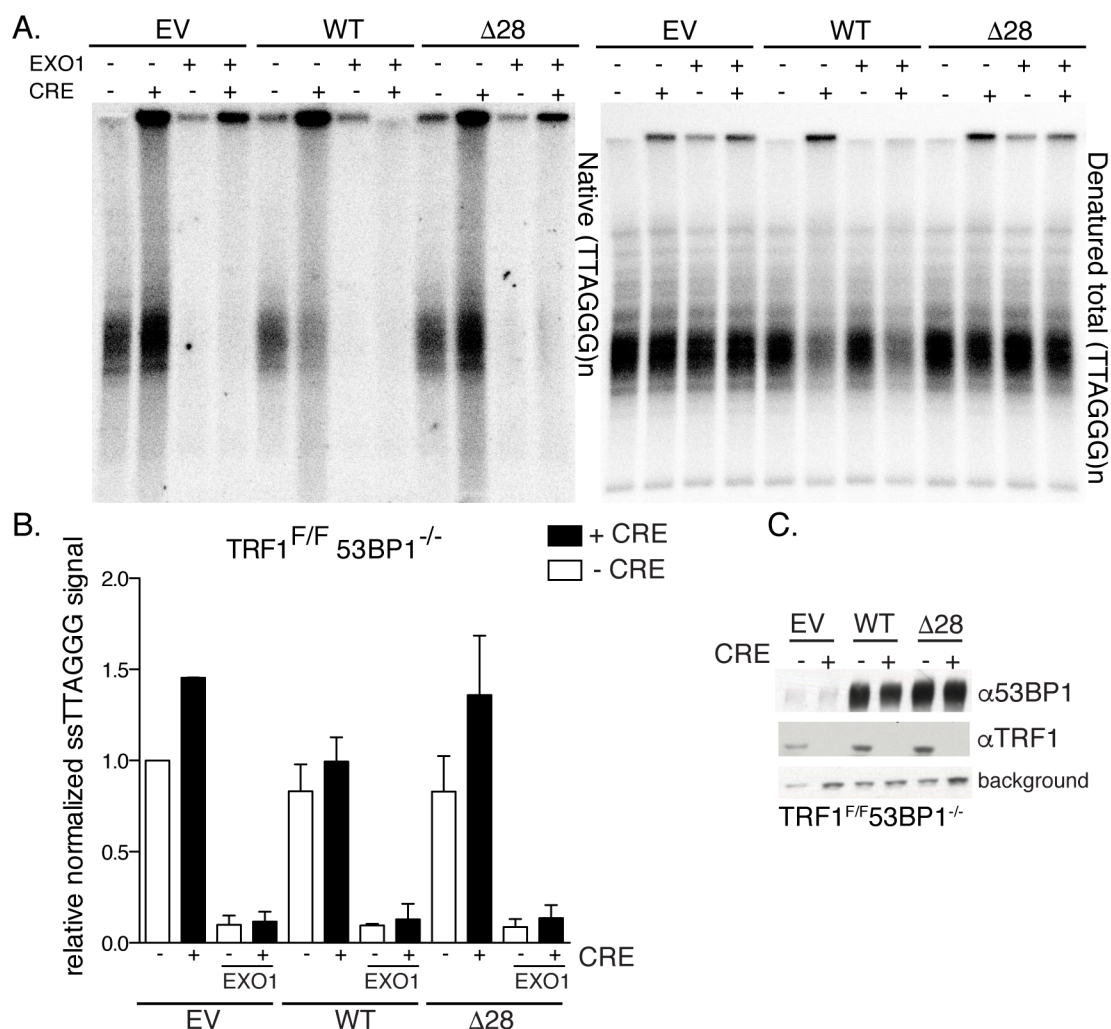


Figure 3.12 Telomere overhang gel in TRF1^{F/F} 53BP1^{-/-} cells

(A) Telomere overhang assay of MboI/AluI digested DNA from TRF1^{F/F} 53BP1^{-/-} MEFs expressing the indicated mutant 53BP1 alleles. Telomeric DNA was analyzed 96 h after Cre-mediated deletion of TRF1 using the in-gel hybridization assay. Left panel shows native telomeric ssDNA signal, right panel displays the denatured total amount of telomeric DNA. Where indicated, telomeric DNA was treated with Exo1 to remove ssDNA at the 3' overhang. (B) Quantification of the overhang signal as in (A) from two independent experiments. Numbers were obtained by normalizing the native ssDNA signal to the total telomeric DNA signal in the same lane in the denatured gel. The values of the Cre-treated samples were obtained by comparison with the no-Cre empty vector control lane, which was set to 1.0. Means and SDs from two independent experiments are shown. (C) Western blot with 53BP1 and TRF1 reactive antibodies from TRF1^{F/F} 53BP1^{-/-} MEFs expressing the indicated 53BP1 allele. Cells were harvested 72 h after deletion of TRF1.

blot (Fig. 3.11b). Similar to the setting of TRF2 deletion, IF-FISH showed that localization of 53BP1^{S/TQ} to telomeres lacking TRF1 was not affected by mutating the S/TQ sites (Fig. 3.11c). Furthermore, Rif1 was recruited to 53BP1 in cells expressing 53BP1^{WT}, 53BP1^{ΔPTIP}, and 53BP1^{ΔMOB} but not to 53BP1^{Δ28} or 53BP1^{ΔRif1}, similar to the situation upon deletion of TRF2 (Fig. 3.11c).

TRF1 deletion itself does not unleash resection at the telomere end but co-deletion of 53BP1 results in a mild hyper-resection phenotype (Sfeir et al., 2009; Sfeir and de Lange, 2012). To confirm that resection is increased in absence of 53BP1, a telomere overhang analysis was done in TRF1^{F/F}53BP1^{-/-} cells expressing empty vector, 53BP1^{WT} or 53BP1^{Δ28} (Fig. 3.12a-c). Samples were analyzed with or without treatment with the E. coli Exol 3' exonuclease to verify that the observed ssDNA is at the overhang and not telomere internal. Indeed, all telomeric signals disappeared from the native gel upon treatment with Exol confirming that the ssDNA is at the telomere end (Fig. 3.12a and b). As expected from experiments in TRF2^{F/F} MEFs, expression of 53BP1^{WT} allele was able to rescue the mild hyper-resection phenotype seen in cells expressing empty vector (Sfeir and de Lange, 2012). Moreover, 53BP1^{Δ28} was unable to rescue the resection phenotype suggesting a similar role for 53BP1 (and Rif1) in blocking resection at telomeres upon TRF1 deletion as at DSBs.

Next, metaphase spreads from TRF1^{F/F}53BP1^{-/-} MEFs were analyzed and SAs and fragile telomeres scored (Fig. 3.13a). Interestingly, SAs were significantly reduced when 53BP1 was absent (Fig. 3.13b). This is in agreement

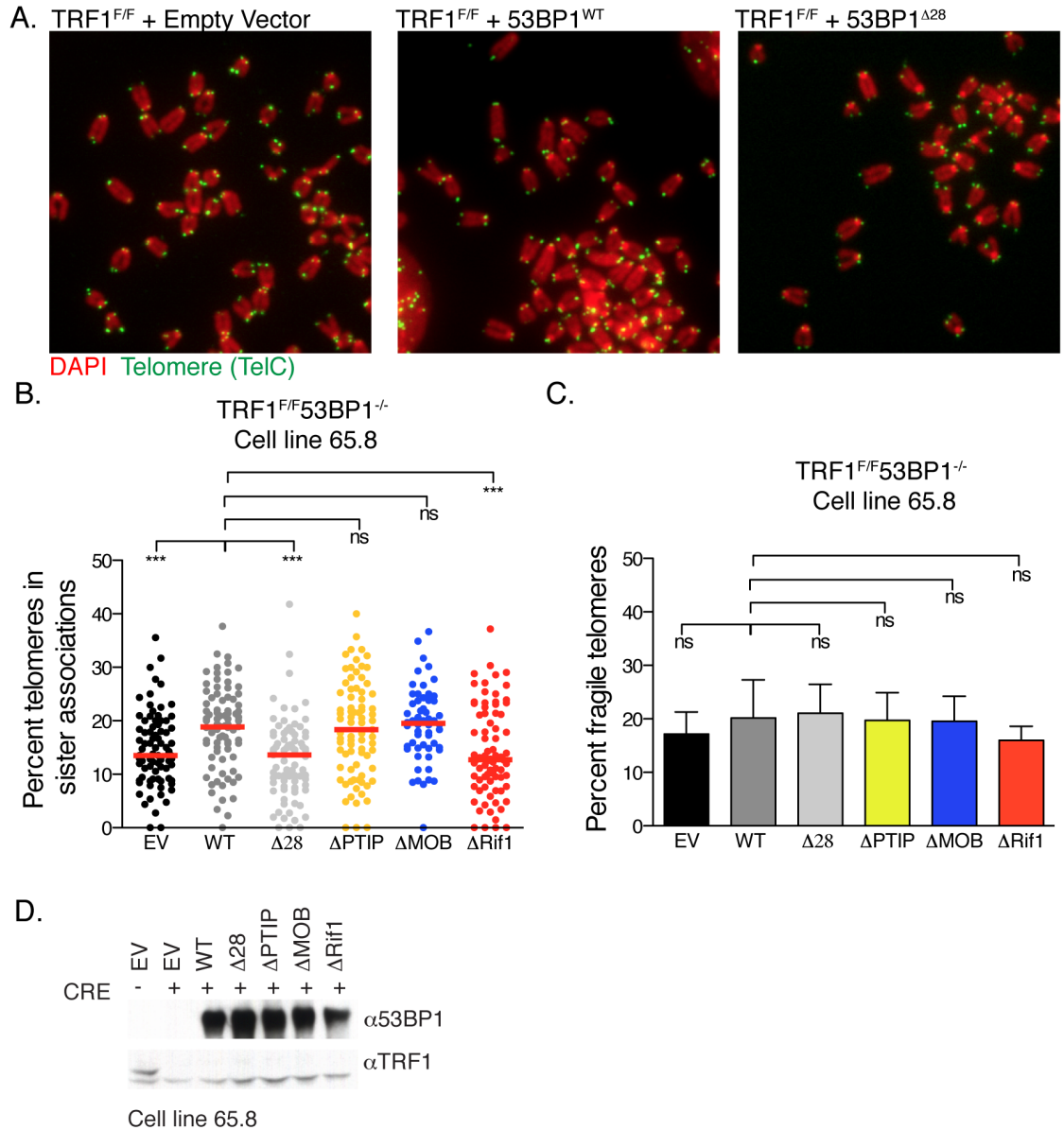


Figure 3.13 53BP1 S/TQ sites affect the frequency of SAs

(A) Examples of metaphase spreads of TRF1^{F/F}53BP1^{-/-} MEFs expressing indicated 53BP1 allele, harvested 96 h after deletion of TRF1. (B) Frequency of SAs in TRF1^{F/F}53BP1^{-/-} MEFs expressing the indicated 53BP1 allele, 96 h after the deletion of TRF1. Bars represent median % of SAs from three independent experiments. Each dot represents a metaphase spread. (C) Analysis of telomere fragility in the same metaphase spreads as in (B). Values represent means and SDs from three independent experiments. P-values determined by a two-sided Students T-test (***) $p < 0.001$, ns: not significant). (D) Western blot visualizing the equal expression of the indicated 53BP1 alleles in TRF1^{F/F}53BP1^{-/-} MEFs. Cells were harvested 72 h after deletion of TRF1.

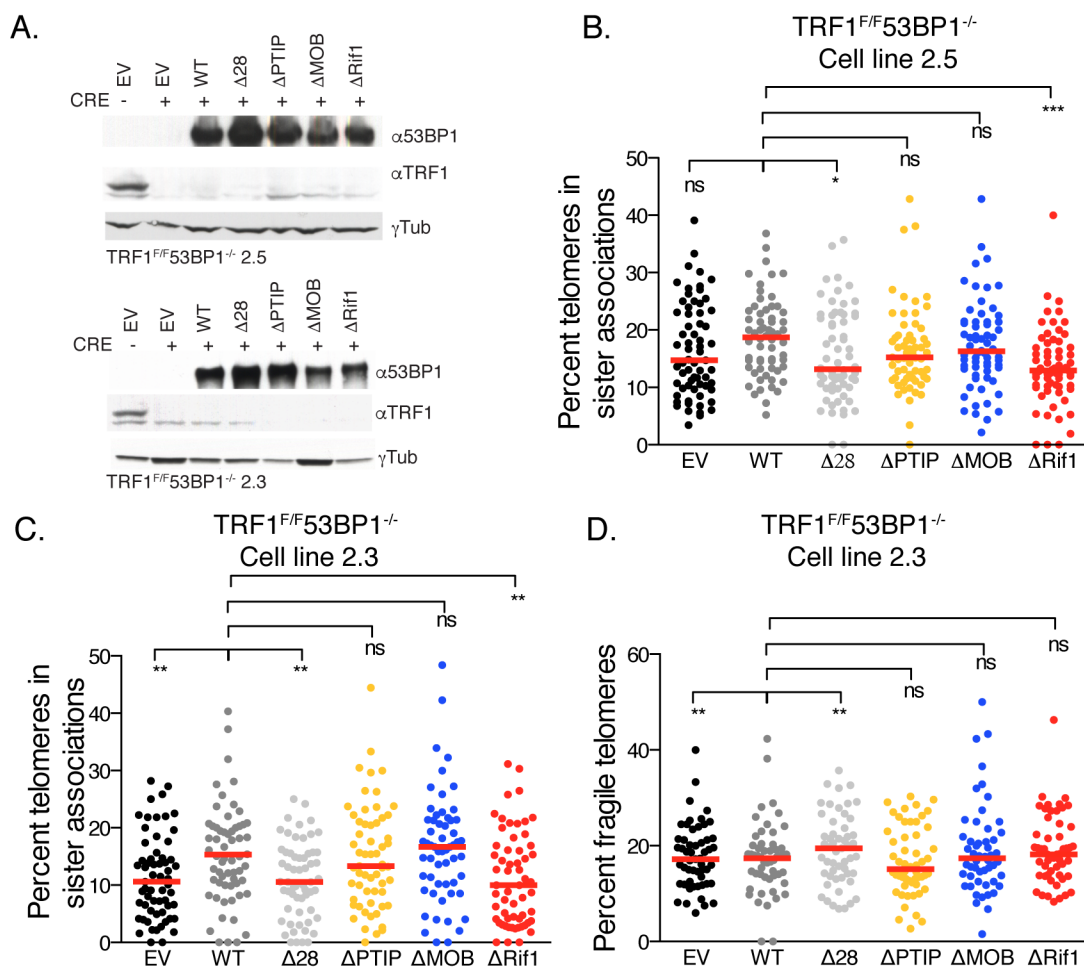


Figure 3.14 53BP1 S/TQ sites affect SAs in two additional cell lines

(A) Western blot visualizing the equal expression of the indicated 53BP1 alleles in two additional TRF1^{F/F}53BP1^{-/-} MEF cell lines. Cells were harvested 72 h after deletion of TRF1. (B and C) Frequency of SAs in TRF1^{F/F}53BP1^{-/-} cell line 2.5 (B) and 2.3 (C). Cells express the indicated 53BP1 allele and were harvested 96 h after the deletion of TRF1. Bars represent median % of SAs from three independent experiments. Each dot represents a metaphase spread. (D) Analysis of telomere fragility in cell line 2.3 on the metaphase spreads from (C). Values represent means and SDs from three independent experiments. P-values determined by a two-sided Students T-test (* p<0.05, ** p<0.01, *** p<0.001, ns: not significant).

with a previous report that noted reduced levels of sister chromatid fusion in absence of 53BP1 (Martinez et al., 2012). The reduction in SAs appeared to be dependent on phosphorylation of 53BP1 as 53BP1^{Δ28} displayed a similar decrease in SAs as the empty vector control (Fig. 3.13b). There was no difference between 53BP1^{ΔMOB} and 53BP1^{ΔPTIP} compared to 53BP1^{WT}, indicating that these domains play no role in the formation of SAs. However, cells expressing 53BP1^{ΔRif1} displayed reduced levels of SAs similar to empty vector control, suggesting that 53BP1 recruits Rif1 to help the formation of SAs. Telomere fragility was also analyzed but no difference was observed with any of the 53BP1 alleles (Fig. 3.13c).

To confirm these results, additional TRF1^{F/F}53BP1^{-/-} MEFs were made to ascertain that this phenotype was not cell line specific. To generate MEFs, TRF1^{F/F}53BP1^{+/-} mice were intercrossed to obtain TRF1^{F/F}53BP1^{-/-} genotypes. MEFs were isolated from E12.5 embryos and immortalized through introduction of the SV40 large T antigen. Two different TRF1^{F/F}53BP1^{-/-} cell lines were analyzed (2.3 and 2.5) upon expression of the different 53BP1 alleles using the same experimental conditions as used in Figure 3.13. Again, SAs were lowered in absence of 53BP1 or when 53BP1^{Δ28} or 53BP1^{ΔRif1} was expressed (Fig. 3.14b and c). Telomere fragility was not affected by any of the mutant 53BP1 alleles indicating that 53BP1 has no role in their formation (Fig. 3.14d). Together, these results suggest that 53BP1 promotes formation of SAs through the recruitment of Rif1.

3.2.7 Rif1 acts downstream of 53BP1 to promote Sister Associations

To further assess the function of Rif1 in the formation of SAs, TRF1^{F/F}Rif1^{F/F}53BP1^{-/-} triple knockout cells were analyzed. If Rif1 is required downstream of 53BP1, there should be no difference in the level of SAs between any of the mutant 53BP1 alleles when Rif1 is absent. To create the TRF1^{F/F}Rif1^{F/F}53BP1^{-/-} cell line, the 53BP1 locus was edited in TRF1^{F/F}Rif1^{F/F} MEFs using CRISPR/Cas9. Since 53BP1 is a large protein (encoded by 5760 bp in 27 exons), early exons in the gene were targeted to maximize the chance of deleting the entire protein instead of generating a possibly functional truncation mutant (Fig. 3.15a). Three different guide RNAs (gRNAs) were designed targeting exon 2 and exon 3 and TRF1^{F/F}Rif1^{F/F} MEFs transiently transfected with one of the gRNA vector together with Cas9. MEFs were subcloned and subsequently screened via western blot for deletion of 53BP1. Several clones were identified that lost expression of 53BP1 and two clones were picked for further analysis (Fig. 3.15b). Sequencing confirmed a frame shift mutation in clone g3#3 and g5#7, although for both clones only one allele variant was detected (Fig. 3.15c). Possibly, the mutation in the second alleles is so substantial that the PCR amplification required for sequencing failed or the clones became hemizygous.

To address the role of Rif1 in the formation of SAs, selected 53BP1^{S/TQ} alleles were expressed in the TRF1^{F/F}Rif1^{F/F}53BP1^{-/-} MEF clones g3#3 and clone g5#7. The mutant 53BP1 alleles were expressed equally as gleaned from

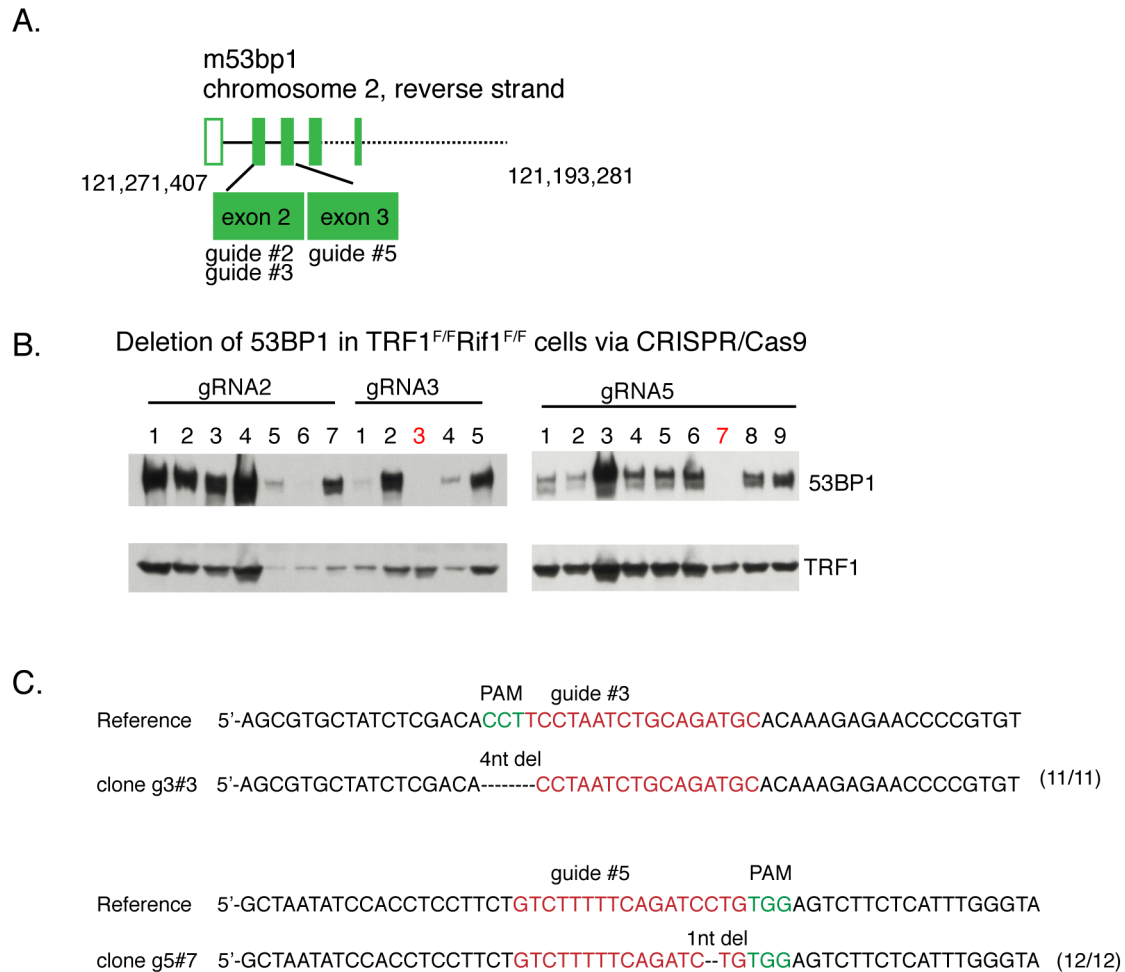
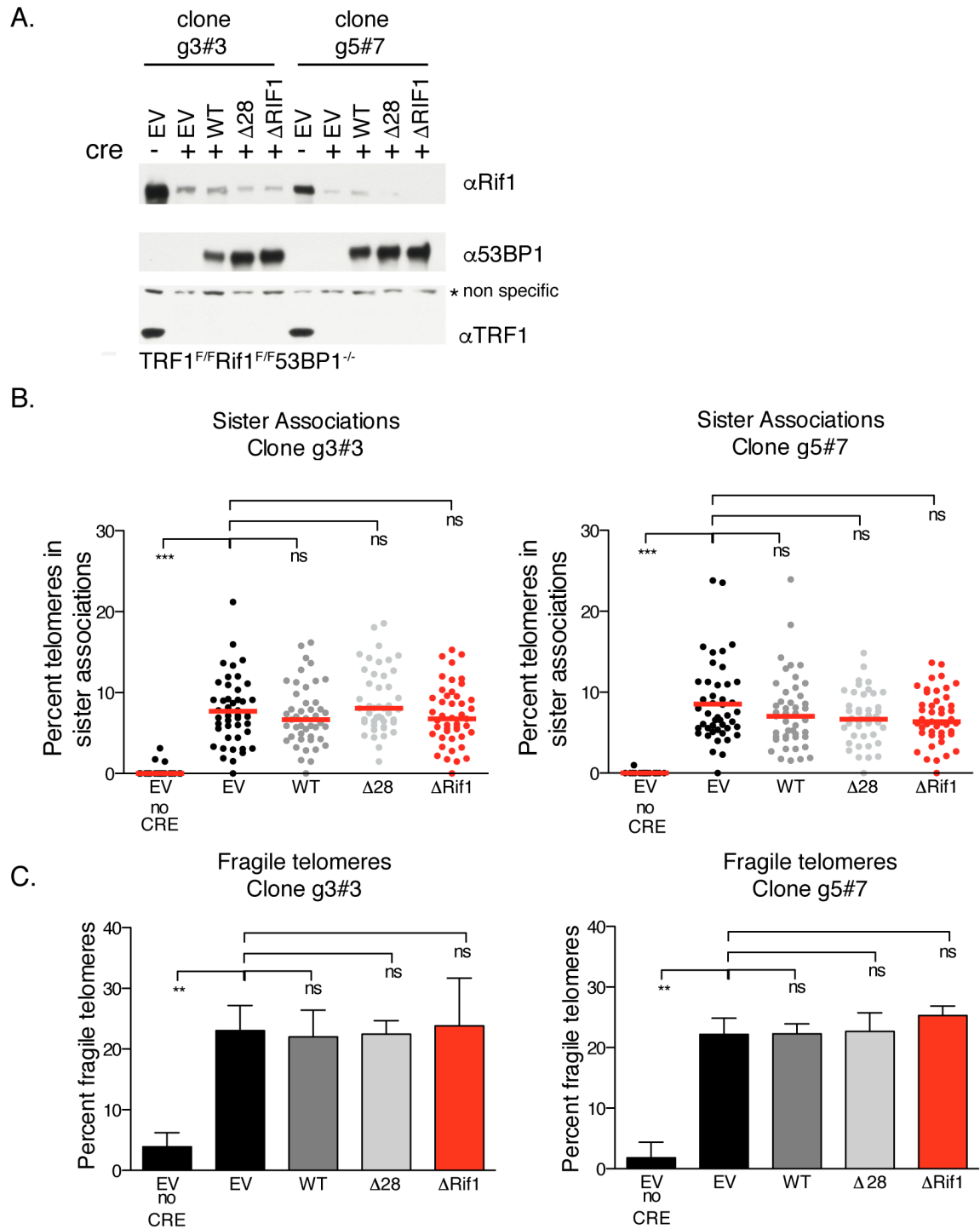


Figure 3.15 CRISPR/Cas9 editing of 53BP1 in TRF1^{F/F}Rif1^{F/F} MEFs

(A) Schematic of the mouse 53BP1 locus on chromosome 2, only the first 5 exons (of 27) are shown. The gRNAs target either exon2 or exon3 as indicated. (B) Immunoblot for 53BP1 in MEF clones picked after targeting with the indicated gRNAs, showing several clones with deletion of 53BP1. Clone g3#3 and g5#7 (in red) were picked for further analysis. Immunoblot for TRF1 is used as loading control. (C) DNA sequencing of clones g3#3 and g5#7. The reference sequence shows the untargeted DNA with the gRNA sequence (red) and PAM (green). For both clones, only one allele was found with sequencing (out of 11 or 12 sequences analyzed) suggesting the other allele has a larger deletion that was not PCR amplified.

Figure 3.16 Analysis of SAs and fragility in TRF1^{F/F}Rif1^{F/F}53BP1^{-/-} MEFs

(A) Immunoblot of TRF1^{F/F}Rif1^{F/F}53BP1^{-/-} MEFs clone g3#3 and g5#7. Cells were harvested 72 h after Cre and analyzed with TRF1, Rif1 and 53BP1 reactive antibodies. (B) Frequency of SAs in metaphase spreads from clone g3#3 (left) and clone g5#7 (right) expressing the indicated 53BP1 allele 96 h after Cre. Bars represent median % of SAs from three independent experiments. Each dot represents a metaphase spread. (C) Analysis of telomere fragility on the metaphase spreads from (B). Values represent means and SDs from three independent experiments. P-values determined by a two-sided Students T-test (***) $p > 0.001$, ns: not significant).



western blot analysis (Fig. 3.16a). SAs and telomere fragility were analyzed in metaphase spreads harvested 96 h after deletion of TRF1 and Rif1. Interestingly, there was no longer a difference in the level of SAs in absence of 53BP1 (Fig. 3.16b). All mutant 53BP1 alleles displayed a similar frequency of SAs compared to empty vector control. The results were comparable in the two CRISPR clones analyzed substantiating this finding. Telomere fragility was also unaltered upon expression of any 53BP1 allele (Fig. 3.16c).

These results strongly suggest that 53BP1 recruits Rif1 to aid the formation of SAs. Of note, the overall levels of SAs are much lower in these TRF1^{F/F}Rif1^{F/F}53BP1^{-/-} clones compared to other cell lines analyzed (median ~8% versus ~15-20%) (Compare Figs 3.13/3.14 and 3.16b). It is interesting to speculate that this lower level of SAs in TRF1^{F/F}Rif1^{F/F}53BP1^{-/-} MEFs is due to the absence of Rif1 but it is also possible that this is a clonal effect. The frequency of SAs changes slightly between the different cell types analyzed, with wild type levels ranging from ~15-20%. It would be interesting to overexpress Rif1 in TRF1^{F/F}Rif1^{F/F}53BP1^{-/-} MEFs cells to examine if this increases the frequency of SAs. However, Rif1 is a large protein and difficult to express and this experiment was therefore not attempted.

The main known function of Rif1 downstream of 53BP1 is to control end resection via Rev7 (Callen et al., 2013; Di Virgilio et al., 2013; Zimmermann et al., 2013; Boersma et al., 2015; Xu et al., 2015). If SAs are formed by a-NHEJ, limited resection is required to expose the microhomology needed for the

reaction to occur. It is therefore unclear why loss of Rif1 and 53BP1 reduces the levels of SAs. Absence of these proteins increases the amount of end resection, which should increase the prevalence of SAs instead of reducing them. Possibly, the extensive end resection that occurs in absence of 53BP1/Rif1 instead channels repair to HR.

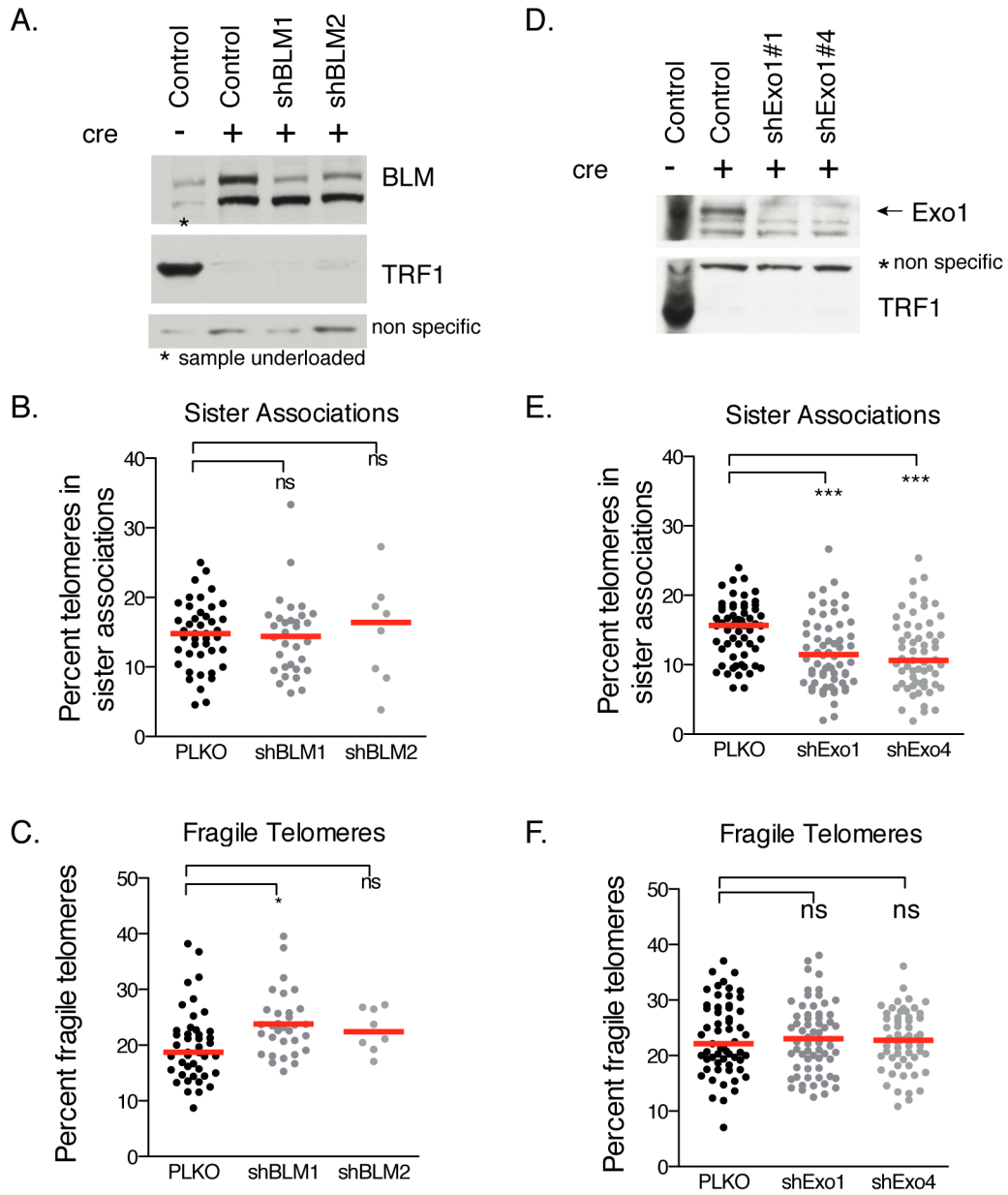
3.2.8 A enigmatic role for Exo1 in the formation of Sister Associations

To better understand the role for end resection in the formation of SAs, the effect of shRNAs against BLM and Exo1 was examined. At DSBs, end resection is initiated by the MRN complex and CtIP, followed by more extensive resection by Exo1, BLM, DNA2 and WRN (Sartori et al., 2007; Mimitou and Symington, 2008; Nimonkar et al., 2008). Whether this process is similar at stalled replication forks is not well understood.

To examine whether BLM and Exo1 are involved in the development of SAs, TRF1^{F/F} cells were treated with shRNAs against these proteins. Since cells do not divide well after knockdown of either BLM or Exo1, MEFs were treated with Cre prior to the shRNA infection to minimize effects on cell growth. Metaphase spreads were analyzed 96 h after Cre infection, which corresponds to 72 h after the first shRNA infection. Two independent shRNA against BLM were tested and both display reduced BLM expression by western blot (Fig 3.17a). However, the frequency of SAs was not affected by BLM depletion (Fig. 3.17b). This is not surprising since a previous paper already described that BLM has no

Figure 3.17 Analysis of SAs and fragility upon deletion of Exo1 or BLM

(A) Immunoblot of TRF1^{F/F} MEFs treated with shRNA against BLM. Cells were harvested 72 h after Cre and analyzed with TRF1 and BLM reactive antibodies. (B) Frequency of SAs in metaphase spreads from TRF1^{F/F} MEFs after depletion of BLM, 96 h after Cre. Bars represent median % SAs from three independent experiments. Each dot represents a metaphase spread. For MEFs treated with shBLM2, few metaphases were analyzed because cells were sick and not many spreads were obtained. (C) Analysis of telomere fragility on the metaphase spreads from B. Bars represent the median % of fragility from three independent experiments. (D) Immunoblot of TRF1^{F/F} MEFs treated with shRNA against Exo1. Cells were harvested 72 h after Cre and analyzed with TRF1 and Exo1 specific antibodies. (E) Frequency of SAs in metaphase spreads from TRF1^{F/F} cells after depletion of Exo1, 96 h after Cre. Bars represent median % SAs from 4 independent experiments. (D) Analysis of telomere fragility on the metaphase spreads from E. Bars represent the median % of fragile telomeres from 4 experiments. P-values determined by a two-sided Students T-test (* p>0.05, *** p>0.001, ns: not significant).



effect on SAs (Zimmermann et al., 2014). As expected, telomere fragility was slightly increased in absence of BLM consistent with its role in removing G4 structure in the lagging strand template (Fig. 3.17c).

Next, shRNA against Exo1 were examined. Knockdown of Exo1 by shRNA was efficient as indicated by western blot and loss of Exo1 did not affect telomere fragility (Fig. 3.17d and f). Surprisingly, the level of SAs was significantly decreased upon knockdown of Exo1 (Fig. 3.17e). This is unexpected given the finding the Rif1, an inhibitor of end resection, also reduces SAs (Fig. 3.13 and 3.14).

3.3 Summary of findings

The results in this chapter elucidate the molecular nature of SAs that arise when replication stress occurs at telomeres upon loss of TRF1. The results indicate that telomeres lacking TRF1 are subject to the a-NHEJ pathway and fusion of sister chromatids, which are visible as SAs on metaphase spreads. The results show that SAs are dependent on PARP1 as both shRNA and PARP1 inhibition by olaparib reduced their appearance (Fig. 3.3b and e). Furthermore, depletion of Lig3 also reduced the prevalence of SAs, further implicating that the a-NHEJ pathway is involved (Fig. 3.4b). However, deletion of Ku70, a known inhibitor of a-NHEJ, did not increase the level of SAs (Fig. 3.6b). Possibly, the interaction between TRF2 and Ku prevents the latter from affecting a-NHEJ upon TRF1 deletion (Ribes-Zamora et al., 2013). Ku is strictly suppressed at telomeres by

TRF2 to prevent c-NHEJ and telomere fusions. Thus, upon deletion of TRF1, Ku is still bound by TRF2 and kept away from telomere ends. Therefore it is unable to influence a-NHEJ, explaining why loss of Ku loss has no effect on SAs.

Consistent with SAs being formed by a-NHEJ, live cell imaging experiments indicates mitotic abnormalities upon deletion of TRF1 (Fig. 3.7). The fusion of sister chromatids creates dicentric chromosomes that form anaphase bridges in mitotic cells. Indeed, around 70-80% of cells display this phenotype upon deletion of TRF1 consistent with SAs representing fused telomeres. Interestingly, PICH was also recruited to anaphase bridges (Fig. 3.8b). PICH is a marker for UFBs that arise from centromeric regions and fragile sites, and are thought to represent underreplicated regions or replication intermediates that require additional processing for resolution during anaphase (Chan et al., 2007; Chan et al., 2009). However, the anaphase bridges detected upon loss of TRF1 were mostly DAPI or H2B-venus positive indicating that they might not be true UFBs. It is possible that the resolution of the live cell-imaging microscope was not high enough to detect true UFBs in these cells. But, even though the appearance of UFBs awaits further investigation, the results clearly show the appearance of mitotic defects upon TRF1 loss.

The function of 53BP1 and Rif1 in the formation of SAs is more complicated. The results indicate that 53BP1 recruits Rif1 to promote the formation of SAs as loss of either protein reduces the frequency of SAs (Fig. 3.13b and 3.16b). However, if SAs are formed by a-NHEJ, there is a requirement

for end-resection to expose the microhomology domains, a process inhibited by 53BP1 and Rif1. Therefore, the results are counterintuitive, as loss of 53BP1 and Rif1 would be expected to promote resection and increase the levels of SAs. Possibly, the resection occurring in absence of 53BP1/Rif1 is too extensive for a-NHEJ and promotes HR-mediated repair instead. Alternatively, it could mean that Rif1 has another function at the replication fork that is independent from resection. On the other hand, the effect of Exo1 inhibition could be easily explained if Exo1 is the main nuclease involved in the end-resection at telomeres lacking TRF1. The defect in resection would be expected to result in a lack of 3' overhangs that are used by a-NHEJ to form the SAs. Further studies are required to fully understand the role of 53BP1/Rif1 and Exo1 at telomeres lacking TRF1.

Chapter 4: Gen1 cleaves fused sister telomeres

4.1 Introduction

Results from the previous chapter indicate that SAs are sister telomeres fused via a-NHEJ. The level of SAs is around 15-20% and therefore most cells contain 5-10 SAs after deletion of TRF1 (SV-40 MEFs have variable chromosome numbers). If these were covalently fused telomeres, more chromosomal instability and mitotic defects would be expected than is reported for TRF1 deletion (Sfeir et al., 2009). Specifically, when sister telomeres fuse, isochromosomes should appear in the next metaphase when the chromosome with sister fusions mis-segregates into one daughter cell occurs and is replicated (Fig. 3.2b). However, isochromosomes are not prominent upon deletion of TRF1.

To explain this discrepancy, we considered the possibility that the fused sister telomeres are cleaved after metaphase. Fused telomeres are different from chromosome internal fusions and translocations, as fusion of the repetitive TTAGGG sequence always creates a palindromic sequence. Such palindromes can form cruciform DNA structures (Leach, 1994) (Fig. 4.1a), which are similar to a Holliday junction and might therefore be subject to cleavage by HJ resolvases. Thus, it is possible that fused telomeres (SAs) are cleaved by HJ resolvases during mitosis, resulting in their resolution and normal segregation of the two sister chromatids. Some evidence for cleavage of fused telomeres exists from studies in the budding yeast *S. cerevisiae* (Pobiega and Marcand, 2010). In these experiments, the fate of dicentric chromosomes formed by telomere fusions was followed. Interestingly, these dicentrics often break at the telomere fusion site

during mitosis. However, dicentrics with fusions elsewhere in the chromosome did not break and remained until after cytokinesis, indicating that a special feature of telomeres caused it to be prone to breakage/cleavage (Lopez et al., 2015). Since fused telomeres can form cruciform structures, HJ resolvases could possibly act on them (Pobiega and Marcand, 2010).

Mammalian cells have three pathways for Holliday Junction processing (Fig. 4.1b). The first pathway is mediated by BLM together with Topolla and RMI1 and RMI2 and (BTR complex) (Wu and Hickson, 2003). This pathway involves branch-migration of two HJs to produce a hemicatenane that can be untangled by topoisomerase action. This is an error-free pathway resulting in non-crossover products during HR. However, the dissolution pathway requires double HJs, which are not expected at fused telomeres where only a single HJ can be formed (Fig. 4.1a). Therefore, the BLM dissolution pathway is not expected to be relevant for fused telomere resolution. In agreement with this, shRNA mediated depletion of BLM did not affect the frequency of SAs in a TRF1 null setting (Fig. 3.15b). If BLM were indeed responsible for cleaving fused telomeres, an increase in SAs would be expected in metaphase spreads upon loss of BLM, but this is not observed. Furthermore, SAs are not increased in TRF1^{F/F}BLM^{F/F} MEFs after Cre confirming the shRNA results (Zimmermann et al., 2014).

Two additional HJ resolvase pathways function by endonucleolytic cleavage of a single HJ structure, specifically Mus81 and Gen1 (Ciccia et al.,

2003; Ip et al., 2008; Wyatt et al., 2013). Both these pathways can result in crossover and non-crossover products. Mus81 belongs to the XPF family of nucleases and forms a complex with its regulatory subunit EME1. Mus81 alone is inefficient on intact HJs but works well on 3'-flaps, replication forks and nicked HJs (Wyatt et al., 2013). Nicked HJs can be created by the nucleases SLX4 and SLX1, which form a scaffold for Mus81. Cooperatively, the two complexes can thus cleave intact HJs by a nick and counter-nick mechanism. Gen1 is also a member of the XPG family of nucleases but unlike Mus81, it cleaves HJs symmetrically (Ip et al., 2008; Rass et al., 2010). Contrary to Mus81, Gen1 has no known interaction partners.

Recent studies have shown the temporal and spatial organization of HJ resolvases during the cell cycle (Fig. 4.1b). Since dissolution of dHJs by BLM results only in harmless non-crossovers, this appears to be the pathway of choice for cells. BLM is active throughout S/G2 to untangle any dHJs that arise through replication. However, BLM does not act on single HJs that are formed during DNA repair and some dHJs might be refractory to its action. These HJs require processing by Mus81 or Gen1. Since these resolvases can result in crossovers, their action is limited to later stages of the cell cycle, possibly to allow most processing to be done by BLM. At the onset of mitosis, high CDK1 activity triggers the association of Mus81 with SLX4/SLX1 (Wyatt et al., 2013). How this association is formed precisely is unclear but SLX4, Mus81 and EME1 are all phosphorylated in a CDK1-dependent manner. Gen1 is even more restricted than

Mus81, being actively excluded from the nucleus by a nuclear export signal (Matos et al., 2011; Chan and West, 2014). Only upon nuclear envelope breakdown does Gen1 gain access to any remaining HJs. This spatial and temporal regulation of Gen1 and Mus81 may have evolved to ensure that dHJs are preferentially untangled by dissolution (BLM) to prevent crossover formation and potential loss of heterozygosity.

This chapter is focused on examining the function of the Holliday junction resolvase Gen1, and to a lesser extent Mus81, at telomeres lacking TRF1 to investigate whether they can cleave fused telomeres.

4.2 Results

4.2.1 Gen1 loss induces chromatin bridges after TRF1 loss

To examine the role of Gen1 at telomeres lacking TRF1, CRISPR/Cas9 was used to edit the Gen1 locus in TRF1^{F/F} cells. The gRNAs were designed to target exon 2 of the mouse Gen1 locus on chromosome 12 (Fig. 4.2a). Gen1 contains a XPG-N terminal (XPG-N), XPG-Internal (XPG-I) and helix-hairpin-helix domain in its N-terminus that are required for nuclease activity (Rass et al., 2010). The C-terminus of Gen1 contains a nuclear export signal but otherwise has no known function (Chan and West, 2014). The designed gRNAs target the XPG-N domain in the N-terminus and are thus expected to inactivate Gen1 even if an in-frame deletion is generated (Fig. 4.2a). TRF1^{F/F} cells were transiently infected with Cas9 and two distinct gRNAs and then subcloned. Analysis of isolated clones by

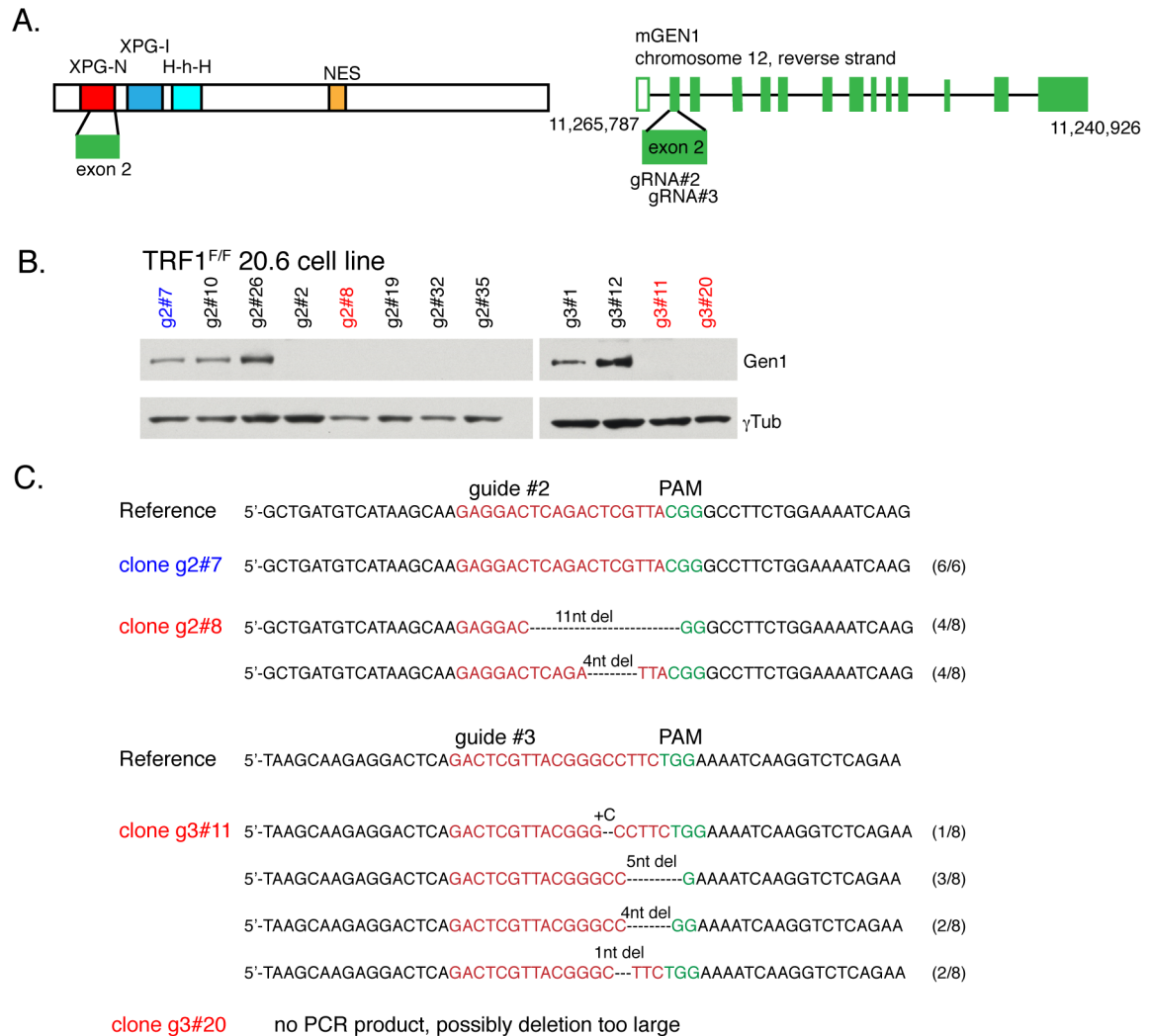


Figure 4.2 CRISPR/Cas9 editing of Gen1 in TRF1^{F/F} MEFs

(A) Schematic of the functional domains of mouse Gen1 with the nuclease domains in red and blue boxes is shown on the left. A nuclear export signal (NES) is shown in yellow. A schematic of the mouse Gen1 locus is shown on the right. The gRNAs 2 and 3 target exon 2, which corresponds to part of the XPG nuclease domain. (B) Immunoblot for Gen1 in clones from TRF1^{F/F} cell line 20.6 targeted with gRNA 2 or 3. Clones in blue (control) and red (null) were used for experiments. (C) DNA sequencing of control clone g2#7 and TRF1^{F/F} Gen1^{-/-} clones g3#11, g2#8 and g3#20, the total number of sequences identified is shown on the right. The reference sequence shows the untargeted DNA with the gRNA sequence (red) and PAM (green). No PCR product was generated from clone g3#20, possibly because the deletions were too large.

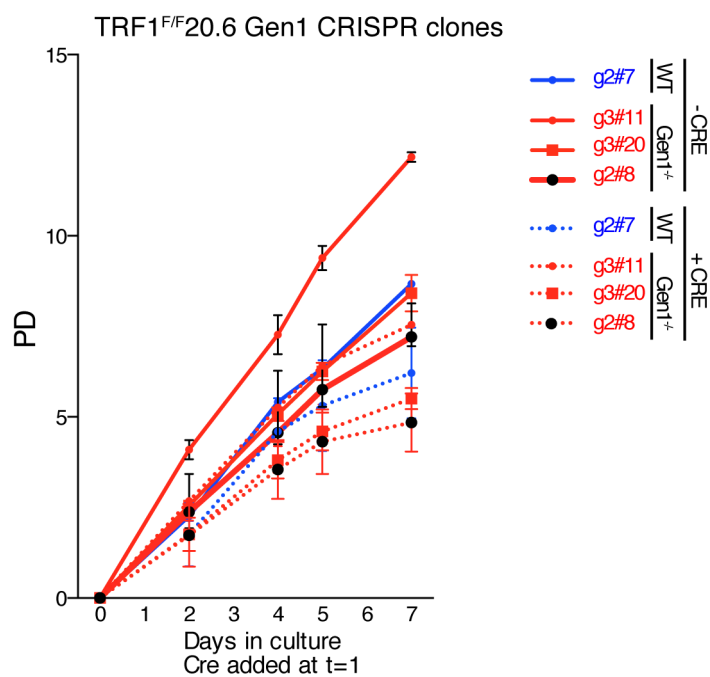


Figure 4.3 Growth curve

Growth curve of the TRF1^{F/F}20.6Gen1 WT (blue) or TRF1^{F/F}20.6Gen1^{-/-} (red) clones before (solid line) and after (dashed line) deletion of TRF1. Cre virus was added at day 1. The means and SEM of two experiments is shown.

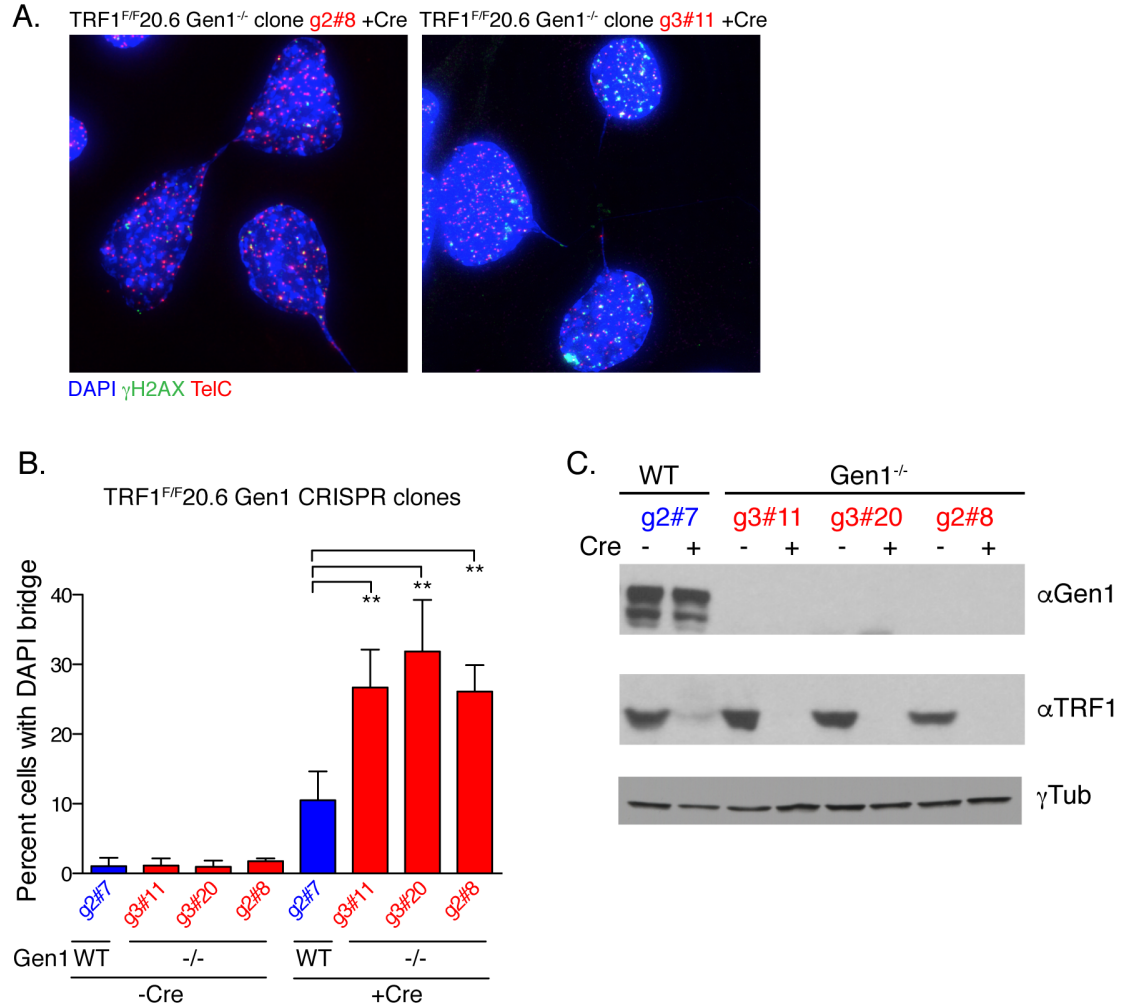


Figure 4.4 Gen1 null cells display increased chromatin bridges after deletion of TRF1

(A) Example of chromatin bridges in TRF1^{F/F}20.6Gen1^{-/-} clones g2#8 (left) and g3#11 (right). Cells were analyzed by IF-FISH 72 h after deletion of TRF1. Bridges often contain telomeric signals (TelC, red). DNA is stained with DAPI and γH2AX in green. (B) Quantification of the percent of cells with chromatin bridges in the indicated cell clones before and 72 h after the deletion of TRF1. Clones in red are Gen1 null whereas the control is in blue. Results represent means and SDs from three independent experiments. At least 200 cells were counted for each condition. P-values determined by a two-sided Student's t-test (* p<0.05, ** p<0.01). (C) Immunoblot with antibodies specific for TRF1, Gen1 and γTub from the cells in B. Cells were harvested 72 h after deletion of TRF1.

western blot indicated efficient editing of Gen1 (Fig. 4.2b). One TRF1^{F/F}20.6Gen1^{+/+} control clone and three TRF1^{F/F}20.6Gen1^{-/-} clones from the parental cell line 20.6 were selected for analysis and targeting of the Gen1 locus was verified by sequencing (Fig. 4.2c). All TRF1^{F/F}20.6Gen1^{-/-} clones grew well and showed no obvious phenotype (Fig. 4.3). This was expected, as Gen1 loss is only lethal when combined with SLX4 or Mus81 depletion (Wechsler et al., 2011; Garner et al., 2013).

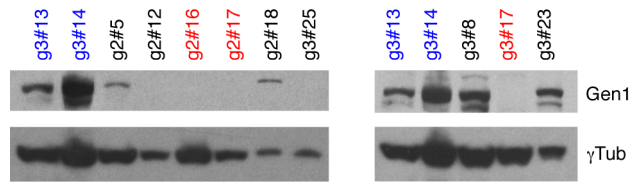
TRF1 was deleted from the TRF1^{F/F}20.6Gen1^{-/-} and control clones and cells were analyzed by IF-FISH for DNA damage markers 72 h later. Interestingly, the TRF1^{F/F}20.6Gen1^{-/-} clones displayed significantly higher levels of chromatin bridges after TRF1 deletion compared to the Gen1-proficient cells (Fig 4.4a-c). Between 25-30% of Gen1 null cells contained these bridges compared to only 10% of Gen1 positive control cells. Without TRF1 deletion, chromatin bridges were rarely seen in any of the cells analyzed. The chromatin bridges were different from the mitotic anaphase bridges described earlier as the chromatin bridges in Gen1 null cells remained after mitosis into the next G1 and were visible by a thin DAPI or Hoechst positive bridge (Fig.4.4a).

A second TRF1^{F/F} parental cell line (9.3) was edited with the same gRNAs targeting the Gen1 locus to verify the results in an independent cell line. Two control TRF1^{F/F}9.3Gen1^{+/+} and three TRF1^{F/F}9.3Gen1^{-/-} clones were picked based on Gen1 expression analyzed by western blot (Fig. 4.5a). Targeting of the Gen1 locus was verified by sequencing (Fig. 4.5b). Again, 72 h after deletion of TRF1

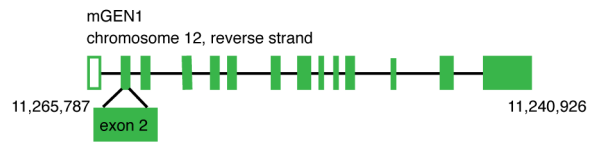
Figure 4.5 CRISPR/Cas9 editing of Gen1 in TRF1^{F/F} cell line 9.3

(A) Immunoblot of isolated clones from TRF1^{F/F} cell line 9.3 with antibodies specific for Gen1 or γ -tubulin control. Clones in blue (control) and red (Gen1^{-/-}) were picked for further analysis. (B) Schematic of the mouse Gen1 locus, as in Fig. 4.2. DNA sequencing of control clones (blue) and Gen1^{-/-} clones (red) is shown below. The reference sequence displays the untargeted DNA with the gRNA sequence (red) and PAM (green). No PCR products were generated from clones g2#17 and g3#17, possibly because the deletion was too large. (C) Quantification of chromatin bridges in the indicated cell clones before and 72 h after deletion of TRF1. Clones in red are Gen1 null cells and controls are blue. Values represent means and SDs from three independent experiments, at least 200 cells were counted per condition. P-values determined by a two-sided Student's t-test (* p<0.05, ** p<0.01, ns: not significant).

A. TRF1^{F/F} 9.3 cell line



B. TRF1^{F/F} 9.3 cell line



Reference 5'-GCTGATGTCATAAGCAAGAGGACTCAGACTCGTTACGGGCCTTCTGGAAAATCAAG (3/4)
 clone 2#16 5'-GCTGATGTCAT-----58nt del----- (3/4)
 5'-GCTGATGTCATAAGCAAGA-----31nt del-----ATCAAG (1/4)
 clone 2#17 no PCR product, possibly deletion too large

Reference 5'-TAAGCAAGAGGACTCAGACTCGTTACGGGCCTTCTGGAAAATCAAGGTCTCAGAA

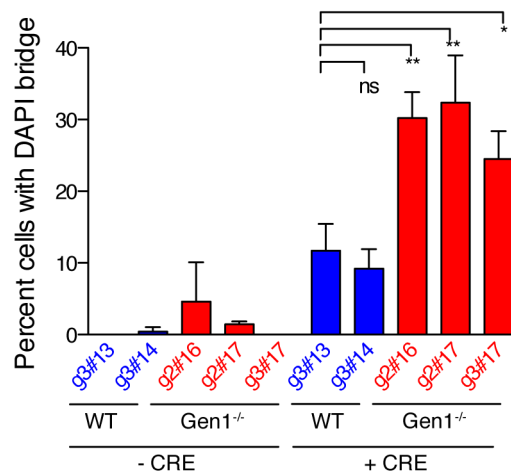
clone g3#13 5'-TAAGCAAGAGGACTCAGACTCGTTACGGGCCTTCTGGAAAATCAAGGTCTCAGAA

clone g3#14 5'-TAAGCAAGAGGACTCAGACTCGTTACGGGCCTTCTGGAAAATCAAGGTCTCAGAA

clone g3#17 no PCR product, possibly deletion too large

C.

TRF1^{F/F} 9.3 Gen1 CRISPR clones



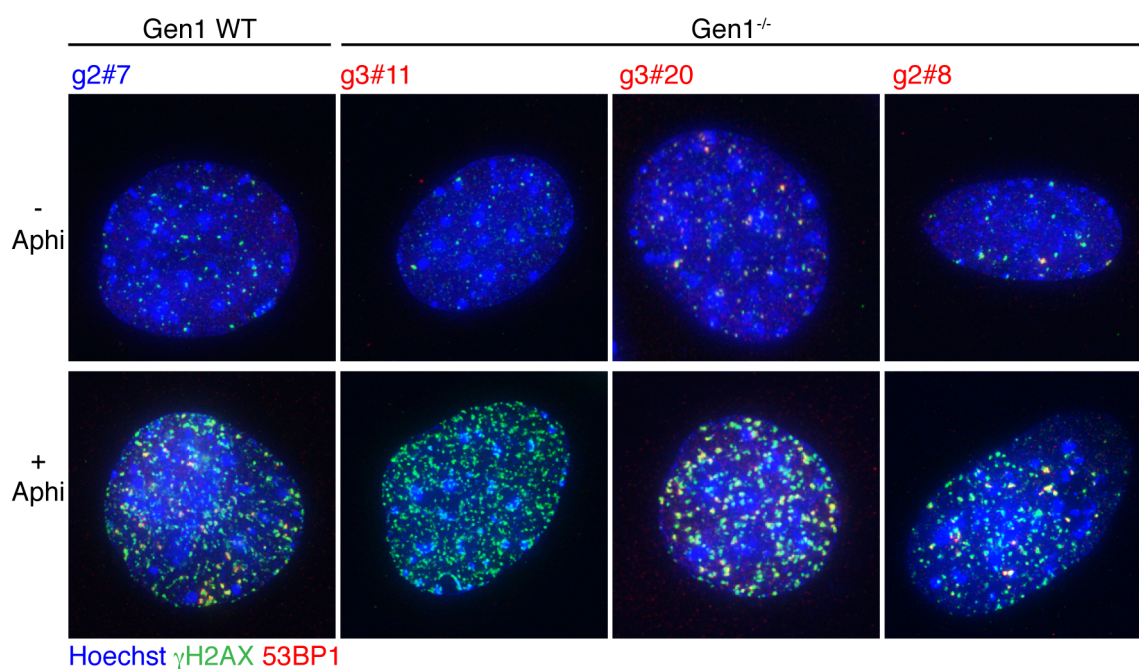
the clones without Gen1 displayed a higher level of chromatin bridges (Fig. 4.5c). The bridges were specific to the deletion of TRF1 as no defect was seen in clones not treated with Cre. The chromatin bridges were often (partially) covered by γ H2AX staining indicating DNA damage signaling. A telomeric signal could frequently be observed in these bridges, suggesting the presence of fused telomeres (Fig. 4.4a). The results suggest that Gen1 indeed has an important role in resolving chromatin bridges formed after deletion of TRF1

4.2.2 Aphidicolin does not induce chromatin bridges

To examine whether the chromatin bridges in Gen1 null cells are the result of general replication stress at telomeres or specific to a particular phenotype that occurs upon deletion of TRF1, cells were treated with the DNA polymerase inhibitor aphidicolin. It is known that aphidicolin leads to CFS expression and exacerbates the telomere fragility seen upon TRF1 deletion (Glover et al., 1984; Martinez et al., 2009; Sfeir et al., 2009). Additionally, aphidicolin treatment induces telomere fragility even in presence of TRF1. However, aphidicolin has no effect on SAs and they remain absent when TRF1^{F/F} cells are treated with aphidicolin without TRF1 deletion (Sfeir et al., 2009). Therefore, this treatment allows separating the effect of general replication stress at telomeres from the SAs seen upon TRF1 deletion.

TRF1^{F/F} 20.6Gen1 CRISPR clones were treated with 0.5 μ M aphidicolin for 16 h and harvested for IF analysis immediately after. Cells displayed a strong

A. TRF1^{F/F}20.6 CRISPR Clones



B. TRF1^{F/F}20.6 Gen1 CRISPR clones

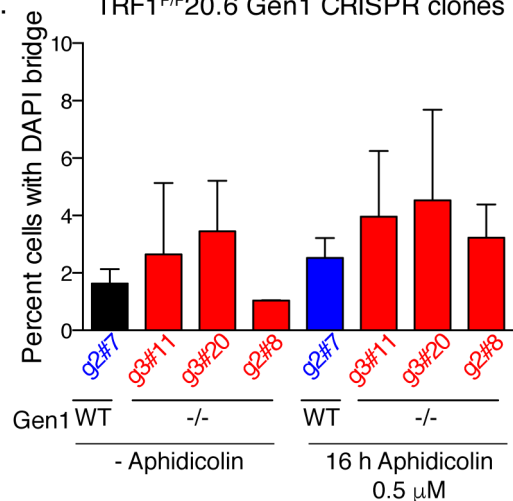


Figure 4.6 Aphidicolin treatment does not induce chromatin bridges in TRF1^{F/F}Gen1^{-/-} MEFs

(A) Representative images of indicated TRF1^{F/F}20.6Gen1^{-/-} (red) or control clones (blue) before and 16 h after aphidicolin treatment (CRISPR clones from Fig. 4.2). Cells were stained with Hoechst, 53BP1 (red) and γH2AX (green). (B) Quantification of chromatin bridges after aphidicolin treatment. Clones in red are Gen1 null clones and blue are controls. Values represent means and SDs from three experiments; at least 200 cells were counted per condition. Differences are not significant.

increase in the level of γ H2AX upon aphidicolin treatment, indicative of replication stress (Fig. 4.6a). However, chromatin bridges were not induced by aphidicolin treatment (Fig. 4.6b). This suggests that the chromatin bridges seen in TRF1^{F/F}Gen1^{-/-} cells after Cre are the result of a TRF1 specific phenotype, in agreement with the hypothesis that Gen1 acts on SAs.

4.2.3 Gen1 loss does not affect the frequency of SAs or telomere fragility

To determine whether the increase in chromatin bridges in Gen1 null cells is due to an increase in SAs, metaphase spreads from TRF1^{F/F}20.6Gen1^{-/-} clones were analyzed 96 h after deletion of TRF1. A difference in the percentage of SAs was observed between the different clones analyzed (Fig. 4.7a). However, the difference did not correlate with the presence or absence of Gen1. For example, Gen1^{-/-} clone g3#11 had a higher level of SAs than the control clone whereas Gen1^{-/-} clone g3#20 had lower levels. This suggests that there is clonal variation in the level of SAs but that Gen1 itself has no effect on their prevalence. Gen1 is actively excluded from the nucleus until nuclear envelope breakdown and therefore not expected to gain access to SAs before metaphase. Thus, the absence of an effect of Gen1 on the level of SAs in metaphase is likely due to its late action in the cell cycle. Telomere fragility was also analyzed on the same metaphase spreads (Fig. 4.7b). As expected, Gen1 did not affect the level of telomere fragility.

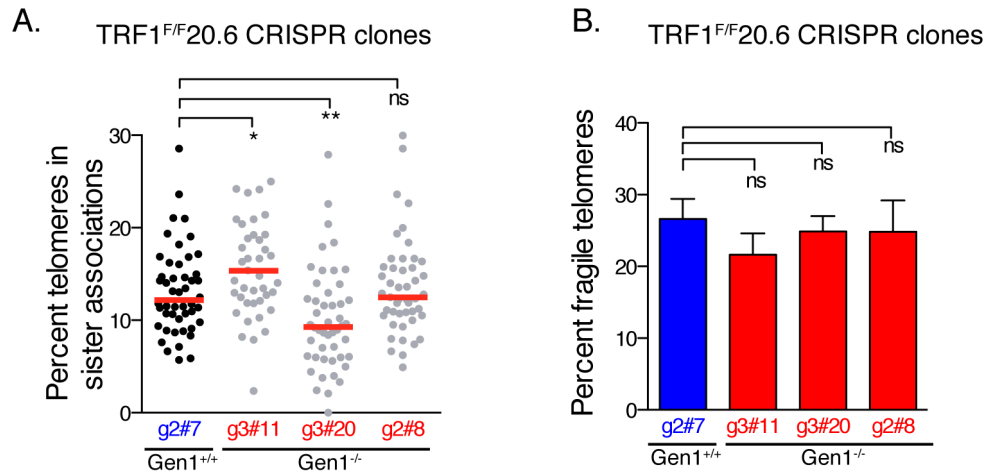


Figure 4.7 SAs and telomere fragility in TRF1^{F/F}20.6Gen1^{-/-} clones

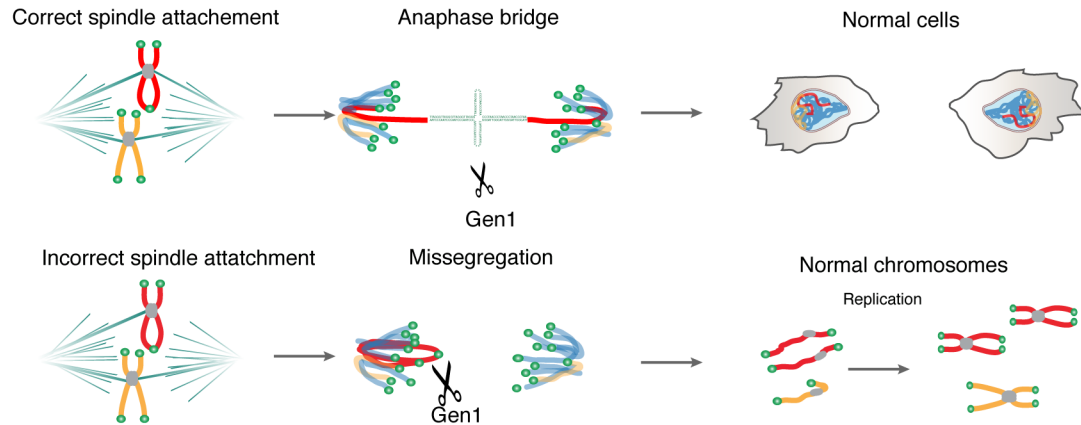
(A) Frequency of SAs in metaphase spreads 96 h after Cre. Clones in red are TRF1^{F/F}20.6Gen1^{-/-} cells and those in blue are control (CRISPR clones from Fig. 4.2). Bars represent the median % of SAs from 3 independent experiments; each dot represents a metaphase spread. (B) Analysis of telomere fragility on the metaphase spreads from A. Values represent mean and SDs from three independent experiments. SAs and fragility were counted on the long arm only. P-values determined by a two-sided Student's t-test (* p<0.05, ** p<0.01, *** p<0.001, ns: not significant).

4.2.4 Gen1 loss increases the frequency of isochromosomes

As argued in the introduction of Chapter 3, sister telomere fusions are expected to result in isochromosomes in the following metaphase, but these are not commonly observed after TRF1 loss (Sfeir et al., 2009). Their absence can be explained if Gen1 cleaves the sister fusions to allow faithful chromosome separation (Fig. 4.8a). If this model is correct, isochromosomes are expected to arise in TRF1^{F/F}Gen1^{-/-} cells, since cleavage of SAs would not occur. In absence of Gen1, a chromosome with fused sister telomeres would have two fates (Fig. 4.8b). If the spindle forms correct attachments to the centromere, it will try to separate this chromosome into two daughter nuclei resulting in an anaphase/chromatin bridge at the fused telomere, as frequently observed in TRF1^{F/F}Gen1^{-/-} cells. But if the spindle forms incorrect attachments or when for another reason the entire chromosome is missegregated into one daughter cell, an isochromosome would be formed after the next DNA replication (Fig. 4.8b). To test whether the level of isochromosomes is indeed higher in Gen1 null cells, metaphase spreads were analyzed in TRF1^{F/F}20.6Gen1^{-/-} cells after deletion of TRF1.

Discriminating between isochromosomes and other types of chromosome fusions in MEFs is not straightforward as many mouse chromosomes are of similar size and all mouse chromosomes are acrocentric. The following criteria were applied to identify isochromosomes. They should show either long arm to long arm (L-L) fusions or short arm to short arm (S-S) fusions and the two long

A. TRF1^{F/F} wild type



B. TRF1^{F/F} No Gen1

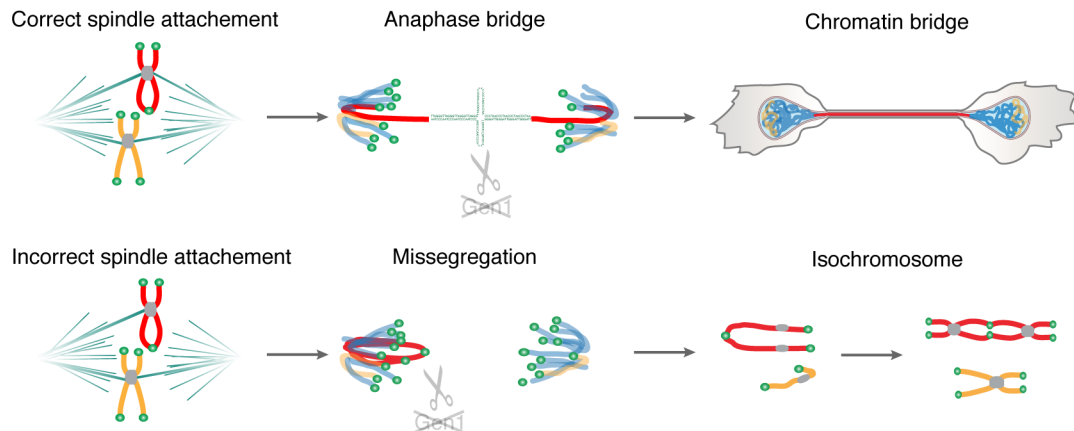


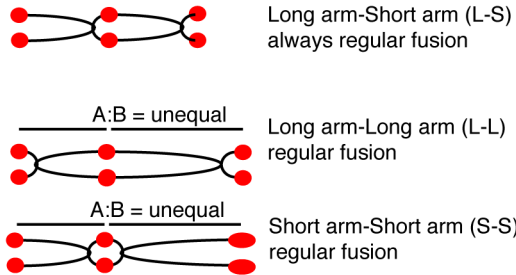
Figure 4.8 Faith of a sister fusion in absence of Gen1

(A) Upon deletion of TRF1, anaphase bridges can form when a chromosome with a sister telomere fusion (red) is separated (top). Cleavage of the telomere fusion by Gen1 still allows faithful chromosome segregation. When the spindle forms an incorrect attachment or loses its connection (bottom), the entire chromosome is missegregated into one daughter cell. Cleavage by Gen1 can prevent the formation of isochromosomes. (B) In absence of Gen1, a chromosome with a sister fusion can follow two fates in mitosis. If the spindle forms a correct attachment, the fused chromosome will form a chromatin bridge (top). When the spindle forms an incorrect attachment or loses its connection, the entire chromosome is missegregated into one daughter cell (bottom). Replication in the next S-phase will result in the formation of an isochromosome (red).

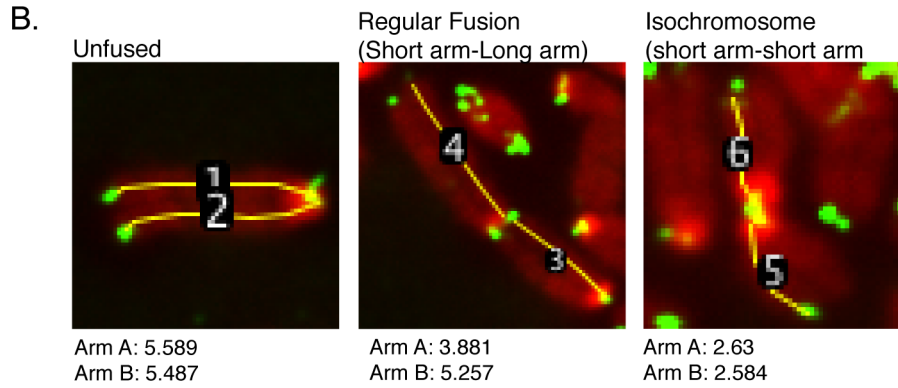
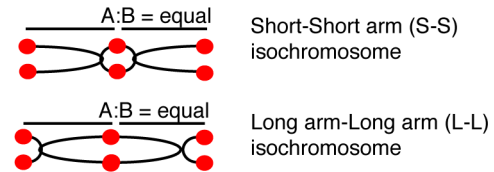
Figure 4.9 Verification of isochromosome analysis

(A) Schematics of different forms of fusions detected. Chromosomes fused via Long arm-Short arm (L-S) are always regular fusions (left panel). Long arm-Long arm (L-L) or Short arm-Short arm (S-S) are regular fusions if the arm lengths are unequal (left). However, S-S and L-L fusions are scored as isochromosomes if the arm lengths are equal (right panel). (B) Examples of different forms of fused chromosomes. The lines represent the arm lengths measured in image J, which were used to calculate arm length ratio. (C) An example calculation of arm ratios from A is shown in the table. For each chromosome, the values of arm A and B used to determine the ratio between the longer and shorter arm (values >1). (D) The arm ratios of chromosome arms from three independent experiments are shown. Long arm sister chromatids were compared on unfused chromosomes as a control for the accuracy of the imageJ measurements. Chromosome fusions after deletion of TRF2 were used to display the variability in arm length in regular fusions. The blue dots represent the arm ratio of regular fusions in the indicated Gen1 WT (blue) or Gen1^{-/-} (red) cells 96 h after deletion of TRF1, which are either L-L, S-S or L-S as explained in A. The arm ratio of chromosomes counted as isochromosomes is shown in green dots for each clone, which are either L-L or S-S with equal arm length. Every dot represents a (fused) chromosome. The average, SD and numbers (n) are shown in top of the graph. (E) The mean and SDs of the arm ratios from D is shown. Values are from 3 independent experiments and 10 metaphase spreads were analyzed per condition for the Gen1 CRISPR clones. For unfused and TRF2 fusions, only 2-5 metaphase spreads were analyzed per experiment since the number of analyzable chromosomes (unfused or TRF2 fused resp) is much higher per spread. P-values determined by a two-sided Student's t-test (* p<0.05, ** p<0.01, *** p<0.001, ns: not significant).

A. Schematic of regular fusion types

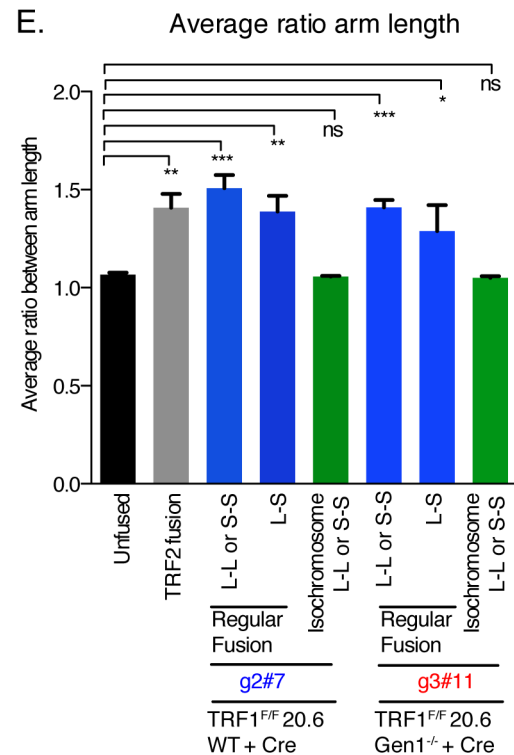
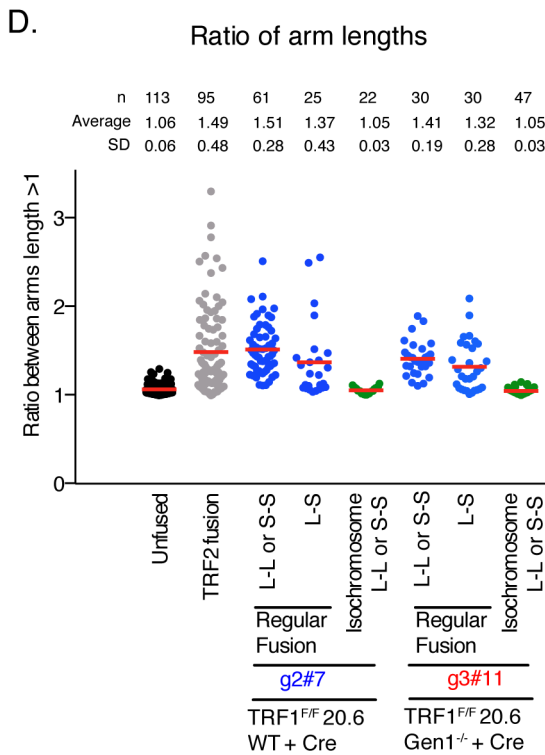


Schematic of isochromosome types



C.

	Arm A	Arm B	Ratio		Value >1
			Arm A/B	Arm B/A	
Unfused	5.589	5.487	1.018	0.982	1.018
Regular Fusion	3.881	5.257	0.738	1.355	1.355
Isochromosome	2.63	2.584	1.018	0.983	1.018



arms in the fusion should be of the same length (Fig. 4.9a). Fusion chromosomes that fit these two criteria are scored as isochromosomes in this study. By contrast, a chromosome that is fused long arm to short arm (L-S) is classified as a regular type fusion as are L-L or S-S fusions with unequal arm length (Fig. 4.9a).

Isochromosomes were counted according to these visual criteria. To ensure that the chromosomes visually counted as an isochromosome indeed have equal arm lengths, these lengths were measured using Image J. A subset of the analyzed metaphase spreads from TRF1^{F/F}20.6Gen1^{-/-} clone g3#11 and control clone g2#7 were used for this Image J analysis. The measurements were made using the following method. First, the arm length of both long arm (sister) chromatids of unfused chromosomes was measured to identify the variability in measuring arm length with imageJ (Fig. 4.9b-e) and the ratio between the longer and the shorter value of the two sister chromatids was calculated (Fig. 4.9c). As seen in Figure 4.9d, the ratio of the sister chromatids of unfused chromosomes is close to 1 (average 1.067, SD 0.060 n=113). This controls for the variability in measuring arm length using Image J. Next, the chromosome arm length of telomere fusions detected upon TRF2 deletion were analyzed to visualize the distribution of regularly fused chromosomes (Fig. 4.9b-e). As telomere fusion after TRF2 deletion occurs primarily in G1, sister fusions and thus isochromosomes will be infrequent. The length of the arms on either side of the fusion was measured and the ratios calculated (Fig. 4.8c). As seen in Figure 4.8c

and d, the ratios are widely distributed (average 1.488, SD 0.48, n= 94) as expected based on random fusion of the telomeres of different chromosomes. Next, fusions from TRF1^{F/F}20.6Gen1^{-/-} or TRF1^{F/F}Gen1^{+/+} MEFs were analyzed. In these metaphase spreads, both regular fusions and isochromosomes are observed, although TRF1^{F/F}Gen1^{+/+} MEFs have fewer isochromosomes. The arm length on either side of the fusion was measured, similar as for the telomeres fusions after TRF2 deletion (Fig. 4.9c). In the chromosomes that were considered an isochromosome (L-L or S-S as explained in Figure 4.9a), the ratio is very close to 1 similar to the unfused chromosomes suggesting that these are indeed isochromosomes (Fig. 4.9d and e). Furthermore, arm ratios of regularly fused chromosomes in these TRF1^{F/F}Gen1^{-/-} or TRF1^{F/F}Gen1^{+/+} MEFs were analyzed as well. A distinction was made between L-S fusions and L-L or S-S, as the latter type of fusion could possibly be an isochromosome (schematic 4.9a). However, the ratios of L-L, S-S and L-S are widely distributed similarly to fused chromosomes observed after TRF2 deletion, indicating that none of these are isochromosomes (Fig. 4.9d and e). This approach verifies that the chromosomes visually counted as isochromosomes indeed have arm ratios similar to unfused chromosomes, strengthening assumption that they represent real isochromosomes. While the isochromosomes measured using this method visually appear as isochromosomes, this cannot definitely be ascertained without chromosome paint (SKY) analysis. Some of the chromosomes counted as isochromosomes might therefore be regular fusions of two chromosomes of similar length. It is therefore

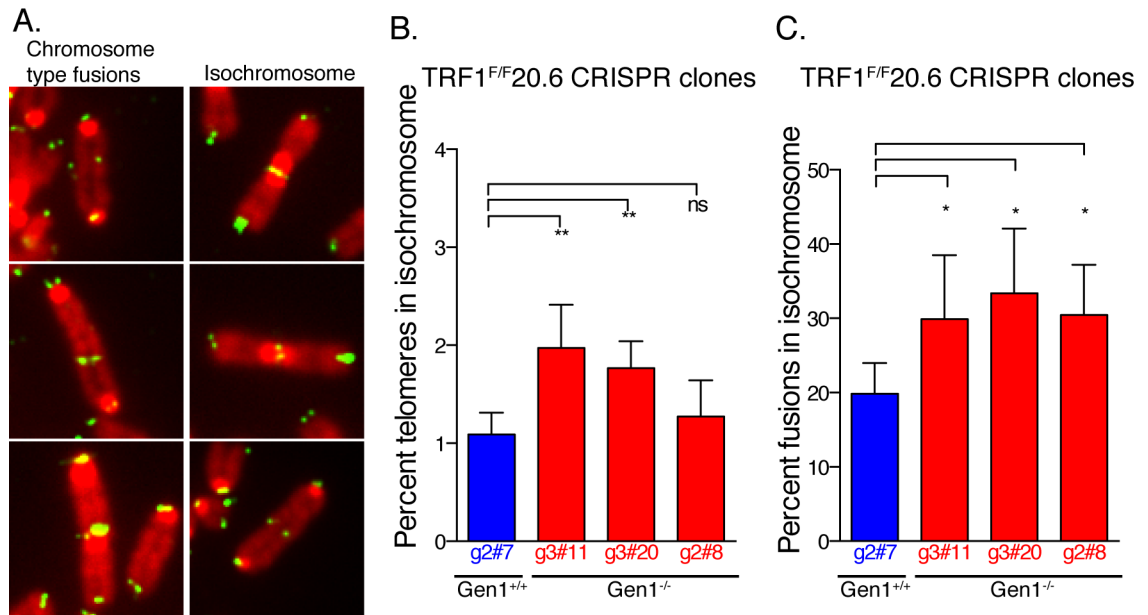


Figure 4.10 Isochromosomes are increased in Gen1 null cells

(A) Examples of normal chromosome type fusions (left) and isochromosomes (right) in metaphase spreads. Telomeres are in green, DAPI in red. (B) Percentage of telomeres in isochromosomes in TRF1^{F/F}20.6Gen1 CRISPR clones. The values represent mean and SDs from 5 independent experiments. (C) Representation of the values from D as percent fusions in isochromosomes, to correct for differences in overall telomere fusion rate. The values represent mean and SDs from 5 experiments. Detailed explanation of isochromosome count can be found in Figure 4.9. P-values determined by a two-sided Student's t-test (* p<0.05, ** p<0.01, *** p<0.001, ns: not significant).

required to correct for the total number of chromosome type fusions between clones, as this can influence the analysis. Accordingly, isochromosome frequencies are given both as the percent of telomeres present in isochromosomes and as the percent of chromosome fusions that are isochromosomes.

Using the described approach and rules, isochromosomes were counted on metaphase spreads from the TRF1^{F/F}20.6Gen1 CRISPR clones after deletion of TRF1 (Fig. 4.10a-c). Interestingly, a 1.5-2fold increase in the number of isochromosomes was observed in Gen1^{-/-} clone g3#11 and g3#20 compared to control cells. Clone g2#8 also showed an increase in the number of isochromosomes but this increase was not significant. Possibly, this is due to the slower growth of this particular clone, since the detection of isochromosomes depend on the rate at which cells progress to the next mitosis (Fig. 4.3). Combined, the results suggest that isochromosome formation in TRF1 KO cells is indeed increased in absence of Gen1.

4.2.5 TRF1^{F/F}Gen1^{-/-} cells display increased mitotic failure

The experiments using live cell imaging from chapter 3 showed that TRF1^{F/F} cells display high numbers of mitotic abnormalities when TRF1 is deleted from cells (Fig. 3.7b). To examine the behavior of TRF1^{F/F}Gen1^{-/-} cells during mitosis, TRF1^{F/F}9.3Gen1^{-/-} clones were examined by live cell imaging. Cells were retrovirally infected with the H2B-venus construct and a population of high

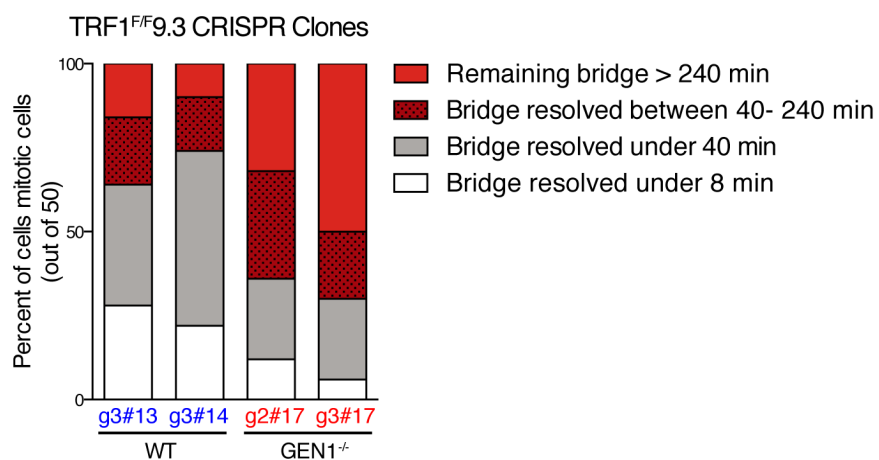


Figure 4.11 Anaphase bridges in TRF1^{F/F}Gen1^{-/-} cells persist longer

Analysis of a live cell imaging experiment of indicated TRF1^{F/F}9.3Gen1^{-/-} or control clones expressing H2B-venus (CRISPR clones from Figure 4.5). Cells were imaged on a spinning disk confocal microscope and Z-stacks taken 4 minutes apart. At least 50 mitotic cells were followed per condition and the time counted until an anaphase bridge disappeared. Mitotic cells without anaphase bridges are counted as bridge resolved under 8 minutes.

expressing cells isolated using FACS sorting to allow visualization of chromosome dynamics. Cells were imaged with the same experimental setup as used for the analysis of mitotic cells after TRF1 deletion (Chapter 3.2.4). Briefly, cells were imaged 72 h after Cre using a Yokogawa spinning-disk confocal system and images (Z-stacks) were acquired every 4 minutes. Analysis of mitotic cells in the movies showed that there was no difference in the prevalence of anaphase bridges between the Gen1 positive and negative clones, which is not surprising given that they occur at 80% in Gen1 positive cells. However, there was a substantial increase in the persistence of the bridges in Gen1 null cells (Fig. 4.11). Whereas in two TRF1^{F/F}9.3Gen1^{+/+} control clones the majority of the bridges were resolved under 40 minutes, the majority of anaphase bridges in TRF1^{F/F}9.3Gen1^{-/-} clones remained much longer or did not disappear for the duration of the movie (Fig. 4.11). This supports the observation that chromatin bridges are frequently observed between post-mitotic interphase cells in TRF1^{F/F}Gen1^{-/-} clones after deletion of TRF1 (Figs. 4.4b and 4.5c).

4.2.6 Overexpression of mutant Gen1 alleles in TRF1^{F/F}Gen1^{-/-} MEFs

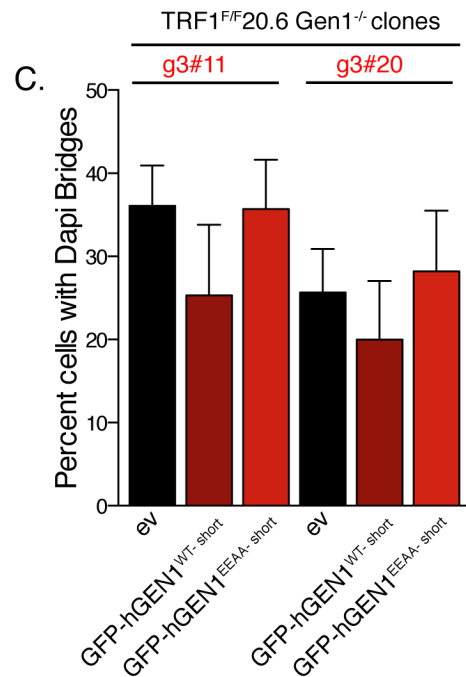
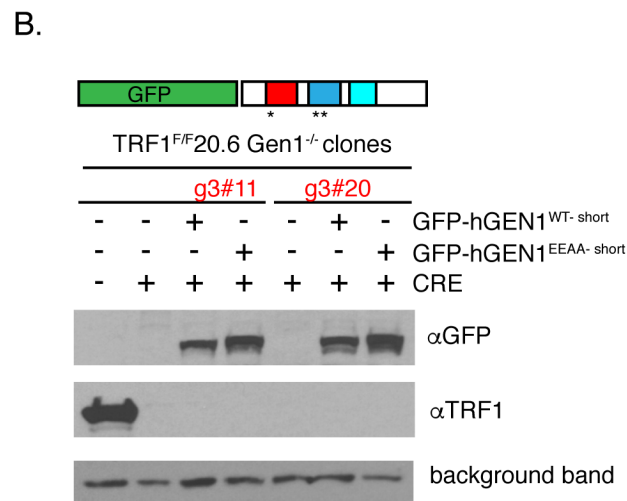
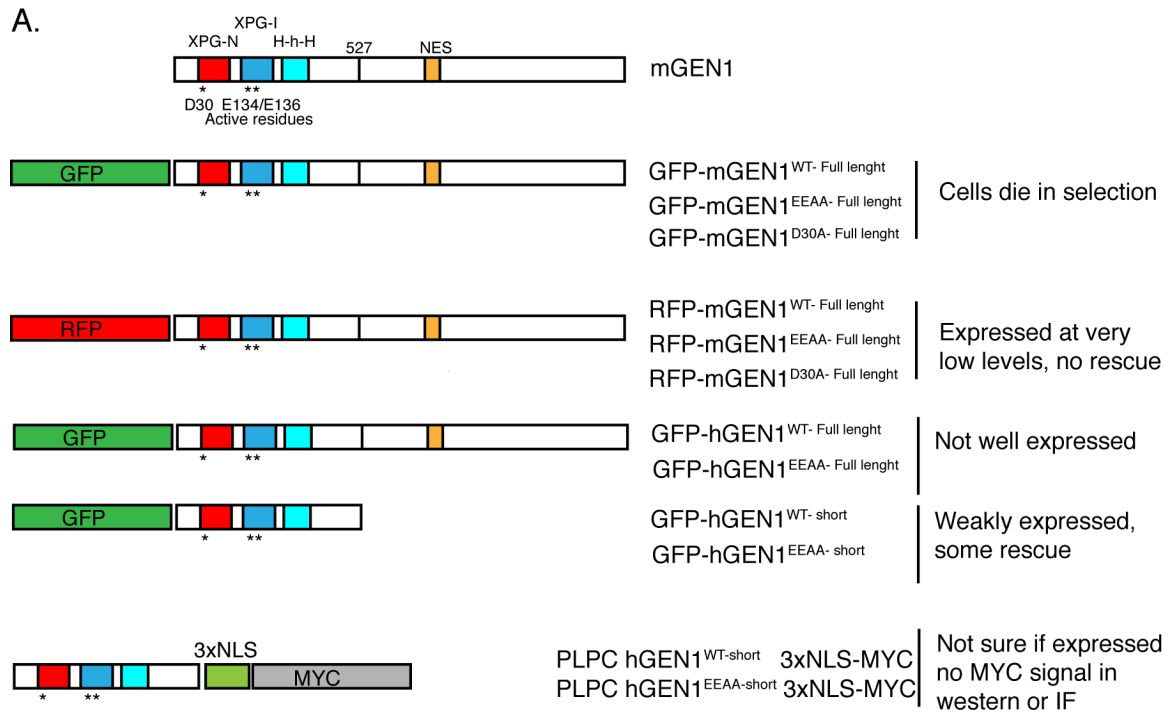
The persistent chromatin bridges in TRF1^{F/F}Gen1^{-/-} cells upon deletion of TRF1 are a striking phenotype. This phenotype was observed in two separate cell lines with two independent gRNAs against Gen1, strongly suggesting that the bridges are due to the loss of Gen1 and not an off-target effect of the CRISPR/Cas9. However, an attempt was made to rescue the phenotype by overexpressing

Gen1 in the TRF1^{F/F}20.6Gen1^{-/-} cells. The catalytic activity of Gen1 is dependent on its N-terminal XPG nuclease domain and a flanking helix-hairpin-helix domain (Ip et al., 2008) (Fig. 4.12a, top). Previous in vitro experiments with a truncated form of Gen1 (aa 1-527) indicated that the N-terminus contains all Holliday junction resolvase activity (Rass et al., 2010). Although the C-terminus is not needed for catalytic activity, it contains a nuclear export signal (NES) that is required to actively keep Gen1 from accessing chromatin until nuclear envelope breakdown in mitosis (Chan and West, 2014). Access of Gen1 to the nucleus in interphase was accomplished by mutating both the NES and addition of a nuclear localization signal.

To attempt to rescue the chromatin bridge formation in TRF1^{F/F}20.6Gen1^{-/-} cells, plasmids were cloned containing an N-terminal RFP or GFP tag followed by a catalytically active or inactive mouse Gen1 (mGen1) (Fig. 4.12a). For inactive Gen1, either the E30A mutant or E134/E136A (EEAA) mutations was created since these sites were previously shown to be required for the catalytic activity (Chan and West, 2014). However, none of these constructs expressed well upon retroviral infection of MEFs. Cells quickly lost the construct or died in antibiotic selection medium. Since previous publications used human Gen1 (hGen1) in overexpression experiments, N-terminal GFP tagged constructs were cloned with hGen1, either the active or an inactive (EEAA) form. However, overexpression of these constructs in MEFs resulted in a similar defect in expression. Since a truncated version of Gen1 (Gen1⁵²⁷) contains all catalytic activity and was

Figure 4.12 TRF1^{F/F} Gen1^{-/-} cells with overexpressed Gen1

(A) Schematic of wild type mouse Gen1 and a variety of tagged constructs (mouse and human). Red and blue boxes in the schematic on top represent the domains of Gen1 required for nuclease activity (XPG-N-terminal, XPG-Internal and Helix-hairpin-Helix). The EEAA mutants have residues E134 and E136 mutated to alanine, the D30A has active site D30 mutated to alanine. The constructs with a shorted Gen1 contain amino acids 1-527. Most constructs did not express well, as indicated on the right. (B) Immunoblot showing the expression of a short form of hGen1 containing an N-terminal GFP tag in TRF1^{F/F}20.6Gen1^{-/-} clones g3#11 and g3#20 (CRISPR clones from Figure 4.2). Cells were harvested 72 h after Cre. (C) Quantification of chromatin bridges 72 h after Cre mediated deletion of TRF1 in TRF1^{F/F}20.6Gen1^{-/-} clones g3#11 and g3#20, expressing the indicated hGen1 construct. Results represent the mean and SD from 4 experiments. Expression level of constructs and the number of bridges varied widely and the results are not significant.



previously shown to rescue human Gen1^{-/-} cells, this construct was cloned with an N-terminal GFP tag. Upon retroviral infection of TRF1^{F/F}20.6Gen1^{-/-} clone g3#20 and g2#8, the active and inactive versions of this construct were weakly expressed (Fig. 4.12b). TRF1 was deleted in these cells using H&R Cre virus and chromatin bridges analyzed by IF 72 h later. Interestingly, a slight rescue was seen with the active version of Gen1 but not Gen1^{EEAA} (Fig. 4.12c). However, these experiments were not reproducible and expression levels of the constructs varied indicating that cells still struggled keeping these constructs expressed.

Possibly, the N-terminal GFP or RFP tag interferes with the expression of Gen1. Previous studies used C-terminally tagged protein and thus a construct was cloned with a C-terminal myc tag. The truncated version of Gen1 was used in this construct. Additionally, a 3xNLS was added to promote nuclear localization of the construct (Chan and West, 2014). However, upon infection of MEFs with this construct, no signal for myc was detected on Western blot (Fig. 4.12b). Furthermore, no reduction in chromatin bridges was detected indicating that this construct was not functional. Further attempts to rescue the TRF1^{F/F}Gen1^{-/-} clones were halted.

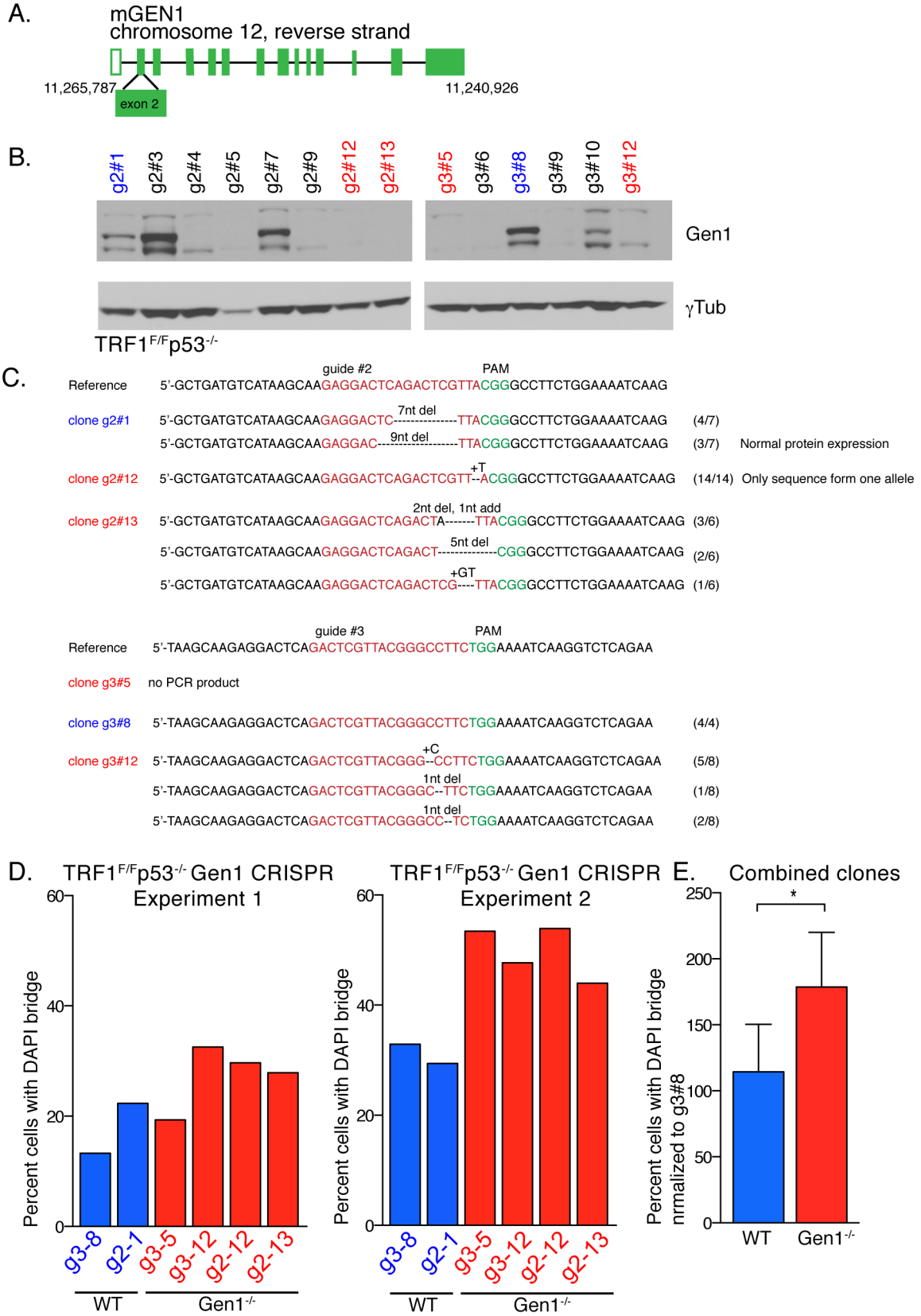
4.2.7 Chromatin bridges are not an SV40 artifact

Since rescue of the TRF1^{F/F}Gen1^{-/-} clones was not possible, an additional control experiment was done to verify that the chromatin bridges observed in Gen1 null cells are not due to the experimental conditions used. Both TRF1^{F/F} cell lines that

were used for CRISPR/Cas9 mediated editing of the Gen1 locus were immortalized using SV40 large T antigen. Since SV40 large T antigen may have uncharacterized functions, it is not excluded that the phenotypes we detect are due to the combined effect of TRF1 loss, Gen1 deficiency and SV40 immortalization. Therefore, an additional Gen1 knockout cell line was created in a parental cell line that lacks p53 but does not express SV40 large T antigen. The same gRNAs were used as described previously and several Gen1 null and control clones were isolated from this TRF1^{F/F}p53^{-/-} cell line (Fig. 4.13a,b). Sequencing confirmed efficient targeting of the Gen1 locus in the Gen1^{-/-} clones g2#12, g2#13 and g3#12 whereas no PCR product was amplified from clone g3#5, likely because the deletion is too large (Fig. 4.13c). Sequencing of the control clone g3#8 confirmed that this clone only contains the unedited Gen1 sequence. However, control clone g2#1 is not completely wild type as it has lost one allele due to a 7-nucleotide deletion and the other allele in this clone contains a 9-nucleotide deletion. This 9 nt deletion does not disrupt protein expression but the western blot signal for Gen1 in this clone is lower than in the other control clones, confirming the loss of one allele. Next, TRF1 was deleted in these TRF1^{F/F}p53^{-/-}Gen1 clones and cells harvested for analysis of chromatin bridges 72 h later. Two separate experiments were done and although there was variability between the experiments, the TRF1^{F/F}p53^{-/-}Gen1^{-/-} cells displayed a higher frequency of bridges than the control clones (Fig. 4.13d and e). These

Figure 4.13 CRISPR/Cas9 editing of Gen1 in TRF1^{F/F}p53^{-/-} MEFs

(A) Schematic of the Gen1 locus on chromosome 12, exon 2 was targeted with the same gRNAs as in Fig. 4.2. (B) Western blot of indicated TRF1^{F/F}p53^{-/-} clones targeted with gRNA2 or gRNA3, showing the deletion of Gen1. Clones in blue (control) and red (null) were used for experiments. (C) DNA sequencing of the indicated clones showing targeting of the Gen1 locus. Clones g2#1 and g3#8 are control clones whereas clones g3#5, g3#12, g2#12 and g2#13 are Gen1^{-/-}. (D) Analysis of chromatin bridges in indicated Gen1 control (blue) and Gen1^{-/-} (red) clones, 72 h after Cre mediated deletion of TRF1. The percentage of bridges from two experiments is shown side by side. The baseline levels of chromatin bridges between these experiments varied greatly thus the results are shown separate. At least 200 cells were analyzed per condition. (E) The percent chromatin bridges of Gen1 control (blue) and Gen1^{-/-} (red) clones from the two experiments in D were pooled as WT and Gen1^{-/-}. The percent chromatin bridges of each clone were compared to the level in control clone g3#8, which was set to 100. The values represent the mean and SDs of all values from clones in D. P-values determined by a two-sided Student's t-test (* p<0.05).



experiments indicate that the phenotype of the $\text{Gen1}^{-/-}$ cells is unlikely due to confounding effects of the SV40 immortalization.

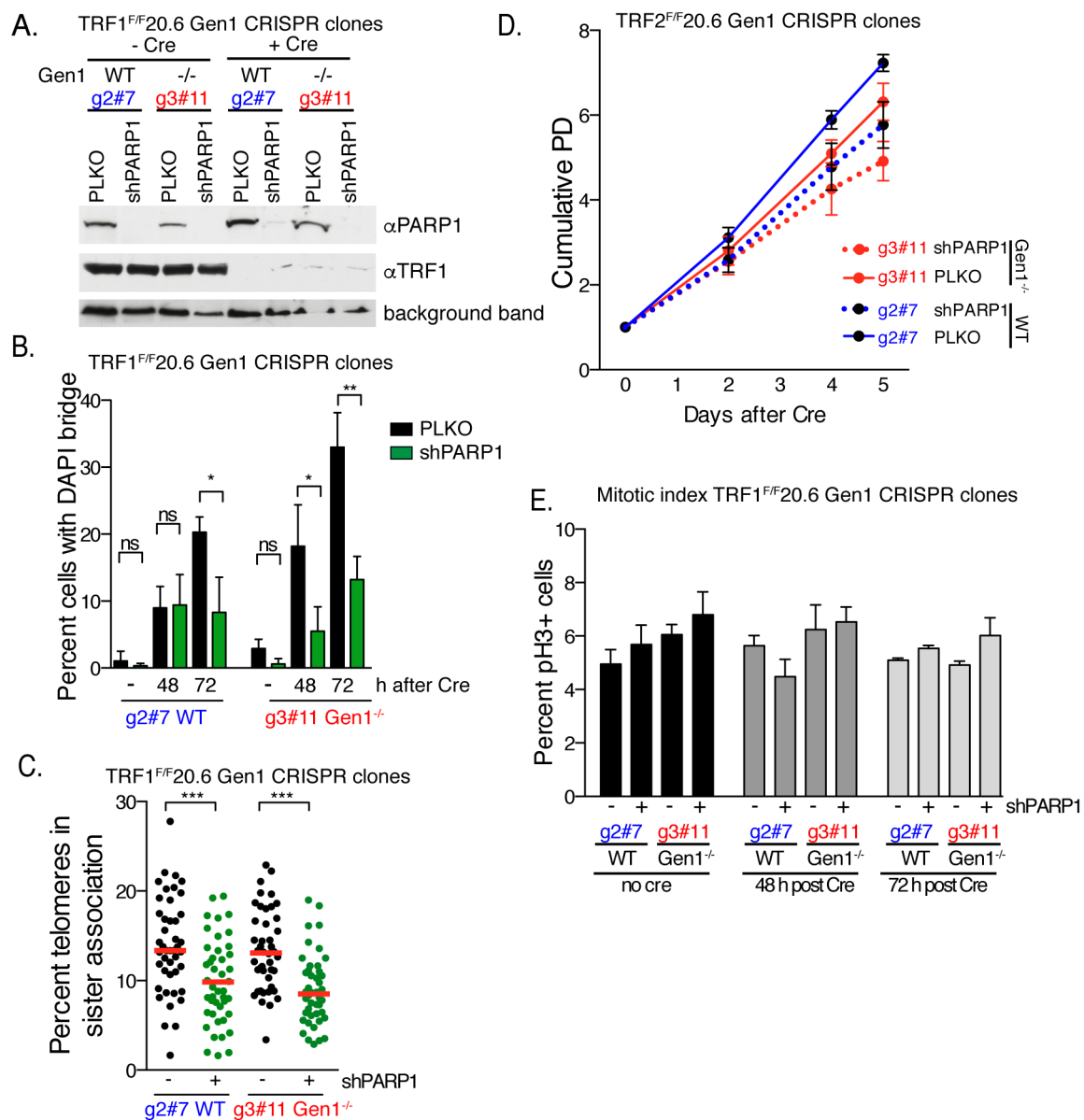
4.2.8 PARP1 deletion rescues chromatin bridge formation

The results so far suggest that Gen1 plays a critical role at telomeres, where it is required to cleave a structure formed upon deletion of TRF1 but not in response to telomere fragility induced by aphidicolin. This suggests that Gen1 cleaves SAs since they are induced specifically when TRF1 is deleted but not after aphidicolin treatment. To further examine this, $\text{TRF1}^{F/F}20.6\text{Gen1}^{-/-}$ cells were treated with shRNAs against PARP1. As described in Chapter 3, SAs are formed via a-NHEJ in a process dependent on PARP1 (Figs. 3.3b and e). Thus, blocking a-NHEJ in $\text{TRF1}^{F/F}\text{Gen1}^{-/-}$ cells should reduce the prevalence of SAs. If Gen1 indeed acts by cleaving SAs, chromatin bridges should be reduced upon treatment with PARP1 shRNAs. For these experiments, $\text{TRF1}^{F/F}20.6\text{Gen1}^{-/-}$ clone g3#11 and control clone g2#7 were used. In both cell lines, shPARP1 efficiently depleted PARP1 as gleaned from western blot (Fig. 4.14a). Chromatin bridges were analyzed 48 or 72 h after deletion of TRF1. Interestingly, shPARP1 drastically reduced the chromatin bridges, not only in the $\text{TRF1}^{F/F}20.6\text{Gen1}^{-/-}$ cells but also partly in the control cells (Fig. 4.14b). The results were more pronounced 72 h after deletion of TRF1, when the percent of chromatin bridges was reduced to 10% in both control and Gen1 null cells after PARP1 depletion. Metaphase spreads were analyzed 96 h after Cre and as expected, shPARP1 significantly reduced the

Figure 4.14 Knockdown of PARP1 reduces chromatin bridge formation in TRF1^{F/F}Gen1^{-/-} cells

(A). Immunoblot for PARP1 and TRF1 after shRNA mediated depletion of PARP1 (sh353). Cells from TRF1^{F/F}20.6Gen1^{-/-} clone g3#11 (red) and control clone g2#7 (blue) were harvested 72 h after deletion of TRF1 (CRISPR clones from Figure 4.2). (B) Frequency of chromatin bridges in TRF1^{F/F}20.6Gen1^{-/-} clone g3#11 (red) and control clone g2#7 (blue). Bridges were analyzed in fixed cells at different time points after Cre (0, 48, 72 h). Values represent mean and SDs from 4 independent experiments and at least 200 cells were counted per condition. (C) Frequency of SAs in the indicated Gen1 clones treated with shRNA against PARP1. Metaphase spreads were harvested 96 h after Cre. Bars represent median % of SAs from 3 independent experiments and every dot represents a metaphase spread. SAs were counted on the long arm only. (D) Growth curve of TRF1^{F/F}20.6Gen1^{-/-} clone g3#11 and control clone g2#7 after deletion of TRF1 and depletion of PARP1. Values represent the means and SEMs from 4 experiments. (E) Mitotic index of indicated cell clones before and 48 or 72 h after deletion of TRF1, treated with shRNA against PARP1. Mitotic index was scored by IF in two experiments by staining with a pH3 specific antibody. The values represent mean and SEM.

P-values determined by a two-sided Student's t-test (* p<0.05, ** p<0.01, *** p<0.001, ns: not significant).



prevalence of SAs in both cell lines (Fig. 4.14c). These results strongly suggest that Gen1 indeed cleaves SAs. One potential caveat of these experiments is that the shRNA against PARP1 affects cell viability and defective cell cycle progression could explain the reduced levels of chromatin bridges, as cells need to go through mitosis for these bridges to form (Fig. 4.14d). However, the mitotic index of cells treated with the shRNA, analyzed by counting pH3 positive mitotic cells, showed no difference upon PARP1 depletion (Fig. 4.14e). Thus, although there were fewer cells after treatment with the shRNA, there was no difference in the percentage of cells in mitosis confirming that the reduced chromatin bridges are the result of PARP1 loss. Combined, the results further confirm the hypothesis that Gen1 cleaves SAs.

4.2.9 Mus81 depletion aggravates the Gen1^{-/-} effect

Mammalian cells have another pathway that resolves HJs and replication intermediates in mitosis that is dependent on Mus81 and not Gen1. As described in the introduction to this chapter, the substrates for Mus81 are nicked HJs but combined with the endonuclease activity of SLX4-SLX1, it is able to cleave intact HJs. Interestingly, SLX4 is associated with telomeres through an interaction with TRF2 (Svendsen et al., 2009).

To examine whether Mus81 can cleave SAs similar to Gen1, shRNAs were used to deplete Mus81. This was done both in Gen1-proficient and deficient cell lines. Antibodies to detect mouse Mus81 on western blot were not effective

and knockdown of Mus81 was therefore analyzed by qPCR. Two primer pairs showed substantial (60-80%) knockdown of Mus81 with two different shRNAs, both in TRF1^{F/F}20.6 Gen1^{-/-} clone g3#11 and control clone g2#7 (Fig. 4.15a,b). Cell viability was affected by the shRNAs against Mus81 as can be seen in a growth curve (Fig. 4.16). However, this effect was not specific for deletion of TRF1 as MEFs not treated with Cre show this loss of viability as well.

Next, chromatin bridges were analyzed by Hoechst staining, 72 h after deletion of TRF1 (Fig. 4.17a-c). Interestingly, chromatin bridges were slightly increased in both TRF1^{F/F}Gen1^{+/+} and TRF1^{F/F}Gen1^{-/-} cells upon Mus81 depletion, although the increase was not statistically significant. Possibly, the level of knockdown is not high enough to obtain higher levels of chromatin bridges. However, the Mus81 depleted cells show a clear phenotype after deletion of TRF1. Many cells appeared to have a clear segregation defect containing multiple nuclei (Fig. 4.17a). This effect is seen both in TRF1^{F/F}Gen1^{+/+} and TRF1^{F/F}Gen1^{-/-} clones although it was more apparent in TRF1^{F/F}Gen1^{-/-} cells.

The observation that shMus81 increased the levels of chromatin bridges and affects nuclear morphology in both TRF1^{F/F}Gen1^{+/+} and TRF1^{F/F}Gen1^{-/-} clones, suggests that it functions independently of Gen1. The activity of Mus81 is induced at the onset of mitosis by high CDK1 activity, prior to nuclear envelope breakdown (Wyatt et al., 2013). Therefore it is possible that Mus81 cleaves a subset of the SAs and that Gen1 cleaves the remaining fusions after nuclear envelope breakdown, explaining the additive effect.

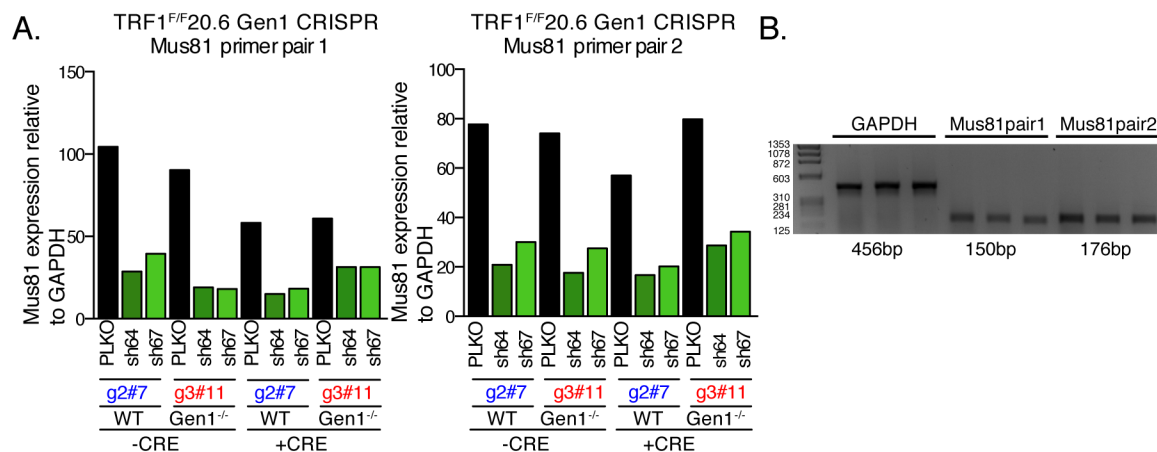


Figure 4.15 Quantification of Mus81 knockdown by qPCR

(A) qPCR for Mus81 in the indicated MEF clones treated with the indicated shRNA against Mus81 (sh64 or sh67, green bars). Two different exon spanning primer pairs were used and values were normalized to GAPDH expression. RNA was isolated from samples before and 72 h after Cre mediated deletion of TRF1 from TRF1^{F/F}20.6Gen1^{-/-} clone g3#11 (red) and control clone g2#7 (blue) as indicated (CRISPR clones from Figure 4.2). (B) Agarose gel with three samples of qPCR amplified DNA from each primer pair, showing a single band of the expected size for GAPDH and the Mus81 primer pairs indicating the specificity of the qPCR.

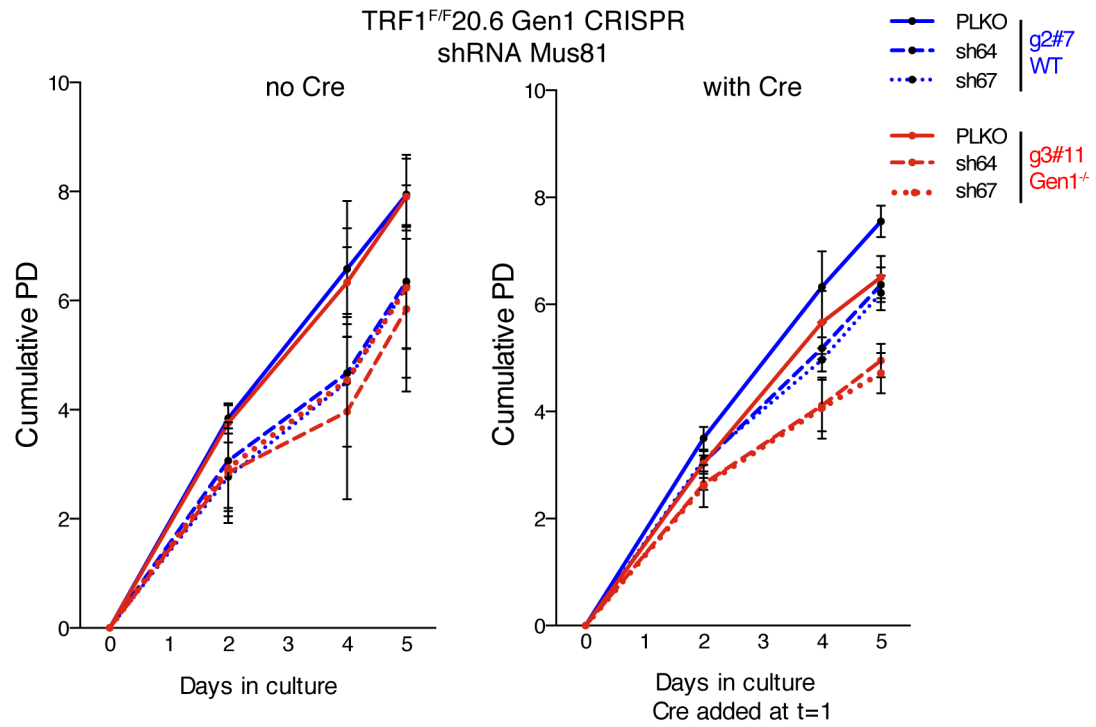


Figure 4.16 Growth curve of Gen1 clones after depletion of Mus81

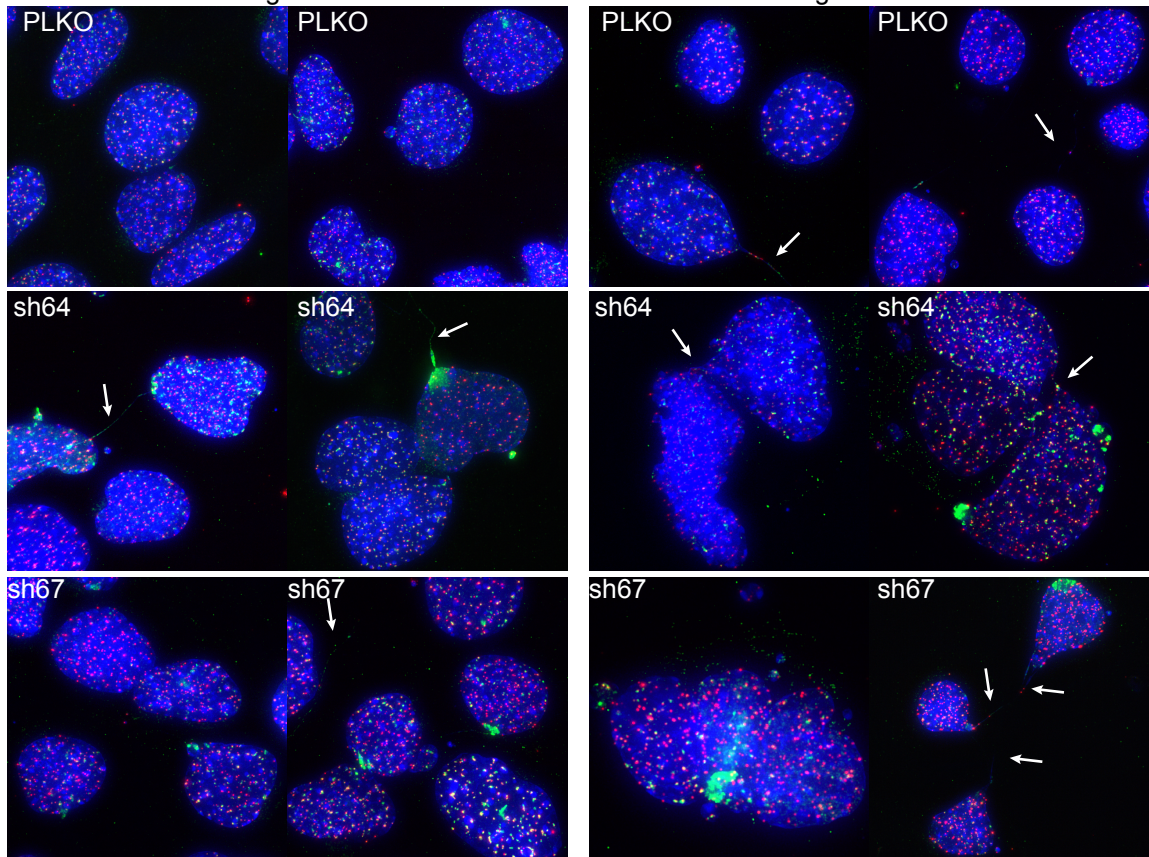
Growth curve of TRF1^{F/F}20.6Gen1^{+/+} (g2#7, blue) and TRF1^{F/F}Gen1^{-/-} (g3#11, red) cells before (left panel) and after (right panel) deletion of TRF1. The shRNAs against Mus81 (dashed lines) affect cell growth in both cell lines. The means and SEM of three experiments are shown.

Figure 4.17 Chromatin bridges are increased after depletion of Mus81

(A) Examples of IF-FISH images from Gen1 positive (g2#7, left) and negative (g3#11, right) TRF1^{F/F}20.6 CRISPR clones, treated with the indicated shRNA against Mus81 (CRISPR clones from Figure 4.2). Cells were fixed 72 h after deletion of TRF1. Cells were stained with Hoechst (blue), γ H2AX (green) and telomere FISH (red). Arrows point to chromatin bridges between cells.

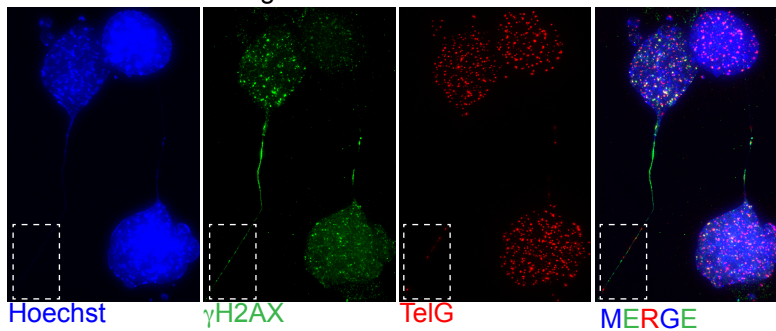
(B) Example of a chromatin bridge in TRF1^{F/F}20.6Gen1^{-/-} clone g3#11 after Mus81 depletion with sh64, 72 h after deletion of TRF1. The chromatin bridge is fully covered in γ H2AX and contains multiple telomeric signal, as is clear from the magnification on the right. (C) Quantification of chromatin bridges in the indicated cell clones before and 72 h after deletion of TRF1. The values represent mean and SDs from 4 independent experiments. At least 200 cells were analyzed per condition. P-values determined by a two-sided Student's t-test (* p<0.05, ns: not significant).

A. $TRF1^{F/F}20.6Gen1^{+/+}g2\#7 + shMus81$ 72 h Cre $TRF1^{F/F}20.6Gen1^{-/-}g3\#11 + shMus81$ 72 h Cre



Hoechst γ H2AX TelG

B. $TRF1^{F/F}20.6Gen1^{-/-}g3\#11 + shMus81\#64$ 72 h after Cre

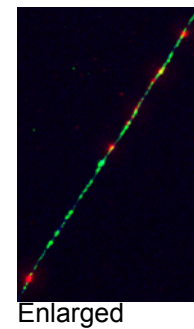


Hoechst

γ H2AX

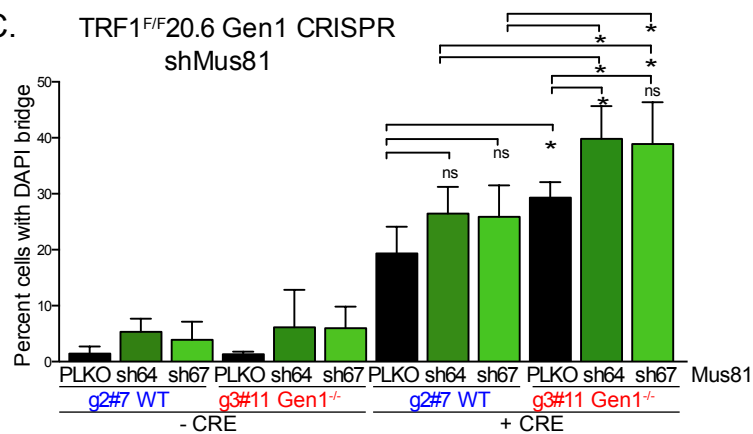
TelG

MERGE



Enlarged

C. $TRF1^{F/F}20.6 Gen1$ CRISPR
shMus81

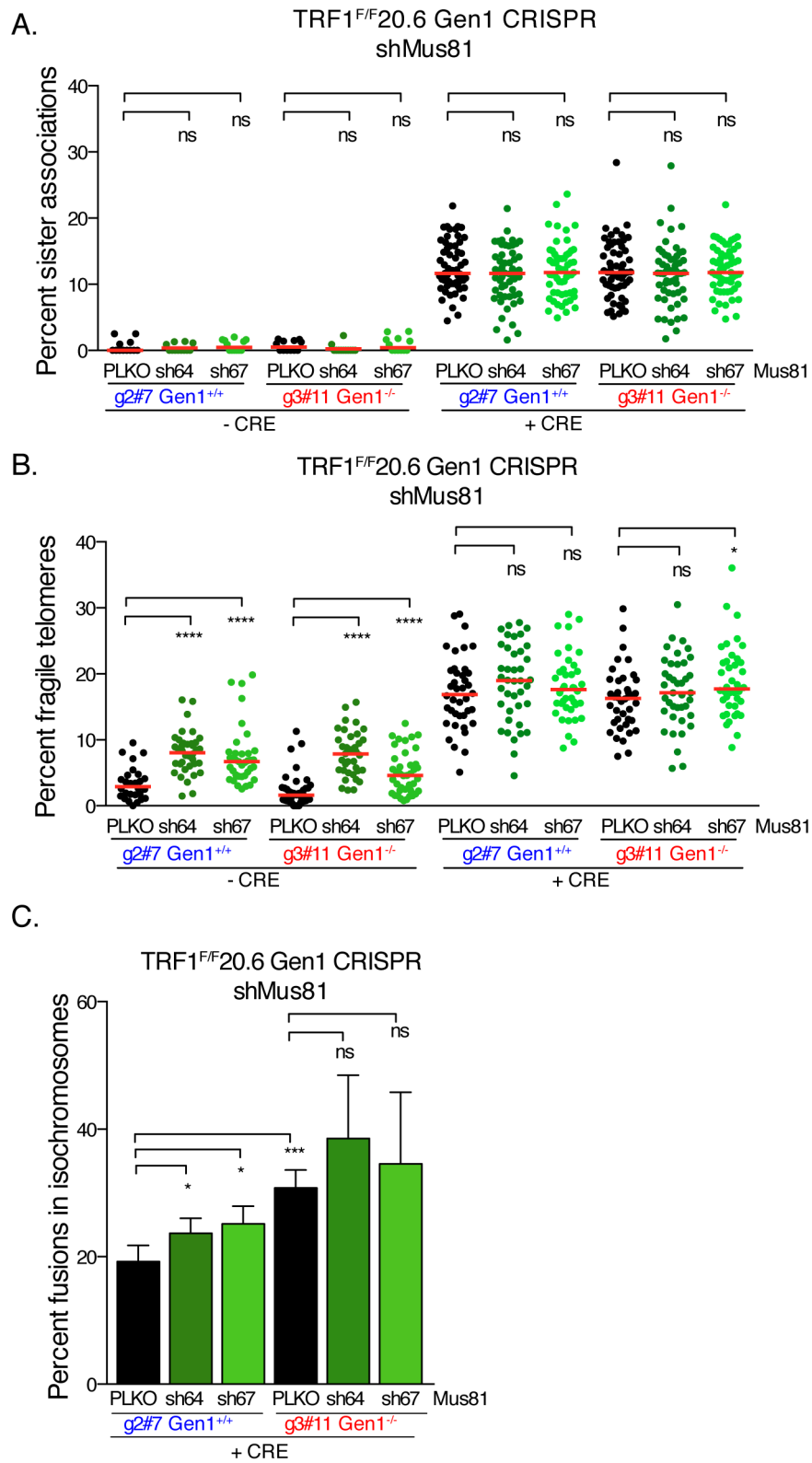


To further understand whether Mus81 might cleave SAs, metaphase spreads were analyzed. Since the activity of Mus81 is already induced at the onset of mitosis, it should increase the prevalence of SAs in metaphase. Metaphase spreads from TRF1^{F/F}Gen1^{-/-} clone g3#11 and control clone g2#7 were analyzed 96 h after deletion of TRF1 (Fig. 4.18a). However, no difference in the level of SAs was observed in either of the cell lines tested. There are several possible explanations why no difference in SAs occurs. The most obvious explanation is that Mus81 is not active on SAs. Mus81 cannot cleave intact HJs and needs its associated SLX4 to create a nicked template. Possibly TRF2 blocks the nuclease activity of SLX4 at telomeres since TRF2 is a known interacting factor (Svendsen et al., 2009). Another explanation could be that the full activation of SLX4-Mus81 does not occur before metaphase. The precise timing of SLX4-Mus81 activity is not very well understood. Experiments with nocodazole arrested cells suggested that the complex is active at the time of prometaphase but this has not been further studied (Wyatt et al., 2013). Therefore it cannot be excluded that Mus81 acts later in mitosis on SAs. It is also possible that the level of knockdown with shRNAs was not sufficient to detect a phenotype on metaphase spreads. A CRISPR/Cas9 knockout cell line would be useful but the combined deletion of Gen1 and Mus81 is expected to affect cell viability and was therefore not attempted (see growth curve Fig. 4.16 and (Wechsler et al., 2011)).

Telomere fragility was also assessed on the metaphase spreads from Mus81 depleted cells. There was no difference in telomere fragility 96 h after

Figure 4.18 Telomere SAs, fragility and isochromosomes after Mus81 depletion

(A). Frequency of SAs in metaphase spreads from TRF1^{F/F} 20.6 control (blue) and Gen1^{-/-} (red) MEFs before and 96 h after Cre, treated with the indicated shRNA against Mus81. Bars represent the median % of SAs from 4 experiments and each dot represents a metaphase spread. (B) Analysis of telomere fragility on the metaphase spreads from A. Bars represent the median % of telomere fragility from 3 experiments. SAs and fragility were counted on the long arm only. (C) Frequency of isochromosomes 96 h after deletion of TRF1 from the indicated Gen1 CRISPR clones, given as a percentage fusions in isochromosome. Detailed explanation of isochromosome count can be found in Figure 4.8. P-values determined by a two-sided Student's t-test (* p<0.05, *** p<0.001, **** p<0.0001, ns: not significant).



deletion of TRF1 (Fig. 4.18b). Unexpectedly however, knockdown of Mus81 significantly increased telomere fragility when TRF1 was present. The levels increased from around 3% to just below 10%. This increase in telomere fragility was similar in Gen1 proficient and deficient cells and is reminiscent of a similar defect seen in human cells upon deletion of Mus81 (Saint-Leger et al., 2014). The reason for this increase in telomere fragility is not well understood. Possibly, it is due to the ability of Mus81 to cleave stalled replication forks during S-phase (Formont et al., 2011). Mus81 was shown to generate DSBs at stalled forks in absence of ATR/Chk1 signaling or upon prolonged replication stress. At telomeres, POT1a/b blocks ATR signaling under TRF1 proficient conditions, possibly allowing Mus81 mediated cleavage and DSB dependent fork restart when the replication machinery encounters a barrier (Zimmermann et al., 2014). Absence of Mus81 could therefore result in abnormal fork restart at telomeres resulting in fragility.

4.3 Summary of findings

A prominent phenotype observed after the deletion of TRF1 are SAs, which represent telomeres fused via a-NHEJ, as shown in Chapter 3. The results in this chapter describe an essential role for Gen1 in the resolution of these telomere fusions. The results are consistent with the proposition that fused telomeres can form cruciform DNA structures due to their repetitive nature, which are a substrate for the Holliday junction resolvases Gen1 (Fig. 4.1). Absence of Gen1

resulted in the appearance of chromatin bridges upon deletion of TRF1 (Fig. 4.4 b and 4.5c). These chromatin bridges were not induced by treatment of TRF1^{F/F}Gen1^{-/-} cells with aphidicolin, which results in fragile telomeres (Fig. 4.6) (Sfeir et al., 2009). This suggests that the chromatin bridges are not related to the telomere fragility seen in absence of TRF1 but due to SAs. Further evidence that Gen1 cleaves SAs is provided by the observation that the percentage of isochromosomes was increased upon TRF1 deletion in TRF1^{F/F}Gen1^{-/-} cells (Fig. 4.10a-c). This indicates that Gen1 normally cleaves SAs thereby preventing the accumulation of isochromosomes in wild type conditions.

As SAs are formed by a-NHEJ, the role of PARP1 on chromatin bridges in Gen1 null cells was assessed. Since deletion of PARP1 reduces the level of SAs, chromatin bridges should be reduced when PARP1 is deleted from TRF1^{F/F}Gen1^{-/-} cells if Gen1 is responsible for cleaving these structures (Chapter 3.2.1, Figs. 3.3b and e). Indeed, deletion of PARP1 from TRF1^{F/F}Gen1^{-/-} cells significantly reduced the presence of chromatin bridges (Fig. 4.14b). This indicates that Gen1 is truly capable of cleaving SAs.

A second Holliday junction resolvase that could act on SAs is Mus81 (Fig. 4.1b). This nuclease was depleted using shRNA to analyze whether a similar phenotype is observed as upon deletion of Gen1. Chromatin bridges were indeed increased when Mus81 was depleted an additive effect was seen with the combined deletion of Mus81 and Gen1 (Fig. 4.17c). The results were insignificant however, possibly due to the limited knockdown of Mus81. This might also have

affected the analysis of SAs on metaphase spreads, as no difference could be seen in their levels upon depletion of Mus81 (Fig. 4.18a). Isochromosomes were slightly increased upon the combined deletion of Mus81 and Gen1, but again, the results were not significant (Fig. 4.18c). The data suggest that it is indeed possible for Mus81 to cleave SAs in a similar fashion to Gen1, since chromatin bridges are increased. However, the effect of Mus81 deletion upon TRF1 deletion merits further analysis with better knockdown levels of the protein.

Chapter 5: Discussion

5.1 Dissociation of function mutants of 53BP1

5.1.1 *Rif1 is the only factor downstream of 53BP1 inhibiting resection*

Analysis of a panel of 53BP1 alleles with subsets of N-terminal S/TQ sites mutated to alanine revealed insights into the mechanisms by which 53BP1 promotes NHEJ (Fig. 2.2). It has previously been shown that 53BP1 recruits Rif1 to inhibit CtIP-dependent and -independent resection at DSBs and dysfunctional telomeres (Chapman et al., 2013; Di Virgilio et al., 2013; Escribano-Diaz et al., 2013; Feng et al., 2013; Zimmermann et al., 2013; Kibe et al., 2016). Additionally, PTIP has been suggested to play a role in blocking the resection pathway downstream of 53BP1 at DSBs in PARPi-treated BRCA1^{-/-} cells (Callen et al., 2013). However, the results described here suggest that Rif1 is the only factor downstream of 53BP1 required to inhibit resection at telomeres (Fig. 2.6b). 53BP1^{ΔRif1} displayed similar levels of resection upon deletion of TRF2 as the 53BP1^{Δ28} allele (Fig. 2.6b). Furthermore, 53BP1^{ΔPTIP} behaved as wild type 53BP1 with regards to inhibition of resection. This is consistent with a recent study of TRF2^{F/F}PTIP^{-/-} MEFs which did not show a telomere hyper-resection phenotype (Lottersberger et al., 2015). Even though resection was not altered by PTIP, the telomere fusions were slightly delayed in 53BP1^{ΔPTIP} expressing cells lacking TRF2 compared to cell with wild type 53BP1, similar to the situation in TRF2^{F/F}PTIP^{-/-} MEFs (Fig. 2.7c) (Lottersberger et al., 2015). It is possible that this reduction is due to the role of PTIP in recruiting the Artemis nuclease, which has been shown to mediate end-trimming of obstructed ends (Wang et al., 2014). The

Artemis nuclease activity can open hairpins at DNA ends during V(D)J recombination to promote c-NHEJ (Ma et al., 2002). However, the telomeric sequence is unlikely to form hairpins at the DNA end, suggesting this activity is not responsible for the reduced level of telomere fusions in absence of PTIP. Possibly, PTIP and Artemis are required for other types of nucleolytic processing such as the removal G4 structures in the 3' overhang, which can block Ku loading and NHEJ. Importantly, the absence of PTIP merely caused a delay in telomere fusions that is no longer observed at later time points after TRF2 deletion, suggesting that the activity of PTIP is redundant with other pathways (Lottersberger et al., 2015).

It is unclear by which mechanism Rif1 prohibits end resection. It is unlikely that Rif1 directly inhibits individual components of the resection pathway, such as BLM, Exo1 or CtIP. First, Rif1 blocks resection at shelterin free telomeres mediated by CtIP as well as BLM and Exo1 (Sfeir and de Lange, 2012; Zimmermann et al., 2013). It could be argued that Rif1 only needs to inhibit the initial resection step mediated by CtIP. However, this is unlikely since Rif1 was also shown to inhibit CtIP-independent resection at telomeres after loss of TPP1 (Kibe et al., 2016). Thus, it is likely that the inhibition of resection by Rif1 occurs on a broader scale, such as changes in the chromatin landscape or by binding dsDNA as has been recently suggested by David Shore and colleagues (pers. comm.).

Recent papers have described Rev7 (also known as MAD2L2), a subunit of the translesion polymerase zeta ($\text{pol}\zeta$), as a factor required for inhibition of resection downstream of 53BP1 and Rif1 (Boersma et al., 2015; Xu et al., 2015). This was independent of the role of Rev7 in translesion synthesis, as depletion of Rev3 or Rev1, the other $\text{pol}\zeta$ components, did not recapitulate the resection phenotype. Rev7 was recruited to DSBs in a 53BP1- and Rif1-dependent manner but a direct interaction could not be detected (Xu et al., 2015). However, loss of Rev7 resulted in a similar reduction in telomere fusions after depletion of TRF2 as loss of 53BP1/Rif1 (Boersma et al., 2015). Furthermore, its knockdown restored PARPi resistance in BRCA1 deficient cells similar to Rif1, providing further evidence that Rev7 and Rif1 operate in the same pathway (Xu et al., 2015). But the molecular mechanism by which Rif1 and Rev7 inhibit resection remains the subject of ongoing investigation.

5.1.2 The connection between 53BP1 and the LINC complex

53BP1 promotes the mobility of telomeres after deletion of TRF2 (Dimitrova et al., 2008). Experiments in the lab have shown that this mobility is dependent on the LINC complex and kinesin-mediated movement on microtubules (explained in Chapter 1.2.5). However, the question remains how 53BP1 mediates chromatin mobility through Sun proteins and the rest of the LINC complex. The results described here identified a 53BP1 dissociation of function mutant that harbors the S/TQ sites needed to induce chromatin mobility (Fig. 2.8b-d). Dysfunctional

telomeres in cells expressing 53BP1^{ΔMOB} were unable to fuse to the same extent as in cells expressing the wild type allele. Furthermore, this delay in fusion frequency was dependent on Sun1 and Sun2 (Fig. 2.8c and d). Additionally, time-lapse imaging showed that 53BP1^{ΔMOB} was unable to promote the mobility of dysfunctional telomeres, similar to 53BP1^{Δ28}, confirming that this mutant is deficient in inducing chromatin mobility (2.9c). The results also indicated that 53BP1^{ΔPTIP} behaves as wild type 53BP1 with regards to mobility, similar to results obtained in TRF2^{F/F}PTIP^{-/-} MEFs (Lottersberger et al., 2015).

It is unknown whether 53BP1 associates with the LINC complex. The fact that uncapped telomeres do not show an obvious localization to the nuclear periphery argues against a interaction. However, the MEFs analyzed are flat and the precise localization of DSBs is difficult to assess. Furthermore, nuclear invaginations can position an internal telomere close to the nuclear envelope and a connection can thus be envisioned (Fig. 5.1a). However, multiple co-IP experiments, telomere ChIP, and co-IPs of crosslinked complexes failed to detect an interaction between 53BP1 and Sun1, raising the possibility that there is no physical interaction between 53BP1 and the Sun proteins (Fig. 2.10 to 2.13).

It is therefore possible that the influence of the LINC complex on DSB mobility is indirect (Fig. 5.1b). One hypothesis is that the mobility domain of 53BP1 interacts with factor(s) that increase the flexibility of the chromatin surrounding the uncapped telomere. Chromatin containing DSBs has been

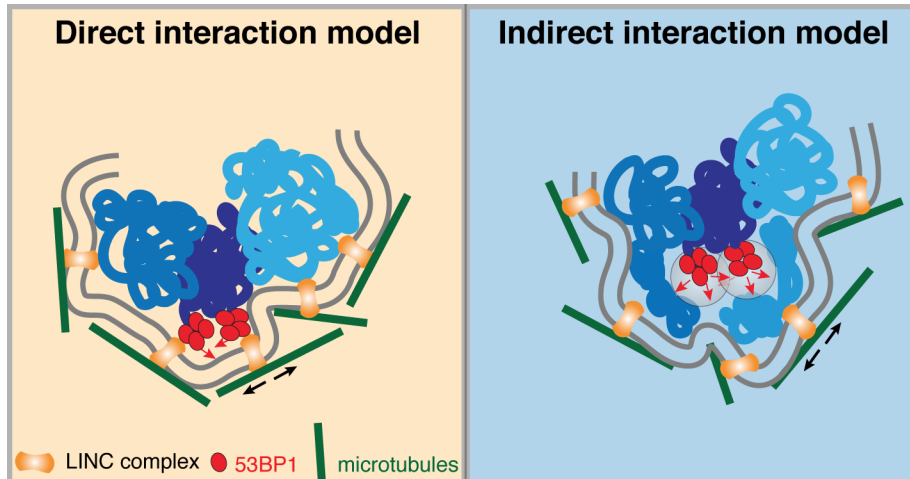


Figure 5.1 Models for the interaction between 53BP1 and Sun1

(A) The direct interaction model predicts an interaction between 53BP1 (red) and the LINC complex (yellow) to permit the transfer of microtubule forces to the DSB. (B) In the indirect interaction model, 53BP1 alters the chromatin structure surrounding the DSB, rendering it more flexible. Random forces transmitted from the cytoplasm into the nucleus through the LINC complex result in increased mobility at the DSB site, due to the altered chromatin structure. Figure provided by F. Lottersberger.

suggested to expand, as evidenced by EM experiments (Kruhlak et al., 2006). If the chromatin near a DSB is more flexible, it is conceivable that the forces exerted by the microtubules could induce mobility of DSBs whereas other regions in the nucleus are less affected (Fig. 5.1).

It will be of interest to identify proteins that interact with the mobility domain of 53BP1. Mass spectrometry could be used to identify proteins that interact with this domain in a DNA damage inducible manner, similar to what was done previously for the 53BP1 S/TQ sites in B-cells (Di Virgilio et al., 2013). Possibly, nucleosome-remodeling complexes could be recruited or activated in a process dependent on 53BP1. Alternatively, the pathway could be more complicated if this domain interacts with a kinase or ubiquitin ligase, that can activate entire signaling cascades. Monitoring the influence of 53BP1 on chromatin status at telomeres would be helpful to address these questions. Telomeric chromatin is heterochromatic and MNase digestion experiments indicated that nucleosome density is not altered in response to DNA damage, when measured after TRF2 loss (Wu and de Lange, 2008). This does not necessarily argue against changes in chromatin structure surrounding DSBs. It is possible that 53BP1 activity affects histone modifications that regulate the flexibility of the chromatin fiber. The increased mobility of flexible chromatin at DSB could be due to regular cytoskeletal forces transmitter through the LINC complex. But it is also possible that DNA damage stimulates an increase in forces on the nucleus. Nuclear invaginations and deformations have been

observed upon etoposide treatment in human fibroblasts (Dellaire et al., 2009). Furthermore, ATM dependent signaling through Chk2 and/or Chk1 could impact the LINC complex directly, as was shown for *C. elegans* meiosis where Chk2 directly phosphorylates the Sun1 N-terminus (Penkner et al., 2009).

5.1.3 The function of chromatin mobility in response to damage

An outstanding question is the functional relevance of increased chromatin mobility in response to DNA damage. Certainly the pathway has not evolved to fuse dysfunctional telomeres. As discussed in Lottersberger et al. 2015, it is possible that the mobility inhibits ectopic repair at sites of damage. In G1, DSBs are quickly repaired by c-NHEJ in response to Ku binding. However, at some DSBs, Ku binding or synapse might fail, resulting in two loose ends that become spatially separated. The 53BP1 dependent mobility might help reconnect these ends to promote their repair (Fig. 5.2a). A downside of this model is that it can be argued that the mobility increases the chance of generating translocations, if the DSB reconnects with an end on another chromosome. However, most cells do not contain more than one persistent DSBs unless under an external genotoxic insult (Wu et al., 2010). Therefore, the possibility that 53BP1 mediated mobility promotes translocations is very limited in biological relevant settings.

Another setting where DSB mobility might play a protective function is at sites of replication stress. A DSB generated at a collapsed fork can be repaired by HR using the sister chromatid as a template. However, if the DNA end loses

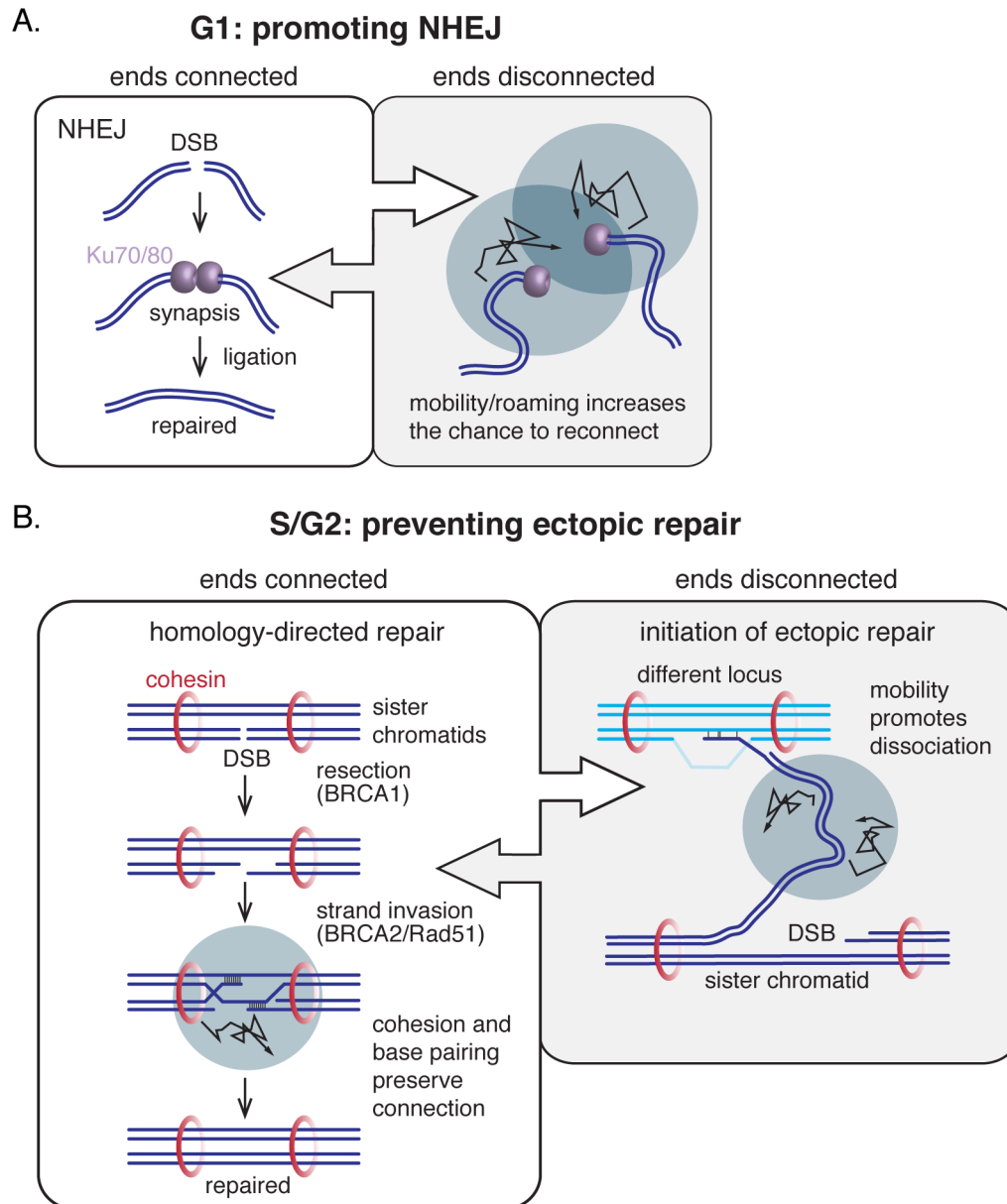


Figure 5.2 Proposed function of 53BP1-dependent mobility of DSBs

(A) In G1, the mobility of DNA ends that have become disassociated would promote their correct rejoining by NHEJ. (B) In S/G2, a DNA end could lose its connection with the sister chromatid at a DSB. Ectopic repair on another locus could be prevented by the 53BP1-dependent mobility stimulating correct repair using HDR on the sister chromatid. Figure from Lottersberger et al. 2015 (Lottersberger et al., 2015).

the connection with the sister chromatid, ectopic repair on another chromosome can occur by strand invasion and microhomology. DNA mobility might be required to tear apart these low affinity interactions to promote correct repair on the sister chromatid (Fig. 5.2b). The use of chromosome mobility to disrupt inaccurate chromosome pairing has previously been suggested to play a role in *C. elegans* meiosis (Sato et al., 2009). Pairing and synapsis of chromosomes is required to accurately separate homologous chromosomes in meiosis I. Synapsis is promoted by a connection between telomeres (pairing centers in *C. elegans*) and Sun1 in the nuclear envelope. Microtubule forces transmitted through the LINC complex induce meiotic chromosome movement along the nuclear envelope that promotes synapsis (Shibuya and Watanabe, 2014). This movement was suggested to improve the accuracy of synapsis since pairing of non-homologous chromosomes results in weaker interactions that can be disrupted by the movement while paired homologues resist this force (Sato et al., 2009). The situation at DBSs is different from meiosis since the damage sites do not appear to connect directly at the nuclear envelope. However, the underlying molecular mechanism to promote accurate pairing could be similar.

5.2 The fusion of sister telomeres by a-NHEJ and cleavage by Gen1

5.2.1 Telomeres are prone to a-NHEJ in absence of TRF1

It was long unknown what structure underlies the manifestation of SAs in metaphase chromosomes. They are not dependent on c-NHEJ, since absence of

Lig4 does not affect their prevalence. Furthermore, they are not related to the telomere fragility that is observed after deletion of TRF1, as explained in detail in Chapter 3.1. The results presented here strongly indicate that SAs are formed via the a-NHEJ pathway since they are dependent on Lig3 and PARP1 (Fig. 3.2 and 3.3). Supporting this finding, SAs are also reduced from ~12% to ~5% in TRF1^{F/F}TRF2^{F/F}Lig4^{-/-} MEFs after deletion of the entire shelterin complex in response to shLig3 depletion (unpublished experiments from A. Sfeir). This reduction is similar to the results reported here (Fig. 3.3). Furthermore, anaphase bridges are seen in mitotic cells after loss of TRF1, indicating chromosome fusion events (Fig. 3.7b). Unexpectedly, telomere fusions are not prominently detected upon analysis of the telomeric restriction fragments from Cre-treated TRF1^{F/F} MEFs, even when mitotic cells are enriched (unpublished experiments from de Lange lab). The absence of molecular evidence for telomere-telomere fusions could be due to several reasons. First, the abundance of SAs might be too low for detection. Upon TRF2 loss, telomere fusions are clearly visible in gels but the percentage of fused telomeres is much higher in those cells (60% in TRF2^{F/F} versus 15% in TRF1^{F/F}). Secondly, if SAs are resolved by Gen1 (or other nucleases), their number would be reduced even further because the fusions would be transient. Third, fusions via a-NHEJ are known to produce mutations at the fusion site. Telomeric DNA is digested with AluI and MboI prior to PFGE, which normally do not cleave fused telomeres. But after a-NHEJ, cleavage sites for these enzymes may appear at the fusion site resulting in their cleavage due to

de novo sequence insertions by PolQ (Mateos-Gomez et al., 2015). Therefore, this observation that fused telomeres are not visible in telomeric gels does not argue against a-NHEJ mediated fusion of sister telomeres upon loss of TRF1.

5.2.2 Incomplete DNA replication does not explain the appearance of SAs

Different models have previously been proposed for the events resulting in the formation of SAs. It can be argued that SAs are sites of incomplete DNA replication. Telomere replication is initiated primarily in the subtelomere from where the replication fork progresses into the telomeric DNA. Replication initiation within the telomeric sequence is infrequent (Sfeir et al., 2009). Telomeric replication is furthermore not a late event but occurs throughout S phase (Ten Hagen et al., 1990; Wright et al., 1999). It can be argued that the replication fork in some replicating telomeres does not reach the telomere end, particularly upon replication fork stalling in absence of TRF1, resulting in unfinished replication leaving the sister chromatids bound together. A similar model for incomplete replication exists for common fragile sites (CFS), regions of the genome that are difficult to replicate and manifest as breaks and gaps on metaphase spreads (Durkin and Glover, 2007). Replication at CFS was recently shown to continue into the prophase, as evidenced by EdU incorporation after entry into mitosis (Minocherhomji et al., 2015). Mitotic DNA synthesis was dependent on Mus81/SLX4, Rad52 and POLD3, resulting in a model where cleavage of the replication fork by Mus81/SLX4 allows D-loop formation by Rad52 on the sister

template and initiation of DNA synthesis by POLD3 (Minocherhomji et al., 2015; Bhowmick et al., 2016). It is possible that SAs at telomeres represent similar areas of incomplete replication after deletion of TRF1, resulting in the appearance of 'fused' telomeres. However, several arguments counter this hypothesis.

First, in contrast to telomeres, most CFSs replicate late in S-phase explaining why they remain incompletely replicated, especially after aphidicolin treatment (Le Beau et al., 1998). Telomeric replication is likely to be finished at the end of S-phase, since they replicate throughout S-phase, even in absence of TRF1 (Wright et al., 1999; Sfeir et al., 2009).

Secondly, EdU incorporation in mitosis could not be detected at telomeres, in absence of TRF1 suggesting that DNA replication has finished in this setting (unpublished experiments). It is possible that the amount of EdU incorporation at telomeres was too limited for detection. However, treatment of cells with aphidicolin treatment did result in EdU signals at or near telomeres (unpublished data Z. Yang). This further suggests that telomeres are fully replicated after TRF1 deletion, except when cells are treated with aphidicolin. Since SAs are not seen at telomeres after aphidicolin treatment, this argues that they do not represent sites of unfinished replication (Sfeir et al., 2009).

Third, Mus81 was shown to be required for mitotic DNA replication, which occurs in prophase but before prometaphase (Minocherhomji et al., 2015). If SAs represent areas of unfinished replication, depletion of Mus81 should have some

effect on the prevalence of SAs since they are visualized in metaphase after mitotic DNA replication has occurred. But the frequency of SAs was not altered in MEFs in absence of Mus81 upon deletion of TRF1 (Fig. 4.16a).

Finally, CFS expression as a consequence of incomplete replication is associated with an increase of UFBs in anaphase cells (Ying et al., 2013). Thus, UFBs should be clearly visible in anaphase cells after deletion of TRF1, if SAs indeed represent sites of unfinished replication. Although the resolution of the microscope was not ideal, there was no indication for high levels of UFBs in TRF1^{F/F} MEFs after deletion of TRF1, as gleaned from PICH recruitment in time-lapse imaging experiments (Fig. 3.8). Although many anaphase bridges were detected upon loss of TRF1, they were almost always DAPI positive suggesting that they represent real fusions instead of sites of unfinished replication (Fig. 3.7b and 3.8d).

Additionally, whereas the reduction of SAs by PARP1 inhibition could potentially be explained by its many distinct functions at the replication fork, the reduction of SAs by Lig3 does not make sense if the SAs represent incompletely replicated telomeres. Combined, the results argue that (at least some of the) SAs are telomeres fused by a-NHEJ and do not represent sites of unfinished replication.

5.2.3 Cohesin defects cannot explain SAs

Another possible model for the molecular nature of SAs could be defective removal of cohesin at telomeres in absence of TRF1. Sister chromatids are held together after replication by cohesin until their separation in mitosis (Nasmyth and Haering, 2009). Most cohesin is removed during prophase but a small amount remains at the centromeres to allow accurate chromosome alignment and spindle formation. At the onset of anaphase, all sister chromatid cohesion is destroyed by the action of separase, allowing chromosomes to fully separate (Nasmyth and Haering, 2009). Telomeres are held together by the SA1-cohesin complex, which in human cells requires the shelterin associated protein tankyrase for its removal from telomeres. Absence of tankyrase-1 was shown to result in persistent telomere associations mediated by SA1 (Dyrek and Smith, 2004; Canudas et al., 2007). It is therefore possible that SAs represent sister telomeres from which SA1-cohesion has not properly been removed. Indeed, sister chromatid fusions were seen in human cells after tankyrase depletion (Hsiao and Smith, 2009). However, other studies argue against SAs being merely cohered telomeres. Sister telomere coherence mediated by SA1 is a non-covalent interaction that is destroyed by the hypotonic treatment used for metaphase spread analysis (Dyrek and Smith, 2004). This coherence is therefore only seen upon direct fixation of mitotic cells. However, SAs upon TRF1 loss are refractory to hypotonic swelling since they are detected in regular metaphase spreads, indicating that they do not represent associations mediated

by SA1-cohesion. Furthermore, the tankyrase-SA1 mediated telomere associations in human cells are dependent on an interaction between tankyrase and TRF1. However, mouse TRF1 does not interact with tankyrase, indicating that SAs are distinct from a telomere cohesion defect (Donigian and de Lange, 2007).

Interestingly however, telomeric cohesion is required for accurate telomere replication. An SA1 knockout mouse displayed defective telomere replication indicated by the appearance of fragile telomeres (Remeseiro et al., 2012). Loss of SA1 did not affect centromeric cohesion but telomeres are seen as doublets in IF analysis representing defective coherence. The level of telomere fragility is of a similar level as induced by TRF1 deletion (20-25%), but SAs were not described. Telomeric sister chromatid exchanges (T-SCE) are decreased in absence of SA1. The reduced level of T-SCE suggests that SA1 facilitates HR-mediated repair of stalled forks by keeping sister telomeres close together. It would be interesting to analyze SAs in TRF1^{F/F} MEFs after depletion of SA1 to see if their levels are altered by loss of cohesion.

5.2.4 Telomere entanglements in yeast

The anaphase bridges seen upon loss of TRF1 are reminiscent of the telomere 'entanglements' observed on gel analysis of fission yeast cells lacking the TRF1/2 ortholog taz1 (Miller and Cooper, 2003). When *taz1Δ* cells are exposed to cold temperatures (20°C) they undergo replication stress similar to the

situation in TRF1 knockout MEFs (Miller et al., 2006). Importantly, *taz1Δ* cells display segregation defects such as anaphase bridges, which are dependent on progression through S-phase (Miller and Cooper, 2003). This segregation defect was independent of Ku or Lig4, indicating that the defect is not the result of telomere fusion by c-NHEJ. It is possible that the telomere entanglements represent telomeres fused by a-NHEJ similar to the SAs in MEFs, but deletion of Lig3 was not tested in these yeast experiments. The cold-sensitivity of *taz1Δ* cells was improved by deletion of topoisomerase II and it was suggested that inappropriate cleavage and rejoining of DNA strands was a causative factor for the appearance of entangled telomeres (Miller and Cooper, 2003). But telomere fusions were not observed in PFGE electrophoreses gels, suggesting that the telomere entanglement were not covalently attached. The molecular nature of these entanglements thus remains unknown.

Intriguingly, subsequent experiments showed that deletion of yeast Rif1 (*rif1+*) rescued the cold sensitivity of *taz1Δ* cells implicating *rif1+* contributes to the formation of telomere entanglements (Miller et al., 2005; Zaaijer et al., 2016). Fission yeast *Rif1+* is different from mammalian Rif1 in that it does not affect c-NHEJ or the 3' overhang at the telomere end. Furthermore, *Rif1+* binds to yeast telomeres in a *taz1* dependent manner indicating that its role in preventing the cold sensitivity of *taz1Δ* cells is independent of its localization to telomeres. Later experiments showed that *Rif1+* localizes to the anaphase mid-region in fission yeast during mitosis suggesting that it prevents untangling at this site (Zaaijer et

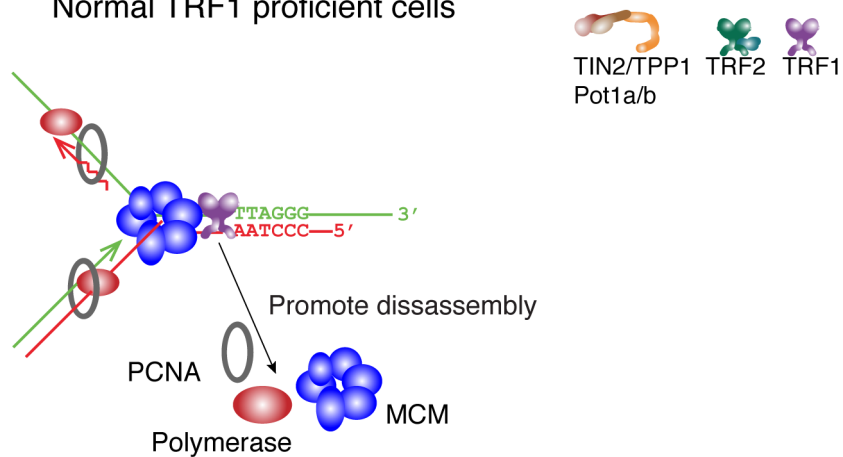
al., 2016). Recently, Rif1 was also detected at UFBs during mitosis in mammalian cells (Hengeveld et al., 2015). However, in contrast to telomere entanglements, resolution of UFBs was worse in absence of Rif1 suggesting that Rif1 performs a function that helps resolve UFBs (Hengeveld et al., 2015; Zaaier et al., 2016). These contradicting functions of Rif1 at telomeres and UFBs could be explained if the telomere entanglements are structurally different from UFBs, for example, if the telomere entanglements actually represent fused sister telomeres, similar to the SAs in TRF1 null cells. In agreement with this hypothesis, SAs were prevented in TRF1^{F/F}53BP1^{-/-} MEFs expressing the 53BP1^{ΔRif1} allele, suggesting a similar function of mammalian Rif1 in promoting telomeric SAs as in fission yeast (Fig. 3.13 and 3.14). However, the role for Rif1 described in this thesis is downstream of 53BP1 in contrast to fission yeast, where *Rif1+* localizes independently. It is possible that the 53BP1 dependent recruitment of mammalian Rif1 evolved later, in agreement with the observation that fission *Rif1+* does not play a role in telomeric overhang regulation. Further experiments are needed to determine whether yeast telomere entanglements are similar to the SAs in TRF1 null cells and what function Rif1 plays at these sites. It is possible that Rif1 is required to promote topoisomerase mediated untangling of UFBs during mitosis. This could explain why Rif1 promotes untangling of replication intermediates but has detrimental consequences at entangled telomeres if these sites represent telomere fusions, since topoisomerase function would not resolve these structures (Hengeveld et al., 2015; Zaaier et al., 2016).

Intriguingly, Rif1 is known to interact with BLM at stalled replication forks, independent from 53BP1, where it prevents the accumulation of stalled forks (Xu et al., 2010). Although the recruitment of Rif1 to UFBs is independent of BLM, it is possible that they act in the same pathway to untangle replication intermediates (Hengeveld et al., 2015).

5.2.5 *What is the substrate for a-NHEJ at sister telomeres?*

A major question arising from this work is what specific substrate allows a-NHEJ to take place between sister telomeres after deletion of TRF1. SAs are not seen after TRF2 loss, even when fusions are limited to S/G2 such as in TRF2^{F/F}ATM^{F/F} or TRF2^{F/F}NBS1^{F/F} MEFs (Dimitrova and de Lange, 2009). Instead, leading-leading chromatid type fusions are observed in these cells. Lagging strand telomeres are protected from these fusions since telomere processing, formation of the 3' overhang, and binding of the POT1 proteins are thought to be incompatible to c-NHEJ. However, replication of the leading strand telomere yields a blunt end. Normally, ATM activation in response to TRF2 removal results in resection of the leading end, providing a 3' overhang incompatible to c-NHEJ in S/G2. But in TRF2^{F/F}ATM^{F/F} (or NBS1^{F/F}) MEFs, ATM dependent-resection is inhibited leaving blunt ended telomeres resulting in leading-leading chromatid fusions. Nevertheless, SAs are not observed upon loss of TRF2 indicating that a TRF1 specific event is required. Given that TRF1 is required for telomere

A. Normal TRF1 proficient cells



B. Fork stabilization in absence of TRF1

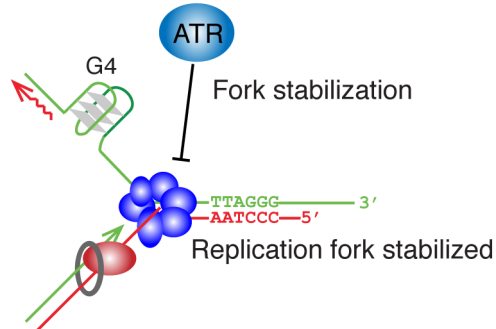


Figure 5.3 Model for the fork stabilization in absence of TRF1

(A) When the replication fork reaches the end of the telomere, TRF1 might promote the disassembly of the replisome. (B) In absence of TRF1, the disassembly of the replisome might not occur efficiently. Furthermore, activation of ATR stabilizes the replication fork even more, which could lead to fork regression.

replication, possibly an event at the terminal replication fork provides the substrate for a-NHEJ.

While many studies focus on understanding the initiation of replication, termination of the fork is not very well understood. It is thought to require topoisomerase function and polyubiquitination, suggesting an active process (Fachinetti et al., 2010; Moreno et al., 2014; Bailey et al., 2015). This has mainly been studied at converging forks at chromosome internal locations. How replication fork dismantling occurs at a DNA end such as a telomere is unknown. Possibly, one of the functions of TRF1 is to promote replication fork disassembly once the fork has reached the end of the DNA (Fig. 5.3a and b). In absence of TRF1, ATR is activated which has a stabilizing function on the replisome (Lopes et al., 2001; Tercero and Diffley, 2001; Cobb et al., 2003; Lucca et al., 2004). It is therefore possible that the replisome remains associated at the telomere after DNA replication in TRF1 null cells. Stalled replication forks can give rise to abnormal DNA structures such as reversed forks, which form cruciform structures (Neelsen and Lopes, 2015). At chromosome internal locations, the reversed forks can help replication fork restart or bypass of DNA lesions. But at the telomere there is just the DNA end and repair would not be possible.

What could occur at these terminal forks was assessed in a study examining the fate of a replication fork reaching a DSB, not unlike the situation at a chromosome end (Doksani et al., 2009). It was speculated that the combined action of MRN, CtIP and ATM prevents the formation of pathological chicken-foot

structures at the stalled fork encountering the DSB, allowing disassembly of the replication complex. In absence of these proteins, fork reversal and the accumulation of cruciform structures were observed at the fork, which was speculated to be a substrate for sister fusion. Although the situation at telomeres is not exactly similar to internal DSBs, it is possible that a comparable process occurs in absence of TRF1 (Fig. 5.4). Initially, the situation is similar to fork reversal at replication forks elsewhere in the genome, resulting in a regressed fork. Resection of the newly replicated 5' end by nucleases such as Exo1, Dna2 or WRN takes place, creating a 3' overhang at the reversed end. What is unique at telomeres is that this overhang generates a potential substrate for a-NHEJ because there is already a 3' overhang present nearby at the unreplicated telomere end. This ssDNA at the chromosome end contains microhomology with the newly generated overhang (AT-TA). When these 3' overhangs anneal, fusion by a-NHEJ could occur resulting in sister telomere fusion (Fig. 5.4). An interesting experiment to test the requirement for TRF1 loss in the formation of SAs would be to treat Pot1a null cells with aphidicolin. This would result in ATR activation, due to the unprotected 3' overhang, together with aphidicolin induced replication stress at the telomere. An increase in SAs in this setting would argue against a direct effect of TRF1 on the terminal replication fork, but indicate that ATR activation at the terminal fork by itself is sufficient to induce sister fusions.

Interestingly, there is experimental evidence suggesting that sister telomere fusions occur when there is complementarity in the telomeric sequence

Telomeric replication fork at the chromosome end without TRF1

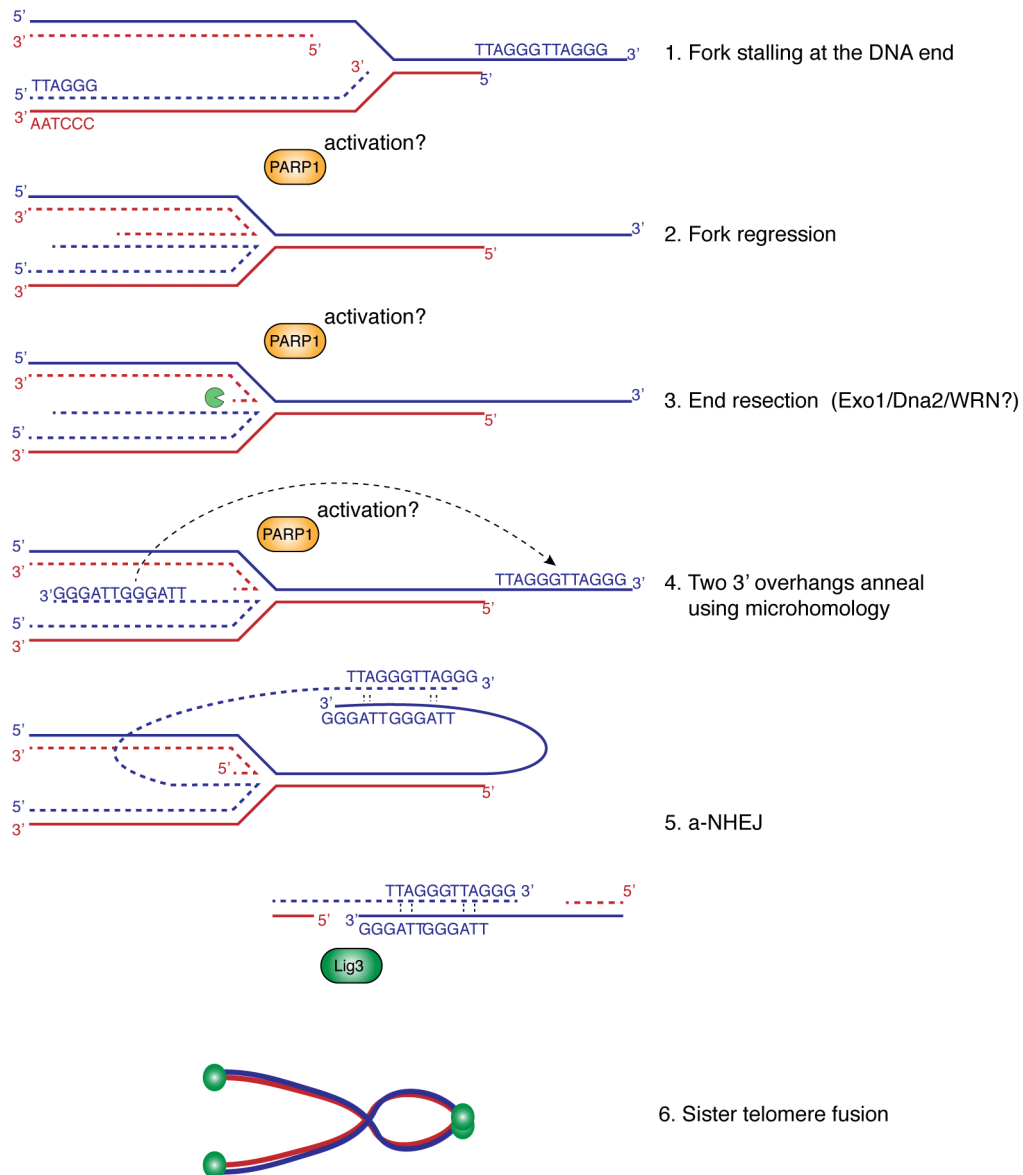


Figure 5.4 Model for the formation of sister telomere fusions upon TRF1 loss

A schematic of the terminal replication fork is shown (Shelterin and replisome are not included for clarity). In absence of TRF1, the replication fork would stall at the telomere end. Unwinding of the newly synthesized DNA strands would occur resulting in fork regression. At the reversed fork, the nucleases (Exo1/Dna2 or WRN) would act on the 5' end resulting in a 3' overhang. Since there is already a 3' overhang present at the telomere end, annealing can occur between the overhangs due to the microhomology present in the telomeric sequence, resulting in a-NHEJ mediated by PARP1 and Lig3. How and where PARP1 is activated is not known.

(Stohr et al., 2010). An experiment with a mutated telomerase enzyme that incorporates different 'telomeric' sequences to the DNA end than the typical TTAGGG sequence has provided evidence for this. A telomerase enzyme incorporating "TATATATA" caused sister telomere fusions and isochromosomes, which occurred in an ATM independent manner. However, incorporation of TTTGGG sequences did not have this effect and solely led to chromosome type telomere fusions, that required ATM (likely because telomeres become uncapped since TRF2 does not bind this sequence). These experiments suggest that microhomology within the telomeric sequence might indeed be required for SAs, in support of the model presented here.

While this model can explain how sister fusions are formed, several questions remain unanswered. How is PARP1 activated at the regressed fork and why is its activation not inhibited by TRF2? Does TRF1 indeed promote the disassembly of the replication fork? And if so, does TRF1 promote replisome disassembly through preventing ATR activation? Is the RNA primer at the lagging strand removed prior to fork stalling? How is 53BP1/Rif1 involved in this process? Future experiments should attempt to answer these questions.

5.2.6 The role of Ku in preventing a-NHEJ at telomeres

An interesting observation is that Ku70/80 did not prevent SAs after deletion of TRF1 (Fig. 3.6b). This was surprising given that Ku can block a-NHEJ upon loss of TRF2 or the entire shelterin complex (Celli et al., 2006; Sfeir and de

Lange, 2012). Ku is thought to block a-NHEJ by competing with PARP1 for DNA ends (Wang et al., 2006). One explanation for why Ku does not inhibit a-NHEJ in the TRF1 null setting is that TRF2 is still present. In vitro experiments suggested that TRF2 directly interacts with Ku to prevent it from stimulating NHEJ. Thus, upon deletion of TRF1, Ku may still be inhibited by TRF2 explaining why loss of Ku does not result in higher levels of SAs. Arguing against this hypothesis is the fact that Ku appears to prevent SAs in a TRF1^{F/F}TPP1^{F/F} setting. When Ku is deleted from these MEFs, the level of SAs increases from 13 to 30% (unpublished data from T. Kibe). These results raise the possibility that POT1a/b limits the activity of Ku in the formation of SAs. Possibly, the ssDNA binding capability of POT1a/b limits the accessibility of Ku for the DNA end. Although the levels of the TIN2/TPP1/POT1a/b axis of shelterin are reduced when TRF1 is missing, enough residual POT1a/b remains to protect the 3' overhang since a POT1a/b null phenotype is not observed in absence of TRF1 (Frescas and de Lange, 2014). It would be interesting to analyze the contribution of Ku to SAs in a POT1a^{F/F}TRF1^{F/F} setting.

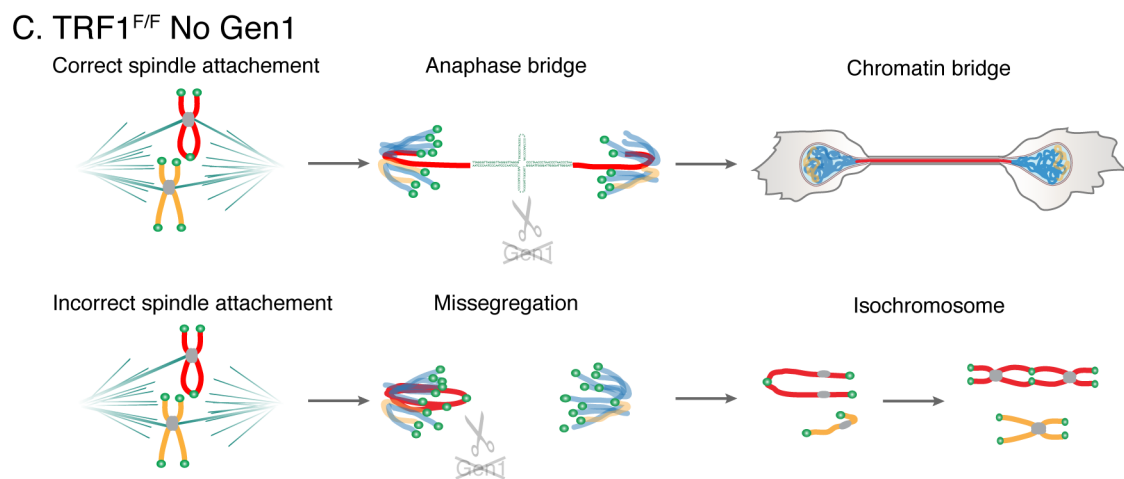
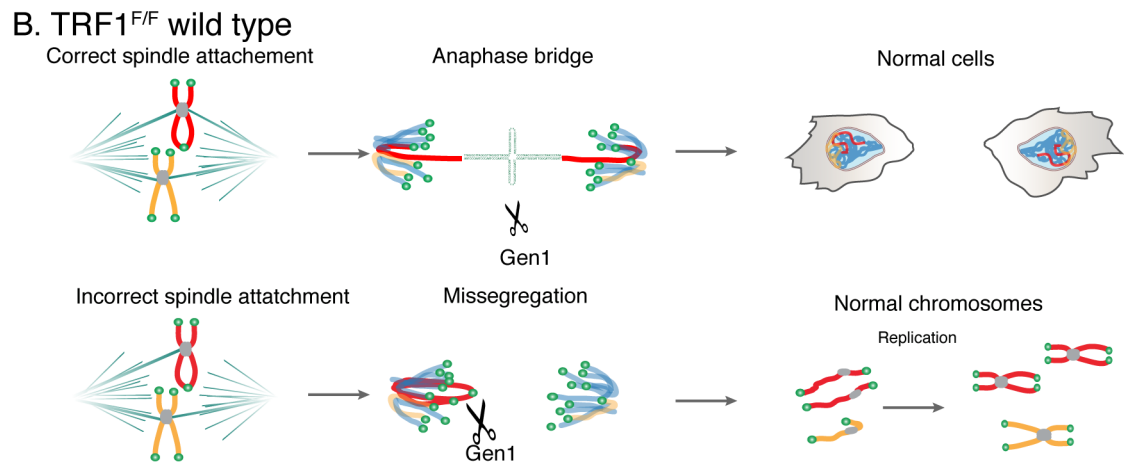
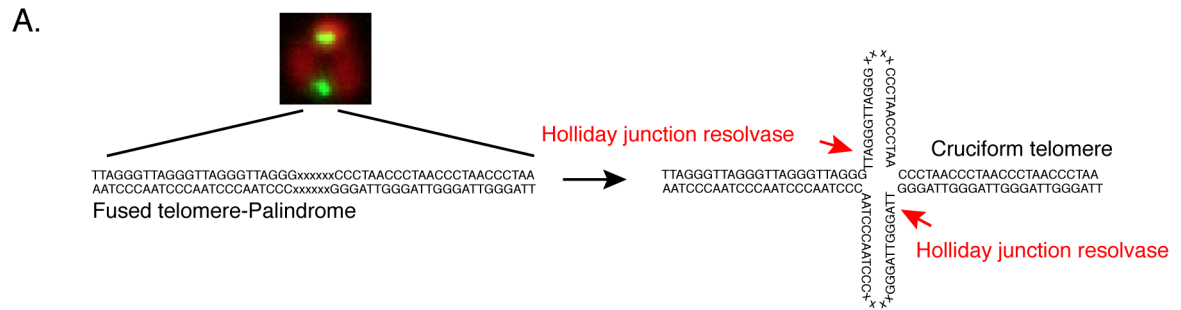
An alternative explanation for the lack of suppression of SAs by Ku could simply be the structure of the DNA end. We do not know on a molecular level what structure gives rise to a-NHEJ in absence of TRF1. Possibly, the end is incompatible to Ku loading, thus explaining why its loss does not affect SAs. However, this cannot explain the increased level of SAs in the TRF1^{F/F}TPP1^{F/F}Ku^{-/-} setting.

5.2.7 *Gen1 cleaves SAs*

The results in Chapter 4 revealed a unique mechanism for cleavage of sister telomere fusions by the HJ resolvases Gen1 (Fig. 5.5a-c). Since telomere fusions create a palindromic sequence, a Holliday junction can be formed which can be cleaved by HJ resolvases. The absence of Gen1 results in the accumulation of chromatin bridges, but only when TRF1 was removed from telomeres. It is unclear from the results presented here whether Gen1 is the only HJ resolvase capable of cleaving fused telomeres. Whereas Mus81 loss increased the percentage of chromatin bridges, it cannot be ascertained that this is due to a TRF1 specific effect or because of its role at CFS throughout the genome. An additive effect was seen for Gen1 and Mus81 depletion, but the results were not significant. This could be due to the inefficiency of the shRNAs against Mus81, which led to only a 60-80% reduction in expression levels. However, it is also possible that Mus81 is not as efficient as Gen1 in cleaving telomeres. Mus81 requires a nicked substrate for HJ cleavage, which might not be efficiently generated at telomeres (Wyatt et al., 2013). Interestingly, a recent paper analyzed the sequence specificity of Gen1. Even though it shows broad cleavage activity on a variety of sequences, it preferentially cleaves TTxGG substrates, suggesting that telomeric TTaGGg sequences form an ideal substrate for Gen1 (Shah Punatar et al., 2017). A remaining question is whether Gen1 cleaves all types of telomere fusions or just the ones arising through a-NHEJ. Preliminary experiments indicate that Gen1 does not cleave telomere fusions that occur after

Figure 5.5 Model for the role of Gen1 at telomeres fused by a-NHEJ.

(A) Schematic of a fused sister telomere is shown on the left. Fusion junctions in a-NHEJ often contain insertions/deletions that are depicted by xxx. The formation of a cruciform structure from a telomere fusion is shown on the right. (B) Upon deletion of TRF1, anaphase bridges can form when a chromosome with a sister telomere fusion (red) is separated (top). Cleavage of the telomere fusion by Gen1 still allows faithful chromosome segregation. When the spindle forms an incorrect attachment or loses its connection (bottom), the entire chromosome is missegregated into one daughter cell. Cleavage by Gen1 can prevent the formation of isochromosomes. (C) In absence of Gen1, a chromosome with a sister fusion can follow two fates in mitosis. If the spindle forms a correct attachment, the fused chromosome will form a chromatin bridge (top). When the spindle forms an incorrect attachment or loses its connection, the entire chromosome is missegregated into one daughter cell (bottom). Replication in the next S-phase will result in the formation of an isochromosome (red).



expression of a dominant negative TRF2 allele, TRF2^{ΔBΔM}, which results in chromatid type telomere fusion in human cells (van Steensel et al., 1998). The level of telomere fusion was not increased in Gen1 null cells, suggesting it is not capable of cleaving these fusions (unpublished data S. Dewhurst). Possibly, Gen1 only cleaves fusions formed via a-NHEJ. This pathway is known to promote mutations and insertions at the fusion site and the mismatches could help to destabilize the helix and promote protrusion of the cruciform DNA structure. Cruciform DNA structures are energetically unfavorable and do not form easily. However, increasing their length or by introducing negative supercoiling, their extrusion can be promoted (Mizuuchi et al., 1982; Gellert et al., 1983). This opens the possibility that transcription of TERRA, the telomeric RNA, promotes the expression of the cruciform, since transcription induces negative supercoiling (Gilbert and Allan, 2014). Alternatively, perhaps the activities of BLM and PICH during anaphase promote the protrusion of cruciform structures.

5.2.8 Critically short telomeres in human cells fuse via a-NHEJ

The results presented here are relevant with regard to telomere shortening in human cancer. Studies have shown that fusions of critically short telomeres in human cells occur via sister chromatid fusion and are dependent on a-NHEJ (Letsolo et al., 2010; Jones et al., 2014; Liddiard et al., 2016). Microhomology is also observed at telomere fusion sites in cancer, consistent with a-NHEJ (Lin et al., 2010). In a system of experimentally induced telomere erosion, telomere

fusions in surviving Lig4^{-/-} cells were predominantly intra-chromosomal consistent with Lig3-mediated sister chromatid fusion (Jones et al., 2014). Conversely, Lig4 facilitated inter-chromosomal fusions, indicating they are formed by c-NHEJ. Interestingly, the inter-chromosomal fusions often retained telomeric repeats at the fusion sites whereas intra-chromosomal fusions (Lig3) involved the subtelomeric region (Letsolo et al., 2010; Jones et al., 2014). Given the results presented here, it is interesting to speculate that sister telomere fusions by a-NHEJ in the telomeric region are cleaved by Gen1, until the degradation reaches into the subtelomeric region where a substrate for a cruciform DNA structure no longer exists. In agreement with this, escape from telomere-driven crisis is dependent on a functional Lig3, suggesting that cells with a-NHEJ mediated sister fusions have a mechanisms to survive (Jones et al., 2014).

Liddiard et al. suggested that the basis for intra-chromosomal fusions lies in interplay with the DNA replication machinery, consistent with the model presented here (Liddiard et al., 2016). Critically short telomeres were inferred to contain an average of 6 TTAGGG repeats at the time of stable fusion product formation (Capper et al., 2007). This might not be enough for efficient telomere protection by shelterin but telomeres of this size are still thought to contain a 3' overhang (Jones et al., 2014). Therefore it is possible that our model for the generation of sister fusions at the terminal replication fork takes place at critically short telomeres after DNA replication. The short telomere tract no longer contains enough TRF1 to promote disassembly of the replication machinery resulting to

fork stalling and reversal. Since the 3' overhang is still formed at these critically short telomeres, a-NHEJ mediated fusion can occur. But further studies are required to test this hypothesis.

Chapter 6: Materials and Methods

6.1 Cell culture techniques

6.1.1 Mammalian cell culture

MEFs were cultured in DMEM (GIBCO) supplemented with 15% fetal bovine serum (GIBCO), 2 mM L-glutamine, 100 U/ml penicillin (Sigma), 0.1 mg/ml streptomycin (Sigma), 0.1 mM nonessential amino acids (Invitrogen), 1 mM sodium pyruvate (Sigma) and 50 mM β -mercaptoethanol (Chemicon). Primary MEFs were isolated from E13.5 embryos using standard techniques. Primary MEFs were immortalized at PD2 or 3 by retroviral infections with pBabe-SV40-LT (a gift from G. Hannon) and cultured additionally for 10-15 PDs to achieve immortalization. Human 293T and Phoenix packaging cell lines were grown in DMEM supplemented with 10% bovine calf serum (Hyclone), 2 mM L-glutamine, 100U/ml penicillin (Sigma), 0.1 mg/ml streptomycin (Sigma), 0.1 mM nonessential amino acids (Invitrogen) and 1 mM sodium pyruvate (Sigma). For subculturing, cells were washed with PBS pH 7.4, trypsinized and resuspended in fresh serum containing medium to inactivate trypsin. Cells passaged 1:5 or plated as required and when necessary, counted with a Coulter Z1 counter. All cell lines were grown at 37°C with 5% CO₂.

293T and Phoenix cells were grown in 10% bovine serum (GIBCO), 2 mM L-glutamine, 100 U/ml penicillin (Sigma), 0.1 mg/ml streptomycin (Sigma), 0.1 mM nonessential amino acids (Invitrogen) and 1 mM sodium pyruvate (Sigma). Cells were passaged 1:10 or plated as required. Cells were used for a maximum of 15-20 passages. A list of cell lines used is found in Chapter 6.4.

6.1.2 Calcium phosphate precipitation transfection of 293T and Phoenix cells

3-5X10⁶ 293T or Phoenix cells were seeded in 10 cm dishes 20-24 h prior to transfection. For each plate, plasmid DNA (10-20 µg) was combined with 50 µl of 2.5 M CaCl₂ and ddH₂O in a total volume of 500 µl. The solution was incubated for 1-2 minutes at room temperature after which 500µl of 2x HBS (50 mM HEPES pH 7.05, 10 mM KCL, 12 mM dextrose, 280 mM NaCl, 1.5 mM Na₂PO₄) was added dropwise while airing the solution with a pipet. The solution was incubated for 1-2 minutes and carefully added to the 10 cm dish containing 293T or Phoenix cells. Medium was exchanged 12-16 h after transfection.

6.1.3 Retroviral gene delivery

For retroviral gene delivery, 3-5X10⁶ Phoenix packaging cells (ATCC) were transfected with 10-20 µg of plasmid using calcium phosphate precipitation. After 12-16 h, medium was replaced by MEF medium. Virus particles were first collected 48 h after transfection, filtered through a 0.45 µM filter and supplemented with 4 µg/ml polybrene before infecting target MEFs that were seeded 12 h prior in a 10 cm dish (3-5X10⁵ cells/plate). The Phoenix cell media was replenished and infections repeated every 12 h for a total of 3 or 4 infections.

For selection, MEFs were collected 12 h after the last infection and seeded in fresh medium containing the appropriate antibiotics (1.5-2 µg/ml puromycin, 90 µg/ml hygromycin). Cells were maintained in selection until

uninfected control cells were dead. A list of shRNA targets is provided in Chapter 6.5.

6.1.4 Lentiviral gene delivery of shRNAs

Lentiviral PLKO vectors were used for shRNA-mediated knockdown of protein expression in MEFs, except for BLM as discussed below. Briefly, $4\text{-}5 \times 10^6$ 293T cells were seeded in 10 cm dishes 24 h prior to transfection. Calcium phosphate precipitation was used to transfect 10 μg shRNA plasmid together with plasmids encoding viral packaging proteins (5 μg RRE, 3 μg VSV, 2.5 μg REV). Medium was exchanged 12 h after transfection and replaced with MEF medium. Virus was collected as described in Chapter 6.1.3 with the first collection and infection 36 h after transfection of 293Ts. MEFs were infected 3 times total 12 h apart. Selection of MEFs was done as described in 6.1.3, but only when the shRNA did not strongly affect cell viability (TopBP1, Ligase 1). When shRNA resulted in a rapid drop in cell viability, the selection process was omitted and Cre infection done 12 h after the last shRNA infection, to ensure cells remained healthy throughout the experiment (Mus81, PARP1, CCDC124, CCDC9, CCDC79). For the shRNA against Exo1 and Lig3, the shRNA infection had such a strong effect on cell viability that the Cre infection was done prior to shRNA infection. Where possible, efficient shRNA mediated knockdown was checked by western blot or qPCR.

For BLM depletion, a retroviral expression vector was used (pSuperior) as described in Zimmermann et al. 2014 (Zimmermann et al., 2014). For the experiment, $3\text{-}5 \times 10^6$ Phoenix cells were transfected with 10 μg shBLM or control. Media exchanged for MEF media 12 h after transfection and virus was collected as described in Chapter 6.1.3, with the first collection 36 h after transfection. As for shExo1, target MEFs were first infected with Cre virus, immediately followed by 2 shRNA infections to increase cell viability after BLM depletion.

6.1.5 Cre mediated gene deletion

For Cre recombinase mediated gene deletion, MEFs seeded at $2\text{-}5 \times 10^5$ cells in a 10 cm dish and infected 3 times using a pMMP Hit&Run Cre retrovirus. Infections were done 12 h at room temperature in media containing 4 $\mu\text{g}/\text{ml}$ polybrene. For timed experiments, time point zero was set at the time of the 2nd Cre infection. For Cre-ER inducible cell lines, Cre expression was activated by addition of 1 μM 4OH-tamoxifen to the cell growth media and exchanged for regular media 12-24 h later. Addition of 4OH-tamoxifen was set at time point zero for timed experiments.

6.1.6 Generation of CRISPR/Cas9 knockout cell lines

Target sequences for CRISPR/Cas9 mediated gene knockouts were identified by ZiFit (<http://zifit.parners.org>, see list below). Targets were cloned into an AflII-linearized gRNA cloning vector (Addgene) by Gibson Assembly. gRNA plasmids

were transiently co-transfected with a hCas9 expression plasmid into target MEF cell lines using nucleofection (Lonza) using the MEF2 nucleofection kit. Briefly, $2-4 \times 10^6$ cells were collected and mixed with electroporation buffer, 5 μ g Cas9 plasmid and 5 μ g gRNA plasmid and electroporated using program A023. Cells were rapidly transferred into a 10 cm dish containing pre-warmed media and, which was refreshed 12 h afterwards to remove dead cells. The transfection was repeated after 48 h to obtain maximum efficiency of the CRISPR/Cas9 system. After the second round of transfection, cells were left to recover for 24-48 h and subcloned into 96-well plates at several dilutions ranging from 1 to 0.05 cells per well. After two weeks, multiple (~30-50) clones were grown to confluence in a 6-well plate and clones screened for gene deletion by immunoblotting. Targeting was further verified by sequencing clones of TOPO-TA cloned PCR products according to manufactures' instructions (Thermo Fisher).

Target of gRNAs for mouse 53BP1:

gRNA2-GAGAATCTTCTATTATC

gRNA3-GCATCTGCAGATTAGGA

gRNA5-GTCTTTTTCAGATCCTG

Target of gRNAs for mouse Gen1:

gRNA2-GAGGACTCAGACTCGTTA

gRNA3-GACTCGTTACGGGCCTTC

TOPO-TA sequencing primers mouse 53BP1:

FW: CTCGATCTCACACTTCCGCC, RV: TCTTTGGGATGAATCAGCAGGT

TOPO-TA sequencing primers mouse Gen1:

FW: TGTCATATGCTTGCCTGGTCT, RV: TCAAGTCCCTACCACGGGTT

6.1.7 PARPi treatment of cells

For PARP inhibitor treatment (olaparib AZD2281 Selleck chemicals), MEFs were first infected with Cre virus in 10 cm dish as described previously. Olaparib was dissolved in DMSO and added to cells in fresh media at a final concentration of 2 μ M. Treatment lasted for the final 24-48 h of the experiment until colcemid was added for 45 minutes prior to harvest. To control for PARPi efficiency, western blot analysis was done in MEFs grown separately in 6 cm dish and treated with Olaparib as above. To promote phosphorylation, MEFs were treated with/without H₂O₂ (2.55 μ l in 5 ml media, 5 mM) for 20 minutes immediately prior to harvest for western blot.

6.2 Molecular techniques

6.2.1 Cloning techniques

53BP1 mutant alleles were generated via Gibson cloning (Gibson et al., 2009) (Fig. 2.1). 53BP1DB (wild type 53BP1 lacking the C-terminal BRCT domains) or

53BP1^{Δ28} in a PMX backbone were used as template for the reactions (Bothmer et al., 2011). All PCR reactions were done with PfuUltra II Fusion polymerase (Agilent). Briefly, the domain of 53BP1 containing the mutated STQ residues was PCR amplified from 53BP1^{Δ28}. The remainder of 53BP1 and the backbone PMX vector were PCR amplified from the 53BP1DB plasmid using primers that are the reverse complement of the primers used on 53BP1^{Δ28} creating a homologous sequence on either end of the PCR products. PCR products were gel-purified and combined using Gibson cloning. This Gibson mix contains

Mutant	Template	Forward primer	Reverse primer
ΔPTIP =	53BP1DB	GAAAACAAGGTTGCAGACCCTGTGGATTCTTC	GAATTCGGATCCGGCAGTCTAGAGGATGGTCCACC
Δ1	53BP1Δ28	GGTGGACCATCCTCTAGACTGCCGGATCCGAATTC	GAAGAATCCACAGGGTCTGCAACCTTGTTTTTC
ΔMOB =	53BP1DB	GGTGGACCATCCTCTAGACTGCCGGATCCGAATTC	GTGCCTCAGATCGAGTAGCTGGTGACGGAAGT
Δ4	53BP1Δ28	CAGTTCCGTCACCAGCTACTCGATCTGAGGCAC	GAATTCGGATCCGGCAGTCTAGAGGATGGTCCACC
ΔRif1	53BP1DB	TTCCTGCTGAAAATGATAGTATCCTGATGAATCC	CAACTGTGATGAGGCAGTATCTTCAGCACCAAG
	53BP1Δ28	CTTGGTGCTGAAGATACTGCCTCATCACAGTTG	GGATTCATCAGGATACTATCATTTTCAGCAGGAA
ΔOligo	53BP1Δ28	CTGAGGAGACTGAAGAGCCAATTG	GCTGAGGCATATCAAACCTTCTTCTTC
Δ28	PCR #1	GAAGAAGAGTTTGATATGCCTCAGCCTGAGGAG ACTGAAGAGCCAATTG	CAATTGGCTCTTCAGTCTCCTCAGGCTGAGGCA TATCAAACCTTCTTCTTC
ΔOligo	53BP1DB	CTGATGTGGATGCTAATACTGCAATTAAG	GTGCCTCAGATCGAGTAGCTGGTGACGGAAGT
Δ1,2,4	53BP1Δ28	CTTAATTGCAGTATTAGCATCCACATCAG	CAGTTCCGTCACCAGCTACTCGATCTGAGGCAC
	ΔOligo		
ΔOligo	53BP1DB	GGTGGACCATCCTCTAGACTGCCGGATCCGAATTC	CTTAATTGCAGTATTAGCATCCACATCAG
Δ3,4	53BP1Δ28	CTGATGTGGATGCTAATACTGCAATTAAG	GAATTCGGATCCGGCAGTCTAGAGGATGGTCCACC
	ΔOligo		
ΔOligo	53BP1DB	GGTGGACCATCCTCTAGACTGCCGGATCCGAATTC	GAAGAATCCACAGGGTCTGCAACCTTGTTTTTC
Δ2,3,4	53BP1Δ28	GAAAACAAGGTTGCAGACCCTGTGGATTCTTC	GAATTCGGATCCGGCAGTCTAGAGGATGGTCCACC
	ΔOligo		
Mutants used for initial Rif1 localization experiments, not used for any other experiments.			
Δ1,2	53BP1DB	CTGATGTGGATGCTAATACTGCAATTAAG	GAATTCGGATCCGGCAGTCTAGAGGATGGTCCACC
	53BP1Δ28	GGTGGACCATCCTCTAGACTGCCGGATCCGAATTC	CTTAATTGCAGTATTAGCATCCACATCAG
Δ3	53BP1DB	CTTAATTGCAGTATTAGCATCCACATCAG	CAGTTCCGTCACCAGCTACTCGATCTGAGGCAC
	53BP1Δ28	CTGATGTGGATGCTAATACTGCAATTAAG	GTGCCTCAGATCGAGTAGCTGGTGACGGAAGT
Δ1,2,3	53BP1DB	CAGTTCCGTCACCAGCTACTCGATCTGAGGCAC	GAATTCGGATCCGGCAGTCTAGAGGATGGTCCACC
	53BP1Δ28	GGTGGACCATCCTCTAGACTGCCGGATCCGAATTC	GTGCCTCAGATCGAGTAGCTGGTGACGGAAGT
Δ1,2,4	53BP1DB	CTGATGTGGATGCTAATACTGCAATTAAG	GTGCCTCAGATCGAGTAGCTGGTGACGGAAGT
	53BP1Δ28	CAGTTCCGTCACCAGCTACTCGATCTGAGGCAC	CTTAATTGCAGTATTAGCATCCACATCAG
Δ3,4	53BP1DB	GGTGGACCATCCTCTAGACTGCCGGATCCGAATTC	CTTAATTGCAGTATTAGCATCCACATCAG
	53BP1Δ28	CTGATGTGGATGCTAATACTGCAATTAAG	GAATTCGGATCCGGCAGTCTAGAGGATGGTCCACC
Δ2,3,4	53BP1DB	GGTGGACCATCCTCTAGACTGCCGGATCCGAATTC	GAAGAATCCACAGGGTCTGCAACCTTGTTTTTC
	53BP1Δ28	GAAAACAAGGTTGCAGACCCTGTGGATTCTTC	GAATTCGGATCCGGCAGTCTAGAGGATGGTCCACC

a 5' exonuclease that generates ssDNA at the homologous sequences on either end of the PCR products enabling them to ligate together. A taq ligase and phusion polymerase fills in the gaps creating a full-length plasmid composed of both PCR fragments. The 53BP1^{ΔoligoΔ28} mutant was created in a similar fashion. First, a PCR around the 53BP1^{Δ28} vector was done with primers that were targeted to each side of the oligomerization domain (amino acids 1231-1270) creating a long PCR product lacking this domain. Next, a second PCR was done on the same template using primers with extension that overlapped on either side of the deletion. The final PCR product was then ligated together using the Gibson mix. The other 53BP1 oligomerization mutants were created as described for the 53BP1-S/TQ mutants using 53BP1^{ΔoligoΔ28} and 53BP1^{DB} as templates.

GFP-PICH and RFP-PICH constructs were created using Gateway cloning according to manufacturers protocol (Clontech). Briefly, mouse PICH cDNA was amplified and cloned into a pDONR vector. The construct was then shuttled into an N-terminal GFP or RFP retroviral destination vector (pQCXIP). Mouse and human Gen1 constructs were cloned from cDNA into pQCXIP retroviral vectors using Gateway cloning, as described for PICH. Mutations of the active sites were made using quickchange mutagenesis on the cDNA in the pDONR vector, prior to shuttling to the pQCXIP destination vector. The C-terminally myc tagged hGen1-3xNLS-PLPC constructs were made using Infusion cloning (Clontech) using the manufactures instructions. First, the 3xNLS sequence was inserted upstream of the myc tag using an EcoRI site using annealed oligos to create a

PLPC-3xNLS-Myc construct. Then, the PCR amplified hGEN1 amino acids 1-527 were inserted using BAMH1/EcoRI sites by Infusion cloning.

6.2.2 Co-immunoprecipitation in 293T cells

To examine the interaction between Sun1, PTIP and 53BP1, $4-5 \times 10^6$ 293T cells were plated in a 10 cm dish 20-24 h prior to transfection by CaPO₄ precipitation using 10 µg each plasmid DNA as indicated. Medium was changed 12 h after transfection and 24-28 h later cells were incubated with 100 µg/ml zeocin (Invitrogen) for 20 min, harvested by scraping in cold PBS on ice, and collected by centrifugation. For irradiation experiment, cells were irradiated with 10 Gray, left to recover for 1 h and harvested by scraping in cold PBS on ice and collected by centrifugation. Cells were lysed in lysis buffer (20 mM Tris pH 8.0, 0.5% NP-40, 150 mM NaCl, 1 mM CaCl₂, 1 mM MgCl₂, 1 mM EDTA, Complete protease inhibitor mix (Roche) and PhosSTOP phosphatase inhibitor mix (Roche)) for 30 minutes on ice, and centrifuged at 15,000 rpm in an tabletop eppendorf centrifuge for 10 min at 4°C. Lysate was incubated with beads for immunoprecipitation for 1 h with 50 µl pre-blocked Protein G beads per 1 ml of lysate. For myc: 1.2 µl antibody (9B11) was used per co-IP. For FLAG, pre-conjugated M2-sepharose beads were used (Sigma). For experiments using FLAG magnetic beads, M-270 Epoxy beads were conjugated with anti-FLAG M2 antibody (Sigma) as described (Subbotin and Chait, 2014)).

An alternative lysis condition was used in some experiments with similar

results. After collection, cells were resuspended in 0.5 ml hypotonic lysis buffer (10% glycerol, 10 mM KCl, 10 mM Hepes (pH 7.9), 0.1 mM EDTA, 0.5% NP-40, 1.5 mM MgCl_2 , Complete protease inhibitor mix (Roche), and PhosSTOP phosphatase inhibitor mix (Roche)). The KCl concentration was then raised to 400 mM and samples sonicated for 1 min in water bath solicitor and equal amount of lysis buffer, without KCl, was added to reduce KCl concentration to 200 mM. After centrifugation at 15,000 rpm in a tabletop eppendorf centrifuge or 10 min at 4°C, the IP was done as described above. Beads were washed 7 times with the lysis buffer containing 150 mM KCl and immunoprecipitated proteins were eluted with 50 µl of 2xLaemmli buffer. Samples were boiled for 5 min before separation on SDS-PAGE.

To test the interaction between Sun1 and 53BP1, several experiments were done using the two cell lysis methods described above with untagged Sun1 or myc-tagged Sun1 and FLAG tagged 53BP1. Additionally, the following lysis buffers were tested using the first protocol described above.

- RIPA lysis buffer (150 mM NaCl, 1% NP-40, 0.5% Sodium deoxycholate, 0.1% SDS, 50 mM Tris pH 8.0 + Complete protease inhibitor mix and PhosSTOP phosphatase inhibitor mix)
- DNase treatment (100 mM NaCl, 1.5 mM MgCl_2 , 1.5 mM CaCl_2 , 20 mM Tris pH 8.0, 0.5% NP-40 + Complete protease inhibitor mix and PhosSTOP phosphatase inhibitor mix supplemented with 5 units DNaseI/500 µl (Promega))

6.2.3 Co-immunoprecipitation of endogenous Sun1 from MEFs

To test the interaction between FLAG-53BP1 and endogenous Sun1, MEFs were infected with 53BP1 constructs as described. Cells were collected 72 h after Cre by scraping, one confluent 15 cm dish per condition was used. Where indicated, cells were treated prior to scraping with DSP crosslinker for 15 minutes in 10 ml media containing 1 mM DSP (Thermo Scientific, 50 mM stock in DMSO), which was quenched by addition of 20 ml Tris pH 7.4 buffer. Cells were either lysed whole or nuclei pre-isolated prior to lysis. For nuclear isolation, cells were incubated for 10 min in hypotonic lysis buffer (10 mM Hepes pH 7.9, 10 mM KCl, 0.1 mM EGTA, 10% Glycerol, 1.5mM MgCl₂, 0.1% NP-40, Complete protease inhibitor mix (Roche), and PhosSTOP phosphatase inhibitor mix (Roche)), and centrifuged to collect nuclei. Cells or isolated nuclei were then resuspended in 500 µl hypotonic lysis buffer (10% glycerol, 10 mM KCl, 20 mM Hepes (pH 7.9), 0.1 mM EDTA, 0.5% NP-40, 1.5 mM MgCl₂, Complete protease inhibitor mix (Roche), and PhosSTOP phosphatase inhibitor mix (Roche)) and the KCl concentration raised to 400 mM. Cells were lysed by 1-5 min sonication in a waterbath. Equal amounts of lysis buffer without KCl, was added to reduce KCl concentration to 200 mM and after centrifugation at 16,000 rpm for 10 min at 4°C, the IP was done as described in Chapter 6.2.3 using magnetic beads conjugated to M2 FLAG antibody. Beads were washed 7 times with the lysis buffer containing 150 mM KCl and immunoprecipitated proteins were eluted with 50 ml

of 2xLaemmli buffer containing 50 mM DTT. Samples were boiled for 5 min before separation on SDS-PAGE.

6.2.4 Western blotting

Western blot was performed using standard methods. Briefly, cells were lysed in 2X laemmli buffer (100 mM Tris pH 6.8, 20% Glycerol, 4% SDS, 0.04% bromophenol blue, 5% 2-mercaptoethanol) at 5×10^3 cells/ μ l and the lysate denatured for 10 min at 100°C before shearing with a 28 ½ gauge insulin needle. Lysate was briefly centrifuged to remove debris and subsequently resolved using SDS/PAGE and transferred to a nitrocellulose membrane. For large proteins (53BP1 and Rif1), transfer was done overnight in a cold room to enhance transfer efficiency. Membranes were blocked in 1-5% milk in PBS with 0.1% Tween-20 and incubated with primary antibody for 1 h at room temperature or overnight at 4°C. Membranes were washed 3x in PBS-T and incubated for 1 h at room temperature with horse-radish-peroxidase-conjugated sheep anti-mouse or donkey anti-rabbit secondary antibodies. After three washes in PBS-T, membranes developed using enhanced chemiluminescence (Amersham). For phosphor-specific antibodies, TBS-T was used instead of PBS-T and membranes were blocked in 5% BSA.

6.2.5 List of antibodies used

TRF1 (1255 de lange lab), TRF2 (1499 de lange lab), Rif1 (de lange lab), 53BP1 (175933 abcam or 612522 BD Biosciences or 100-304A Novus Biologicals), γ H2AX (JBW301 Millipore), Ku70 (m19 Santa Cruz), γ Tubulin (GTU88 Abcam), Sun1 (ab74758 Abcam), Sun2 (ab87036 Abcam), Ligase 3 (611876 BD Biosciences), Ligase 1 (18051 Proteintech), pSTQ ATR/ATM substrate (2851 Cell Signaling), BLM (2179 Abcam), Ku70 (m19 Santa Cruz), PARP1 (C2-10 Enzo life sciences), Anti-Poly(ADP-ribose) (4335 Trevigen), TopBP1 (ab2402 Abcam), Exo1 (Bethyl), Gen1 (kind gift from Steve West lab), FLAG epitope (M2 FLAG Sigma), myc tag (9B11 Cell Signaling), GFP tag (50430 Proteintech)

6.2.6 Chromatin immunoprecipitation (ChIP)

ChIP was performed as previously described (Loayza and de Lange, 2003). Briefly, cells were fixed 1% paraformaldehyde/culture medium for 60 min at room temperature. Glycine was added to 0.2 M to stop the cross-linking. Cells were pelleted by centrifugation and washed with ice-cold PBS, followed by a final wash in PBS/1 mM PMSF. The cells were resuspended in cell lysis buffer (1% SDS, 10 mM EDTA pH 8.0, 50 mM Tris-HCl pH 8.0, 1 mM PMSF, protease inhibitor cocktail from Roche), incubated on ice for 15 min and sonicated for 10 min (30 sec on/30 sec off) in a water-bath sonicator. Supernatants of lysates were incubated with antibody at 4 °C overnight. Following antibodies were used: TRF1 (1449 crude serum), 53BP1 (ab175933, Abcam), Sun1 (ab74758, Abcam),

Sun2 (ab87036, Abcam). ChIP-grade protein G magnetic beads were added for 45 minutes (Dyna, Invitrogen). Immunoprecipitated DNA was washed, eluted from the beads, and precipitated with ethanol after reversal of the cross-links and Proteinase K treatment. The DNA samples were dissolved in water, boiled and loaded on dot blots, and hybridized with the Sty11 probe (telomeres) or BAMHI probe labeled with ^{32}P -alpha CTP using Klenow. Signal intensity measured by ImageQuant software was normalized to the signals of the input DNA on the same blot.

6.2.7 Telomere overhang analysis

1×10^6 cells were harvested by trypsinization, resuspended in PBS, mixed 1:1 with 2% agarose in PBS and cast into plugs. The plugs were then digested overnight at 50°C with 1 mg/ml Proteinase K (Roche) in 10 mM Tris HCl pH 8.0, 250 mM EDTA, 0.2% sodium deoxycholate and 1% sodium lauryl sarcosine. The next day, the plugs were washed five times for 1 h each with TE (1 mM PMSF was added to the fourth wash) and once with sterile water (20 min). DNA in the plugs was subsequently digested by AluI and MboI (NEB; 60 U of each per plug, in 500 μl cutSMART buffer) overnight at 37°C shaking. The next morning, plugs were washed once with 1 ml TE and equilibrated with 1 ml 0.5x TBE. The samples were loaded onto a 1% agarose/0.5x TBE gel and run on a CHEFTDRII pulse field electrophoresis apparatus (BioRad). The electrophoresis parameters were as follows: Initial pulse: 5 s, final pulse: 5 s, voltage: 6 V/cm, run time: 24 h.

The gel was then dried and pre-hybridized with Church mix for 1 h at 50°C. DNA in the gel was hybridized overnight at 50°C in Church mix with 50 ng of ^{32}P end-labeled [AACCCT]₄ probe. After hybridization, the gel was washed three times 30 min with 4x SSC at 55°C, once with 4xSSC/0.1% SDS and exposed to a phosphorimager screen overnight or longer. After exposure, the screen was scanned on a STORM phosphorimager (Molecular Dynamics) and the gel was denatured in 0.5 M NaOH, 1.5 M NaCl for 30 min, neutralized twice (15 min each) with 0.5 M Tris HCl pH 7.5, 3 M NaCl, pre-hybridized in Church mix (0.5 M Na⁺ phosphate pH 7.2, 1 mM EDTA, 1% BSA, 7% SDS) for 1 h at 55°C and hybridized overnight with the same probe as above at 55°C. The next day, the gel was washed and exposed as above. The ssDNA and dsDNA signals were quantified using ImageQuant software (Molecular Dynamics). The telomeric 3' overhang signal was quantified based on the signal obtained after annealing a labeled CT strand telomeric oligonucleotide to native telomeric DNA. The ssDNA signal was normalized to the total telomeric DNA signal in each lane obtained after in situ denaturation of the DNA and re-hybridization with the same probe. The normalized signals are then compared between samples to determine the effect of genotypes or treatments on the relative normalized 3' overhang signals. To determine if the telomeric ssDNA signal in the in-gel hybridization assay represented a *bona fide* terminal 3' overhang structure, the DNA in agarose plugs were digested with the *E. coli* 3' exonuclease ExoI prior to restriction digest. After the plugs had been washed 5x in TE as described above, they were washed with

ddH₂O and 1x Exol buffer (NEB) for 1 h each. The DNA in the plugs was digested with 100 units Exol in 300 µl 1x Exol buffer per plug overnight at 37°C. The next day, 60 units of fresh Exol was added and the plugs were digested for an additional 2 h. After the digestion, the plugs were washed 2 times with TE for 1 h each and loaded onto a 1% agarose gel as described above.

6.2.8 Quantitative PCR analysis

For qPCR analysis, RNA was isolated from MEFs using a Qiagen RNA isolation kit (Invitrogen). cDNA was prepared from 1 µg of total RNA by using Thermoscript Reverse Transcriptase (Invitrogen). Quantitative PCR reactions were performed using Life Technologies SYBR Green Master Mix on an Applied Biosystems 7900HT Sequence Detection System. Differences between samples were calculated using QuantStudio software (Applied Biosystems) using the Δ CT method and were normalized to GAPDH. For Mus81, two different primers pairs were designed, both spanning an exon-exon junctions to prevent amplification of genomic DNA. Primers used:

Mus81_FW_1: TCGTGTTTCAAAGGCATTGC

Mus81_RV_1 TCACCGCCTGATGCTAGGT

Mus81_FW_2: TGCTGCAACTCTACAGGGAG

Mus81_RV_2: GCCGATGCGTTCCAAGGAT

GAPDH_FW: GGGTGAGGCCGGTGCTGAGTAT (from H. Takai)

GAPDH_RV: CCTTCCGTGTTCTACCCCAA (from H. Takai)

6.3 Imaging techniques

6.3.1 IF and IF-FISH

IF and IF-FISH were conducted as previously described (Dimitrova and de Lange, 2006). Briefly, cells grown on coverslips were fixated for 10 min in 3% paraformaldehyde and 2% sucrose in PBS at room temperature, followed by three PBS washes. Coverslips were incubated in blocking solution (1 mg/ml BSA, 3% goat serum, 2% donkey serum, 0.1% TritonX-100, 1 mM EDTA in PBS) for 30 min, followed by incubation with primary antibodies diluted in blocking solution for 1 h at room temperature. Cells were washed three times for 5 min with PBS and then incubated with secondary antibodies diluted in blocking solution for 30 min at room temperature. For IF, samples were washed in three 5-min washes with PBS. DNA was stained with DAPI or Hoechst33342 (Tocris, Fisher Scientific) in the PBS washes and coverslips were mounted using antifade reagent ProLong Gold from Life Technologies. For IF-FISH, coverslips were washed after the secondary antibody incubation and fixed for an additional 10 min in 3% paraformaldehyde. After 3 additional 5-min PBS washes, coverslips were dehydrated with 70%, 95% and 100% ethanol and allowed to dry. Hybridizing solution (70% formamide, 0.5% blocking reagent from Roche, 10 mM Tris-HCl pH 7.2 and 488-OO-[CCCTAA]₃ or Cy3-OO-[TTAGGG]₃ PNA or AF647-OO-[TTAGGG]₃ probe from Applied Biosystems) was added to each coverslip and denatured at 80°C for 5 min, followed by a 1h incubation at room temperature. Two 15-min washes in 70% formamide/10 mM Tris-HCl pH 7.2 and

three 5-min washes with PBS were performed. DNA was stained with DAPI or Hoechst 33342 in the PBS washes and coverslips were mounted using antifade reagent ProLong Gold from Life Technologies. Images were captured using a Zeiss AxioPlan II microscope with a Hamamatsu C4742-95 camera using Volocity software from Perkin Elmer or with an image restoration system (DeltaVision; Applied Precision) equipped with a cooled charge-coupled device camera (CoolSnap QE; Photometrics), a PlanApo 60x 1.40 NA objective (Olympus America, Inc) and SoftWoRx software.

Primary antibodies used for IF: Rif1 (de lange lab), 53BP1 (175933 Abcam or 612522 BD Biosciences) FLAG epitope (M2 FLAG Sigma), MYC tag (9B11 Cell Signaling). Secondary antibodies used for IF: AF488 Goat- α Mouse (Invitrogen), AF555 Goat- α Rabbit (Invitrogen), AF647- Goat- α Rabbit (Invitrogen).

6.3.2 Chromatin bridge analysis

To analyze chromatin bridges between nuclei, cells grown on coverslips were fixed for 10 min in 3% paraformaldehyde/2% sucrose at room temperature, followed by three PBS washes. Cells were either processed for regular IF as described in 6.3.1. Alternatively, coverslips were directly incubated for 5 min in 5 μ g/ml Hoechst 33342 or DAPI and washed three times in PBS. Coverslips were then mounted using antifade reagent ProLong Gold from Life Technologies. Coverslips were analyzed using a Zeiss AxioPlan II microscope with a Hamamatsu C4742-95 camera. Since the intensity of many bridges is too low to

capture by camera, bridges were counted manually at the microscope. For each coverslip, at least 200 cells were counted in fields next to each other and the percent of cells with a bridge was counted (every cell that has a bridge protruding from it is counted as positive, independent of whether the cell on the other end of the bridge was visible in the field of view).

6.3.3 Metaphase telomeric FISH

Telomeric FISH was conducted as previously described (van Steensel et al., 1998; Celli et al., 2006). Briefly, colcemid was added to cells 0.75-1 hour prior to harvest. Cells were collected by trypsinization, swollen in 0.075 M KCl and fixed overnight at 4°C in methanol:acetic acid (3:1). Metaphase spreads were dropped on glass slides and aged overnight. Slides were hybridized with AF488-OO-[CCCTAA]₃ or Cy3-OO-[TTAGGG]₃ PNA probe in hybridizing solution, denatured at 80°C for 10 min and incubated for 2 h at room temperature. Two 15-min washes in 70% formamide/10 mM Tris-HCl pH 7.2 and three 5 min PBS washes. Slides were dehydrated in 70%, 95%, and 100% ethanol and mounted using Vectashield mounting medium with DAPI from Vector Laboratories. Images were captured using a Zeiss AxioPlan II microscope with a Hamamatsu C4742-95 camera using Volocity software from Perkin Elmer.

6.3.4 Isochromosome analysis

Isochromosomes were counted on metaphase spreads based on their visual appearance. The details of the analysis are fully described in Chapter 4.2.4.

6.3.5 Live-cell imaging for chromatin mobility analysis

Dysfunctional telomeres were visualized using mCherry-BP1-2 (h53BP1, amino acid 1220-1711) as described previously (Dimitrova et al., 2008). Cre-treated TRF2^{F/F} cells were plated onto MatTek glass bottom plates and grown for 2 days before imaging. An hour before imaging, cells were changed into Leibovitz's L-15 medium (Gibco) supplemented with 15% FBS, non-essential amino acids, L-glutamine, penicillin/streptomycin and 50 mM β -mercaptoethanol, and allowed to equilibrate for one hour. Imaging was done at 37°C using an environmental chamber using a DeltaVision microscope system (Applied Precision) with a PlanApo 60x 1.40 NA objective lens (Olympus America, Inc.). 5 μ m Z-stacks at 0.5 μ m steps were acquired using SoftWoRx software with 50 msec exposure time, every 30 sec over 10 min (t=20 frames) at 2 x 2 binning with 512 x 512 pixels in final size. Images were deconvolved and 2D-maximum intensity projection images were obtained using SoftWoRx software. Tracking of mCherry-BP1-2 foci was performed with ImageJ software for at least 10 cells per condition. Cells were registered by the StackReg plugin using Rigid Body (Thevenaz et al., 1998). Next, particles were detected and tracked using the Mosaic Particle Detector and Tracker plugin (Sbalzarini and Koumoutsakos,

2005) with the following parameters: radius=1-2 pixels; cutoff=1-2 pixels; percentile=1-6; link range=1; displacement=5 pixels. The x and y coordinates of each trajectory were output for further calculation. Per cell, all mCherry-BP1-2 foci that were continuously tracked for at least 19 of the 20 frames were analyzed. The analysis of the eGFP-TRF1-marked telomeres was similarly conducted using the following parameters: radius=1 pixels; cutoff=1 pixels; percentile=8-12; link range=1; displacement=5 pixels. Distorted nuclei were discarded based on the methods described in Lottersberger et al. 2015 (Lottersberger et al., 2015).

6.3.6 Live-cell imaging for mitotic abnormalities

Live cell imaging was performed as described in (Maciejowski et al., 2015).

Briefly, cells were plated onto 35 mm glass bottom dishes (MatTek) 48 h before imaging. One hour before imaging, cell culture media was replaced with phenol red-free DMEM medium. Live cell imaging was performed using a CellVoyager CV1000 spinning disk confocal system (Yokogawa, Olympus) equipped with 445, 488, and 561 nm lasers, a Hamamatsu 512 x 512 EMCCD camera. Pinhole size was 50 μm . Images were acquired at the indicated intervals using a UPlanSApo 60x/1.3 silicone oil objective with the correction collar set to 0.17. The pixel size in the image was 0.27 μm . The following emission filters were used for image acquisition: 525/488 for Venus- tagged proteins, and 617/61 for RFP-tagged proteins. 12 μm z-stacks were collected at 2.0 μm steps. Temperature was maintained at 37°C in a temperature-controlled enclosure with CO₂. Maximum

intensity projection of z-stacks and adjustment of brightness and contrast were performed using Fiji software. Image stitching was done with the Fiji plugin Grid/Collection stitching (Preibisch et al., 2009) with 20% tile overlap, linear blending, a 0.30 regression threshold, a 2.50 max/avg. displacement threshold, and a 3.50 absolute displacement threshold. Images were cropped and assembled into figures using Fiji and Photoshop CS5.1 (Adobe).

6.4 Lists of cell lines used

Genotype	Source	Cell line #
293T	ATCC	
Phoenix cells	ATCC	
TRF2 ^{F/F} Rosa26 Cre-ER ^{T2}	De Lange lab	
TRF2 ^{F/F} 53BP1 ^{-/-} Lig4 ^{-/-} Rosa26 Cre-ER ^{T2}	De Lange lab	78600.1
TRF2 ^{F/F} 53BP1 ^{-/-}	De Lange lab	
TRF2 ^{F/F} 53BP1 ^{-/-} Sun1 ^{-/-} Sun2 ^{-/-}	De Lange lab	60318.7
TRF2 ^{F/F} 53BP1 ^{-/-} Sun1 ^{+/+} Sun2 ^{+/+}	De Lange lab	53618.4
TRF1 ^{F/F} 53BP1 ^{-/-} late passage	De Lange lab	76565.5
TRF1 ^{F/F} 53BP1 ^{-/-}	This work	78882.3
TRF1 ^{F/F} 53BP1 ^{-/-}	This work	78882.5
TRF1 ^{F/F}	De Lange lab	9.3
TRF1 ^{F/F} Gen1 ^{+/+} CRISPR	This work	g3#13, g3#14

TRF1 ^{F/F} Gen1 ^{-/-} CRISPR	This work	g3#17,g2#16,g2#17
TRF1 ^{F/F}	De Lange lab	39020.6
TRF1 ^{F/F} Gen1 ^{+/+} CRISPR	This work	g2#7
TRF1 ^{F/F} Gen1 ^{-/-} CRISPR	This work	g2#8, g3#11, g3#20
TRF1 ^{F/F} Rif1 ^{F/F}	De Lange lab	65.8
53BP1 ^{-/-} CRISPR	This work	g3#3, g5#7
TRF1 ^{F/F} mTR ^{+/-}	De Lange lab	370.5
TRF1 ^{F/F} mTR ^{+/+}	De Lange lab	370.2
TRF1 ^{F/F} TIN2 ^{+/+} Ku70 ^{-/-}	De Lange lab	82263.2
TRF1 ^{F/F} TIN2 ^{+/+} Ku70 ^{+/+}	De Lange lab	82263.8
TRF1 ^{F/F} TRF2 ^{F/+} Lig4 ^{-/-}	De Lange lab	305-1
TRF1 ^{F/F} p53 ^{-/-}	De Lange lab	75023.9

6.5 List of shRNA used

Target	TRC	Backbone	Target sequence
CCDC9	TRCN0000250760	PLKO	GGACGTGAGTGAAGATGTTAC
CCDC79	TRCN0000113325	PLKO	CGGTCCTTTGTTTGGACTCTT
	TRCN0000113326	PLKO	CCTGAGGTAATTCGACCTATA
	TRCN0000113327	PLKO	CCTGTAGAAGAAGACAACCTT
CCDC124	TRCN0000181504	PLKO	GAAGGAGCTGGAAGATGCTTA
	TRCN0000181941	PLKO	GCTGGAAGATGCTTACTGGAA

	TRCN0000181879	PLKO	GCCACTGGAAGAGAACCTTAA
	TRCN0000181658	PLKO	GAAACAGAAGGAGCTGGAAGA
	TRCN0000181793	PLKO	GCTGATGCCAAGAAACAGAAG
Gen1	TRCN0000246735	PLKO	ATGTTGACTGTTACACGATAT
	TRCN0000246737	PLKO	TGAACGTAATGGATGCATATT
	TRCN0000246738	PLKO	GGCATCAGACAGACCATAATA
PARP1	TRCN0000353959	PLKO	GAGTACATTGTCTACGACATT
	TRCN0000325059	PLKO	GCCCTTGGAAACATGTATGAA
Mus81	TRCN0000241267	PLKO	TAGTGCCTGGAAGTTCGAAAC
	TRCN0000241266	PLKO	CCAGTCTGTGCGAGAAGTATT
	TRCN0000241264	PLKO	CAGAAATGCTCCGAGAGTTAC
Lig3	TRCN0000070979	PLKO	GCAATGAAGAAGTGTCCCAAT
	TCRN0000070980	PLKO	CCAGTGAAAGGTGCTTCGTTT
Lig1	TRCN0000071154	PLKO	CCTTGGATGTTGATGCCACTT
	TRCN0000071155	PLKO	CCTTCCAAGAATAACTATCAT
	TRCN0000071157	PLKO	CGAGAGTGATTCTCCAGTGAA
TopBP1	TRCN0000124220	PLKO	GCTCTTAGAAACTGCGAGAAT
	TRCN0000124223	PLKO	GCCAGAAGAGTTTCCTTGTTT
shBLM	from Michal	pSuperior	GCATCCTAATAAAGAGTTA
	from Michal	pSuperior	GGAGGGTTATTATCAAGAA

References

1. **Adams, M.M., Wang, B., Xia, Z. et al.Carpenter, P.B.** (2005) 53BP1 oligomerization is independent of its methylation by PRMT1. *Cell Cycle*, *4*, 1854–1861.
2. **Anderson, L., Henderson, C., and Adachi, Y.** (2001) Phosphorylation and rapid relocalization of 53BP1 to nuclear foci upon DNA damage. *Mol Cell Biol*, *21*, 1719–1729.
3. **Bailey, R., Priego Moreno, S., and Gambus, A.** (2015) Termination of DNA replication forks: “Breaking up is hard to do”. *Nucleus*, *6*, 187–196.
4. **Barefield, C., and Karlseder, J.** (2012) The BLM helicase contributes to telomere maintenance through processing of late-replicating intermediate structures. *Nucleic Acids Res*, *40*, 7358–7367.
5. **Bass, T.E., Luzwick, J.W., Kavanaugh, G. et al.Cortez, D.** (2016) ETAA1 acts at stalled replication forks to maintain genome integrity. *Nat Cell Biol*, *18*, 1185–1195.
6. **Baumann, C., Körner, R., Hofmann, K. et al.Nigg, E.A.** (2007) PICH, a centromere-associated SNF2 family ATPase, is regulated by Plk1 and required for the spindle checkpoint. *Cell*, *128*, 101–114.
7. **Baumann, P., Benson, F.E., and West, S.C.** (1996) Human Rad51 protein promotes ATP-dependent homologous pairing and strand transfer reactions in vitro. *Cell*, *87*, 757–766.
8. **Becker, A., Durante, M., Taucher-Scholz, G. et al.Jakob, B.** (2014) ATM alters the otherwise robust chromatin mobility at sites of DNA double-strand breaks (DSBs) in human cells. *PLoS One*, *9*, e92640.
9. **Bermudez, V.P., Lindsey-Boltz, L.A., Cesare, A.J. et al.Sancar, A.** (2003) Loading of the human 9-1-1 checkpoint complex onto DNA by the checkpoint clamp loader hRad17-replication factor C complex in vitro. *Proc Natl Acad Sci USA*, *100*, 1633–1638.
10. **Bhowmick, R., Minocherhomji, S., and Hickson, I.D.** (2016) RAD52 Facilitates Mitotic DNA Synthesis Following Replication Stress. *Mol Cell*, *64*, 1117–1126.
11. **Boboila, C., Yan, C., Wesemann, D.R. et al.Alt, F.W.** (2010) Alternative end-joining catalyzes class switch recombination in the absence of both Ku70 and DNA ligase 4. *J Exp Med*, *207*, 417–427.

12. **Boersma, V., Moatti, N., Segura-Bayona, S. et al. Jacobs, J.J.** (2015) MAD2L2 controls DNA repair at telomeres and DNA breaks by inhibiting 5' end resection. *Nature*, *521*, 537–540.
13. **Bosco, N., and de Lange, T.** (2012) A TRF1-controlled common fragile site containing interstitial telomeric sequences. *Chromosoma*, *121*, 465–474.
14. **Bothmer, A., Robbiani, D.F., Di Virgilio, M. et al. Nussenzweig, M.C.** (2011) Regulation of DNA end joining, resection, and immunoglobulin class switch recombination by 53BP1. *Mol Cell*, *42*, 319–329.
15. **Bothmer, A., Robbiani, D.F., Feldhahn, N. et al. Nussenzweig, M.C.** (2010) 53BP1 regulates DNA resection and the choice between classical and alternative end joining during class switch recombination. *J Exp Med*, *207*, 855–865.
16. **Bothmer, A., Rommel, P.C., Gazumyan, A. et al. Robbiani, D.F.** (2013) Mechanism of DNA resection during intrachromosomal recombination and immunoglobulin class switching. *J Exp Med*, *210*, 115–123.
17. **Botuyan, M.V., Lee, J., Ward, I.M. et al. Mer, G.** (2006) Structural basis for the methylation state-specific recognition of histone H4-K20 by 53BP1 and Crb2 in DNA repair. *Cell*, *127*, 1361–1373.
18. **Bouwman, P., Aly, A., Escandell, J.M. et al. Jonkers, J.** (2010) 53BP1 loss rescues BRCA1 deficiency and is associated with triple-negative and BRCA-mutated breast cancers. *Nat Struct Mol Biol*, *17*, 688–695.
19. **Brown, E.J., and Baltimore, D.** (2000) ATR disruption leads to chromosomal fragmentation and early embryonic lethality. *Genes Dev*, *14*, 397–402.
20. **Brown, E.J., and Baltimore, D.** (2003) Essential and dispensable roles of ATR in cell cycle arrest and genome maintenance. *Genes Dev*, *17*, 615–628.
21. **Bryan, T.M., Marusic, L., Bacchetti, S. et al. Reddel, R.R.** (1997) The telomere lengthening mechanism in telomerase-negative immortal human cells does not involve the telomerase RNA subunit. *Hum Mol Genet*, *6*, 921–926.
22. **Bryant, H.E., Petermann, E., Schultz, N. et al. Helleday, T.** (2009) PARP is activated at stalled forks to mediate Mre11-dependent replication restart and recombination. *EMBO J*, *28*, 2601–2615.

23. **Buis, J., Wu, Y., Deng, Y. et al.Ferguson, D.O.** (2008) Mre11 nuclease activity has essential roles in DNA repair and genomic stability distinct from ATM activation. *Cell*, *135*, 85–96.
24. **Bunting, S.F., Callen, E., Wong, N. et al.Nussenzweig, A.** (2010) 53BP1 inhibits homologous recombination in Brca1-deficient cells by blocking resection of DNA breaks. *Cell*, *141*, 243–254.
25. **Burma, S., Chen, B.P., Murphy, M. et al.Chen, D.J.** (2001) ATM phosphorylates histone H2AX in response to DNA double-strand breaks. *J Biol Chem*, *276*, 42462–42467.
26. **Callen, E., Di Virgilio, M., Kruhlak, M.J. et al.Nussenzweig, A.** (2013) 53BP1 Mediates Productive and Mutagenic DNA Repair through Distinct Phosphoprotein Interactions. *Cell*, *153*, 1266–1280.
27. **Canudas, S., Houghtaling, B.R., Kim, J.Y. et al.Smith, S.** (2007) Protein requirements for sister telomere association in human cells. *EMBO J*, *26*, 4867–4878.
28. **Cao, L., Xu, X., Bunting, S.F. et al.Finkel, T.** (2009) A selective requirement for 53BP1 in the biological response to genomic instability induced by Brca1 deficiency. *Mol Cell*, *35*, 534–541.
29. **Capper, R., Britt-Compton, B., Tankimanova, M. et al.Baird, D.M.** (2007) The nature of telomere fusion and a definition of the critical telomere length in human cells. *Genes Dev*, *21*, 2495–2508.
30. **Carney, J.P., Maser, R.S., Olivares, H. et al.Petrini, J.H.** (1998) The hMre11/hRad50 protein complex and Nijmegen breakage syndrome: linkage of double-strand break repair to the cellular DNA damage response. *Cell*, *93*, 477–486.
31. **Celli, G.B., and de Lange, T.** (2005) DNA processing is not required for ATM-mediated telomere damage response after TRF2 deletion. *Nat Cell Biol*, *7*, 712–718.
32. **Celli, G.B., Lazzerini Denchi, E., and de Lange, T.** (2006) Ku70 stimulates fusion of dysfunctional telomeres yet protects chromosome ends from homologous recombination. *Nat Cell Biol*, *8*, 885–890.
33. **Chan, K.L., North, P.S., and Hickson, I.D.** (2007) BLM is required for faithful chromosome segregation and its localization defines a class of ultrafine anaphase bridges. *EMBO J*, *26*, 3397–3409.

34. **Chan, K.L., Palmai-Pallag, T., Ying, S. et al.Hickson, I.D.** (2009) Replication stress induces sister-chromatid bridging at fragile site loci in mitosis. *Nat Cell Biol*, *11*, 753–760.
35. **Chan, Y.W., and West, S.C.** (2014) Spatial control of the GEN1 Holliday junction resolvase ensures genome stability. *Nat Commun*, *5*, 4844.
36. **Chang, H.H., Watanabe, G., Gerodimos, C.A. et al.Lieber, M.R.** (2016) Different DNA End Configurations Dictate Which NHEJ Components Are Most Important for Joining Efficiency. *J Biol Chem*, *291*, 24377–24389.
37. **Chanoux, R.A., Yin, B., Urtishak, K.A. et al.Brown, E.J.** (2009) ATR and H2AX cooperate in maintaining genome stability under replication stress. *J Biol Chem*, *284*, 5994–6003.
38. **Chapman, J.R., Barral, P., Vannier, J.B. et al.Boulton, S.J.** (2013) RIF1 is essential for 53BP1-dependent nonhomologous end joining and suppression of DNA double-strand break resection. *Mol Cell*, *49*, 858–871.
39. **Chapman, J.R., and Jackson, S.P.** (2008) Phospho-dependent interactions between NBS1 and MDC1 mediate chromatin retention of the MRN complex at sites of DNA damage. *EMBO Rep*, *9*, 795–801.
40. **Chaturvedi, P., Eng, W.K., Zhu, Y. et al.Zhou, B.B.** (1999) Mammalian Chk2 is a downstream effector of the ATM-dependent DNA damage checkpoint pathway. *Oncogene*, *18*, 4047–4054.
41. **Chen, H., Lisby, M., and Symington, L.S.** (2013) RPA Coordinates DNA End Resection and Prevents Formation of DNA Hairpins. *Mol Cell*, *50*, 589–600.
42. **Ciccia, A., Constantinou, A., and West, S.C.** (2003) Identification and characterization of the human mus81-eme1 endonuclease. *J Biol Chem*, *278*, 25172–25178.
43. **Cimprich, K.A., and Cortez, D.** (2008) ATR: an essential regulator of genome integrity. *Nat Rev Mol Cell Biol*, *9*, 616–627.
44. **Cobb, J.A., Bjergbaek, L., Shimada, K. et al.Gasser, S.M.** (2003) DNA polymerase stabilization at stalled replication forks requires Mec1 and the RecQ helicase Sgs1. *EMBO J*, *22*, 4325–4336.
45. **Cortez, D., Guntuku, S., Qin, J. et al.Elledge, S.J.** (2001) ATR and ATRIP: partners in checkpoint signaling. *Science*, *294*, 1713–1716.

46. **Costanzo, V., Robertson, K., Ying, C.Y. et al. Gautier, J.** (2000) Reconstitution of an ATM-dependent checkpoint that inhibits chromosomal DNA replication following DNA damage. *Mol Cell*, *6*, 649–659.
47. **Costanzo, V., Shechter, D., Lupardus, P.J. et al. Gautier, J.** (2003) An ATR- and Cdc7-dependent DNA damage checkpoint that inhibits initiation of DNA replication. *Mol Cell*, *11*, 203–213.
48. **Cotta-Ramusino, C., McDonald, E.R., Hurov, K. et al. Elledge, S.J.** (2011) A DNA damage response screen identifies RHINO, a 9-1-1 and TopBP1 interacting protein required for ATR signaling. *Science*, *332*, 1313–1317.
49. **Cuadrado, M., Martinez-Pastor, B., Murga, M. et al. Fernandez-Capetillo, O.** (2006) ATM regulates ATR chromatin loading in response to DNA double-strand breaks. *J Exp Med*, *203*, 297–303.
50. **Cuella-Martin, R., Oliveira, C., Lockstone, H.E. et al. Chapman, J.R.** (2016) 53BP1 Integrates DNA Repair and p53-Dependent Cell Fate Decisions via Distinct Mechanisms. *Mol Cell*, *64*, 51–64.
51. **Dantzer, F., de La Rubia, G., Ménissier-De Murcia, J. et al. Schreiber, V.** (2000) Base excision repair is impaired in mammalian cells lacking Poly(ADP-ribose) polymerase-1. *Biochemistry*, *39*, 7559–7569.
52. **Davies, A.A., Masson, J.Y., McIlwraith, M.J. et al. West, S.C.** (2001) Role of BRCA2 in control of the RAD51 recombination and DNA repair protein. *Mol Cell*, *7*, 273–282.
53. **de Jager, M., van Noort, J., van Gent, D.C. et al. Wyman, C.** (2001) Human Rad50/Mre11 is a flexible complex that can tether DNA ends. *Mol Cell*, *8*, 1129–1135.
54. **de Lange, T., Shiue, L., Myers, R.M. et al. Varmus, H.E.** (1990) Structure and variability of human chromosome ends. *Mol Cell Biol*, *10*, 518–527.
55. **Delacroix, S., Wagner, J.M., Kobayashi, M. et al. Karnitz, L.M.** (2007) The Rad9-Hus1-Rad1 (9-1-1) clamp activates checkpoint signaling via TopBP1. *Genes Dev*, *21*, 1472–1477.
56. **Dellaire, G., Kepkay, R., and Bazett-Jones, D.P.** (2009) High resolution imaging of changes in the structure and spatial organization of chromatin, gamma-H2A.X and the MRN complex within etoposide-induced DNA repair foci. *Cell Cycle*, *8*, 3750–3769.

57. **Denchi, E.L., and de Lange, T.** (2007) Protection of telomeres through independent control of ATM and ATR by TRF2 and POT1. *Nature*, *448*, 1068–1071.
58. **Deriano, L., and Roth, D.B.** (2013) Modernizing the nonhomologous end-joining repertoire: alternative and classical NHEJ share the stage. *Annu Rev Genet*, *47*, 433–455.
59. **Deshpande, R.A., Lee, J.H., Arora, S. et al. Paull, T.T.** (2016) Nbs1 Converts the Human Mre11/Rad50 Nuclease Complex into an Endo/Exonuclease Machine Specific for Protein-DNA Adducts. *Mol Cell*, *64*, 593–606.
60. **Di Virgilio, M., Callen, E., Yamane, A. et al. Nussenzweig, M.C.** (2013) Rif1 prevents resection of DNA breaks and promotes immunoglobulin class switching. *Science*, *339*, 711–715.
61. **Difilippantonio, S., Gapud, E., Wong, N. et al. Nussenzweig, A.** (2008) 53BP1 facilitates long-range DNA end-joining during V(D)J recombination. *Nature*, *456*, 529–533.
62. **Dimitrova, N., Chen, Y.C., Spector, D.L. et al. de Lange, T.** (2008) 53BP1 promotes non-homologous end joining of telomeres by increasing chromatin mobility. *Nature*, *456*, 524–528.
63. **Dimitrova, N., and de Lange, T.** (2006) MDC1 accelerates nonhomologous end-joining of dysfunctional telomeres. *Genes Dev*, *20*, 3238–3243.
64. **Dimitrova, N., and de Lange, T.** (2009) Cell cycle dependent role of MRN at dysfunctional telomeres: ATM signaling-dependent induction of NHEJ in G1 and resection-mediated inhibition of NHEJ in G2. *Mol Cell Biol*, *29*, 5552–5563.
65. **Ding, H., Schertzer, M., Wu, X. et al. Lansdorp, P.M.** (2004) Regulation of murine telomere length by Rtel: an essential gene encoding a helicase-like protein. *Cell*, *117*, 873–886.
66. **Doil, C., Mailand, N., Bekker-Jensen, S. et al. Lukas, C.** (2009) RNF168 binds and amplifies ubiquitin conjugates on damaged chromosomes to allow accumulation of repair proteins. *Cell*, *136*, 435–446.
67. **Doksani, Y., Bermejo, R., Fiorani, S. et al. Foiani, M.** (2009) Replicon dynamics, dormant origin firing, and terminal fork integrity after double-strand break formation. *Cell*, *137*, 247–258.

68. **Doksani, Y., and de Lange, T.** (2014) The role of double-strand break repair pathways at functional and dysfunctional telomeres. *Cold Spring Harb Perspect Biol*, *6*, a016576.
69. **Doksani, Y., Wu, J.Y., de Lange, T. et al. Zhuang, X.** (2013) Super-resolution fluorescence imaging of telomeres reveals TRF2-dependent T-loop formation. *Cell*, *155*, 345–356.
70. **Donigian, J.R., and de Lange, T.** (2007) The role of the poly(ADP-ribose) polymerase tankyrase1 in telomere length control by the TRF1 component of the shelterin complex. *J Biol Chem*, *282*, 22662–22667.
71. **Dudley, D.D., Chaudhuri, J., Bassing, C.H. et al. Alt, F.W.** (2005) Mechanism and control of V(D)J recombination versus class switch recombination: similarities and differences. *Adv Immunol*, *86*, 43–112.
72. **Dunham, M.A., Neumann, A.A., Fasching, C.L. et al. Reddel, R.R.** (2000) Telomere maintenance by recombination in human cells. *Nat Genet*, *26*, 447–450.
73. **Durkin, S.G., and Glover, T.W.** (2007) Chromosome fragile sites. *Annu Rev Genet*, *41*, 169–192.
74. **Dynek, J.N., and Smith, S.** (2004) Resolution of sister telomere association is required for progression through mitosis. *Science*, *304*, 97–100.
75. **Escribano-Diaz, C., Orthwein, A., Fradet-Turcotte, A. et al. Durocher, D.** (2013) A cell cycle-dependent regulatory circuit composed of 53BP1-RIF1 and BRCA1-CtIP controls DNA repair pathway choice. *Mol Cell*, *49*, 872–883.
76. **Fachinetti, D., Bermejo, R., Cocito, A. et al. Foiani, M.** (2010) Replication termination at eukaryotic chromosomes is mediated by Top2 and occurs at genomic loci containing pausing elements. *Mol Cell*, *39*, 595–605.
77. **Feng, L., Fong, K.W., Wang, J. et al. Chen, J.** (2013) RIF1 Counteracts BRCA1-mediated End Resection during DNA Repair. *J Biol Chem*, *288*, 11135–11143.
78. **Forment, J.V., Blasius, M., Guerini, I. et al. Jackson, S.P.** (2011) Structure-specific DNA endonuclease Mus81/Eme1 generates DNA damage caused by Chk1 inactivation. *PLoS One*, *6*, e23517.

79. **Fouche, N., Ozgur, S., Roy, D. et al. Griffith, J.D.** (2006) Replication fork regression in repetitive DNAs. *Nucleic Acids Res*, *34*, 6044–6050.
80. **Fradet-Turcotte, A., Canny, M.D., Escribano-Diaz, C. et al. Durocher, D.** (2013) 53BP1 is a reader of the DNA-damage-induced H2A Lys 15 ubiquitin mark. *Nature*, *499*, 50–54.
81. **Frescas, D., and de Lange, T.** (2014) TRF2-Tethered TIN2 Can Mediate Telomere Protection by TPP1/POT1. *Mol Cell Biol*, *34*, 1349–1362.
82. **Frit, P., Barboule, N., Yuan, Y. et al. Calsou, P.** (2014) Alternative end-joining pathway(s): bricolage at DNA breaks. *DNA Repair (Amst)*, *17*, 81–97.
83. **Garcia, V., Phelps, S.E., Gray, S. et al. Neale, M.J.** (2011) Bidirectional resection of DNA double-strand breaks by Mre11 and Exo1. *Nature*, *479*, 241–244.
84. **Garner, E., Kim, Y., Lach, F.P. et al. Smogorzewska, A.** (2013) Human GEN1 and the SLX4-associated nucleases MUS81 and SLX1 are essential for the resolution of replication-induced Holliday junctions. *Cell Rep*, *5*, 207–215.
85. **Ge, X.Q., Jackson, D.A., and Blow, J.J.** (2007) Dormant origins licensed by excess Mcm2-7 are required for human cells to survive replicative stress. *Genes Dev*, *21*, 3331–3341.
86. **Gellert, M., O’Dea, M.H., and Mizuuchi, K.** (1983) Slow cruciform transitions in palindromic DNA. *Proc Natl Acad Sci U S A*, *80*, 5545–5549.
87. **Gibson, D.G., Young, L., Chuang, R.Y. et al. Smith, H.O.** (2009) Enzymatic assembly of DNA molecules up to several hundred kilobases. *Nat Methods*, *6*, 343–345.
88. **Gilbert, N., and Allan, J.** (2014) Supercoiling in DNA and chromatin. *Curr Opin Genet Dev*, *25*, 15–21.
89. **Giunta, S., Belotserkovskaya, R., and Jackson, S.P.** (2010) DNA damage signaling in response to double-strand breaks during mitosis. *J Cell Biol*, *190*, 197–207.
90. **Glover, T.W., Berger, C., Coyle, J. et al. Echo, B.** (1984) DNA polymerase alpha inhibition by aphidicolin induces gaps and breaks at common fragile sites in human chromosomes. *Hum Genet*, *67*, 136–142.

91. **Gong, Y., and de Lange, T.** (2010) A Shld1-controlled POT1a provides support for repression of ATR signaling at telomeres through RPA exclusion. *Mol Cell*, *40*, 377–387.
92. **Gong, Z., Cho, Y.W., Kim, J.E. et al.Chen, J.** (2009) Accumulation of Pax2 transactivation domain interaction protein (PTIP) at sites of DNA breaks via RNF8-dependent pathway is required for cell survival after DNA damage. *J Biol Chem*, *284*, 7284–7293.
93. **Gravel, S., Chapman, J.R., Magill, C. et al.Jackson, S.P.** (2008) DNA helicases Sgs1 and BLM promote DNA double-strand break resection. *Genes Dev*, *22*, 2767–2772.
94. **Greider, C.W., and Blackburn, E.H.** (1985) Identification of a specific telomere terminal transferase activity in Tetrahymena extracts. *Cell*, *43*, 405–413.
95. **Greider, C.W., and Blackburn, E.H.** (1987) The telomere terminal transferase of Tetrahymena is a ribonucleoprotein enzyme with two kinds of primer specificity. *Cell*, *51*, 887–898.
96. **Greider, C.W., and Blackburn, E.H.** (1989) A telomeric sequence in the RNA of Tetrahymena telomerase required for telomere repeat synthesis. *Nature*, *337*, 331–337.
97. **Griffith, J.D., Comeau, L., Rosenfield, S. et al.de Lange, T.** (1999) Mammalian telomeres end in a large duplex loop. *Cell*, *97*, 503–14.
98. **Haahr, P., Hoffmann, S., Tollenaere, M.A. et al.Mailand, N.** (2016) Activation of the ATR kinase by the RPA-binding protein ETAA1. *Nat Cell Biol*, *18*, 1196–1207.
99. **Harper, J.W., and Elledge, S.J.** (2007) The DNA damage response: ten years after. *Mol Cell*, *28*, 739–745.
100. **Harrigan, J.A., Belotserkovskaya, R., Coates, J. et al.Jackson, S.P.** (2011) Replication stress induces 53BP1-containing OPT domains in G1 cells. *J Cell Biol*, *193*, 97–108.
101. **Hartsuiker, E., Neale, M.J., and Carr, A.M.** (2009) Distinct requirements for the Rad32(Mre11) nuclease and Ctp1(CtIP) in the removal of covalently bound topoisomerase I and II from DNA. *Mol Cell*, *33*, 117–123.
102. **Hayflick, L.** (1965) The limited in vitro lifetime of human diploid cell strains. *Exp Cell Res*, *37*, 614–636.

103. **Hecht, F., and Glover, T.W.** (1984) Cancer chromosome breakpoints and common fragile sites induced by aphidicolin. *Cancer Genet Cytogenet*, *13*, 185–188.
104. **Hellman, A., Zlotorynski, E., Scherer, S.W. et al. Kerem, B.** (2002) A role for common fragile site induction in amplification of human oncogenes. *Cancer Cell*, *1*, 89–97.
105. **Helmrich, A., Ballarino, M., and Tora, L.** (2011) Collisions between replication and transcription complexes cause common fragile site instability at the longest human genes. *Mol Cell*, *44*, 966–977.
106. **Henderson, E., Hardin, C.C., Walk, S.K. et al. Blackburn, E.H.** (1987) Telomeric DNA oligonucleotides form novel intramolecular structures containing guanine-guanine base pairs. *Cell*, *51*, 899–908.
107. **Hengeveld, R.C., de Boer, H.R., Schoonen, P.M. et al. van Vugt, M.A.** (2015) Rif1 Is Required for Resolution of Ultrafine DNA Bridges in Anaphase to Ensure Genomic Stability. *Dev Cell*, *34*, 466–474.
108. **Hockemeyer, D., Daniels, J.P., Takai, H. et al. de Lange, T.** (2006) Recent expansion of the telomeric complex in rodents: Two distinct POT1 proteins protect mouse telomeres. *Cell*, *126*, 63–77.
109. **Hockemeyer, D., Sfeir, A.J., Shay, J.W. et al. de Lange, T.** (2005) POT1 protects telomeres from a transient DNA damage response and determines how human chromosomes end. *EMBO J.*, *24*, 2667–2678.
110. **Hoeijmakers, J.H.** (2009) DNA damage, aging, and cancer. *N Engl J Med*, *361*, 1475–1485.
111. **Hopfner, K.P., Craig, L., Moncalian, G. et al. Tainer, J.A.** (2002) The Rad50 zinc-hook is a structure joining Mre11 complexes in DNA recombination and repair. *Nature*, *418*, 562–566.
112. **Hsiao, S.J., and Smith, S.** (2009) Sister telomeres rendered dysfunctional by persistent cohesion are fused by NHEJ. *J Cell Biol*, *184*, 515–526.
113. **Huber, M.D., Lee, D.C., and Maizels, N.P.** (2002) G4 DNA unwinding by BLM and Sgs1p: substrate specificity and substrate-specific inhibition. *Nucleic Acids Res*, *30*, 3954–3961.
114. **Huen, M.S., Grant, R., Manke, I. et al. Chen, J.** (2007) RNF8 transduces the DNA-damage signal via histone ubiquitylation and checkpoint protein assembly. *Cell*, *131*, 901–914.

115. **Huyen, Y., Zgheib, O., Ditullio, R.A., Jr et al.Halazonetis, T.D.** (2004) Methylated lysine 79 of histone H3 targets 53BP1 to DNA double-strand breaks. *Nature*, *432*, 406–411.
116. **Ibarra, A., Schwob, E., and Mendez, J.** (2008) Excess MCM proteins protect human cells from replicative stress by licensing backup origins of replication. *Proc Natl Acad Sci U S A*, *105*, 8956–8961.
117. **Ip, S.C., Rass, U., Blanco, M.G. et al.West, S.C.** (2008) Identification of Holliday junction resolvases from humans and yeast. *Nature*, *456*, 357–361.
118. **Iwabuchi, K., Bartel, P.L., Li, B. et al.Fields, S.** (1994) Two cellular proteins that bind to wild-type but not mutant p53. *Proc Natl Acad Sci USA*, *91*, 6098–6102.
119. **Iwabuchi, K., Li, B., Massa, H.F. et al.Fields, S.** (1998) Stimulation of p53-mediated transcriptional activation by the p53-binding proteins, 53BP1 and 53BP2. *J Biol Chem*, *273*, 26061–26068.
120. **Jackson, S.P., and Bartek, J.** (2009) The DNA-damage response in human biology and disease. *Nature*, *461*, 1071–1078.
121. **Jazayeri, A., Falck, J., Lukas, C. et al.Jackson, S.P.** (2006) ATM- and cell cycle-dependent regulation of ATR in response to DNA double-strand breaks. *Nat Cell Biol*, *8*, 37–45.
122. **Jensen, R.B., Carreira, A., and Kowalczykowski, S.C.** (2010) Purified human BRCA2 stimulates RAD51-mediated recombination. *Nature*, *467*, 678–683.
123. **Jones, R.E., Oh, S., Grimstead, J.W. et al.Baird, D.M.** (2014) Escape from telomere-driven crisis is DNA ligase III dependent. *Cell Rep*, *8*, 1063–1076.
124. **Jowsey, P., Morrice, N.A., Hastie, C.J. et al.Rouse, J.** (2007) Characterisation of the sites of DNA damage-induced 53BP1 phosphorylation catalysed by ATM and ATR. *DNA Repair (Amst)*, *6*, 1536–1544.
125. **Kabotyanski, E.B., Gomelsky, L., Han, J.O. et al.Roth, D.B.** (1998) Double-strand break repair in Ku86- and XRCC4-deficient cells. *Nucleic Acids Res*, *26*, 5333–5342.

126. **Karlseder, J., Broccoli, D., Dai, Y. et al. de Lange, T.** (1999) p53- and ATM-dependent apoptosis induced by telomeres lacking TRF2. *Science*, *283*, 1321–1325.
127. **Kibe, T., Osawa, G.A., Keegan, C.E. et al. de Lange, T.** (2010) Telomere Protection by TPP1 Is Mediated by POT1a and POT1b. *Mol Cell Biol*, *30*, 1059–1066.
128. **Kibe, T., Zimmermann, M., and de Lange, T.** (2016) TPP1 Blocks an ATR-Mediated Resection Mechanism at Telomeres. *Mol Cell*, *61*, 236–246.
129. **Kim, N.W., Piatyszek, M.A., Prowse, K.R. et al. Shay, J.W.** (1994) Specific association of human telomerase activity with immortal cells and cancer. *Science*, *266*, 2011–5.
130. **Konishi, A., and de Lange, T.** (2008) Cell cycle control of telomere protection and NHEJ revealed by a ts mutation in the DNA-binding domain of TRF2. *Genes Dev*, *22*, 1221–1230.
131. **Krawczyk, P.M., Borovski, T., Stap, J. et al. Aten, J.A.** (2012) Chromatin mobility is increased at sites of DNA double-strand breaks. *J Cell Sci*, *125*, 2127–2133.
132. **Kremer, E.J., Pritchard, M., Lynch, M. et al. Richards, R.I.** (1991) Mapping of DNA instability at the fragile X to a trinucleotide repeat sequence p(CCG)_n. *Science*, *252*, 1711–1714.
133. **Kruhlak, M.J., Celeste, A., Dellaire, G. et al. Nussenzweig, A.** (2006) Changes in chromatin structure and mobility in living cells at sites of DNA double-strand breaks. *J Cell Biol*, *172*, 823–834.
134. **Kumagai, A., Lee, J., Yoo, H.Y. et al. Dunphy, W.G.** (2006) TopBP1 activates the ATR-ATRIP complex. *Cell*, *124*, 943–955.
135. **Le Beau, M.M., Rassool, F.V., Neilly, M.E. et al. McKeithan, T.W.** (1998) Replication of a common fragile site, FRA3B, occurs late in S phase and is delayed further upon induction: implications for the mechanism of fragile site induction. *Hum Mol Genet*, *7*, 755–761.
136. **Le Tallec, B., Dutrillaux, B., Lachages, A.M. et al. Debatisse, M.** (2011) Molecular profiling of common fragile sites in human fibroblasts. *Nat Struct Mol Biol*, *18*, 1421–1423.
137. **Leach, D.R.** (1994) Long DNA palindromes, cruciform structures, genetic instability and secondary structure repair. *Bioessays*, *16*, 893–900.

138. **Lee, J.H., and Paull, T.T.** (2004) Direct activation of the ATM protein kinase by the Mre11/Rad50/Nbs1 complex. *Science*, *304*, 93–96.
139. **Lee, J.H., and Paull, T.T.** (2005) ATM activation by DNA double-strand breaks through the Mre11-Rad50-Nbs1 complex. *Science*, *308*, 551–554.
140. **Lee, M.S., Edwards, R.A., Thede, G.L. et al. Glover, J.N.** (2005) Structure of the BRCT repeat domain of MDC1 and its specificity for the free COOH-terminal end of the gamma-H2AX histone tail. *J Biol Chem*, *280*, 32053–32056.
141. **Lee, S.E., Moore, J.K., Holmes, A. et al. Haber, J.E.** (1998) Saccharomyces Ku70, Mre11/Rad50, and RPA Proteins Regulate Adaptation to G2/M Arrest after DNA Damage. *Cell*, *94*, 399–409.
142. **Lejnine, S., Makarov, V.L., and Langmore, J.P.** (1995) Conserved nucleoprotein structure at the ends of vertebrate and invertebrate chromosomes. *Proc Natl Acad Sci USA*, *92*, 2393–2397.
143. **Letsolo, B.T., Rowson, J., and Baird, D.M.** (2010) Fusion of short telomeres in human cells is characterized by extensive deletion and microhomology, and can result in complex rearrangements. *Nucleic Acids Res*, *38*, 1841–1852.
144. **Liddiard, K., Ruis, B., Takasugi, T. et al. Baird, D.M.** (2016) Sister chromatid telomere fusions, but not NHEJ-mediated inter-chromosomal telomere fusions, occur independently of DNA ligases 3 and 4. *Genome Res*, *26*, 588–600.
145. **Lieber, M.R.** (1999) The biochemistry and biological significance of nonhomologous DNA end joining: an essential repair process in multicellular eukaryotes. *Genes Cells*, *4*, 77–85.
146. **Lieber, M.R.** (2010) The mechanism of double-strand DNA break repair by the nonhomologous DNA end-joining pathway. *Annu Rev Biochem*, *79*, 181–211.
147. **Lillard-Wetherell, K., Machwe, A., Langeland, G.T. et al. Groden, J.** (2004) Association and regulation of the BLM helicase by the telomere proteins TRF1 and TRF2. *Hum Mol Genet*, *13*, 1919–1932.
148. **Lim, D.S., Kim, S.T., Xu, B. et al. Kastan, M.B.** (2000) ATM phosphorylates p95/nbs1 in an S-phase checkpoint pathway. *Nature*, *404*, 613–617.

149. **Lin, T.T., Letsolo, B.T., Jones, R.E. et al. Baird, D.M.** (2010) Telomere dysfunction and fusion during the progression of chronic lymphocytic leukemia: evidence for a telomere crisis. *Blood*, *116*, 1899–1907.
150. **Lingner, J., Hughes, T.R., Shevchenko, A. et al. Cech, T.R.** (1997) Reverse transcriptase motifs in the catalytic subunit of telomerase. *Science*, *276*, 561–567.
151. **Liu, Q., Guntuku, S., Cui, X.S. et al. Elledge, S.J.** (2000) Chk1 is an essential kinase that is regulated by Atr and required for the G(2)/M DNA damage checkpoint. *Genes Dev*, *14*, 1448–1459.
152. **Lo, K.W., Kan, H.M., Chan, L.N. et al. Zhang, M.** (2005) The 8-kDa dynein light chain binds to p53-binding protein 1 and mediates DNA damage-induced p53 nuclear accumulation. *J Biol Chem*, *280*, 8172–8179.
153. **Loayza, D., and de Lange, T.** (2003) POT1 as a terminal transducer of TRF1 telomere length control. *Nature*, *424*, 1013–1018.
154. **Lomant, A.J., and Fairbanks, G.** (1976) Chemical probes of extended biological structures: synthesis and properties of the cleavable protein cross-linking reagent [35S]dithiobis(succinimidyl propionate). *J Mol Biol*, *104*, 243–261.
155. **Lopes, M., Cotta-Ramusino, C., Pelliccioli, A. et al. Foiani, M.** (2001) The DNA replication checkpoint response stabilizes stalled replication forks. *Nature*, *412*, 557–561.
156. **Lopez, V., Barinova, N., Onishi, M. et al. Marcand, S.** (2015) Cytokinesis breaks dicentric chromosomes preferentially at pericentromeric regions and telomere fusions. *Genes Dev*, *29*, 322–336.
157. **Lotterberger, F., Bothmer, A., Robbiani, D.F. et al. de Lange, T.** (2013) Role of 53BP1 oligomerization in regulating double-strand break repair. *Proc Natl Acad Sci U S A*, *110*, 2146–2151.
158. **Lotterberger, F., Karssemeijer, R.A., Dimitrova, N. et al. de Lange, T.** (2015) 53BP1 and the LINC Complex Promote Microtubule-Dependent DSB Mobility and DNA Repair. *Cell*, *163*, 880–893.
159. **Lou, Z., Minter-Dykhouse, K., Franco, S. et al. Chen, J.** (2006) MDC1 maintains genomic stability by participating in the amplification of ATM-dependent DNA damage signals. *Mol Cell*, *21*, 187–200.

160. **Lu, G., Duan, J., Shu, S. et al. Zhang, Y.** (2016) Ligase I and ligase III mediate the DNA double-strand break ligation in alternative end-joining. *Proc Natl Acad Sci U S A*, *113*, 1256–1260.
161. **Lucca, C., Vanoli, F., Cotta-Ramusino, C. et al. Foiani, M.** (2004) Checkpoint-mediated control of replisome-fork association and signalling in response to replication pausing. *Oncogene*, *23*, 1206–1213.
162. **Lukas, C., Savic, V., Bekker-Jensen, S. et al. Lukas, J.** (2011) 53BP1 nuclear bodies form around DNA lesions generated by mitotic transmission of chromosomes under replication stress. *Nat Cell Biol*, *13*, 243–253.
163. **Ma, Y., Pannicke, U., Schwarz, K. et al. Lieber, M.R.** (2002) Hairpin opening and overhang processing by an Artemis/DNA-dependent protein kinase complex in nonhomologous end joining and V(D)J recombination. *Cell*, *108*, 781–794.
164. **MacDougall, C.A., Byun, T.S., Van, C. et al. Cimprich, K.A.** (2007) The structural determinants of checkpoint activation. *Genes Dev*, *21*, 898–903.
165. **Maciejowski, J., Li, Y., Bosco, N. et al. de Lange, T.** (2015) Chromothripsis and Kataegis Induced by Telomere Crisis. *Cell*, *163*, 1641–1654.
166. **Mailand, N., Bekker-Jensen, S., Faustrup, H. et al. Lukas, J.** (2007) RNF8 ubiquitylates histones at DNA double-strand breaks and promotes assembly of repair proteins. *Cell*, *131*, 887–900.
167. **Mailand, N., Falck, J., Lukas, C. et al. Lukas, J.** (2000) Rapid destruction of human Cdc25A in response to DNA damage. *Science*, *288*, 1425–9.
168. **Makovets, S., Herskowitz, I., and Blackburn, E.H.** (2004) Anatomy and dynamics of DNA replication fork movement in yeast telomeric regions. *Mol Cell Biol*, *24*, 4019–4031.
169. **Martinez, P., Flores, J.M., and Blasco, M.A.** (2012) 53BP1 deficiency combined with telomere dysfunction activates ATR-dependent DNA damage response. *J Cell Biol*, *197*, 283–300.
170. **Martinez, P., Thanasoula, M., Munoz, P. et al. Blasco, M.A.** (2009) Increased telomere fragility and fusions resulting from TRF1 deficiency lead to degenerative pathologies and increased cancer in mice. *Genes Dev*, *23*, 2060–2075.

171. **Mateos-Gomez, P.A., Gong, F., Nair, N. et al.Sfeir, A.** (2015) Mammalian polymerase theta promotes alternative NHEJ and suppresses recombination. *Nature*, *518*, 254–257.
172. **Matos, J., Blanco, M.G., Maslen, S. et al.West, S.C.** (2011) Regulatory control of the resolution of DNA recombination intermediates during meiosis and mitosis. *Cell*, *147*, 158–172.
173. **Matsuoka, S., Ballif, B.A., Smogorzewska, A. et al.Elledge, S.J.** (2007) ATM and ATR substrate analysis reveals extensive protein networks responsive to DNA damage. *Science*, *316*, 1160–1166.
174. **Matsuoka, S., Huang, M., and Elledge, S.J.** (1998) Linkage of ATM to cell cycle regulation by the Chk2 protein kinase. *Science*, *282*, 1893–1897.
175. **Matsuoka, S., Rotman, G., Ogawa, A. et al.Elledge, S.J.** (2000) Ataxia telangiectasia-mutated phosphorylates Chk2 in vivo and in vitro. *Proc Natl Acad Sci U S A*, *97*, 10389–10394.
176. **Mattiroli, F., Vissers, J.H., van Dijk, W.J. et al.Sixma, T.K.** (2012) RNF168 ubiquitinates K13-15 on H2A/H2AX to drive DNA damage signaling. *Cell*, *150*, 1182–1195.
177. **McClintock, B.** (1941) The stability of broken ends of chromosomes in *Zea mays*. *Genetics*, *26*, 234–282.
178. **Mejat, A., and Misteli, T.** (2010) LINC complexes in health and disease. *Nucleus*, *1*, 40–52.
179. **Miller, K.M., and Cooper, J.P.** (2003) The telomere protein Taz1 is required to prevent and repair genomic DNA breaks. *Mol Cell*, *11*, 303–313.
180. **Miller, K.M., Ferreira, M.G., and Cooper, J.P.** (2005) Taz1, Rap1 and Rif1 act both interdependently and independently to maintain telomeres. *EMBO J*, *24*, 3128–3135.
181. **Miller, K.M., Rog, O., and Cooper, J.P.** (2006) Semi-conservative DNA replication through telomeres requires Taz1. *Nature*, *440*, 824–828.
182. **Mimitou, E.P., and Symington, L.S.** (2008) Sae2, Exo1 and Sgs1 collaborate in DNA double-strand break processing. *Nature*, *455*, 770–774.

183. **Minocherhomji, S., Ying, S., Bjerregaard, V.A. et al.Hickson, I.D.** (2015) Replication stress activates DNA repair synthesis in mitosis. *Nature*, *528*, 286–290.
184. **Mirzoeva, O.K., and Petrini, J.H.** (2001) DNA damage-dependent nuclear dynamics of the Mre11 complex. *Mol Cell Biol*, *21*, 281–288.
185. **Mizuuchi, K., Mizuuchi, M., and Gellert, M.** (1982) Cruciform structures in palindromic DNA are favored by DNA supercoiling. *J Mol Biol*, *156*, 229–243.
186. **Moreno, S.P., Bailey, R., Campion, N. et al.Gambus, A.** (2014) Polyubiquitylation drives replisome disassembly at the termination of DNA replication. *Science*, *346*, 477–481.
187. **Moynahan, M.E., Chiu, J.W., Koller, B.H. et al.Jasin, M.** (1999) Brca1 controls homology-directed DNA repair. *Mol Cell*, *4*, 511–518.
188. **Moynahan, M.E., and Jasin, M.** (2010) Mitotic homologous recombination maintains genomic stability and suppresses tumorigenesis. *Nat Rev Mol Cell Biol*, *11*, 196–207.
189. **Muller, H.J.** (1938) The remaking of chromosomes. *The Collecting Net*, Woods Hole, *8*, 182–195.
190. **Munoz, I.M., Jowsey, P.A., Toth, R. et al.Rouse, J.** (2007) Phospho-epitope binding by the BRCT domains of hPTIP controls multiple aspects of the cellular response to DNA damage. *Nucleic Acids Res*, *35*, 5312–5322.
191. **Myers, J.S., and Cortez, D.** (2006) Rapid activation of ATR by ionizing radiation requires ATM and Mre11. *J Biol Chem*, *281*, 9346–9350.
192. **Naim, V., and Rosselli, F.** (2009) The FANC pathway and BLM collaborate during mitosis to prevent micro-nucleation and chromosome abnormalities. *Nat Cell Biol*, *11*, 761–768.
193. **Naim, V., Wilhelm, T., Debatisse, M. et al.Rosselli, F.** (2013) ERCC1 and MUS81-EME1 promote sister chromatid separation by processing late replication intermediates at common fragile sites during mitosis. *Nat Cell Biol*, *15*, 1008–1015.
194. **Nakamura, T.M., Morin, G.B., Chapman, K.B. et al.Cech, T.R.** (1997) Telomerase catalytic subunit homologs from fission yeast and human. *Science*, *277*, 955–959.

195. **Nasmyth, K., and Haering, C.H.** (2009) Cohesin: its roles and mechanisms. *Annu Rev Genet*, *43*, 525–558.
196. **Nassif, N., Penney, J., Pal, S. et al.Gloor, G.B.** (1994) Efficient copying of nonhomologous sequences from ectopic sites via P-element-induced gap repair. *Mol Cell Biol*, *14*, 1613–1625.
197. **Neelsen, K.J., and Lopes, M.** (2015) Replication fork reversal in eukaryotes: from dead end to dynamic response. *Nat Rev Mol Cell Biol*, *16*, 207–220.
198. **Nelms, B.E., Maser, R.S., MacKay, J.F. et al.Petrini, J.H.** (1998) In situ visualization of DNA double-strand break repair in human fibroblasts. *Science*, *280*, 590–592.
199. **Neumaier, T., Swenson, J., Pham, C. et al.Costes, S.V.** (2012) Evidence for formation of DNA repair centers and dose-response nonlinearity in human cells. *Proc Natl Acad Sci U S A*, *109*, 443–448.
200. **Nielsen, C.F., Huttner, D., Bizard, A.H. et al.Hickson, I.D.** (2015) PICH promotes sister chromatid disjunction and co-operates with topoisomerase II in mitosis. *Nat Commun*, *6*, 8962.
201. **Nikitina, T., and Woodcock, C.L.** (2004) Closed chromatin loops at the ends of chromosomes. *J Cell Biol*, *166*, 161–165.
202. **Nimonkar, A.V., Genschel, J., Kinoshita, E. et al.Kowalczykowski, S.C.** (2011) BLM-DNA2-RPA-MRN and EXO1-BLM-RPA-MRN constitute two DNA end resection machineries for human DNA break repair. *Genes Dev*, *25*, 350–362.
203. **Nimonkar, A.V., Ozsoy, A.Z., Genschel, J. et al.Kowalczykowski, S.C.** (2008) Human exonuclease 1 and BLM helicase interact to resect DNA and initiate DNA repair. *Proc Natl Acad Sci U S A*, *105*, 16906–16911.
204. **Noon, A.T., Shibata, A., Rief, N. et al.Goodarzi, A.A.** (2010) 53BP1-dependent robust localized KAP-1 phosphorylation is essential for heterochromatic DNA double-strand break repair. *Nat Cell Biol*, *12*, 177–184.
205. **Ochi, T., Blackford, A.N., Coates, J. et al.Jackson, S.P.** (2015) DNA repair. PAXX, a paralog of XRCC4 and XLF, interacts with Ku to promote DNA double-strand break repair. *Science*, *347*, 185–188.

206. **Olovnikov, A.M.** (1973) A theory of marginotomy. The incomplete copying of template margin in enzymic synthesis of polynucleotides and biological significance of the phenomenon. *J Theor Biol*, *41*, 181–190.
207. **Orthwein, A., Fradet-Turcotte, A., Noordermeer, S.M. et al.Durocher, D.** (2014) Mitosis inhibits DNA double-strand break repair to guard against telomere fusions. *Science*, *344*, 189–193.
208. **Ozeri-Galai, E., Bester, A.C., and Kerem, B.** (2012) The complex basis underlying common fragile site instability in cancer. *Trends Genet*, *28*, 295–302.
209. **Ozeri-Galai, E., Lebofsky, R., Rahat, A. et al.Kerem, B.** (2011) Failure of origin activation in response to fork stalling leads to chromosomal instability at fragile sites. *Mol Cell*, *43*, 122–131.
210. **Palm, W., and de Lange, T.** (2008) How shelterin protects mammalian telomeres. *Annu Rev Genet*, *42*, 301–334.
211. **Palm, W., Hockemeyer, D., Kibe, T. et al.de Lange, T.** (2009) Functional dissection of human and mouse POT1 proteins. *Mol Cell Biol*, *29*, 471–482.
212. **Panier, S., and Boulton, S.J.** (2014) Double-strand break repair: 53BP1 comes into focus. *Nat Rev Mol Cell Biol*, *15*, 7–18.
213. **Pannunzio, N.R., Li, S., Watanabe, G. et al.Lieber, M.R.** (2014) Non-homologous end joining often uses microhomology: implications for alternative end joining. *DNA Repair (Amst)*, *17*, 74–80.
214. **Paul, K., Wang, M., Mladenov, E. et al.Iliakis, G.** (2013) DNA ligases I and III cooperate in alternative non-homologous end-joining in vertebrates. *PLoS One*, *8*, e59505.
215. **Paull, T.T.** (2015) Mechanisms of ATM Activation. *Annu Rev Biochem*, *84*, 711–738.
216. **Pelliccia, F., Bosco, N., Curatolo, A. et al.Rocchi, A.** (2008) Replication timing of two human common fragile sites: FRA1H and FRA2G. *Cytogenet Genome Res*, *121*, 196–200.
217. **Penkner, A.M., Fridkin, A., Gloggnitzer, J. et al.Jantsch, V.** (2009) Meiotic chromosome homology search involves modifications of the nuclear envelope protein Matefin/SUN-1. *Cell*, *139*, 920–933.

218. **Peterson, S.E., Li, Y., Wu-Baer, F. et al. Gautier, J.** (2013) Activation of DSB processing requires phosphorylation of CtIP by ATR. *Mol Cell*, *49*, 657–667.
219. **Pichierri, P., and Rosselli, F.** (2004) The DNA crosslink-induced S-phase checkpoint depends on ATR-CHK1 and ATR-NBS1-FANCD2 pathways. *EMBO J*, *23*, 1178–1187.
220. **Pirzio, L.M., Pichierri, P., Bignami, M. et al. Franchitto, A.** (2008) Werner syndrome helicase activity is essential in maintaining fragile site stability. *J Cell Biol*, *180*, 305–314.
221. **Pobiega, S., and Marcand, S.** (2010) Dicentric breakage at telomere fusions. *Genes Dev*, *24*, 720–733.
222. **Poulet, A., Buisson, R., Faivre-Moskalenko, C. et al. Giraud-Panis, M.J.** (2009) TRF2 promotes, remodels and protects telomeric Holliday junctions. *EMBO J*, *28*, 641–651.
223. **Rainey, M.D., Black, E.J., Zachos, G. et al. Gillespie, D.A.** (2008) Chk2 is required for optimal mitotic delay in response to irradiation-induced DNA damage incurred in G2 phase. *Oncogene*, *27*, 896–906.
224. **Rappold, I., Iwabuchi, K., Date, T. et al. Chen, J.** (2001) Tumor suppressor p53 binding protein 1 (53BP1) is involved in DNA damage-signaling pathways. *J Cell Biol*, *153*, 613–620.
225. **Rass, U., Compton, S.A., Matos, J. et al. West, S.C.** (2010) Mechanism of Holliday junction resolution by the human GEN1 protein. *Genes Dev*, *24*, 1559–1569.
226. **Remeseiro, S., Cuadrado, A., Carretero, M. et al. Losada, A.** (2012) Cohesin-SA1 deficiency drives aneuploidy and tumorigenesis in mice due to impaired replication of telomeres. *EMBO J*, *31*, 2076–2089.
227. **Ribes-Zamora, A., Indiviglio, S.M., Mihalek, I. et al. Bertuch, A.A.** (2013) TRF2 interaction with Ku heterotetramerization interface gives insight into c-NHEJ prevention at human telomeres. *Cell Rep*, *5*, 194–206.
228. **Rizzo, A., Salvati, E., Porru, M. et al. Biroccio, A.** (2009) Stabilization of quadruplex DNA perturbs telomere replication leading to the activation of an ATR-dependent ATM signaling pathway. *Nucleic Acids Res*, *37*, 5353–5364.

229. **Rogakou, E.P., Pilch, D.R., Orr, A.H. et al.Bonner, W.M.** (1998) DNA double-stranded breaks induce histone H2AX phosphorylation on serine 139. *J Biol Chem*, *273*, 5858–5868.
230. **Saint-Leger, A., Koelblen, M., Civitelli, L. et al.Gilson, E.** (2014) The basic N-terminal domain of TRF2 limits recombination endonuclease action at human telomeres. *Cell Cycle*, *13*, 2469–2474.
231. **Salvati, E., Leonetti, C., Rizzo, A. et al.Biroccio, A.** (2007) Telomere damage induced by the G-quadruplex ligand RHPS4 has an antitumor effect. *J Clin Invest*, *117*, 3236–3247.
232. **Sanchez, Y., Wong, C., Thoma, R.S. et al.Elledge, S.J.** (1997) Conservation of the Chk1 checkpoint pathway in mammals: linkage of DNA damage to Cdk regulation through Cdc25. *Science*, *277*, 1497–1501.
233. **Sartori, A.A., Lukas, C., Coates, J. et al.Jackson, S.P.** (2007) Human CtIP promotes DNA end resection. *Nature*, *450*, 509–514.
234. **Sato, A., Isaac, B., Phillips, C.M. et al.Dernburg, A.F.** (2009) Cytoskeletal forces span the nuclear envelope to coordinate meiotic chromosome pairing and synapsis. *Cell*, *139*, 907–919.
235. **Sfeir, A., and de Lange, T.** (2012) Removal of shelterin reveals the telomere end-protection problem. *Science*, *336*, 593–597.
236. **Sfeir, A., Kabir, S., van Overbeek, M. et al.de Lange, T.** (2010) Loss of Rap1 induces telomere recombination in the absence of NHEJ or a DNA damage signal. *Science*, *327*, 1657–1661.
237. **Sfeir, A., Kosiyatrakul, S.T., Hockemeyer, D. et al.de Lange, T.** (2009) Mammalian telomeres resemble fragile sites and require TRF1 for efficient replication. *Cell*, *138*, 90–103.
238. **Shah Punatar, R., Martin, M.J., Wyatt, H.D. et al.West, S.C.** (2017) Resolution of single and double Holliday junction recombination intermediates by GEN1. *Proc Natl Acad Sci U S A*,
239. **Shamanna, R.A., Lu, H., de Freitas, J.K. et al.Bohr, V.A.** (2016) WRN regulates pathway choice between classical and alternative non-homologous end joining. *Nat Commun*, *7*, 13785.
240. **Shibuya, H., Ishiguro, K., and Watanabe, Y.** (2014) The TRF1-binding protein TERB1 promotes chromosome movement and telomere rigidity in meiosis. *Nat Cell Biol*, *16*, 145–156.

241. **Shibuya, H., and Watanabe, Y.** (2014) The meiosis-specific modification of mammalian telomeres. *Cell Cycle*, *13*, 2024–2028.
242. **Shieh, S.Y., Ahn, J., Tamai, K. et al.Prives, C.** (2000) The human homologs of checkpoint kinases Chk1 and Cds1 (Chk2) phosphorylate p53 at multiple DNA damage-inducible sites. *Genes Dev*, *14*, 289–300.
243. **Simsek, D., Brunet, E., Wong, S.Y. et al.Jasin, M.** (2011) DNA ligase III promotes alternative nonhomologous end-joining during chromosomal translocation formation. *PLoS Genet*, *7*, e1002080.
244. **Simsek, D., and Jasin, M.** (2010) Alternative end-joining is suppressed by the canonical NHEJ component Xrcc4-ligase IV during chromosomal translocation formation. *Nat Struct Mol Biol*, *17*, 410–416.
245. **Smogorzewska, A., Karlseder, J., Holtgreve-Grez, H. et al.de Lange, T.** (2002) DNA Ligase IV-Dependent NHEJ of Deprotected Mammalian Telomeres in G1 and G2. *Curr Biol*, *12*, 1635.
246. **Snouwaert, J.N., Gowen, L.C., Latour, A.M. et al.Koller, B.H.** (1999) BRCA1 deficient embryonic stem cells display a decreased homologous recombination frequency and an increased frequency of non-homologous recombination that is corrected by expression of a *brca1* transgene. *Oncogene*, *18*, 7900–7907.
247. **Soutoglou, E., Dorn, J.F., Sengupta, K. et al.Misteli, T.** (2007) Positional stability of single double-strand breaks in mammalian cells. *Nat Cell Biol*, *9*, 675–682.
248. **Stark, J.M., and Jasin, M.** (2003) Extensive loss of heterozygosity is suppressed during homologous repair of chromosomal breaks. *Mol Cell Biol*, *23*, 733–743.
249. **Starr, D.A., and Fridolfsson, H.N.** (2010) Interactions between nuclei and the cytoskeleton are mediated by SUN-KASH nuclear-envelope bridges. *Annu Rev Cell Dev Biol*, *26*, 421–444.
250. **Stephens, P.J., Greenman, C.D., Fu, B. et al.Campbell, P.J.** (2011) Massive genomic rearrangement acquired in a single catastrophic event during cancer development. *Cell*, *144*, 27–40.
251. **Stewart, G.S., Maser, R.S., Stankovic, T. et al.Taylor, A.M.** (1999) The DNA double-strand break repair gene hMRE11 is mutated in individuals with an ataxia-telangiectasia-like disorder. *Cell*, *99*, 577–587.

252. **Stewart, G.S., Wang, B., Bignell, C.R. et al.Elledge, S.J.** (2003) MDC1 is a mediator of the mammalian DNA damage checkpoint. *Nature*, *421*, 961–966.
253. **Stewart, G.S., Panier, S., Townsend, K. et al.Durocher, D.** (2009) The RIDDLE syndrome protein mediates a ubiquitin-dependent signaling cascade at sites of DNA damage. *Cell*, *136*, 420–434.
254. **Stohr, B.A., Xu, L., and Blackburn, E.H.** (2010) The terminal telomeric DNA sequence determines the mechanism of dysfunctional telomere fusion. *Mol Cell*, *39*, 307–314.
255. **Stracker, T.H., and Petrini, J.H.** (2011) The MRE11 complex: starting from the ends. *Nat Rev Mol Cell Biol*, *12*, 90–103.
256. **Sturzenegger, A., Burdova, K., Kanagaraj, R. et al.Janscak, P.** (2014) DNA2 cooperates with the WRN and BLM RecQ helicases to mediate long-range DNA end resection in human cells. *J Biol Chem*, *289*, 27314–27326.
257. **Subbotin, R.I., and Chait, B.T.** (2014) A pipeline for determining protein-protein interactions and proximities in the cellular milieu. *Mol Cell Proteomics*, *13*, 2824–2835.
258. **Sun, H., Karow, J.K., Hickson, I.D. et al.Maizels, N.P.** (1998) The Bloom's syndrome helicase unwinds G4 DNA. *J Biol Chem*, *273*, 27587–27592.
259. **Svendsen, J.M., Smogorzewska, A., Sowa, M.E. et al.Harper, J.W.** (2009) Mammalian BTBD12/SLX4 assembles a Holliday junction resolvase and is required for DNA repair. *Cell*, *138*, 63–77.
260. **Szostak, J.W., Orr-Weaver, T.L., Rothstein, R.J. et al.Stahl, F.W.** (1983) The double-strand-break repair model for recombination. *Cell*, *33*, 25–35.
261. **Takai, H., Jenkinson, E., Kabir, S. et al.de Lange, T.** (2016) A POT1 mutation implicates defective telomere end fill-in and telomere truncations in Coats plus. *Genes Dev*, *30*, 812–826.
262. **Takai, H., Smogorzewska, A., and de Lange, T.** (2003) DNA damage foci at dysfunctional telomeres. *Curr Biol*, *13*, 1549–1556.
263. **Takai, K.K., Kibe, T., Donigian, J.R. et al.de Lange, T.** (2011) Telomere protection by TPP1/POT1 requires tethering to TIN2. *Mol Cell*, *44*, 647–659.

264. **Ten Hagen, K.G., Gilbert, D.M., Willard, H.F. et al.Cohen, S.N.** (1990) Replication timing of DNA sequences associated with human centromeres and telomeres. *Mol Cell Biol*, *10*, 6348–6355.
265. **Tercero, J.A., and Diffley, J.F.** (2001) Regulation of DNA replication fork progression through damaged DNA by the Mec1/Rad53 checkpoint. *Nature*, *412*, 553–557.
266. **Thorslund, T., Ripplinger, A., Hoffmann, S. et al.Mailand, N.** (2015) Histone H1 couples initiation and amplification of ubiquitin signalling after DNA damage. *Nature*, *527*, 389–393.
267. **Tibbetts, R.S., Brumbaugh, K.M., Williams, J.M. et al.Abraham, R.T.** (1999) A role for ATR in the DNA damage-induced phosphorylation of p53. *Genes Dev*, *13*, 152–7.
268. **Tomimatsu, N., Mukherjee, B., Deland, K. et al.Burma, S.** (2012) Exo1 plays a major role in DNA end resection in humans and influences double-strand break repair and damage signaling decisions. *DNA Repair (Amst)*, *11*, 441–448.
269. **Truong, L.N., Li, Y., Shi, L.Z. et al.Wu, X.** (2013) Microhomology-mediated End Joining and Homologous Recombination share the initial end resection step to repair DNA double-strand breaks in mammalian cells. *Proc Natl Acad Sci U S A*, *110*, 7720–7725.
270. **Uziel, T., Lerenthal, Y., Moyal, L. et al.Shiloh, Y.** (2003) Requirement of the MRN complex for ATM activation by DNA damage. *Embo J*, *22*, 5612–5621.
271. **van Steensel, B., Smogorzewska, A., and de Lange, T.** (1998) TRF2 protects human telomeres from end-to-end fusions. *Cell*, *92*, 401–413.
272. **Vannier, J.B., Pavicic-Kaltenbrunner, V., Petalcorin, M.I. et al.Boulton, S.J.** (2012) RTEL1 Dismantles T Loops and Counteracts Telomeric G4-DNA to Maintain Telomere Integrity. *Cell*, *149*, 795–806.
273. **Vannier, J.B., Sandhu, S., Petalcorin, M.I. et al.Boulton, S.J.** (2013) RTEL1 is a replisome-associated helicase that promotes telomere and genome-wide replication. *Science*, *342*, 239–242.
274. **Verkaik, N.S., Esveltd-van Lange, R.E., van Heemst, D. et al.van Gent, D.C.** (2002) Different types of V(D)J recombination and end-joining defects in DNA double-strand break repair mutant mammalian cells. *Eur J Immunol*, *32*, 701–709.

275. **Walker, J.R., Corpina, R.A., and Goldberg, J.** (2001) Structure of the Ku heterodimer bound to DNA and its implications for double-strand break repair. *Nature*, *412*, 607–614.
276. **Walworth, N.C., and Bernards, R.** (1996) rad-dependent response of the chk1-encoded protein kinase at the DNA damage checkpoint. *Science*, *271*, 353–356.
277. **Wang, H., Perrault, A.R., Takeda, Y. et al.Iliakis, G.** (2003) Biochemical evidence for Ku-independent backup pathways of NHEJ. *Nucleic Acids Res*, *31*, 5377–5388.
278. **Wang, H., Shi, L.Z., Wong, C.C. et al.Wu, X.** (2013) The interaction of CtIP and Nbs1 connects CDK and ATM to regulate HR-mediated double-strand break repair. *PLoS Genet*, *9*, e1003277.
279. **Wang, J., Aroumougame, A., Lobrich, M. et al.Gong, Z.** (2014) PTIP associates with Artemis to dictate DNA repair pathway choice. *Genes Dev*, *28*, 2693–2698.
280. **Wang, M., Wu, W., Wu, W. et al.Iliakis, G.** (2006) PARP-1 and Ku compete for repair of DNA double strand breaks by distinct NHEJ pathways. *Nucleic Acids Res*, *34*, 6170–6182.
281. **Wang, R.C., Smogorzewska, A., and de Lange, T.** (2004) Homologous recombination generates T-loop-sized deletions at human telomeres. *Cell*, *119*, 355–368.
282. **Wang, X., Takenaka, K., and Takeda, S.** (2010) PTIP promotes DNA double-strand break repair through homologous recombination. *Genes Cells*, *15*, 243–254.
283. **Ward, I., Kim, J.E., Minn, K. et al.Chen, J.** (2006) The tandem BRCT domain of 53BP1 is not required for its repair function. *J Biol Chem*, *281*, 38472–38477.
284. **Ward, I.M., Minn, K., van Deursen, J. et al.Chen, J.** (2003) p53 Binding protein 53BP1 is required for DNA damage responses and tumor suppression in mice. *Mol Cell Biol*, *23*, 2556–2563.
285. **Ward, I.M., and Chen, J.** (2001) Histone H2AX is phosphorylated in an ATR-dependent manner in response to replicational stress. *J Biol Chem*, *276*, 47759–47762.

286. **Ward, I.M., Reina-San-Martin, B., Olaru, A. et al.Chen, J.** (2004) 53BP1 is required for class switch recombination. *J Cell Biol*, *165*, 459–464.
287. **Waters, C.A., Strande, N.T., Wyatt, D.W. et al.Ramsden, D.A.** (2014) Nonhomologous end joining: a good solution for bad ends. *DNA Repair (Amst)*, *17*, 39–51.
288. **Watson, J.D.** (1972) Origin of concatemeric T7 DNA. *Nat New Biol*, *239*, 197–201.
289. **Wechsler, T., Newman, S., and West, S.C.** (2011) Aberrant chromosome morphology in human cells defective for Holliday junction resolution. *Nature*, *471*, 642–646.
290. **Weinstock, D.M., Brunet, E., and Jasin, M.** (2007) Formation of NHEJ-derived reciprocal chromosomal translocations does not require Ku70. *Nat Cell Biol*, *9*, 978–981.
291. **Wilson, M.D., Benlekhir, S., Fradet-Turcotte, A. et al.Durocher, D.** (2016) The structural basis of modified nucleosome recognition by 53BP1. *Nature*, *536*, 100–103.
292. **Wold, M.S.** (1997) Replication protein A: a heterotrimeric, single-stranded DNA-binding protein required for eukaryotic DNA metabolism. *Annu Rev Biochem*, *66*, 61–92.
293. **Wold, M.S., and Kelly, T.** (1988) Purification and characterization of replication protein A, a cellular protein required for in vitro replication of simian virus 40 DNA. *Proc Natl Acad Sci U S A*, *85*, 2523–2527.
294. **Wong, A.K., Pero, R., Ormonde, P.A. et al.Bartel, P.L.** (1997) RAD51 interacts with the evolutionarily conserved BRC motifs in the human breast cancer susceptibility gene *brca2*. *J Biol Chem*, *272*, 31941–31944.
295. **Woodward, A.M., Gohler, T., Luciani, M.G. et al.Blow, J.J.** (2006) Excess Mcm2-7 license dormant origins of replication that can be used under conditions of replicative stress. *J Cell Biol*, *173*, 673–683.
296. **Wright, W.E., Tesmer, V.M., Liao, M.L. et al.Shay, J.W.** (1999) Normal human telomeres are not late replicating. *Exp Cell Res*, *251*, 492–499.

297. **Wu, J., Prindle, M.J., Dressler, G.R. et al. Yu, X.** (2009) PTIP regulates 53BP1 and SMC1 at the DNA damage sites. *J Biol Chem*, *284*, 18078–18084.
298. **Wu, L., and Hickson, I.D.** (2003) The Bloom's syndrome helicase suppresses crossing over during homologous recombination. *Nature*, *426*, 870–874.
299. **Wu, P., Takai, H., and de Lange, T.** (2012) Telomeric 3' Overhangs Derive from Resection by Exo1 and Apollo and Fill-In by POT1b-Associated CST. *Cell*, *150*, 39–52.
300. **Wu, P., van Overbeek, M., Rooney, S. et al. de Lange, T.** (2010) Apollo Contributes to G Overhang Maintenance and Protects Leading-End Telomeres. *Mol Cell*, *39*, 1–12.
301. **Wu, P., and de Lange, T.** (2008) No overt nucleosome eviction at deprotected telomeres. *Mol Cell Biol*, *28*, 5724–5735.
302. **Wyatt, H.D., Sarbajna, S., Matos, J. et al. West, S.C.** (2013) Coordinated actions of SLX1-SLX4 and MUS81-EME1 for holliday junction resolution in human cells. *Mol Cell*, *52*, 234–247.
303. **Wyatt, H.D., and West, S.C.** (2014) Holliday junction resolvases. *Cold Spring Harb Perspect Biol*, *6*, a023192.
304. **Xing, M., Yang, M., Huo, W. et al. Xu, D.** (2015) Interactome analysis identifies a new paralogue of XRCC4 in non-homologous end joining DNA repair pathway. *Nat Commun*, *6*, 6233.
305. **Xu, D., Muniandy, P., Leo, E. et al. Wang, W.** (2010) Rif1 provides a new DNA-binding interface for the Bloom syndrome complex to maintain normal replication. *EMBO J*, *29*, 3140–3155.
306. **Xu, G., Chapman, J.R., Brandsma, I. et al. Rottenberg, S.** (2015) REV7 counteracts DNA double-strand break resection and affects PARP inhibition. *Nature*, *521*, 541–544.
307. **Yan, C.T., Boboila, C., Souza, E.K. et al. Alt, F.W.** (2007) IgH class switching and translocations use a robust non-classical end-joining pathway. *Nature*, *449*, 478–482.
308. **Ying, S., Minocherhomji, S., Chan, K.L. et al. Hickson, I.D.** (2013) MUS81 promotes common fragile site expression. *Nat Cell Biol*, *15*, 1001–1007.

309. **Yoo, H.Y., Kumagai, A., Shevchenko, A. et al. Dunphy, W.G.** (2007) Ataxia-telangiectasia mutated (ATM)-dependent activation of ATR occurs through phosphorylation of TopBP1 by ATM. *J Biol Chem*, *282*, 17501–17506.
310. **Zaaijer, S., Shaikh, N., Nageshan, R.K. et al. Cooper, J.P.** (2016) Rif1 Regulates the Fate of DNA Entanglements during Mitosis. *Cell Rep*, *16*, 148–160.
311. **Zgheib, O., Pataky, K., Brugger, J. et al. Halazonetis, T.D.** (2009) An oligomerized 53BP1 tudor domain suffices for recognition of DNA double-strand breaks. *Mol Cell Biol*, *29*, 1050–1058.
312. **Zhu, Z., Chung, W.H., Shim, E.Y. et al. Ira, G.** (2008) Sgs1 helicase and two nucleases Dna2 and Exo1 resect DNA double-strand break ends. *Cell*, *134*, 981–994.
313. **Zimmermann, M., and de Lange, T.** (2014) 53BP1: pro choice in DNA repair. *Trends Cell Biol*, *24*, 108–117.
314. **Zimmermann, M., Kibe, T., Kabir, S. et al. de Lange, T.** (2014) TRF1 negotiates TTAGGG repeat-associated replication problems by recruiting the BLM helicase and the TPP1/POT1 repressor of ATR signaling. *Genes Dev*, *28*, 2477–2491.
315. **Zimmermann, M., Lottersberger, F., Buonomo, S.B. et al. de Lange, T.** (2013) 53BP1 regulates DSB repair using Rif1 to control 5' end resection. *Science*, *339*, 700–704.
316. **Zou, L., and Elledge, S.J.** (2003) Sensing DNA damage through ATRIP recognition of RPA-ssDNA complexes. *Science*, *300*, 1542–1548.